METHYLMERCURY-INDUCED DISRUPTION OF CALCIUM HOMEOSTASIS AND SUBSEQUENT CYTOTOXICITY IN THE RENSHAW AREA

By

Mónica Ríos-Cabanillas

A DISSERTATION

Submitted to
Michigan State University
in partial fulfillment of the requirements
for the degree of

Comparative Medicine and Integrative Biology – Environmental Toxicology – Doctor of Philosophy

2019

ABSTRACT

METHYLMERCURY-INDUCED DISRUPTION OF CALCIUM HOMEOSTASIS AND SUBSEQUENT CYTOTOXICITY IN THE RENSHAW AREA

By

Mónica Ríos-Cabanillas

Methylmercury (MeHg) is an environmental neurotoxicant of current concern. It bioaccumulates in humans, via consumption of contaminated fish, causing deficiencies in motor function. The mechanism(s) underlying the MeHg-induced neuronal injury are not yet understood, but nerve cells die. Due to the prevalence of MeHg in the environment, superimposed with the high incidence for sporadic Amyotrophic Lateral Sclerosis (Guallar et al.), gene and environmental interactions have been proposed. At the Renshaw area, excitatory motor neurons (MNs) and inhibitory Renshaw cells (RCs) participate in a negative-feedback mechanism that control hindlimb muscles. Disruption of recurrent inhibition by too much excitation or too low inhibition disrupts this circuit towards a state of hyperexcitability. MeHg affects both excitatory and inhibitory neurotransmission, being the later the most sensitive. Also, MeHg-induced cell death is associated to increases in intracellular calcium (Ca^{2+}) concentration ($[Ca^{2+}]_i$). In detail, MeHg triggers Ca^{2+} efflux from intracellular Ca^{2+} stores followed by Ca^{2+} influx from the extracellular solution. Cholinergic receptors participate of MeHg-mediated alterations of $Ca^{2+}{}_i$ homeostasis in CGCs. The purpose of this research is to determine whether known targets of MeHg neurotoxicity contribute to dysfunction in cells that degenerate in ALS. Specifically, to examine the role of the nicotinic acetylcholine receptor (nAChR), γ-aminobutyric acid type A receptor ($GABA_AR$), glycine receptor (GlyR), and intracellular Ca^{2+} stores to the acute effects of MeHg neurotoxicity. The heteropentameric nAChR contributes to MeHg (*in vitro*)-induced increase in $[Ca^{2+}]_i$ and subsequent cell death. Furthermore, this occurred in an extracellular Ca^{2+}-dependent fashion. The

nAChR and $GABA_AR$, but not GlyR, contributes to the MeHg (*in situ*)-induced increase in $[Ca^{2+}]_i$. Intracellular Ca^{2+} pools also participate of the MeHg-mediated increase in $[Ca^{2+}]_i$. However, only the $GABA_AR$ is involved during MeHg-induced cell death in the Renshaw area. This research contributes to our understanding the effects of metal-induced neuronal injury in a group of cells that degenerate during ALS.

To my STAR and my family

ACKNOWLEDGEMENTS

My doctoral research project and my development as a scientist was only possible because of the love, guidance and support from many people. I would love to express my deepest gratitude towards the following:

Dr. William D. Atchison, thank you for believing and taking a chance on me. For providing the opportunity to achieve my goals of becoming a neurotoxicologist. For teaching me critical thinking, as well as, paying ultimate attention to detail. For your advice and patience during my years in the laboratory and for given me the opportunity to be a mentor.

To the members of my committee: Dr. Susan Barman, Dr. Timothy Collier, Dr. Patricia Ganey, and Dr. Irving Vega. For your willingness to serve as mentors on my committee, taking time to assist with thoughtful suggestions and insightful feedback on my experiments and writing skills. For meeting personally in order for me to provide project updates on my research progress and for asking thought-provoking questions. Your guidance and advice were essential throughout this entire experience.

To the Comparative Medicine and Integrative Biology Program, Institute of Integrative Toxicology, Dr. Vilma Yuzbasiyan-Gurkan, and Dr. Robert Roth. For giving me the opportunity to be part of these programs. To the Department of Toxicology and Pharmacology, Bridge to the PhD in Neuroscience Program and Summer Research Opportunity Program for the opportunity to conduct research in the company of such excellent scientists. To the supportive staff members of the department and programs. In particular to Dimity, Shari, Wendy, Beverly, Erica, Stephen and Bradley. Again, to the Institute of Integrative Toxicology and Dr. Atchison, for providing travel

awards and funding which allowed me to focus on my research and present my research at National meetings.

To Dr. Hajela and Dr. Yuan for your mentorship, patience and teaching me all the techniques I know today. Your continued support and guidance through my time in the laboratory is appreciated. To my laboratory friends: Dr. Jaiman, Dr. Bailey, Melissa Jaiman, Noge Wiwatratana, and Gretchen Rivera. For your collaborative spirit, brainstorming, encouragement, mentorship, many conversations, lunch dates, coming to my desk to say, 'what up?!', and overall support. Thank you all for helping me so much in the lab! Alberto Pérez, for your support and saving my experiments when I needed last minute materials. Ivelisse Cruz, for being an unconditional friend and, although we're in long distance, sharing our PhD journey together. Your support and encouragement were needed and appreciated. To my mentees: Yolimar Colón, Nicole Rivera, Andrea Aldaz and Romina González, Erin Formiller and Paige McKeon. For your help and technical assistance in this research project. I could not have done so many experiments without your help and assistance. For motivating me to be a better mentor. There were never silly questions. I learned a lot about teaching every one of you.

I am forever grateful to my family, Mom (Cusy), Dad (Tony), Ricky, Abi, Papo, Beatriz, Nico, Jose, Pri, Manuel and Vale. Thank you for always believing in me. Your love and support cannot be measured. Specifically, to my parents, for setting me up for success, fostering the importance of an education and always being there for me. Abi, you are my everything. Papo, you have been a role model in the arduous journey of completing a PhD. Also, for giving me a sense of social/environmental consciousness and awareness. Family time during my visits to Puerto Rico refilled my heart, gave me strength and purpose. To my other family in California, Terri, Adrianna, Jackson, Taita and Bob. For your support, love, and reminding me to always keep my eyes on the

prize. Your visits to Michigan provided a sense of comfort and family environment. Finally, I would like to thank Carlos, the love of my life. For everything he did and does for me. Who moved across the nation and who put up with many of my most intense moments. This journey would had been very difficult without you. Thank you for making me smile every day.

TABLE OF CONTENTS

LIST OF FIGURES

KEY TO ABBREVIATIONS

$[Ca^{2+}]_e$ Extracellular calcium concentration

$[Ca^{2+}]_i$ Intracellular calcium concentration

$^{45}Ca^{2+}$ Radiolabeled calcium

ACh Acetylcholine

ALS Amyotrophic Lateral Sclerosis

AMPA α-amino-3-hydroxy-5-methyl-4-isoxazolepropionic acid

ANOVA Analysis of variance

ATP Adenosine 5'-triphosphate

BAPTA-AM 1,2-Bis(2-aminophenoxy)ethane-N,N,N′,N′-tetra acetic acid tetrakis(acetoxymethyl ester)

BBB Blood brain barrier

BZs Benzodiazepines

Ca^{2+} Calcium

$Ca^{2+}{}_e$ Extracellular calcium

$Ca^{2+}{}_i$ Intracellular calcium

$CaCl_2$ Calcium chloride

Calcein AM Calcein acetoxymethyl ester

CCCP Carbonyl cyanide m-chlorophenyl hydrazone

Cl^- Chloride

CNS Central nervous system

CO_2 Carbon dioxide

DHβE Dihydro-β-erythroidine

DNA Deoxyribonucleic acid

EAA Excitatory amino acid

EAAT Excitatory amino acid transporter

EC_{50} Half maximal response concentration

EGTA egtazic acid

EPA Environmental Protection Agency

EtHD-1 Ethidium homodimer-1

F_{340} Fura-2 fluorescence signal at 340 nm excitation

$F_{340/380}$ Fura-2 fluorescence ratio

F_{380} Fura-2 fluorescence signal at 380 nm excitation

fALS Familial Amyotrophic Lateral Sclerosis

FDA Food and Drug Administration

FITC Fluorescein isothiocyanate

Fluo-4 AM acetoxymethyl ester

Fura-2 AM Fura-2 acetoxymethyl ester

GABA γ-aminobutyric acid

$GABA_AR$ γ-aminobutyric acid receptor

Glu Glutamate

GluR Glutamate receptor

Gly Glycine

GlyR Glycine receptor

HBS HEPES-buffered saline

HEPES 4-(2-hydroxyethyl)-1-piperazineethanesulfonic acid

Hg^0 Mercury

Hg^+ Mercurous

Hg^{2+} Mercuric

hr Hour

IACUC Institutional Animal Care and Use Committee

IP_3 Inositol 1,4,5-triphosphate

K^+ Potassium

KCl Potassium chloride

KH_2PO_4 Monopotassium phosphate

M Molar

MEC Mecamylamine

MeHg Methylmercury

mEPP Miniature end plate potential

Mg Milligrams

Mg^{2+} Magnesium

$MgCl_2$ Magnesium chloride

$MgSO_4$ Magnesium sulfate

min Minute

mL Milliliter

MLA Methyllycaconitine

mm Millimeter

mM Millimolar

MN Motor neuron

MNs Motor neurons

Na^+ Sodium

nAChR Nicotinic acetylcholine receptor

NaCl Sodium chloride

NIH National Institute of Health

nm Nanometer

NMDA N-methyl-D-aspartate

NMDG N-methyl-D-glucamine

NMJ Neuromuscular junction

NW No wash

O^2 Oxygen

PBS Phosphate-buffered saline

PC12 Pheochromocytoma 12

PIP2 Phosphatidylinositol biphosphate

PND Postnatal day

PNS Peripheral nervous system

ppm Parts per million

RCs Renshaw cells

RfD Reference dose

RR Ruthenium red

s Second

sALS Sporadic Amyotrophic Lateral Sclerosis

SEM Standard error of the mean

THP Thapsigargin

TPEN N,N,N',N'-tetrakis (2-pyridylmethyl) ethane-1,2-diamine

VGCCs Voltage-gated calcium channels

w/v Weight per volume

Zn^{2+} Zinc

µg Microgram

µL Microliter

µm Micrometer

µM Micromolar

CHAPTER ONE:

INTRODUCTION

Background

Methylmercury (MeHg) in the environment

Mercury (Hg^0) is also known as quicksilver for its mobility and silver liquid appearance at room temperature. The Latin name for Hg^0 is hydrargyrum, which translates to liquid silver. Hg^0 originates from natural and anthropogenic sources. Environmental sources that emit Hg^0 include degassing of the crust of the earth and emissions released by volcanic activity (United Nations Environment Programme., International Labour Organisation., World Health Organization., & International Program on Chemical Safety., 1990). Depositions of Hg^0 increase during the summer months as the result from the warmer temperatures (Vanarsdale et al., 2005). Nonetheless, Hg^0 is present in snow (15 ng/L or less) but in less amount compared to rain (15 ng/L or more) (Landis, Vette, & Keeler, 2002). Anthropogenic sources that add to the total atmospheric Hg^0 include burning of coal and fossil fuels, smelting of sulfide ores, production of iron and steel, and incineration of municipal and medical wastes (Clarkson, 1995; Mohapatra, Nikolova, & Mitchell, 2007). The current leading source of Hg^0 pollution is artisanal gold mining (Ashe, 2012; Wade, 2013). Together, these sources have exacerbated the toxicological effects of Hg^0 throughout time. The global distribution of Hg^0 and its atmospheric residence time makes this heavy metal a potential threat to humans (Perry, Norton, Kamman, Lorey, & Driscoll, 2005). Hg^0 is a stable gas, heavier than air (Cherry, Lowry, Velez, Cotrell, & Keyes, 2002). In the atmosphere, Hg^0 oxidizes and intercalates with the water cycle. In the environment, Hg^0 vapor undergoes two oxidation states: mercurous (Hg^+) and mercuric (Hg^{2+}). Hg^{2+} returns to the surface of the earth in rainwater, where it is deposited on land and open bodies of water. Methylation of Hg^{2+} to produce methylmercury (MeHg) takes place on sediments in fresh and ocean waters by methanogenic sulfate-reducing bacteria (Ekstrom, Morel, & Benoit, 2003). These bacteria use sulfur as a part of

their respiration system and they uptake Hg^{2+} via passive diffusion (Benoit, Mason, & Gilmour, 1999). Methylation of Hg^{2+} occurs through a mechanism that involves methyl-cobalamine compounds as the result of the bacterial synthesis (Jensen & Jernelov, 1969; Jones et al., 2019; Ridley, Dizikes, & Wood, 1977; Siciliano, O'Driscoll, & Lean, 2002; Wood, Kennedy, & Rosen, 1968). A decrease in the atmospheric deposition of Hg^0 lowers concentrations of MeHg in fish (R. C. Harris et al., 2007). Thus, MeHg is a worldwide concern, especially for fish-eating populations (Clarkson, 1995; Knobeloch, Gliori, & Anderson, 2007; Mergler et al., 2007).

MeHg is a persistent environmental neurotoxicant found in biota (King, Kostka, Frischer, & Saunders, 2000). Specifically, MeHg localizes in the aquatic food-chain, where it enters by rapid diffusion (J. Sherlock, Hislop, Newton, Topping, & Whittle, 1984; J. C. Sherlock, Lindsay, Hislop, Evans, & Collier, 1982). MeHg is absorbed by zooplankton, which in turn feeds the fish populations. Hence, MeHg biomagnifies in the seafood food-chain (Clarkson, 1995). Large predatory species, such as tuna, marlin and sea mammals (pilot whale) contain the highest concentrations of MeHg (Mason, Heyes, & Sveinsdottir, 2006). Individuals that depend on a piscivorous diet are exposed to a low-dose exposure of MeHg through the consumption of contaminated fish (Clarkson, 1995; Mahaffey et al., 2011; Mergler et al., 2007). MeHg bioaccumulates in animals and humans due to its slow rate of excretion (Hammerschmidt, Fitzgerald, Lamborg, Balcom, & Tseng, 2006). Studies have demonstrated a direct correlation between consumption of contaminated seafood and high blood levels of Hg^0 (Mahaffey, Clickner, & Jeffries, 2009; Schober et al., 2003). The mechanism(s) by which MeHg exerts its selective neurotoxicity are unknown.

Past and current human exposures to methylmercury

MeHg is responsible for two mass outbreaks in history. The first event occurred in Japan, 1950s. The Chisso Corporation was using inorganic Hg^0 as a catalyst to make acetaldehyde. MeHg was generated as a byproduct from this reaction. The MeHg waste was discharged into the Minamata Bay (Clarkson, 1995; M. Harada, 1995; Tsuda, Yorifuji, Takao, Miyai, & Babazono, 2009). Human ingestion of contaminated fish with MeHg (5-35 ppm) through a chronic exposure did not produce observable behavioral effects during years (M. Harada, 1995; Takeuchi, 1982; Takeuchi, Eto, & Tokunaga, 1989; Tsuda et al., 2009; B. Weiss, Clarkson, & Simon, 2002). Also, pregnant women exposed to MeHg reported severe cognitive and motor deficits in fetus (Y. Harada, Miyamoto, Nonaka, Ohta, & Ninomiya, 1968). Clinical signs of MeHg include irreversible damage and degeneration of neuronal populations, referred to "Minamata Disease" (Mc & Araki, 1958). These cause adult and developmental neurotoxicity (Bakir et al., 1973; Eto, Tokunaga, Nagashima, & Takeuchi, 2002). Approximately, 1,043 deaths were attributed to MeHg poisoning in Minamata, Japan (M. Harada, 1995).

The second mass outbreaks occurred during winter months in Iraq, 1970s. Iraqi farmers received grain shipments from Mexico that had been previously treated with MeHg as a fungicide. The grains containing MeHg were meant to be washed. Instead, Iraqi famers used the seed for flour production to prepare bread and feed their livestock. Iraqi victims presented signs of poisoning weeks and months after the occurrence of this exposure (Al-Mufti, Copplestone, Kazantzis, Mahmoud, & Majid, 1976; Bakir et al., 1973; Greenwood, 1985; Kazantzis, Al-Mufti, Al-Jawad, et al., 1976; Kazantzis, Al-Mufti, Copplestone, Majid, & Mahmoud, 1976). Furthermore, a high incidence of "myasthenia gravis"-like syndrome was reported (Rustam, Von Burg, Amin-Zaki, &

El Hassani, 1975). Approximately, 6,000 hospital admissions and 400 deaths were attributed to MeHg poisoning in Iraq (Bakir et al., 1973). The symptoms of neuromuscular weakness were ameliorated with acetylcholinesterase inhibitors (United Nations Environment Programme. et al., 1990). Treatment with neostigmine, to inhibit the hydrolysis of acetylcholine (ACh), alleviated MeHg-mediated symptoms of motor weakness (Rustam et al., 1975). Thus, MeHg disrupts the cholinergic neurotransmission at the motor end plate.

Together, these outbreaks demonstrate that the signs and symptoms associated with MeHg poisoning are similar following chronic and acute exposures (Clarkson & Magos, 2006). Symptoms of MeHg poisoning characteristics of the Minamata Disease include paresthesia, blurred vision, muscle weakness, dysarthria, dysphagia, ataxia and death (Bakir et al., 1973; L. W. Chang, 1977; Eto, 1997; M. Harada, 1995). Ataxia, due to cerebellar degeneration, is associated with a body burden of 200-312 mg Hg or blood levels of 19.5 μM Hg (Bakir et al., 1973). Severity of the symptoms depend on factors such as the dose and duration of exposure, and the developmental stage at which the MeHg poisoning occurred. Symptoms of MeHg poisoning are not immediate. Thus, it shows a latency period between MeHg exposure and the pathological consequences. The reason for the latency period is unknown. However, it could be due to MeHg-induced cerebellum cytotoxicity (Hunter & Russell, 1954; B. Weiss et al., 2002). Additionally, in Canada, Cree Indian mothers consumed seafood contaminated with MeHg and their children presented abnormal motor coordination (McKeown-Eyssen & Ruedy, 1983).

Following these MeHg outbreaks, two long-term studies were conducted in populations that primarily eat fish to further understand effects of MeHg poisoning. Studies in the Seychelles and

the Faroe Islands have been monitoring prenatal effects of a low dose to MeHg for decades. The Seychelles Islands is an archipelago off the eastern coast of Africa. No prenatal adverse effects were detected in this population (Myers & Davidson, 1998; Myers et al., 2003). Also, they did not show neurological dysfunctions associated with MeHg poisoning (Cernichiari et al., 1995; Davidson et al., 2011). The Faroe Islands is an archipelago between the Norwegian Sea and the North Atlantic Ocean. Besides eating seafood, this population also eat marine mammals (pilot whale), which accumulate polychlorinated biphenyls (PCBs) (Nakai & Satoh, 2002; Weihe, Grandjean, Debes, & White, 1996). Unlike the Seychelles population, this Nordic community presented dysfunctions associated with MeHg poisoning. A correlation was detected between prenatal exposure to MeHg and mental retardation and deficits in the motor system (Debes, Budtz-Jorgensen, Weihe, White, & Grandjean, 2006; Grandjean et al., 1997). Adult brains in this cohort reported levels of 300 ng/g MeHg in the brain (Bjorklund et al., 2007; B. Weiss, Stern, Cox, & Balys, 2005). The factors that account for the differences in susceptibility between these populations to MeHg are not known. However, their genetics and the type of fish consumption could be involved. The neurotoxicity observed in the population of the Faroe Islands could had been provoked by the consumption of contaminated meat from whales (Booth & Zeller, 2005). Furthermore, adverse effects in cognitive functions as the result of exposure to MeHg may become evident with age (Weihe et al., 1996).

Currently, the largest known source in the world of Hg^0 pollution is artisanal and small-scale gold mining (ASGM) (Veiga et al., 2004; Wade, 2013). In detail, Hg^0 is mixed with gold ore to form an amalgam. Then, the amalgam is heated followed by the evaporation of Hg^0. This separates the gold from the rock and sediments allowing the miners to collect the gold. Hence, Hg^0 vapors enter

the environment. Hg^0 comprises about 37% of the total atmospheric emissions (Sakamoto, Nakamura, & Murata, 2018). Additionally, miners are a fish-eating population. Therefore, the miners are simultaneously exposed to MeHg through dermal absorption and fish consumption. The main site for ASGM is in Madre de Dios, Peru (Ashe, 2012; Fraser, 2016; Gardner, 2012). In 2012, a report indicated that 11% of the population at Madre de Dios had levels of hair mercury above 16 mg/g (Ashe, 2012). This concentration is associated with neurotoxic symptoms (United Nations Environment Programme. et al., 1990). Other locations for ASGM include Africa (Odumo et al., 2014; Rajaee, Long, Renne, & Basu, 2015), French Guiana (Frery et al., 2001), China (Gunson, 2004) and Indonesia (Nakazawa et al., 2016). These populations could present neurological signs similar to those observed with Minamata Disease (Bailey, Colon-Rodriguez, & Atchison, 2017).

The first association between a neurodegenerative disease and an environmental toxicant occurred in Guam (Johnson & Atchison, 2009). The Chamorro indigenous people were exposed to the non-protein amino acid β-methylamino-L-alanine through consumption of cycad seeds and flying fox (Armon, 2003). They presented high incidence of amyotrophic lateral sclerosis (Guallar et al.). Furthermore, veterans of the Persian Gulf War (1990-1992) presented incidence of nonspecific neurological symptoms, which it is known as the "Gulf War Syndrome". Clinical observations concluded that incidence of ALS in this population increased significantly (Haley, 2003; Horner et al., 2003). Also, onset of ALS was hastened, occurring at earlier time points compared to the general population (Schmidt et al., 2008). Thus, military personnel developed ALS following an environmental or occupational exposure (Weisskopf, Cudkowicz, & Johnson, 2015). Therefore, gene and environmental (GxE) interactions may hasten onset or cause neurodegenerative diseases (Johnson et al., 2011; Roos, Vesterberg, & Nordberg, 2006).

MeHg neurotoxicity has been reported in United States. Particularly, the fish population in the Great Lakes has been reported to exceed the reference dose (RfD) for MeHg (Gerstenberger & Dellinger, 2002; Gilbertson & Carpenter, 2004; D. C. Rice, 1995; Weis, 2004). The Environmental Protection Agency (EPA) suggested RfD for the daily intake of MeHg during chronic exposure is 4-5 μg/L blood and approximately 0.1 μg/kg per day (Keating, United States. Environmental Protection Agency. Office of Air Quality Planning and Standards., & United States. Environmental Protection Agency. Office of Research and Development., 1997; G. Rice, Swartout, Mahaffey, & Schoeny, 2000; Schoen, 2004). The RfD value was based from MeHg exposure in the Faroe Islands and contains two uncertainty factors: pharmacodynamic and pharmacokinetics variabilities (Grandjean et al., 1997). Additionally, the RfD takes in consideration research on children exposed in utero during the Iraq poisoning (Marsh et al., 1987). Fish consumption of 7 ounces or less per week is recommended for the general population.

Pharmacokinetics of MeHg

Thiol groups are ubiquitously found within cells. MeHg binds to thiol forming a covalent bond via an oxidation reaction (H. H. Harris, Pickering, & George, 2003; Kostyniak & Clarkson, 1981). Thus, MeHg targets cysteine groups (Hisatome et al., 2000). Cysteine amino acids are conserved residues important for regulatory and catalytic proteins, and binding functions. Cysteine is constantly produced and metabolized, achieving a plasma concentration of 10 μM (Bannai, 1984).

The 95% of MeHg is absorbed in the gastrointestinal tract in rats, mice and humans (Aberg et al., 1969; Bakir et al., 1973; Berlin & Ullberg, 1963; I. R. Rowland, Davies, & Evans, 1980). Thus, MeHg is systemically distributed throughout the body (Clarkson, Vyas, & Ballatori, 2007). The

high affinity that MeHg has with cysteine groups allows it to target the bloodstream (Kerper, Ballatori, & Clarkson, 1992; Simmons-Willis, Koh, Clarkson, & Ballatori, 2002). The MeHg-cysteine complex acts as an amino acid analog similar in structure to methionine (Cernichiari et al., 2007). The large neutral amino-acid carrier transports the MeHg-cysteine complex instead of the methionine complex (Yin et al., 2008). Also, MeHg is lipophilic and it can cross lipid membranes. Thus, MeHg associates with endothelial cells where it forms a new complex with glutathione. Then, MeHg-glutathione complex crosses the placenta and blood brain barrier (BBB), reaching the brain via the glutathione carrier (Kajiwara, Yasutake, Adachi, & Hirayama, 1996; Kerper et al., 1992). MeHg targets the central nervous system (CNS) causing damage to the developmental and adult brain (Castoldi et al., 2008). The process of MeHg absorption to distribution is completed in 3-4 days in humans (Clarkson et al., 2007). The brain MeHg values are the highest in about 5-6 days (Goodman, Gilman, & Brunton, 2008; United Nations Environment Programme. et al., 1990). Furthermore, MeHg reaches brain tissue within 5 min after intravenous injection in the rat (Hirayama, 1985; Thomas & Smith, 1979) and 4 hour (hr) after ingestion in mice (Sager, Doherty, & Rodier, 1982). Excretion of MeHg occurs in its inorganic form (I. R. Rowland, Robinson, & Doherty, 1984). Elimination of MeHg in the brain accounts for 10% of demethylation (Dunn & Clarkson, 1980). Thus, the brain has limited demethylation capability. The liver is the main organ responsible for the elimination of MeHg (Dunn & Clarkson, 1980). The MeHg-glutathione complex is secreted into the bile via glutathione carriers (Ballatori & Clarkson, 1985; Ballatori, Gatmaitan, & Truong, 1995). Then, biliary elimination brakes down the MeHg-glutathione complex into a MeHg-cysteine complex. The latter can be reabsorbed into the bloodstream (Dutczak & Ballatori, 1992, 1994). MeHg reabsorption produces a multiphasic kinetics secretion-reabsorption cycle, called enterohepatic circulation. The mean human half-life

for MeHg elimination is 70 days (Aberg et al., 1969; Birke et al., 1972; Kershaw, Clarkson, & Dhahir, 1980). It corresponds to the loss of the body burden to 1% MeHg every 24 hr (Cernichiari et al., 2007). The 90% of MeHg elimination occurs via the feces (Clarkson et al., 2007). Furthermore, lactation facilitates elimination of MeHg from the blood (Skerfving, 1988). An effective method to remove MeHg from the human body it hemodialysis with n-acetyl penicillamine (Elhassani, 1982). The basis for chelation of MeHg consists in adding free sulfhydryl groups to promote metal mobility within the ligands (Bernhoft, 2012). There is no effective antidote against MeHg poisoning.

Pathophysiology of MeHg

Consumption of seafood contaminated with MeHg highlights the pathophysiology of developmental and adult poisoning. Several brain regions are particularly sensitive to the effects of MeHg. MeHg affects the occipital lobe, specifically the visual cortex and the cerebellum. Chronic exposure to MeHg (2 mg/kg/day) disrupts GABAergic signaling in the occipital cortex of wild minks (Basu et al., 2010). Administration of MeHg *in vivo* causes cell death of GABA-containing neurons in the visual cortex, cerebral cortex and forebrain (J. O'Kusky, 1985; J. R. O'Kusky & McGeer, 1985). Furthermore, impaired spatial vision in the visual cortex was reported in monkeys following a chronic exposure to MeHg (50 mg/kg/day) (D. C. Rice & Gilbert, 1982). Also, a case study of a 23 year old man that was exposed to MeHg in dust revealed contraction of the visual field and ataxia. Specifically, the autopsy revealed atrophy of the cerebellum and occipital lobe (Hunter & Russell, 1954). This study demonstrated a latency period (6 months) between the time of exposure to MeHg and presentation of symptoms. A long latency, delay or "silent phase" caused by MeHg has been previously described (Nierenberg et al., 1998; B. Weiss

et al., 2002; J. H. Weiss & Sensi, 2000). The rationale for this silent phase is unknown. However, mechanisms that involve cell death have been proposed. Particularly, the latency phase suggests that live cells are trying to sustain normal functions and compensate against MeHg-induced cell death (B. Weiss et al., 2002). Furthermore, the case study demonstrated that cerebellar granule cells (CGCs) degenerated more than neighboring Purkinje neurons. Thus, the effects of MeHg neurotoxicity are cell-type specific. This relative sensitivity has been reported *in vitro* (Yuan & Atchison, 2003, 2007). Purkinje cells are larger than CGCs and following MeHg exposure, Purkinje cells accumulated more MeHg than CGCs. Furthermore, Purkinje cells were spared from cytotoxicity following MeHg exposure *in vivo* (Leyshon-Sorland, Jasani, & Morgan, 1994) and *in vitro* (Edwards, Marty, & Atchison, 2005). Thus, neurotoxicity is not dependent solely on the amount of MeHg accumulated within a cell. Perhaps, Purkinje cells metabolize MeHg into organic Hg^{2+} faster than CGCs (Leyshon-Sorland et al., 1994). Also, Purkinje cells express calbindin, while CGCs do not (Celio, 1990). This suggests that presence of calbindin could protect against Ca^{2+}-induced cell death (Mattson, Rychlik, Chu, & Christakos, 1991; McMahon et al., 1998). Furthermore, transfection of calbindin in neuron-like cells demonstrate an increased capacity of these cells to buffer Ca^{2+} ions and protect against cell death (McMahon et al., 1998). Purkinje cells express the α1 subunit while CGCs express the α6 subunit in the $GABA_AR$ (Herden, Pardo, Hajela, Yuan, & Atchison, 2008). Thus, differential expression of the α subunit could underly the preferential neurotoxicity of MeHg. Together, the amount of MeHg accumulated by cells do not correlate to their susceptibility.

Another region in the brain that is particularly sensitive to MeHg poisoning is the hippocampus. In this region, MeHg (5-8 mg/kg/day) alters gene expression, by upregulating the mRNA levels of

the N-methyl-D-aspartate (NMDA) receptors, and impaired cognitive behavior in rats (Baraldi, Zanoli, Tascedda, Blom, & Brunello, 2002; Liu, Wang, Zhang, & Zhou, 2009). Furthermore, MeHg (2 mg/kg/day) increases the density of muscarinic acetylcholine receptors (mAChRs) in the hippocampus and cerebellum (Coccini et al., 2000). Additionally, in the brainstem, as well as, in the occipital lobe and hippocampus, MeHg (10 mg/kg/day) mediates cell death of cortical neurons (Miyamoto et al., 2001) Together data demonstrate that mechanisms involved in motor and cognitive functions are altered by MeHg poisoning.

Amyotrophic Lateral Sclerosis

ALS is a neurodegenerative disorder characterized by the linear progressive degeneration of α-motor neurons (αMNs) located in the cerebral cortex, brainstem and spinal cord (Kanning, Kaplan, & Henderson, 2010; Tandan & Bradley, 1985). This results in a loss of function of skeletal muscles. ALS is the current most common MN disease in humans. Population studies determined an incidence of 5 cases in a population of 100,000 annually. Preferentially, ALS affects white men over the age of 50 (McGuire, Longstreth, Koepsell, & van Belle, 1996). After the initiation of symptoms, the disease culminates in death for 80% of the patients in approximately 5 years (Cleveland & Rothstein, 2001; L. P. Rowland & Shneider, 2001). Signs and symptoms include muscle denervation, atrophy muscular spasticity and paralysis. Ultimately, respiratory failure causes death (Cleveland & Rothstein, 2001). The majority of the ALS cases are sporadic (sALS). Thus, GxE interactions may hasten or trigger ALS in susceptible individuals. Only 10% of the ALS cases are classified as familial (fALS) inheritance with autosomal dominant transmission. Both, sALS and fALS have virtually identical etiology, clinical course and neuropathology (Cleveland & Rothstein, 2001). Thus, both forms share a common pathological mechanism(s),

although their causes may differ. The 20% of the fALS cases are linked to an autosomal dominant mutation in the *superoxide dismutase* (SOD)-1 gene (Swarup & Julien, 2011). This gene is an antioxidant that detoxifies intracellular superoxide anions and free radicals. Specifically, the SOD1-G93A mutation has been a common model to study the pathophysiology of fALS and sALS (Andersen et al., 1996; Synofzik, Fernandez-Santiago, Maetzler, Schols, & Andersen, 2010).This mutation substitutes the glycine amino acid for an alanine at position 93 and leads to a toxic gain of function (Gurney et al., 1994; Sau et al., 2007).

There is not yet a definitive mechanism by which ALS originates. Three theories have been proposed. First, primary damage occurs to αMNs mediated through glutamate (Glu) excitotoxicity, (Braak et al., 2013; Cappello & Francolini, 2017). Second, degeneration of αMNs starts at the nerve ending and progress toward the cell body (Cappello & Francolini, 2017; Fischer et al., 2004; Moloney, de Winter, & Verhaagen, 2014). Regardless of how ALS originates, the neuromuscular junction (NMJ) degenerates leading to impairment of skeletal muscle (Cappello & Francolini, 2017). Third, since ALS is a not an αMN-only disease, the contribution from dysfunctions in astrocytes and microglia has been suggested (Philips & Rothstein, 2014; Qian et al., 2017). Mechanisms involved in the pathology of ALS include: increases in protein aggregation, defects in protein stability, increase in oxidative stress, impairment of the excitatory amino acid transporter 2 (EAAT2), Glu-mediated excitotoxicity, uncontrolled activation of the α-amino-3-hydroxy-5-methyl-4-isoxazolepropionic acid (Campanari, Garcia-Ayllon, Ciura, Saez-Valero, & Kabashi) receptor, dysregulation of Ca^{2+} homeostasis, and mitochondrial dysfunction and altered neuronal excitability (Cleveland & Rothstein, 2001; Ghasemi & Brown, 2018; Pasinelli & Brown, 2006). Also, lack of the Ca^{2+}-binding protein, calbindin, in MNs may increase susceptibility to ALS

neurodegeneration (Shaw & Eggett, 2000). There is no cure or effective treatment against ALS. Riluzole is the first FDA approved drug to treat ALS. However, it alleviates ALS symptoms and delays death of ALS-patients by ~3 months (Bellingham, 2011). Riluzole mechanism of action works by blocking release of Glu. Radicavas is the second FDA approved treatment for ALS. A study indicates its mechanism of action is by reducing oxidative stress in nerve and vascular cells (Nagase, Yamamoto, Miyazaki, & Yoshino, 2016).

Dysfunction of the cholinergic, GABAergic and glycinergic systems have been reported in ALS patients. Downregulation of cholinergic, GABAergic and glycinergic receptors has been observed in ALS patients (Whitehouse et al., 1983; Wootz et al., 2013). Muscle biopsies from ALS patients indicate a reduction in ACh esterase (Frery et al.) (Campanari et al., 2016; Cappello & Francolini, 2017). Results from spinal cord autopsies reveal that ALS patients have reduced binding sites for glycine (Hayashi, Suga, Satake, & Tsubaki, 1981). Furthermore, Recurrent inhibition between Renshaw cells (RCs) and αMNs appears to be abnormally reduced in patients with ALS compared with healthy individuals (Raynor & Shefner, 1994). Dysfunction of excitatory and inhibitory synaptic transmission has also been reported in animal models of ALS. Downregulation of choline acetyltransferase (ChAT) and the vesicular ACh transporter (VAChT) have been reported in humans and mouse models. This suggests that reduced ACh availability in the presynaptic terminals contributes to degeneration of MN (Campanari et al., 2016; Cappello & Francolini, 2017). An increase in ACh level mediated by overexpression of VAChT leads to degeneration of the NMJ and accelerates disease onset in SOD1-G93A mice (Cappello & Francolini, 2017; Sugita et al., 2016). GABA receptors induce more chloride (Cl^-) influx into MNs, accelerating neuronal excitotoxicity in mice (Carunchio, Mollinari, Pieri, Merlo, & Zona, 2008). Furthermore, MNs have

a reduced GABAergic and glycinergic neurotransmission in the SOD1-G93A mouse model (Q. Chang & Martin, 2009, 2011; Nieto-Gonzalez, Moser, Lauritzen, Schmitt-John, & Jensen, 2011). Metals are considered to be an environmental contributor to the manifestation of ALS disease due to their prevalence in the environment (Rooney, 2011). Exposure to an environmental factor on its own may not cause ALS. Conversely, a person with a genetic polymorphism exposed to a neurotoxicant could have hastening of ALS. Additionally, the GxE interaction could cause sufficient damage to MNs in order for the ALS disease to manifest (Mitchell, 2000; Wang, Little, Gomes, Cashman, & Krewski, 2017).

Hg^{2+} exposure affects MN by a syndrome that resembles ALS-mediated neurodegeneration (Adams, Ziegler, & Lin, 1983; Praline et al., 2007; Schwarz, Husstedt, Bertram, & Kuchelmeister, 1996; Sutedja et al., 2009). ALS-like clinical syndrome include progressive weakness of the extremities, muscular atrophy and widespread fasciculations. These all indicate injury of spinal MNs (Brown, 1954; Kantarjian, 1961). Exposure to Hg chloride ($HgCl_2$) causes localized deposits of Hg^{2+} in MNs of the spinal cord and the brainstem (Arvidson, 1992). Also, Hg^{2+} significantly accumulates in spinal cord MNs in mice, and this was not different from the Hg^{2+} accumulated by patients who died from a spinal MN disease (Pamphlett & Waley, 1996). These findings demonstrate possible roles in how exposure to an environmental contaminant contributes to ALS.

MeHg poisoning and ALS disease share a similar toxic mechanism(s). Both, MeHg and ALS increase release of Glu (Cleveland & Rothstein, 2001; Yuan & Atchison, 1997), increase $[Ca^{2+}]_i$ (Grosskreutz, Van Den Bosch, & Keller, 2010; Limke, Heidemann, & Atchison, 2004), causes mitochondrial damage (Cleveland & Rothstein, 2001; Limke & Atchison, 2002), increase reactive

oxygen species (ROS) (Aschner, Syversen, Souza, Rocha, & Farina, 2007; Cleveland & Rothstein, 2001; Pamphlett & Coote, 1998), and impair function of the astrocytic EAAT2 (Aschner, Yao, Allen, & Tan, 2000; Cleveland & Rothstein, 2001). Thus, these mechanisms of excitotoxicity share a common denominator which is the disruption of Ca^{2+} homeostasis.

A study conducted in our laboratory established the first relationship of cause and effect between development of ALS and an exposure to an environmental neurotoxicant (Johnson et al., 2011). In detail, exposure to chronic, low-dose MeHg (3 parts per million (ppm)) caused elevations in internal Ca^{2+} concentrations ($[Ca^{2+}]_i$) in slices from the brainstem slices of SOD1-G93A mice (Johnson et al., 2011). Additionally, MeHg hastened the onset of the ALS phenotype in SOD1-G93A mice (Johnson et al., 2011). In another experiment, treatment with an antagonist for the L-type voltage gated Ca^{2+} channel (VGCC) ablated the MeHg-mediated neurological dysfunctions *in vivo* and *in vitro* (Sakamoto, Ikegami, & Nakano, 1996). Moreover, blocking the L-type VGCC with nimodipine protected against MeHg-induced behavioral toxicity in mice (Bailey, Hutsell, & Newland, 2013).

To date, no specific factor is known to cause ALS disease and the mechanisms that contribute to the hastening of ALS are unknown. Alterations in Ca^{2+} oscillation and Ca^{2+} dynamics have been hypothesized as a risk factor for the onset of neurodegenerative diseases. Hence, GxE interactions are a possible explanation for the sALS cases. This is important because it allows to use MeHg-mediated Ca^{2+} dysregulation and subsequent cytotoxicity as a model to understand mechanisms of ALS pathogenesis (Bailey et al., 2017)

Regulation of Ca^{2+}

Ca^{2+} is an alkaline earth metal. It is the most abundant metal in the body. Ca^{2+} is a 2nd messenger that regulates neuronal activity and downstream pathways through activation of enzymatic cascades. Ca^{2+} regulation of intracellular events controls fundamental neuronal functions including membrane depolarization, neurotransmitter release and synaptic activity. At the biomolecular level Ca^{2+} homeostasis is an extensive, well-regulated and tightly coupled process. In normal conditions, external Ca^{2+} concentration ($[Ca^{2+}]_e$) is in the 1-2 mM range (Kass & Orrenius, 1999). This represents 10,000 times more than cytosolic Ca^{2+}. In normal conditions, unbound $Ca^{2+}{}_i$ is in the 100 nM range but in active zones, it increases to concentrations as high as 100 µM (Bennett, Farnell, & Gibson, 2000). This drastic difference in $[Ca^{2+}]_i$ across the plasma membrane creates a large chemical driving force. The tight coupling between Ca^{2+} buffering and Ca^{2+} release processes causes physiological oscillations to initiate and end electrical activity in the plasma membrane. $Ca^{2+}{}_e$ enters the cell through VGCCs and ligand-gated ion channels (LGICs). These channels alter the concentration of cytoplasmic ions because of their high rate capacity for ion transfer (Hille, 1978). Thus, they are important for regulating the membrane potential, activating secretion of neurotransmitters, initiating gene transcription pathways and second messenger Ca^{2+} signaling, among others.

MeHg disrupts Ca^{2+} homeostasis and drives an uncontrolled and sustained increase in $[Ca^{2+}]_i$ in both primary and transformed cell lines (e.g. rat brain synaptosomes, NG108-15 neuroblastoma cells, CGCs and MNs) (Edwards et al., 2005; Hare, McGinnis, & Atchison, 1993; Kauppinen, Komulainen, & Taipale, 1989; Marty & Atchison, 1997; Ramanathan & Atchison, 2011; T. A. Sarafian, 1993; Yuan & Atchison, 2007, 2016). The MeHg-mediated biphasic $[Ca^{2+}]_i$ increase

consists of two kinetically and temporally distinct phases. “Phase 1” is thought to be due to Ca^{2+} efflux from both mitochondria and the smooth endoplasmic reticulum (SER). “Phase 2” is thought to be due to entry of extracellular Ca^{2+} (Denny, Hare, & Atchison, 1993; Edwards et al., 2005; Hare & Atchison, 1995; Hare et al., 1993; Limke, Bearss, & Atchison, 2004; Marty & Atchison, 1997; Ramanathan & Atchison, 2011). Treatment with specific antagonists for VGCC during MeHg exposure protects against MeHg-mediated increases in $[Ca^{2+}]_i$ (Marty & Atchison, 1997) Furthermore, presence of the $Ca^{2+}{}_i$ chelator, 1,2-Bis(2-aminophenoxy)ethane-N,N,N′,N′-tetra acetic acid tetrakis (BAPTA), protects against Ca^{2+}-dependent cytotoxicity in CGCs (Marty & Atchison, 1998). MeHg neurotoxicity is not exclusive to VGCCs. Thus, other membrane channels participate of MeHg-mediated increase in $[Ca^{2+}]_i$.

Structure and biodiversity of ligand-gated ion channels

LGICs consist of cys-loop receptors, ionotropic Glu receptors (GluRs) and serotonin (5-HT3) channels. LGICs control fast synaptic neurotransmission by converting a chemical signal into a postsynaptic electric signal. The cys-loop family include nicotinic ACh receptors (nAChRs), $GABA_A$Rs and glycine receptors (GlyRs), among others. In the cys-loop of the receptors there are two cysteine residues separated by 13 amino acids that form a disulfide bond. This bond creates a signature loop important for signal transduction following the binding of an agonist at the N-terminal in the extracellular domain (Karlin et al., 1986; Sine & Engel, 2006).

MeHg has high affinity to cysteine residues (Bahr & Moberger, 1954; Hughes, 1957; Kostyniak & Clarkson, 1981; Roberts, Steinrauf, & Blickenstaff, 1980). The presence of these residues on LGICs facilitates MeHg to target them (Hisatome et al., 2000). Interactions of MeHg with cysteine residues on membrane receptors lead to changes in the conformation of the receptor. This interferes

with cellular processes and disrupts synaptic neurotransmission (Denny & Atchison, 1996; Sirois & Atchison, 1996).

LGICs consist of α, β, γ, and δ subunits. The subunit heterogeneity determines the kinetics and characteristics of the receptor. Each subunit contains four conserved transmembrane domains with the second segment the one that forms the central ion pore (Tsetlin, Kuzmin, & Kasheverov, 2011). The α subunit constitutes the pore forming, voltage-sensing and ligand-binding component (Lukas et al., 1999). Thus, it defines the functional kinetics of the channel. The non-α subunits fulfill a role in complementary binding sites.

ACh is the primary neurotransmitter of lower MNs and at the NMJ. ACh is the endogenous agonist for all nAChR subtypes. The binding site for the agonist in the nAChR is formed by two α subunits. These receptors are permeable to K^+ and divalent cations such as Na^+ and Ca^{2+} (Dajas-Bailador & Wonnacott, 2004; Seguela, Wadiche, Dineley-Miller, Dani, & Patrick, 1993). Activation of nAChRs and the generation of an action potential trigger $Ca^{2+}{}_e$ influx and Ca^{2+} release from internal Ca^{2+} stores (Sharma & Vijayaraghavan, 2001; Tsuneki, Klink, Lena, Korn, & Changeux, 2000), which then causes the release of ACh. ACh is synthesized in the motor nerve terminals from acetyl-CoA and choline by the catalysis of ChAT (Hebb, 1972). Effects of ACh are terminated by the action of AChE, which hydrolyzes ACh into acetate and choline. ACh release can occur by either spontaneous or induced by an action potential. Spontaneous release of ACh represents the release from a single quantum (one vesicle). This produces a miniature end plate potential (mEPP) (Katz & Miledi, 1963). A quantum represents a small depolarization because it is not enough to produce an action potential at the postsynaptic membrane. Action potentials that

evoke release of ACh from many quanta in a synchronous way results in a large membrane depolarization or end plate potential (Djiogue et al.) (Del Castillo & Katz, 1954).

The muscle and neuronal nAChRs are two different pentameric receptors. 2 α (2-10), 2 β (2-4) and 1 (γ (1-3), δ, γ, ε) subunits form the nAChR (Albuquerque, Pereira, Alkondon, & Rogers, 2009). Adult skeletal muscle subunit composition consists of (α 1), β, δ, ε with a ratio of 2:1:1:1. The α1 subunit is specific to muscular nAChRs. Neuronal nAChRs are homo- or heteromeric constructed channels. The compositions that predominate the most in the CNS are α7 and α4β2 (Dineley, Pandya, & Yakel, 2015; Gotti, Zoli, & Clementi, 2006). The homomeric α7 nAChRs is the most Ca^{2+} permeable of all the stoichiometries (Seguela et al., 1993; Vernino, Amador, Luetje, Patrick, & Dani, 1992). The nAChRs in the mature spinal cord express α: 2, 3, 4, 5, 7 and β: 2, 3, 4 with a ratio of 2:3, 3:2, or 2:2:1 (Chavez-Noriega et al., 1997; Vincler & Eisenach, 2004). Specifically, nicotine has the highest affinity for the 2 (α 4) - 3 (β 2) stoichiometry (Albuquerque et al., 2009). The specific antagonist to block the nAChR is dependent on the stoichiometry expressed. Methyllycaconitine (MLA) blocks α 7-containing homomeric receptors (Turek, Kang, Campbell, Arneric, & Sullivan, 1995). This competitive antagonist is derived from a camphene, a plant alkaloid (Mogg et al., 2002; Philip, Carpenter, Tyrka, & Price, 2012). Mecamylamine (MEC) blocks α 2-containing heteromeric receptors (Sacco, Bannon, & George, 2004). This non-competitive antagonist developed as an anti-hypertensive drug (Stone, Torchiana, Navarro, & Beyer, 1956). Dihydro-β-erythroidine (DHβE) blocks α 4-containing heteromeric receptors (Chavez-Noriega et al., 1997). This alkaloid is derived from the plant *Erythrina poeppigiana* (Djiogue et al., 2014).

MeHg disrupts cholinergic transmission at the presynaptic and postsynaptic membranes. MeHg-mediated elevations in $[Ca^{2+}]_i$ increase the release of neurotransmitters (Atchison, 1986, 1987; Atchison & Narahashi, 1982), suppresses the amplitude of the EPP (Traxinger & Atchison, 1987), excitatory post-synaptic potential (EPSP) (Yuan & Atchison, 1995, 1997) and inhibitory post-synaptic potential (IPSP) (Yuan & Atchison, 1995). MeHg blocks spontaneous synaptic current (Yuan & Atchison, 2007), suggesting MeHg interacts with the channel itself. Furthermore, exposure to MeHg disrupts the cholinergic neurotransmission. Specifically, MeHg suppresses the nicotinic fast depolarizing response (Quandt, Kato, & Narahashi, 1982). MeHg increases spontaneous release of ACh and decreases the nerve-evoked release of ACh (Atchison, 1986, 1987; Atchison & Narahashi, 1982; Juang & Yonemura, 1975). MeHg blocks binding of ACh to its receptor (Eldefrawi, Mansour, & Eldefrawi, 1977) and MeHg binds to nAChRs (Eldefrawi et al., 1977; Shamoo, Maclennan, & Elderfrawi, 1976) and mAChRs (Abd-Elfattah & Shamoo, 1981; Coccini et al., 2000; Von Burg, Northington, & Shamoo, 1980). Also, MeHg acts on mAChRs causing the release of Ca^{2+} from the inositol-1,4,5-triphosphate (IP3)-sensitive Ca^{2+} pool (Limke, Bearss, et al., 2004). Thus, effects of MeHg in the cholinergic neurotransmission have been well established.

GABA is the most important inhibitory neurotransmitter in the mammalian CNS (Obata, Ito, Ochi, & Sato, 1967; Seeburg et al., 1990). GABA is synthesized in neurons from Glu by the enzymes glutamic acid decarboxylase 65 (GAD65) and 67 (GAD67). $GABA_A$Rs are heteropentameric with four membrane spanning domains. The stoichiometry of the $GABA_A$R consists of α: 1-6, β: 1-3 and γ: 1-3, δ, ε, θ, or π subunits (Mohler et al., 1996) with a ratio of 2:2:1. Also, the $GABA_A$R has an allosteric binding site for benzodiazepines (BZs) (Smith, 2001). Thus, a spectrum of drugs such

as anxiolytics and anesthetic, and toxic agents can interact with the function of the receptor. Zinc (Zn^{2+}) is an allosteric modulator for the $GABA_AR$. The binding site for GABA in the $GABA_AR$ is located between the α and β subunits. The binding site for BZs in the $GABA_AR$ is located between the α and γ subunits (Jacob, Moss, & Jurd, 2008). Activation of the $GABA_AR$ increases the receptors permeability to Cl^-, resulting in an IPSP response that reduces the amplitude of the EPSP. Therefore, the primary role of $GABA_ARs$ is to decrease neuronal excitability and neurotransmission (Long et al., 2009). $GABA_ARs$ mediate phasic inhibition, as well as, tonic inhibition (Farrant & Nusser, 2005). $GABA_ARs$ on Purkinje cells express α 1, β 2, β 3, γ 2 subunits. $GABA_ARs$ on CGCs express α 1, α 6, β 2, β 3, γ 2 subunits (Laurie, Seeburg, & Wisden, 1992). $GABA_ARs$ on MNs of the mature spinal cord express the α 2, α 3 subunits (Carunchio et al., 2008; Wisden, Gundlach, Barnard, Seeburg, & Hunt, 1991). Quantification of the GABAergic interneurons in the spinal cord is not known, but in the brain, they constitute 17%–20% of all the cell populations (Somogyi, Tamas, Lujan, & Buhl, 1998). The antagonist for the $GABA_AR$ is bicuculline (BCC). This alkaloid is a competitive antagonist derived from the plant *Dicentra cucullaria.* Actions of BCC mimic epilepsy.

MeHg suppresses the GABA-mediated Cl^- current in dorsal root ganglion cells (Arakawa, Nakahiro, & Narahashi, 1991). MeHg increases the frequency of occurrence of GABA-mediated IPSCs (Yuan & Atchison, 2003, 2007). MeHg (20, 100 μM) causes a transient stimulation of the IPSP amplitude followed by a complete block of the GABA current (Yuan & Atchison, 1995, 2003, 2007). GABAergic neurotransmission is more sensitive to MeHg neurotoxicity than glutamatergic because inhibitory synaptic transmission is blocked faster (Yuan & Atchison, 1995, 1997). Furthermore, GABAergic synaptic transmission is blocked faster in CGCs than in Purkinje

cells (Yuan & Atchison, 2003). MeHg directly interacts with the α 1 and α 6- containing $GABA_AR$ in oocytes (Tsai, Yuan, Hajela, Philips, & Atchison, 2017). Administration of MeHg *in vivo* causes cell death of GABA-containing neurons in the visual cortex, cerebral cortex and forebrain (J. O'Kusky, 1985; J. R. O'Kusky & McGeer, 1985). Furthermore, MeHg boosts BZs to bind to the $GABA_AR$ in the cerebellum and cerebral cortex (Concas et al., 1983; Corda et al., 1981; Fonfria, Rodriguez-Farre, & Sunol, 2001). Together, these findings suggest that the relative sensitivity of $GABA_ARs$ to MeHg plays a role during MeHg-mediated neurotoxicity. Preferential block of $GABA_ARs$ by MeHg would cause hyperexcitability leading to subsequent increases of $[Ca^{2+}]_i$.

GlyRs open to Cl^- with activation from glycine. Glycine is an inhibitory neurotransmitter predominantly found in the brainstem and spinal cord (Olsen, DeLorey, Gordey, & Kang, 1999; Pycock & Kerwin, 1981). However, they are also localized in the cerebral cortex and hippocampus (Bristow, Bowery, & Woodruff, 1986). The expression of GlyRs at the brainstem and spinal cord is different from the brain. GlyRs at the brainstem and spinal cord express the α 1 subunit, which it is very sensitive to strychnine binding (Becker, Hoch, & Betz, 1988; Bristow et al., 1986). GlyRs in the brain express the α 2 subunit which has low affinity for strychnine binding (Becker et al., 1988; Bristow et al., 1986). GlyRs are homo- and heteropentameric receptors. The stoichiometry of the heteromeric GlyRs consists of α: 1-4 and β: 1, with a ratio of 3:2 (Durisic et al., 2012; Lynch, 2004). The β subunit colocalizes with gephyrin. Gephyrin is an intracellular protein necessary for the anchoring of GlyRs to the membrane. Thus, gephyrin is used to identify the synaptic localization of the GlyRs (Kirsch, Wolters, Triller, & Betz, 1993; Meyer, Kirsch, Betz, & Langosch, 1995). GlyRs on MNs in the mature spinal cord express α 1 (Q. Chang & Martin, 2011; Dutertre, Becker, & Betz, 2012). The antagonist for the GlyR is strychnine. This competitive

antagonist is an alkaloid derived from the tree Strychnos nux-vomica. Actions of strychnine mimic rigidity and seizure. Electrophysiological studies have demonstrated that spinal MNs hyperpolarize in response to strychnine treatment (Curtis, Hosli, & Johnston, 1967; Werman, Davidoff, & Aprison, 1967). Effects of MeHg on glycinergic neurotransmission is less known compared to other LGICs. A study from our laboratory demonstrated that GlyRs in hippocampal CA1 do not participate of MeHg-induced increase of population spikes amplitude (Yuan & Atchison, 1997).

Intracellular Ca^{2+} stores

Intracellular stores dynamically participate in the homeostasis of $[Ca^{2+}]_i$ and generate cytosolic Ca^{2+} signals that potentiate neuronal activity. The two Ca^{2+} stores that contribute to regulation of $[Ca^{2+}]_i$ in the cytoplasm are the mitochondria and the SER. The mitochondria is responsible for the dynamic process of Ca^{2+} homeostasis, storage, regulation and buffering of free $Ca^{2+}{}_i$ ions. This organelle regulates the physiological Ca^{2+} signaling that occurs in response to different stimulation and signaling pathways (Gunter & Gunter, 1994). At resting membrane potentials, the mitochondria is a high-capacity but low-affinity Ca^{2+} store (Somlyo, Bond, & Somlyo, 1985). Thus, for the mitochondria to induce Ca^{2+} uptake it requires a strong driving force. External stimuli such as neurotransmitter release causes the mitochondria to serve as a Ca^{2+} store (Rizzuto, Brini, Murgia, & Pozzan, 1993; Rizzuto, De Stefani, Raffaello, & Mammucari, 2012). Ca^{2+} enters the mitochondria via the inner mitochondrial membrane receptor, the Ca^{2+} uniporter. This uniporter allows Ca^{2+} to move in favor of the electrochemical gradient from the cytosol into the mitochondrial lumen (Gunter & Gunter, 1994). Thus, this is an energetically favorable process because the inner mitochondrial membrane has a negative potential of approximately 140-180 mV.

Inside the mitochondria, Ca^{2+} stimulates synthesis of adenosine 5'- triphosphate (ATP) (Tarasov et al., 2013) because the proton gradient in the mitochondrial internal membrane drives synthesis of ATP (Lehninger, Nelson, & Cox, 2005). Release of Ca^{2+} from the mitochondria triggers the release of neurotransmitters (Rizzuto, 2003; Yang, He, Russell, & Lu, 2003). Furthermore, release of Ca^{2+} from the mitochondria, but not the SER, contributes to spontaneous release of neurotransmitter at the NMJ (Levesque & Atchison, 1988). Mitochondrial Ca^{2+} efflux is controlled by the reversal of the uniporter, the Na^{+}/Ca^{2+} exchanger (Simpson & Russell, 1998) and the opening of the mitochondrial permeability transition pore (mPTP) (Gunter & Gunter, 1994). The mPTP is a non-selective pore across the inner mitochondrial membrane. This pore opens in response to stress signals such as high mitochondrial Ca^{2+}, oxidative stress, depletion of ATP (Bernardi, Scorrano, Colonna, Petronilli, & Di Lisa, 1999; Dubinsky & Rothman, 1991). As a result, the proton gradient in the inner mitochondrial membrane dissipates and the synthesis of ATP is uncoupled (Hillered, Muchiri, Nordenbrand, & Ernster, 1983). These reactions cause the mitochondria to depolarize (White & Reynolds, 1996). Thus, depolarization of the mitochondrial membrane decreases influx of Ca^{2+} and decreases production of ATP. Activation of the mPTP increases cytosolic Ca^{2+} and correlates to mechanisms of Glu-mediated excitotoxicity and subsequent cell death (Bernardi & Petronilli, 1996; Ichas & Mazat, 1998; Lemasters et al., 1998; Schinder, Olson, Spitzer, & Montal, 1996).

MeHg releases $^{45}Ca^{2+}$ from mitochondria while simultaneously preventing mitochondrial Ca^{2+} uptake (Levesque & Atchison, 1991). MeHg release in mitochondrial Ca^{2+} increases $[Ca^{2+}]_i$, which it is delayed by treatment with cyclosporin A in CGCs (Limke & Atchison, 2002; Limke, Otero-Montañez, & Atchison, 2003). Treatment with ruthenium red, to block the mitochondrial Ca^{2+}

uptake, partially suppresses the MeHg-induced increase in the frequency of mEPP (Levesque & Atchison, 1987). MeHg opens the mPTP in human monocytes (InSug, Datar, Koch, Shapiro, & Shenker, 1997) and in lymphocyte cells (Shenker, Guo, & Shapiro, 2000). MeHg-induced release of ACh and norepinephrine depend on the efflux of Ca^{2+} from the mitochondria (Gasso, Sunol, Sanfeliu, Rodriguez-Farre, & Cristofol, 2000; Levesque & Atchison, 1988). Inhibition of the mPTP with bcl-2 protects against MeHg-induced cell death (T. A. Sarafian, Vartavarian, Kane, Bredesen, & Verity, 1994). MeHg exposure increase the generation of ROS, decreases the mitochondrial membrane potential and increases levels of cytochrome-c in CGCs (Bellum, Bawa, Thuett, Stoica, & Abbott, 2007; T. Sarafian & Verity, 1991). Experiments with carbonyl cyanide m-chlorophenyl hydrazine (CCCP) to uncouple the mitochondrial oxidative phosphorylation, and oligomycin to inhibit the mitochondrial ATP synthase, demonstrate that the $Ca^{2+}{}_i$ that enters the mitochondria originates from the SER (Limke & Atchison, 2002). Thus, MeHg releases Ca^{2+} from the mitochondria which then contributes to mechanisms of hyperexcitability and cell death. Other cytosolic Ca^{2+} stores participate during the release of neurotransmitter by MeHg.

The SER is an intracellular Ca^{2+} compartment present in all types of neurons. It buffers the excess of cytosolic Ca^{2+} through the Ca^{2+}-ATPase. Contrary to the mitochondria, the SER is a high-affinity, low-capacity pool (Somlyo et al., 1985). The SER has two main Ca^{2+} pools: ryanodine and IP3. The SER releases Ca^{2+} to the cytosol via ryanodine and IP3 receptors (Berridge, 1998). Stimulation of metabotropic receptors activate phospholipase-c (PLC). PLC hydrolyzes phosphatidylinositol biphosphate (PIP2) producing IP3, which then binds to the IP3 receptor. The SER is able to regulate $Ca^{2+}{}_i$ homeostasis by accumulating, storing and releasing Ca^{2+} ions. Ryanodine and IP3 receptors are involved in Ca^{2+}-induced Ca^{2+}-release mechanisms

(Bezprozvanny, Watras, & Ehrlich, 1991; Simpson, Nahorski, & Challiss, 1996). Ca^{2+} release from IP3 triggers Ca^{2+} release from the ryanodine receptors. Thus, an increase in $Ca^{2+}{}_i$ activates these receptors and further increases $[Ca^{2+}]_i$ (Irving, Collingridge, & Schofield, 1992). Following a transient increase in $Ca^{2+}{}_i$ the restoration of Ca^{2+} homeostasis depends on electrogenic activities. The SER is able to buffer Ca^{2+} through the sarcoendoplasmic reticulum ATPase (SERCA) Ca^{2+} pump. Also, this pump serves as a sensor of how much $[Ca^{2+}]_i$ is inside the SER. Hence, an increase in SER-Ca^{2+} will inhibit functioning of the SERCA pump. The SERCA refills the ryanodine and IP3 Ca^{2+} pools. Thapsigargin (THP) is a pharmacological drug that inhibits Ca^{2+} uptake and the accumulation of Ca^{2+} in the SER by selectively blocking the SERCA pump. THP causes a slow release of Ca^{2+} within neurons. Thus, it prolongs the depolarization induced by transient increases in $[Ca^{2+}]_i$. In this way, THP depletes the SER (Thastrup, Cullen, Drobak, Hanley, & Dawson, 1990). Thiol groups in the SERCA pump (Abramson, Trimm, Weden, & Salama, 1983; Chiu, Mouring, & Haynes, 1983) could interact with MeHg and facilitate Ca^{2+} release from the SER (Limke, Heidemann, et al., 2004). Regulation of $Ca^{2+}{}_i$ is important because it precedes neurotransmitter release and regulates synaptic plasticity.

MeHg stimulates binding of IP3 to the IP3 receptor, suggesting a direct interaction between MeHg and the receptor (Chetty, Rajanna, Hall, Yallapragada, & Rajanna, 1996). MeHg exposure results in a two-fold increase of IP3 receptors in CGCs (T. A. Sarafian, 1993). Moreover, desensitization of IP3 receptor with bethanechol, prior to MeHg exposure, delays MeHg-mediated increase in $[Ca^{2+}]_i$ suggesting that MeHg upregulates IP3 receptors (Limke, Bearss, et al., 2004). Depletion of the IP3-Ca^{2+} pool with the IP3 receptor agonists, bradykinin, reduces MeHg-induced increase in $[Ca^{2+}]_i$ (Hare & Atchison, 1995). Moreover, blocking the IP3 receptor with heparin blocks MeHg-

induced Ca^{2+} release from the SER (Tan, Tang, Castoldi, Manzo, & Costa, 1993). THP partially reduces the MeHg-induced increase in $[Ca^{2+}]_i$ in NG108-15 cells (Hare & Atchison, 1995). MeHg-mediated Ca^{2+} release from the SER is buffered by the mitochondria in CGCs (Limke & Atchison, 2002). However, in NG108-15 cells MeHg-mediated Ca^{2+} release is primarily from the SER (Hare & Atchison, 1995).Together, disruption of the SER by MeHg contributes to cell death via disruption of mitochondrial functions.

Mechanisms of cell death

Prolonged increase in $[Ca^{2+}]_i$ is associated with the activation of mechanisms of cell death (Choi, 1988; Dubinsky, 1993). Uncontrolled Ca^{2+} release from the mitochondria and the SER causes cell death (Kroemer, Petit, Zamzami, Vayssiere, & Mignotte, 1995; Wei, Wei, Bredesen, & Perry, 1998). Loss in the mitochondrial ability to buffer Ca^{2+} results in cell death via activation of cytochrome-c-dependent mechanisms (Bernardi et al., 1999). Cell death via disturbances in Ca^{2+} homeostasis is a common phenomenon in neurodegenerative diseases, including ALS (Mattson, 2000; Wojda, Salinska, & Kuznicki, 2008; Zundorf & Reiser, 2011). Furthermore, disturbances in Ca^{2+} homeostasis mediate degenerations of MNs in ALS (Shaw & Eggett, 2000).

Ca^{2+}-mediated excitotoxicity activates apoptotic and necrotic signaling (Ichas & Mazat, 1998; Kruman & Mattson, 1999; Lemasters et al., 1998; Mattson & Chan, 2003). Apoptosis is characterized by cell shrinkage, chromatin aggregation, plasma membrane blebbing, DNA condensation, loss of ATP maintenance and activation of caspases (Kroemer et al., 1995). Necrosis is characterized by cellular swelling, lysis, loss of cell membrane integrity and depletion of ATP. Nonetheless, both death pathways share similar mechanisms such as elevation in $[Ca^{2+}]_i$ and

damage to the mitochondria (Kruman & Mattson, 1999). MeHg toxicity causes apoptosis and necrosis depending on the duration and concentration of the exposure to MeHg (Miura & Imura, 1987). Low MeHg (0.1 -1 μM) concentrations and *in vivo* exposure is associated with apoptosis (Kunimoto, 1994; Nagashima et al., 1996). High MeHg (5 – 10 μM) concentrations is associated with necrosis (Castoldi, Barni, Turin, Gandini, & Manzo, 2000). However, within 1 hr of MeHg (1 μM) exposure both types of cell death were reported in CGCs (Castoldi et al., 2000).

Increases in $[Ca^{2+}]_i$ mediated by MeHg causes cell death in both primary and immortalized cell lines (Edwards et al., 2005; Hare et al., 1993; Marty & Atchison, 1998). Specifically, increases in $[Ca^{2+}]_i$ occur in a time-and-concentration-dependent manner following exposure to MeHg *in vitro* (Hare et al., 1993; Marty & Atchison, 1997; Ramanathan & Atchison, 2011), *in situ* (Yuan & Atchison, 2007, 2016) and *in vivo* (Johnson et al., 2011). MeHg damages the neurofilaments in the cell membrane in carcinoma-derived neurons (Graff, Falconer, Brown, & Reuhl, 1997). However, mechanisms underlying MeHg-induced cell death are not yet completely understood. Treatment with specific antagonists of VGCCs protects against MeHg-induced cell death *in vitro* and *in vivo* models(Marty & Atchison, 1998; Sakamoto et al., 1996). Thus, block of VGCCs delay the MeHg-mediated increase in $[Ca^{2+}]_i$. This unmasks the involvement of VGCCs during MeHg-mediated alterations in Ca^{2+} homeostasis. Thus, disruptions in the regulation of $Ca^{2+}{}_i$ plays an important role in MeHg-induced cell death. Inhibition of mAChRs with atropine and downregulation of mAChRs with bethanechol protects against MeHg-induced cell death in CGCs (Limke, Bearss, et al., 2004). Thus, the participation of LGICs during MeHg-mediated increase $[Ca^{2+}]_i$ has been identified. Also, inhibition of the mPTP with cyclosporin-A protects against MeHg-induced cell death (Limke & Atchison, 2002). Buffering $Ca^{2+}{}_i$ with BAPTA provides protection against MeHg-induced cell

death at 3.5 but not 24.5 hr post-MeHg exposure (Marty & Atchison, 1998). Antioxidant treatment with lycopene and vitamin E protects from MeHg-induced cytotoxicity (Qu et al., 2013; T. Sarafian & Verity, 1991). Together, these experiments showcase the pivotal role of disruptions in Ca^{2+}_i mechanisms during MeHg-mediated cell death.

The spinal cord

Organization of the motor system

The brain and spinal cord communicate with each other through ascending and descending nerve pathways. Motor output originates in the premotor and primary motor cortices. The corticospinal tract connects the upper MNs that originate in the cortex to lower MNs in the spinal cord (Welniarz, Dusart, & Roze, 2017). Specifically, the MNs that descend from the primary motor cortex, through the lateral corticospinal pathway, control voluntary movement. The MNs that descend from the primary motor cortex through the ventromedial corticospinal pathway control posture and locomotion. The spinal column is divided in four regions and subdivided in levels: cervical, thoracic, lumbar and sacral. The spinal cord has 31 pairs of nerves and 5 of these nerves are in the lumbar region. A transverse section of the spinal cord displays the gray and white matter. The gray matter is comprised of neuronal cells bodies, and glial cells. The white matter is comprised of longitudinal axons and glial cells. The gray matter is divided into different laminae depending on the basis of cytoarchitecture (Waxenbaum & Futterman, 2019). The nuclei of lower MNs are located in the ventral horn. Specifically, MNs are located in the lamina IX, which includes laminae VII and VIII.

Motor neurons

The main type of MNs in the spinal cord is the α subtype. The classification of MNs depend on the muscle fiber that they innervate (Kanning et al., 2010). The αMNs are the biggest (diameter > 30 μm) cells in the ventral horn (Wootz et al., 2013). Spinal αMNs release ACh from their axon terminal causing the postsynaptic cell or sarcolemma to depolarize and initiate muscle contraction. Thus, αMNs innervate extrafusal muscle fibers, which are responsible for the generation of tension and muscle contraction (Burke, Levine, Tsairis, & Zajac, 1973). Dorsal root ganglion cells, upper MNs and interneurons in the spinal cord synapse αMNs.

Renshaw area

The Renshaw area is located in the lamina VII of the lumbar ventral horn. The lumbar region innervates the hindlimb muscles. (Harrison et al., 2013; Rigaud et al., 2008). In detail, αMNs have an axon collateral that synapses on and excites RCs, which in turn inhibit the same αMNs, ultimately modulating their signaling. This negative-feedback mechanism is known as recurrent inhibition (Eccles, Fatt, & Koketsu, 1954; Renshaw, 1946). Thus, RCs control locomotor activity by communicating with αMNs, Ia interneurons and nearby RCs. ACh, GABA and glycine are the principal neurotransmitters that modulate recurrent inhibition (Dourado & Sargent, 2002; Geiman, Zheng, Fritschy, & Alvarez, 2002; Jonas, Bischofberger, & Sandkuhler, 1998; Schneider & Fyffe, 1992). RCs cells receive synaptic inputs from sensory neurons, αMNs and interneurons. Activation of RCs by αMNs causes a high-frequency discharge in the co-release of GABA and glycine (Geiman et al., 2002; Gonzalez-Forero & Alvarez, 2005).

RCs are the only spinal neuron that express gephyrin clusters (Alvarez & Fyffe, 2007). Gephyrin is a postsynaptic scaffolding protein in glycine receptors (GlyRs) (Kirsch & Betz, 1993). This observation has been confirmed in all studied mammalian species (Alvarez & Fyffe, 2007). Also, RCs express high levels of calbindin proteins in rodents and primates (Arvidsson et al., 1992; Carr, Alvarez, Leman, & Fyffe, 1998; Geiman, Knox, & Alvarez, 2000). The development of gephyrin clusters and calbindin reaches plateau by postnatal day (PND) 25 (Geiman et al., 2000). Thus, calbindin immunoreactivity, expression of gephyrin and the anatomical location of the Renshaw area are the criteria used to identify adult RCs. These parameters elucidated that the mean soma diameter of RCs in the adult cat and rat is 20 – 25 μm in size (Fyffe, 1990; Geiman et al., 2000) or less (Wootz et al., 2013). The abundance of RCs is approximately 750 cells in the adult cat (Carr et al., 1998). The ratio of RCs to αMN is 1:5 (Alvarez & Fyffe, 2007). RCs express α 2- and α 4-containing nAChRs (Dourado & Sargent, 2002; Ishii, Wong, & Sumikawa, 2005), α 3- and α 5-containing $GABA_A$Rs (Geiman et al., 2002) and α 1-containing GlyRs (Alvarez & Fyffe, 2007; Geiman et al., 2002; Gonzalez-Forero & Alvarez, 2005). Degeneration of RCs causes rigidity, spasticity and tremors (Alvarez & Fyffe, 2007). A decrease in the recurrent inhibition at the Renshaw area has been reported in ALS patients. Particularly, αMNs degenerate during the early presymptomatic stages of ALS disease while RCs are spared (Wootz et al., 2013). Thus, disruptions in this synaptic circuit occur during late presymptomatic stages of disease via degeneration of αMNs.

Objectives and rationale

Hypothesis

Recurrent inhibition in the Renshaw area controls motor output. An unfavorable change in this negative feedback would influence neurotransmission toward more excitation or less inhibition (Zanette et al., 2002; Ziemann et al., 1997). Furthermore, a reduction in recurrent inhibition underlies the enhanced excitability observed in pyramidal neurons of the motor cortex (Nieto-Gonzalez et al., 2011). Thus, a disruption by MeHg in the mechanism that regulates recurrent inhibition via Ca^{2+}-dependent mechanisms would enhance the susceptibility of the Renshaw Area to degenerate.

Previous studies have demonstrated effects of neurotoxicity mediated by MeHg. Briefly, MeHg disrupts cholinergic transmission in the NMJ (Atchison, 1986; Atchison, Joshi, & Thornburg, 1986; Atchison & Narahashi, 1982; Eldefrawi et al., 1977; Juang, 1976b). MeHg blocks both excitatory and inhibitory neurotransmission in CA1 neurons of hippocampal slices (Yuan & Atchison, 1993, 1995, 1997). Furthermore, the inhibitory neurotransmission is more susceptible to the effects of MeHg than excitatory neurotransmission (Yuan & Atchison, 1995). This is important because MeHg-mediated dysregulation of the inhibitory system precedes disruption of Ca^{2+} homeostasis (Yuan & Atchison, 2016). MeHg, *in vitro* and *in vivo*, increase $[Ca^{2+}]_i$ in MNs (Johnson et al., 2011; Ramanathan & Atchison, 2011). Also, MeHg accumulates $_{in}$ MNs of the ventral horn in rodents (Moller-Madsen, 1991; Pamphlett & Waley, 1996) and degenerates the MNs associated with hindlimb function (M. Su, Wakabayashi, Kakita, Ikuta, & Takahashi, 1998). Additionally, intracellular Ca^{2+} stores participate of MeHg-mediated neurotoxicity (Hare & Atchison, 1995; Levesque & Atchison, 1991; Limke & Atchison, 2002; Limke, Bearss, et al.,

2004). Furthermore, studies have shown a direct correlation between Ca^{2+} dysregulation and activation of cell death pathways (Edwards et al., 2005; Marty & Atchison, 1998).

Ca^{2+} dysregulation induced by MeHg and subsequent cell death through nAChRs has not been characterized. The sensitivity of the Renshaw area during MeHg exposure has not been described. The sensitivity of glycinergic neurotransmission following MeHg exposure has never been studied in the spinal cord. Thus, this research study addresses these gaps in our knowledge. The purpose of this dissertation is to determine whether known targets of MeHg neurotoxicity contribute to dysfunction in cells that degenerate in ALS disease. The aim of my research is to test for the central hypothesis that LGICs and internal Ca^{2+} stores participate of MeHg-mediated increase in $[Ca^{2+}]_i$ leading to degeneration of the Renshaw area. Specifically, I examine the role of nAChRs, $GABA_AR$, GlyR, and intracellular Ca^{2+} stores during MeHg-mediated increase in $[Ca^{2+}]_i$ and cell death. The effects of acute MeHg exposure on Ca^{2+} dysregulation was assessed in three different studies.

Aims

The first study, presented in Chapter 2, aims to determine whether *in vitro* MeHg-induced Ca^{2+} dysregulation and subsequent cell death is prevented or ameliorated using antagonists specific for the heteromeric and homomeric stoichiometry of the nAChR in differentiated PC12 cells.

The second study, presented in Chapter 3, aims to determine for the first time the sensitivity of the Renshaw area to MeHg neurotoxicity. Also, to determine whether MeHg-induced Ca^{2+}

dysregulation and subsequent cell death is prevented or ameliorated with specific antagonists of LGICs in the Renshaw area.

The third study, presented in Chapter 4, aims to determine if MeHg-mediated increase in $[Ca^{2+}]_i$ is due to contributions from the mitochondria and SER, which may lead to cytotoxicity in the Renshaw area. This study is the first to determine the participation of intracellular Ca^{2+} stores during MeHg-mediated neurotoxicity in the Renshaw area.

Model systems

Comparison of an *in vitro* and *in situ* model

An *in vitro* and *in situ* approach was performed in order to characterize the neurotoxic effects caused by MeHg. Experiments were first performed in conditions *in vitro*. This allows for an in-depth exploration of the actions of MeHg. The *in vitro* system characterizes the mechanisms underlying MeHg toxicity without the interactions of different types of cells within the area. Thus, it simplifies the biologic system. Furthermore it excludes glia cells, which can interfere with MeHg neurotoxicity (Ni, Li, Rocha, Farina, & Aschner, 2012). The *in vitro* findings were adapted to a model *in situ*. The *in situ* environment takes in consideration neurons in their natural setting. Furthermore, it excludes mechanisms of pharmacokinetics. A limitation of using slices is that when cutting the tissue, the cells that form the border of the slice get destroyed, as opposed to cell culture or a study *in vivo*. Hence, this leads to progressive degeneration of the tissue (Kasischke, Buchner, Ludolph, & Riepe, 2001). However, by considering the correct parameters for slice culture such as the right control of temperatures and the precise *osmolarity* of the buffer solutions reliefs the tissue from stress.

Experiments in this dissertation consist of an acute exposure to MeHg. A chronic exposure results in direct, as well as, long-term neurotoxicity. On the contrary, an examination of the acute exposure identifies the initiating effects of MeHg neurotoxicity. Thus, an acute exposure to MeHg represents the first crucial steps in determining the chronic effects of MeHg neurotoxicity.

Pheochromocytoma 12 (PC12) cells

The PC12 cell model is an immortalized cell line derived from a rat catecholamine-secreting tumor of the adrenal medulla (Greene & Tischler, 1976). PC12 cells release dopamine, norepinephrine and ACh (Shafer & Atchison, 1991b). These cells express Na^+ and K^+ channels, as well as, VGCCs (Shafer & Atchison, 1991a) and G-protein couple receptors (Shafer & Atchison, 1991b). Additionally, the expression of second messengers, such as PKC (K. M. Harris, Kongsamut, & Miller, 1986) and cAMP (Rabe, Schneider, & McGee, 1982) has been described. Also, PC12 cells contain intracellular Ca^{2+} pools (Fasolato et al., 1991). Undifferentiated PC12 cells resemble noradrenergic adrenal chromaffin cells (Greene & Tischler, 1976). Upon differentiation with NGF, cell proliferation ceases and the PC12 cells transform into sympathetic neuron-like cells in function and morphology (Chamley, Mark, Campbell, & Burnstock, 1972; Greene & Tischler, 1976; Mains & Patterson, 1973; Shafer & Atchison, 1991b). Differentiated PC12 cells express nAChRs and mAChRs, they synthetize ACh in small vesicles and release ACh in a Ca^{2+}-dependent manner (Greene & Rein, 1977). Differentiated PC12 cells have a nicotinic phenotype because exposure to an organosulfur derivative reduced the evoked vesicular ACh release without affecting the content of ACh (Ireland, Yan, Nelson, & Atchison, 1995). PC12 cells do not express GluRs (Shafer & Atchison, 1991b). Previous studies have demonstrated the participation of GluRs during MeHg-induced neurotoxicity (Ramanathan & Atchison, 2011). Hence, this cell line eliminates the

glutamatergic contribution to MeHg-induced toxicity. Together, differentiated PC12 cells provide a unique opportunity to investigate the involvement of neuronal-like heteromeric and homomeric nAChRs during MeHg-induced toxicity.

Lumbar slice

All animal procedures are in accordance with National Institute of Health (Aberg et al.) guidelines for experimental animal use and were approved by the Michigan State University (MSU) Institutional Animal Care and Use Committee (IACUC). C57BL6J mice were obtained from Jackson Laboratories. Briefly, following anesthesia (carbon dioxide) mice (either sex) were decapitated, the spinal cord was removed, and the lumbar region was dissected. The completion of this process was completed in 10 minutes (min) or less, to maintain the viability of the cells. Although C57BL6J female mice have a faster whole-body clearance for MeHg than males, both genders accumulate the same amount of MeHg in their brains. Furthermore, the levels of MeHg in the brain were within the range found in a healthy adult human (10 - 100 ng/g) (Bjorklund et al., 2007; Garcia, Ortega, Domingo, & Corbella, 2001). The use of a mouse to determine the effects of MeHg neurotoxicity is more appropriate than a rat model. Mice have a similar blood to brain ratio compared to humans (Bjorklund et al., 2007; B. Weiss et al., 2005).

Studies on the neurotoxic effects of MeHg have concluded that the CGC is among the first cell type to degenerate following exposure to MeHg. CGCs express the most mAChRs than any other cell in the cerebellum in mice (Neustadt, Frostholm, & Rotter, 1988). The sensitivity of CGCs to MeHg exposure *in vivo* have been demonstrated in humans and rats (Hunter & Russell, 1954; Leyshon-Sorland et al., 1994). In agreement, experiments in CGCs *in vitro* report the heightened

sensitivity of CGCs (Edwards et al., 2005; Marty & Atchison, 1998). This is important because recent experiments in primary cultures of MNs isolated from the spinal cord demonstrates that the sensitivity of MN to MeHg is in par with CGCs (Ramanathan & Atchison, 2011).

Techniques

Calcium imaging

Ca^{2+} homeostasis, transport and function within live cells is often studied with Ca^{2+}-specific fluorescent tools (Limke & Atchison, 2009). Changes in $[Ca^{2+}]_i$ in PC12 cells are measured using single cell microfluorimetry. Ratiometric Ca^{2+} measurements are performed using fura-2 acetoxymethyl ester (AM). Fura-2 is a high affinity intracellular Ca^{2+} fluorophore and does not interact with MeHg (Hare et al., 1993). The AM group makes fura-2 lipid soluble. Thus, it allows the fluorophore to easily cross the cell membrane. Pluronic acid 0.02% (w/v^{-1}) (Molecular Probes) is a vehicle used to increase the transport of fura-2 into the cell. Also, it prevents the AM group to diffuse away from the cytosol before endogenous esterase cleave it from fura-2. During cell loading, fura-2 AM enters the cytoplasm. Esterases cleave the AM group and fura-2 is trapped in the cytoplasm, where it binds to unbound, free Ca^{2+} ions.

Ratiometric differences in the wavelength for dual excitation are taken at 340 nm and 380 nm, ($F_{340/380}$). Fluorescence at 340 nm indicates the bound form of fura-2 to Ca^{2+}. Fluorescence at 380 nm indicates the unbound form of fura-2 to Ca^{2+}. Emission fluorescence is measured at 505 nm (Grynkiewicz, Poenie, & Tsien, 1985; Limke & Atchison, 2009). An increase in the $F_{340/380}$ ratio corresponds to an increase in $[Ca^{2+}]_i$. Binding of fura-2 to Ca^{2+} causes the unbound, free Ca^{2+} form to decrease (380 nm) while the amount of Ca^{2+} bound to fura-2 increases (340 nm). The ratiometric

($F_{340/380}$) difference between the bound and unbound states of fura-2 to Ca^{2+} ions takes in consideration and compensates for differences in the efficiency of cellular loading across the sample population (Grynkiewicz et al., 1985). The fura-2 ratio demonstrates how much of a reaction has moved towards spatial localization as an indication of increases in $[Ca^{2+}]_i$. changes in fura-2 fluorescence are an indirect measure of Ca^{2+} within the cytosol of the cell. Fura-2 maximum can be reached using the Ca^{2+} ionophore: A23187. The latter allows Ca^{2+} to enter the cell and maximize binding of fura-2 to Ca^{2+} ions. On the other hand, fura-2 minimum can be achieved using the anion egtazic acid (EGTA), to chelate extracellular Ca^{2+} ions.

The isobestic point is a wavelength independent of Ca^{2+} measured at 360 nm. At this wavelength fura-2 binds to non-Ca^{2+} cations. Fura-2 binds to Zn^{2+} because shares the commonality of being divalent cations like Ca^{2+}. Furthermore, MeHg induces release of Zn^{2+}, which affects the binding of fura-2 to Ca^{2+}. Thus, measurements of $[Ca^{2+}]_i$ skew (Denny et al., 1993). For this reason, the absolute amplitude quantification of the fura-2 fluorescence response was not determined Therefore, studies in this dissertation refer to relative changes in $[Ca^{2+}]_i$ rather than absolute and quantifiable changes in $[Ca^{2+}]_i$.

Changes in $[Ca^{2+}]_i$ in a slice tissue from the C57BL6J mouse are measured using confocal microscopy. Fluo-4 no wash (fluo-4 NW) with 2.5 mM probenecid is used to study increases in $[Ca^{2+}]_i$. Probenecid inhibits organic-anion transporters from extruding the fluorophore. Unlike fura-2, fluo-4 is not ratiometric. Fluo-4 is excited at 485 nm and emits fluorescence at 520 nm. An increase in fluo-4 fluorescence corresponds to an increase in $[Ca^{2+}]_i$. Confocal microscopy allows the visualization through the slice as opposed to only visualizing the cells in one plane when using

an inverted microscope. Thus, the length of time the microscope takes to scan through the entire slice is a limitation of this approach because it could photo bleach the tissue (Knight, Roberts, Lee, & Bader, 2003). Therefore, studies in this dissertation represent spatial changes in $[Ca^{2+}]_i$ at specific timepoints. While spatial changes elucidate what occurs to a general region, we did not monitor continuous changes in $[Ca^{2+}]_i$, as they were done in experiments with fura-2.

Measurement of cell viability

Cell viability was determined with the Viability/Cytotoxicity Assay (Molecular Probes Inc., OR, USA). The use of calcein AM and ethidium homodimer-1(EtHD-1) have been previously described (Marty & Atchison, 1998). Calcein AM labels viable cells in green while EtHD-1 labels dead cells in red (Papadopoulos et al., 1994). Calcein excites at 495 nm and emits fluorescence at 515 nm. EtHD-1 excites at 528 nm and emits fluorescence at 617 nm. Differentiated PC12 cells were incubated with calcein AM and EtHD-1 for 45 min to 1 hr. Examination of viability was conducted under a Nikon Eclipse fluorescence microscope. Viability changes in the lumbar slice isolated from a C57BL6J mouse were measured using calcein-AM and confocal microscopy. The methodology for measuring viability in tissue is the same as measuring changes in $[Ca^{2+}]_i$, except that fluo-4 AM was replaced by calcein AM. For all the experiments conducted in the presence of specific pharmacologic drugs, the antagonist was applied prior, as well as, during MeHg exposure.

CHAPTER TWO:

ROLE OF NICOTINIC ACETYLCHOLINE RECEPTORS IN METHYLMERCURY-INDUCED TOXICITY IN DIFFERENTIATED PC12 CELLS

Mónica Ríos-Cabanillas[1,2,3] and William D. Atchison[1,2,3]

[1]Comparative Medicine and Integrative Biology Program
[2]Department of Pharmacology and Toxicology
[3]Institute for Integrative Toxicology

Michigan State University
East Lansing, MI, 48824

Abstract

Environmental exposure to methylmercury (MeHg) is a contemporary public health concern. MeHg exposure induces a characteristic biphasic internal calcium (Ca^{2+}_i) response and subsequent cytotoxicity in cells that is in part modulated by ligand-gated ion channels. This event has been studied in undifferentiated pheochromocytoma (PC12) cells, and here we provide the first study examining these events in PC12 cells differentiated to a neuron-like phenotype. We examined whether nicotinic acetylcholine receptors (nAChRs) participate in MeHg-induced Ca^{2+} dysregulation and cytotoxicity using a pharmacological approach, with fura-2 single-cell microfluorimetry to monitor $[Ca^{2+}]_i$ changes and cytotoxicity with a viability assay. Exposure to MeHg (1, 2, 5 μM) induced a kinetically distinct biphasic Ca^{2+}_i increase. The first phase being Ca^{2+} release from intracellular stores followed by a second phase dependent on extracellular Ca^{2+} influx. The time-to-onset of both phases was inversely proportional to MeHg concentrations. Administration of the hetero-pentameric nAChRs inhibitor, mecamylamine (MEC, 5 μM), but not the homo-pentameric inhibitor methyllycaconitine (MLA), significantly delayed fura-2 time-to-onset by 240 sec during phase 1 at 1 μM MeHg compared to control. Low external Ca^{2+} conditions with the Ca^{2+} chelator, egtazic acid (EGTA, 20 μM), in combination with MeHg, significantly delayed MeHg-induced $[Ca^{2+}]_i$ dysregulation at both phases. To determine whether MeHg-induced $[Ca^{2+}]_i$ elevations contribute to cell death, cytotoxicity was measured at immediate (1 hr) and delayed (24 hr) timepoints post-MeHg exposure. At 1 hr post-MeHg, cell viability significantly decreased 7% and 20% from the control values with 2 and 5 μM MeHg, respectively. EGTA during MeHg exposure protected against cell death. MeHg + MEC protected from MeHg-induced cytotoxicity at the immediate timepoint. Thus, specific involvement of heteromeric nAChRs are

implicated in MeHg-mediated increase in $[Ca^{2+}]_i$ and subsequent cytotoxicity in differentiated PC12 cells.

Key Words: Fura-2, Calcein-AM, Ethidium Homodimer-1 (EtHD-1), Toxicity, Intracellular Ca^{2+}

Introduction

Methylmercury (MeHg) is the most prevalent form of organic mercury and represents a current public health concern. Studies *in vivo* have shown that oral administration of 5-10 mg/kg/day MeHg to adult rats accumulates in spinal cord αMNs and causes their degeneration (Moller-Madsen, 1990, 1991; Mori, Tanji, & Wakabayashi, 2000; M. Su et al., 1998). Neuronal degeneration leads to severe pathological effects, via unknown mechanisms. MeHg disrupts calcium (Ca^{2+}) homeostasis and drives an uncontrolled and sustained increase in internal Ca^{2+} concentration ($[Ca^{2+}]_i$) in both primary and transformed cell lines (e.g. rat brain synaptosomes, NG108-15 neuroblastoma cells, cerebellar granule cells (CGCs) and motor neurons (MNs)) (Edwards et al., 2005; Hare et al., 1993; Kauppinen et al., 1989; Marty & Atchison, 1997; Ramanathan & Atchison, 2011; T. A. Sarafian, 1993). The MeHg-mediated biphasic $[Ca^{2+}]_i$ increase consists of two kinetically and temporally distinct phases: first, Ca^{2+} efflux from internal Ca^{2+} stores (phase 1) followed by external Ca^{2+} (Ca^{2+}_e) influx (phase 2) (Denny et al., 1993; Hare et al., 1993; Limke, Bearss, et al., 2004; Limke et al., 2003; Marty & Atchison, 1997; Ramanathan & Atchison, 2011). The mitochondria (Hare et al., 1993; Levesque & Atchison, 1991; Limke & Atchison, 2002) and the smooth endoplasmic reticulum (SER) (Hare & Atchison, 1995; Limke, Bearss, et al., 2004) have both been identified as contributors to increases in $[Ca^{2+}]_i$ during MeHg exposure.

Previous work demonstrates that treatment with voltage-gated calcium channel (VGCC) antagonists during MeHg exposure protects against MeHg-mediated increases in $[Ca^{2+}]_i$ in cerebellar granule cells (CGCs) (Marty & Atchison, 1997) and subsequent neurotoxicity (Marty & Atchison, 1998; Sakamoto et al., 1996). Furthermore, presence of the Ca^{2+}_i chelator, 1,2-Bis(2-

aminophenoxy)ethane-N,N,N′,N′-tetra acetic acid tetrakis (BAPTA), protects against Ca^{2+}-dependent cytotoxicity in CGCs (Marty & Atchison, 1998). Thus, MeHg-mediated Ca^{2+} dysregulation may play an important role in the etiology of MeHg-induced cell death.

Prolonged $[Ca^{2+}]_i$ increase is associated with activation of cell death mechanisms Specifically, inhibition of the mitochondrial permeability transition pore with cyclosporin-A, delays the onset of increased fura-2 fluorescence and protects against cell death in CGCs (Limke & Atchison, 2002). Atropine-mediated inhibition or bethanechol-mediated downregulation of muscarinic acetylcholine (ACh) receptors (mAChRs) delays increased fura-2 time-to-onset and protects against MeHg-induced cytotoxicity in CGCs (Limke, Bearss, et al., 2004). Thus, MeHg activates inositol-1,3,4-triphosphate (IP3) receptors through interaction with mAChRs causing Ca^{2+} release from the SER and reveals a cholinergic contribution to MeHg neurotoxicity (Limke, Heidemann, et al., 2004).

The pheochromocytoma (PC12) cell model is an immortalized cell line derived from a rat catecholamine-secreting tumor of the adrenal medulla (Greene & Tischler, 1976). Undifferentiated PC12 cells are sensitive to MeHg toxicity. Exposure to (0.5 - 5 μM) MeHg causes the characteristic biphasic $[Ca^{2+}]_i$ increase in a concentration- and time-dependent manner followed by cell death (Edwards 2004 dissertation). However, treatment with specific VGCC antagonists delays increased $[Ca^{2+}]_i$ and protects against MeHg toxicity (Edwards 2004 dissertation) (Marty & Atchison, 1998). The PC18 cell line is a subclone from PC12 cells that that does not express functional VGCCs (Hinkle & Osborne, 1994) and does not respond to differentiation by nerve growth factor (NGF) (Roskoski & Roskoski, 1989; Tank, Ham, & Curella, 1986). PC18 cells

remain responsive to MeHg exposure with increased fura-2 fluorescence during phase 1 and phase 2 (Edwards 2004 dissertation). Thus, despite the lack of VGCCs in PC18 cells, MeHg enters the cells, causes Ca^{2+}_i dysregulation and subsequent cell death through non-VGCC pathways (Edwards 2004 dissertation). Furthermore, there is a delay in the MeHg-mediated Ca^{2+}_i dysregulation in PC18 cells compared to undifferentiated PC12 cells. This suggests that MeHg could use membrane channels as a pore to reach the cytoplasm (Edwards 2004 dissertation). Similarly, in the VGCC non-expressing MN hybrid mouse cell line, NSC34, MeHg exposure causes an increase in the incidence of cell death, confirming that MeHg-induced effects are not exclusively dependent on VGCCs (Colón-Rodríguez 2018 dissertation). Therefore, other Ca^{2+} entry pathways are available in neuron-like cells.

PC12 cells contain intracellular Ca^{2+} pools (Fasolato et al., 1991). Upon differentiation with NGF, cell proliferation ceases and the cells transform into sympathetic neuron-like cells in function and morphology (Chamley et al., 1972; Greene & Tischler, 1976; Mains & Patterson, 1973; Shafer & Atchison, 1991b). Differentiated PC12 cells express cholinergic receptors, synthetize ACh in small vesicles and release ACh in a Ca^{2+}-dependent manner (Greene & Rein, 1977). Differentiated PC12 cells have a nicotinic phenotype because exposure to an organosulfur derivative reduced evoked vesicular ACh release without affecting ACh content (Ireland et al., 1995). Specifically, they express pentameric ligand-gated nicotinic ACh receptors (nAChRs) with a cysteine-loop, required for transduction of agonist binding into channel opening (Karlin et al., 1986; Sine & Engel, 2006). This determines the α-subunit type on their extracellular domain (Lukas et al., 1999). Differentiated PC12 cells develop heteromeric α4β2 (slow desensitization, mecamylamine (MEC)-sensitive) (Virginio, Giacometti, Aldegheri, Rimland, & Terstappen, 2002) and

homomeric α7 (fast desensitization, methyllycaconitine (MLA)-sensitive) (Blumenthal, Conroy, Romano, Kassner, & Berg, 1997; Gueorguiev, Zeman, Meyer, & Sabban, 2000; Zhang, Vijayaraghavan, & Berg, 1994) subunit compositions. The extent to which nAChRs contribute to Ca^{2+} permeability depends on the subunit-expression (Seguela et al., 1993). Also, nAChRs could potentially act as a portal for MeHg to enter the cytoplasm initiating Ca^{2+} efflux from intracellular Ca^{2+} pools (Atchison, 1986, 1987; Mirzoian & Luetje, 2002) (Edwards 2004 dissertation). These characteristics of differentiated PC12 cells provide a unique opportunity to investigate the involvement of cholinergic mechanisms in MeHg-induced toxicity.

The purpose of this study is to determine whether acute *in vitro* MeHg-induced Ca^{2+} dysregulation and subsequent cell death is prevented or ameliorated with MEC and/or MLA both nAChR inhibitors, in differentiated PC12 cells. We hypothesize that MeHg-mediates loss of $Ca^{2+}{}_i$ homeostasis through nAChR-dependent mechanisms and that presence of the heteromeric and homomeric nAChR antagonists, MEC and/or MLA, respectively, will delay MeHg-mediated $[Ca^{2+}]_i$ increase and subsequent cytotoxicity. Our findings indicate that heteromeric MEC-sensitive mechanisms, but not homomeric MLA-sensitive mechanisms, participate in MeHg-mediated increase in $[Ca^{2+}]_i$ and cell death in differentiated PC12 cells.

Materials and methods

Materials and experimental solutions

PC12 cells were obtained from American Type Culture Collection (ATCC) (Manassas, VA). Cell culture supplies including Roswell Park Memorial Institute (RPMI) medium, Antibiotic/Antimycin and Horse Serum were purchased from Gibco BRL (Invitrogen, Grand

Island, NY). Fura-2 acetoxymethyl ester (fura-2 AM) and the Live/Dead™ viability/cytotoxicity kit, for mammalian cells, both were purchased from Molecular Probes (Invitrogen, Eugene, OR). NGF was prepared in RPMI media to a stock solution concentration of 100 µg/mL and used on day of experiment at 0.2 µg/mL = 200 ng/mL final concentration. The hetero- and homomeric nAChR blockers, MEC (5 µM) and MLA (5 µM) were purchased from Sigma-Aldrich (St. Louis, MO). MeHg chloride was purchased from ICN Biochemicals Inc. (Aurora, OH). A 10 mM MeHg stock solution was prepared in double-distilled water and stored at 4°C.

Experimental solutions were prepared on the day of the experiment by diluting the MeHg stock solution at the desired working concentrations (1, 2, or 5 µM MeHg) in 4-(2-hydroxyethyl)piperazine-1-ethanesulfonic acid (HEPES)-buffered saline (HBS) solution, which contains (mM): 150 NaCl, 5.4 KCl, 1.8 CaCl2, 0.8 MgSO4, 20 D-glucose, and 20 4-(2-hydroxyethyl)piperazine-1-ethanesulfonic acid (HEPES) Sigma-Aldrich (St. Louis, MO), free acid (pH 7.3), in the absence or presence of drugs. The 40 mM K^+ solution contains the same components as HBS but with 40 mM K^+ and 115.4 mM NaCl. The low [Ca^{2+}] HBS solution used for the ethylene glycol-bis(*β*-aminoethyl ether)N,N,N',N'-tetra acetic acid (EGTA) experiments had the same constituents as HBS minus $CaCl_2$ and addition of 0.02 mM EGTA, purchased from Sigma-Aldrich (St. Louis, MO) (approximately final $[Ca^{2+}]_e$ = 60 nM) (Marty & Atchison, 1997). Disposable or MeHg-contaminated materials used during the preparation and experiment were discarded following the Michigan State University (MSU) Office of Radiation, Chemical, and Biological Safety (ORCBS) guidelines.

PC12 cell culture supplies

PC12 is a classic *in vitro* neuroendocrine clonal cell model derived from the rat adrenal medulla useful for studying disruption by MeHg. PC12 cells are thawed from a liquid nitrogen tank in RPMI media and in 10% dimethyl sulfoxide (DMSO) Sigma-Aldrich (St. Louis, MO). PC12 cells are then grown in RPMI medium supplemented with (v/v): 10% heat-inactivated horse serum, 2.5%, fetal bovine serum, and 1% penicillin-streptomycin (pH 7.3 with tris-(hydroxymethyl)-aminomethane (TRIS)) and cultured using established methods (Greene & Tischler, 1976). PC12 cells from passages 15-30 were cultured in either 25-cm^2 or 75-cm^2 T-flasks in a humidified chamber set at 37°C with 95% air - 5% CO_2. Cells were split every 3-4 days or when the flask is approximately 80-90% confluent. PC12 cells were treated with 50 ng/mL NGF and allowed 48 hr to mature and differentiate into sympathetic-like neurons before experiments.

Measurement of fura-2 fluorescence changes

To measure relative changes in $[Ca^{2+}]_i$, PC12 cultures were detached from the flasks with 0.25% (v/v) trypsin Sigma-Aldrich (St. Louis, MO) and seeded on 35-mm culture dishes coated with poly-D-lysine (PDL) Sigma-Aldrich (St. Louis, MO) at a density of 6 x 10^5 cells/mL. Cells were incubated with the ratio-metric fluorophore fura-2 AM (3 μM) and pluronic acid (3 μM) for 45 min at 37°C with 95% air - 5% CO_2, as previously described (Edwards et al., 2005; Hare et al., 1993; Limke, Bearss, et al., 2004; Marty & Atchison, 1997; Ramanathan & Atchison, 2011). Single-cell microfluorimetry images were obtained with a Diaphot microscope (Nikon, Tokyo, Japan) coupled to an IonOptix cation fluorescence imaging system (IonOptix, Milton, MA). Before the experiment began, multiple soma (5-9) within the same microscopic field were selected to simultaneously and continuously record their emitted fluorescence (505 nm) at excitation

wavelengths of 340 and 380 nm. At these wavelength relative changes in the amount of bound Ca^{2+} and unbound-free Ca^{2+}, respectively, can be detected. Changes in fura-2 fluorescence ratio (340/380 nm) indicate the approximate cytosolic amount of $[Ca^{2+}]_i$. MeHg does not interact with fura-2. Thus, changes in fura-2 fluorescence are the result of MeHg binding to cytosolic free Ca^{2+} (Hare et al., 1993). To examine whether $Ca^{2+}{}_e$ is involved during MeHg-induced elevation in fura-2 fluorescence ratio, experiments were done in the absence or presence of 20 μM EGTA. All experiments began with perfusion of HBS or EGTA-HBS to reach a stable baseline before 1, 2, or 5 μM MeHg perfusion. Only cells with Ca^{2+} buffering capacities following a 40 mM K^+ depolarizing solution during 2-4 min were considered viable for experiments (Edwards et al., 2005; Marty & Atchison, 1997; Ramanathan & Atchison, 2011). To identify the various Ca^{2+} entry pathways as possible targets contributing to Ca^{2+} influx following MeHg exposure, a pharmacologic approach was performed a different day from the control experiments. To examine whether nAChRs blockers could reduce MeHg-induced $[Ca^{2+}]_i$, the non-specific antagonist MEC or the specific α7 subunit antagonist MLA, both at [5 μM], were perfused 5 min prior to, as well as, during exposure to MeHg. This concentration was chosen based on the ability of each antagonist to block the 400 μM nicotine-mediated fura-2 fluorescence increase (results not shown). Because MeHg actions are irreversible only one treatment at a time was applied to differentiated PC12 cells. Perfusion with all buffers followed a 2 mL/min speed throughout the duration of experiment. An experiment was considered complete when fura-2 AM ratio reached plateau. MeHg exposure fixed as time = 0 sec, times-to-onset of phase 1 and phase 2 were measured manually and determined as the point at which fura-2 ratio irreversibly slowly increased over baseline and the point at which fura-2 ratio drastically rises above phase 1, respectively. The phase

1 and phase 2 time-to-onset was calculated for each viable cell in the same experimental field and the mean time-to-onset was determined for that field of cells.

Measurement of differentiated PC12 cell viability

Cell viability was measured using the commercial fluorimetric viability assay consisting of calcein AM and ethidium homodimer-1 (EtHD-1). Calcein AM stains green the cytoplasm of live cells while EtHD-1 stains red the DNA of compromised cells (Papadopoulos et al., 1994). Briefly, PC12 cells were incubated with calcein AM (0.1 μM) and EtHD-1 (0.5 μM) for 45 min at 37°C with 95% air - 5% CO_2, and examined under a Nikon Eclipse epifluorescence microscope as previously described (Limke & Atchison, 2002; Limke, Bearss, et al., 2004; Marty & Atchison, 1998). PC12 cells were plated in a 24-well plate at a density of 6 x 10^5 cells/mL and incubated for 48 hr with NGF treatment at 37°C. Next, RPMI complete media was replaced with HBS containing 0, 1, 2 or 5 μM MeHg for a 1 hr acute MeHg exposure at 37°C. MeHg time exposure paradigm was determined on the results from fura-2 microfluorimetry in which differentiated PC12 cells displayed the characteristic MeHg-induced biphasic $[Ca^{2+}]_i$ increase within 1 hr. Following acute MeHg exposure, cells were allowed to recover in RPMI complete media for 1 or 24 hr before assessing viability. Because MeHg disrupts microtubule stabilization and cell adhesion (Abe, Haga, & Kurokawa, 1975; Imura, Miura, Inokawa, & Nakada, 1980; Vogel, Margolis, & Mottet, 1985) gentle centrifugation (140 *g*, 3 min) was applied before HBS washes after MeHg exposure and prior to assay staining agents. To examine whether nAChRs blockers could delay MeHg-induced cell death, MEC and/or MLA, both at [5 μM] were used. MeHg exposure occurred either in the absence, presence or combination of the nAChR antagonists. A similar exposure paradigm was used for Ca^{2+}_e-free experiments, except that MeHg solutions were made in EGTA-HBS and

cells were incubated in medium containing EGTA (20 μM). Because MeHg actions are irreversible only one treatment at a time was applied to differentiated PC12 cells. Viability was calculated by averaging live and dead cells from 3 distinct regions in the same well and expressed as percentage of control cell viability. Thus, for each set of exposures, data were collected as triplicate measurements within the same well averaged from three distinct wells. The formula for percent viability is as follows:

$$\text{Percent viability} = \frac{(\text{total cells} - \text{dead cells})}{\text{total cells}}$$

Statistics

All experiments consisted of repeated measures, ($n \geq 3$). For fura-2 experiments, one *n* value represents the average response from 5-9 cells in the same microscopic field. For viability experiments, one *n* value represents the average response from 3 different regions in the same microscopic field. All values are expressed as ± standard error of the mean (SEM). To analyze among one or different groups a one-way or two-way analysis of variance, respectively will be made using GraphPad Prism® software (GraphPad Software Inc., San Diego, CA). A p*ost hoc* comparison such as Tukey's or Sidak's were used when significant differences between means were found (Steel & Torrie, 1960). Values are considered statistically significant at $p < 0.05$.

Results

Characteristics of in vitro acute MeHg-induced $Ca^{2+}{}_i$ dysregulation in differentiated PC12 cells

The characteristic MeHg-mediated $[Ca^{2+}]_i$ biphasic response has been observed in a plethora of cell lines, including mouse spinal cord MNs (Ramanathan & Atchison, 2011) and human derived MN-induced pluripotent stem cell model (Colón-Rodríguez 2018 dissertation). This biphasic response has also been observed in undifferentiated PC12 cells (Edwards 2004 dissertation) but has not been studied in differentiated PC12 cells. To identify if Ca^{2+} dysregulation occurs in differentiated PC12 cells we performed fura-2 microfluorimetry recordings. Acute MeHg exposure to differentiated PC12 cells caused the characteristic and kinetically-distinct biphasic $[Ca^{2+}]_i$ increase. This was determined by a rise in the intensity of fura-2 fluorescence. Figure 2.1 shows a representative tracing of fura-2 fluorescence ratio from a differentiated PC12 cell exposed to 5 μM MeHg. In the absence of MeHg, no change in fura-2 fluorescence intensity was observed until the KCl-induced depolarization. Ca^{2+} elevations during phase 1 have canonically been credited to Ca^{2+} release from internal stores while onset of phase 2 depends on $Ca^{2+}{}_e$ entry (Denny et al., 1993; Hare & Atchison, 1995; Limke & Atchison, 2002; Limke, Bearss, et al., 2004; Marty & Atchison, 1997). The biphasic Ca^{2+} response was observed during all MeHg (1, 2 and 5 μM) treatments in differentiated PC12 cells. There was a dose-dependent reduction in time to onset of phase 1 and phase 2 following exposure to MeHg (Fig 2.2). Thus, differentiated PC12 cells are susceptible to MeHg-mediated disruption of $[Ca^{2+}]_i$ in a biphasic manner.

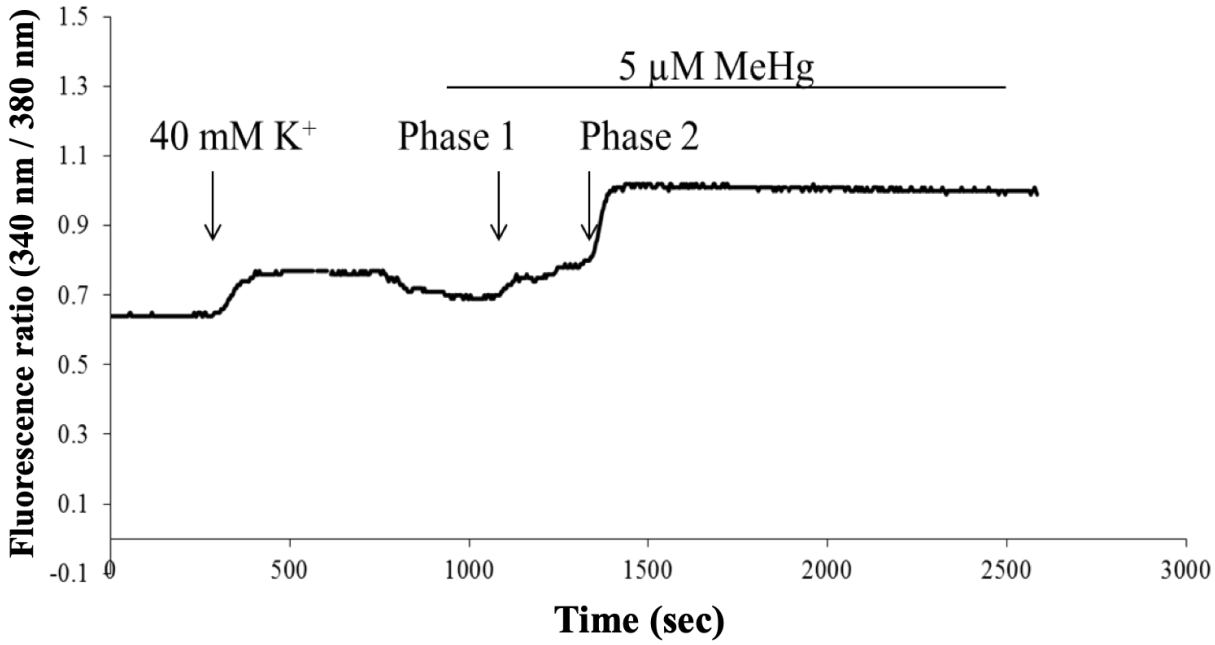

Figure 2.1. Representative tracing of changes in fura-2 fluorescence intensity in a differentiated PC12 cell during a continuous perfusion with 5 μM MeHg. All cells responded to a brief (2-4 min) 40 mM KCl-mediated transient depolarization followed by a return to baseline, demonstrating Ca^{2+}-buffering capacity upon K^+ cessation. A continuous MeHg exposure is depicted with a horizontal line. Onset of K^+-mediated depolarization, phase 1 and phase 2 is shown with vertical arrows. In all experiments the MeHg-induced biphasic fura-2 increase was observed.

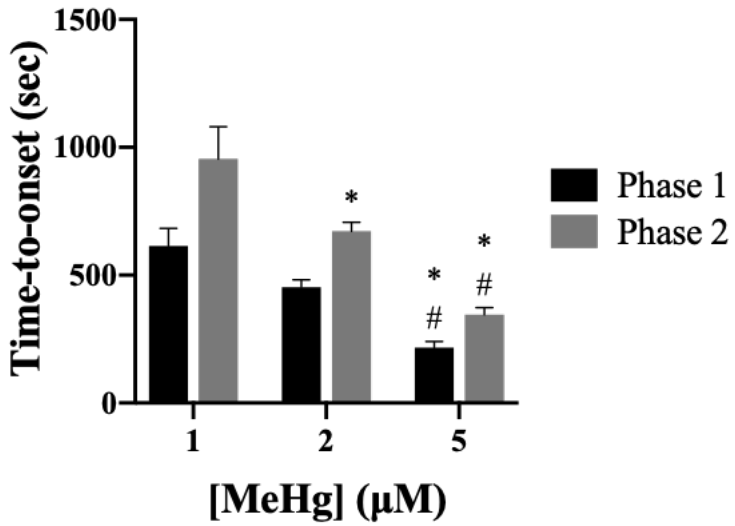

Figure 2.2. MeHg exposure reduces the time-to-onset of phase 1 and phase 2 in $[Ca^{2+}]_i$ elevations in differentiated PC12 cells in a concentration-dependent manner. There were significant differences both for the main effect of MeHg concentrations and time-to-onset. Phase 1 shows a significant difference in time-to-onset at 5 μM MeHg compared to 1 μM MeHg, denoted by the asterisk (*) and compared to 2 μM MeHg, denoted by pound (#). Phase 2 shows a significant difference in time-to-onset at 2 and 5 μM MeHg compared to 1 μM MeHg, denoted by asterisk (*). Phase 2 shows a significant difference in time-to-onset at 5 μM MeHg compared to 2 μM MeHg, denoted by pound (#). MeHg was associated with an inverse correlation between the MeHg concentration and the fura-2 time-to-onset in phase 1 and phase 2. Values are represented as mean ± SEM (n = 10) for 1, 2 and 5 μM MeHg. Each *n* represents the recording of three separate fura-2 fluorescence values from the soma of 5-9 differentiated PC12 cells per cover dish. Each experiment was replicated three times. Two-way analysis of variance followed by Sidak's post-hoc comparison was used. Statistical significance is considered at $p < 0.05$.

Contribution of Ca^{2+}_e to MeHg-mediated Ca^{2+}_i dysregulation in differentiated PC12 cells

To determine the role of extracellular Ca^{2+} during MeHg-induced biphasic alterations in Ca^{2+} homeostasis, Ca^{2+}_e was removed from the perfusion buffer. MeHg exposure occurred in Ca^{2+}_e-free buffer (60 nM). As a result, the fura-2 time-to-onset of phase 1 and phase 2 were significantly delayed compared to 1.8 mM Ca^{2+} during exposure to 5 μM MeHg (Fig 2.3). Presence of phase 2 during Ca^{2+}_e-free circumstances was surprising because previous studies from our laboratory indicate that Ca^{2+}_e is the primary constituent source of Ca^{2+} responsible for onset of phase 2 (Hare et al., 1993; Ramanathan & Atchison, 2011). However, presence of phase 2 during Ca^{2+}_e-free circumstances was also observed in human embryonic kidney (HEK) 293 cells (Hannon 2016 dissertation). Also, our results are the second to indicate a contribution of Ca^{2+}_e in phase 2 Ca^{2+}_i dysregulation during EGTA conditions (Hannon 2016 dissertation). These data suggest that other divalent cations could be contributing to changes in fura-2 fluorescence intensity.

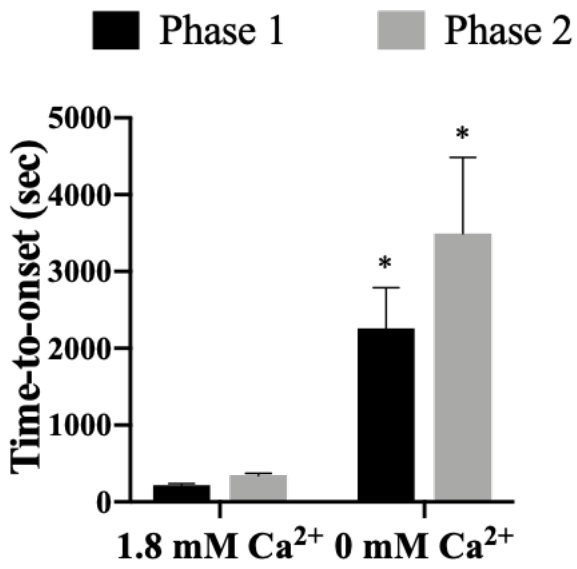

Figure 2.3. Comparative effects of Ca^{2+}_e on times-to-onset of MeHg-induced Ca^{2+}_i elevations in differentiated PC12 cells. Differentiated PC12 cells were perfused with MeHg in either standard HBS (1.8 mM Ca^{2+}_e) or Ca^{2+}-free solution (EGTA-HBS) while simultaneously monitoring changes in fura-2 fluorescence ratio. The time-to-onset of both phases during 5 μM MeHg treatment in the absence of Ca^{2+}_e was significantly delayed when compared to 1.8 mM Ca^{2+}_e treatment, denoted by the asterisk (*). Values are represented as mean ± SEM (n = 10) for 5 μM MeHg. Values are represented as mean ± SEM (n = 3) for 5 μM MeHg + EGTA. Each *n* represents the recording of fura-2 fluorescence value from the soma of 5-9 differentiated PC12 cells per cover dish. Each experiment was replicated three times. Two-way analysis of variance followed by Sidak's post-hoc comparison was used. Statistical significance is considered at $p < 0.05$.

Concentration-dependent death of differentiated PC12 cells occurs after acute MeHg exposure

MeHg-induced cytotoxicity has been linked to $[Ca^{2+}]_i$ elevations (Limke, Bearss, et al., 2004; Marty & Atchison, 1998) and antagonists of VGCCs improve viability after an *in vivo* and *in vitro* MeHg exposure in CGCs (Marty & Atchison, 1998; Sakamoto et al., 1996). We explored the relationship between increases in $[Ca^{2+}]_i$ and consequent reduction of viability in differentiated PC12 cells. Differentiated PC12 cells were exposed to 0, 1, 2 or 5 μM MeHg for 1 hr. This MeHg exposure time is within the biphasic MeHg-induced increase in $[Ca^{2+}]_i$. After MeHg treatment, cells were allowed to recover in culture media for 1 or 24 hr time points to assess short and long-term viability, respectively. The MeHg-induced cell death time course shows that short-term viability of differentiated PC12 cells exposed to 1 μM MeHg was not significantly reduced from control (Fig 2.4). This suggests that perturbations in $Ca^{2+}{}_i$ resulting from 1 μM MeHg exposure are not substantial to induce cell death. However, viability of cells exposed to 2 or 5 μM MeHg was significantly reduced from control in a concentration-dependent manner at immediate timepoint (Fig 2.4A). Long-term viability was significantly reduced from control only at 5 μM MeHg exposure (Fig 2.4B). Thus, cell viability is inversely proportional to MeHg concentrations at both 1 hr post- and 24 hr post-MeHg. Together, the viability assay indicates that differentiated PC12 are susceptible to the toxic effects of MeHg at 1 and 24 hr post-MeHg exposure.

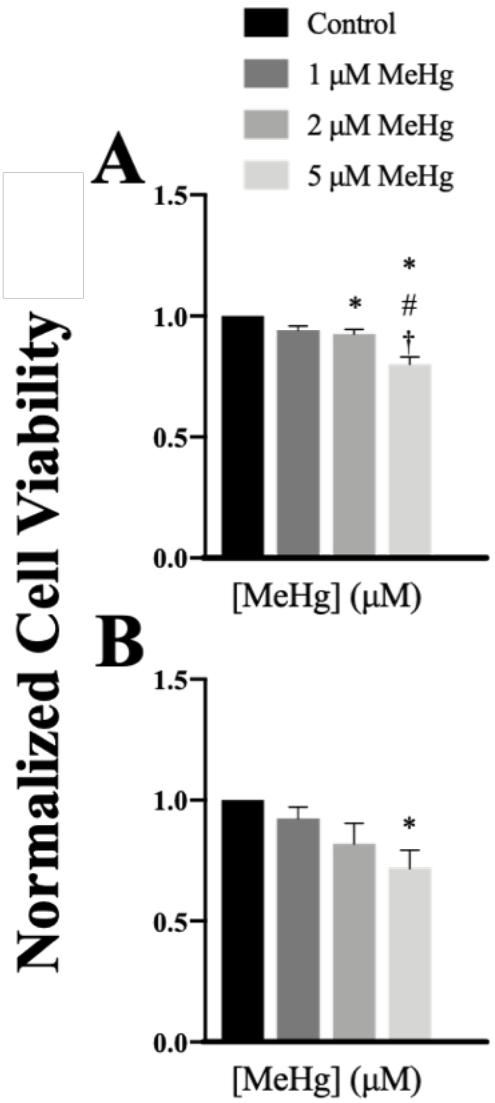

Figure 2.4. Viability of differentiated PC12 cells at immediate (1 hr after MeHg exposure) or delayed (24 hr after MeHg exposure) time points following *in vitro* acute MeHg exposure. (A) Exposure to MeHg leads to a concentration-dependent increase in cell death at the 1 hr post-MeHg time point. At 2 and 5 μM MeHg compared to control, denoted by asterisk (*). At 5 μM MeHg reduced viability is significantly different from 1 and 2 μM MeHg, denoted by dagger (†) and pound (#), respectively. (B) High MeHg concentration shows a significant increase in cell death incidence at 24 hr post-MeHg compared to control, denoted by asterisk (*). Values are

Figure 2.4. (cont'd)

represented as mean ± SEM (n = 7, 7, 7, 6) for 0, 1, 2 and 5 μM MeHg, respectively, for immediate viability. Values are represented as mean ± SEM (n = 7, 7, 6, 5) for 0, 1, 2 and 5 μM MeHg, respectively, for delayed viability. Each experiment was replicated three times. One-way analysis of variance followed by Tukey's multiple comparison test was performed for a concentration-dependent comparison. Two-way analysis of variance followed by Sidak's multiple comparison test was performed for immediate vs delayed time-dependent comparison. Statistical significance is considered at $p < 0.05$.

Contribution of Ca^{2+}_e to acute MeHg-induced cell death in differentiated PC12 cells

Uncontrolled, sustained and prolonged dysregulation of Ca^{2+} leads to cell death (Choi, 1988). Similarly, MeHg exposure causes dysregulation of $[Ca^{2+}]_i$ that contributes to cell death. Next, we examine the contribution of Ca^{2+}_e to the acute phase of neurodegeneration in differentiated PC12 cells. MeHg + EGTA treatment, low Ca^{2+}_e (approximately 60 nM) significantly protected against MeHg cytotoxicity and increased cell viability at 2 and 5 μM MeHg from control (Fig 2.5). Thus, extracellular Ca^{2+} sources contribute to MeHg-induced elevations of $[Ca^{2+}]_i$ at 1 hr post-MeHg exposure in differentiated PC12 cells. Conditions of low Ca^{2+}_e protects against MeHg-induced cell death. Together, data suggest that extracellular Ca^{2+}-dependent pathways contribute MeHg-induced immediate cytotoxicity.

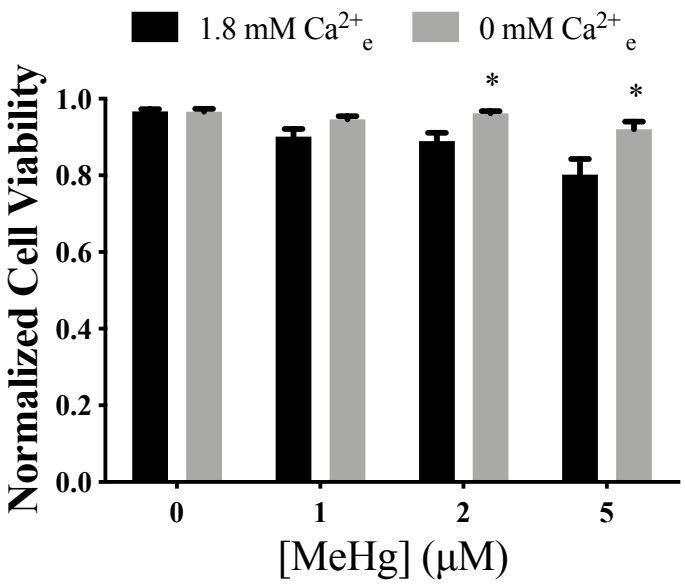

Figure 2.5. EGTA (20 μM) treatment was able to reduce cell death at both 2 and 5 μM MeHg during the acute phase of degeneration. Differentiated PC12 cells were exposed to MeHg for 1 hr and cell viability was assessed. MeHg + EGTA treatment significantly protects against MeHg-induced cell death at 2 and 5 μM MeHg compared to 1.8 mM Ca^{2+}_e, denoted by asterisk (*). Values are represented as mean ± SEM (n = 6) for 0, 1, 2 and 5 μM MeHg, and mean ± SEM (n = 9) for 0, 1, 2 and 5 μM MeHg, respectively, during immediate time point. Each experiment was replicated three times. Two-way analysis of variance followed by Sidak's multiple comparison test was performed. Statistical significance is considered at $p < 0.05$.

Inhibition of heteromeric nAChRs blocks MeHg-induced increases in $[Ca^{2+}]_i$ in differentiated PC12 cells

Experiments on mouse spinal cord MNs have demonstrated that blocking N-methyl D-aspartic acid (NMDA) receptors and VGCCs with their specific antagonists protects against MeHg-mediated $Ca^{2+}{}_i$ dysregulation (Ramanathan & Atchison, 2011). Selective heteromeric or homomeric nAChRs antagonists MEC or MLA, respectively were used separately to determine if cholinergic pathways contribute to the biphasic increase in $[Ca^{2+}]_i$ following MeHg exposure in differentiated PC12 cells. Cells were loaded with fura-2 AM and then exposed to MEC or MLA pretreatment followed by perfusion with 1, 2, or 5 μM MeHg. Exposure to the blocker and MeHg occurred simultaneously during all experiments. MeHg + MEC treatment significantly slowed the fura-2 time-to-onset only for phase 1 during 1 μM MeHg exposure (Fig 2.6A) and not phase 2 (Fig 2.7A). This suggests that heteromeric nAChRs participate in MeHg-mediated $[Ca^{2+}]_i$ dysregulation during phase 1. MLA treatment during MeHg exposure does not affect the MeHg-mediated increase of fura-2 fluorescence (Fig 2.6B, 2.7B). This suggests that homomeric nAChRs do not participate of MeHg-mediated dysregulation of $[Ca^{2+}]_i$. Together, these findings implicate that heteromeric, but not homomeric, nAChRs contribute to the first phase increase in $[Ca^{2+}]_i$ caused by MeHg. Also, it shows that Ca^{2+} influx during phase 2 is not exclusively dependent on cholinergic receptors because blocking them did not affect phase 2.

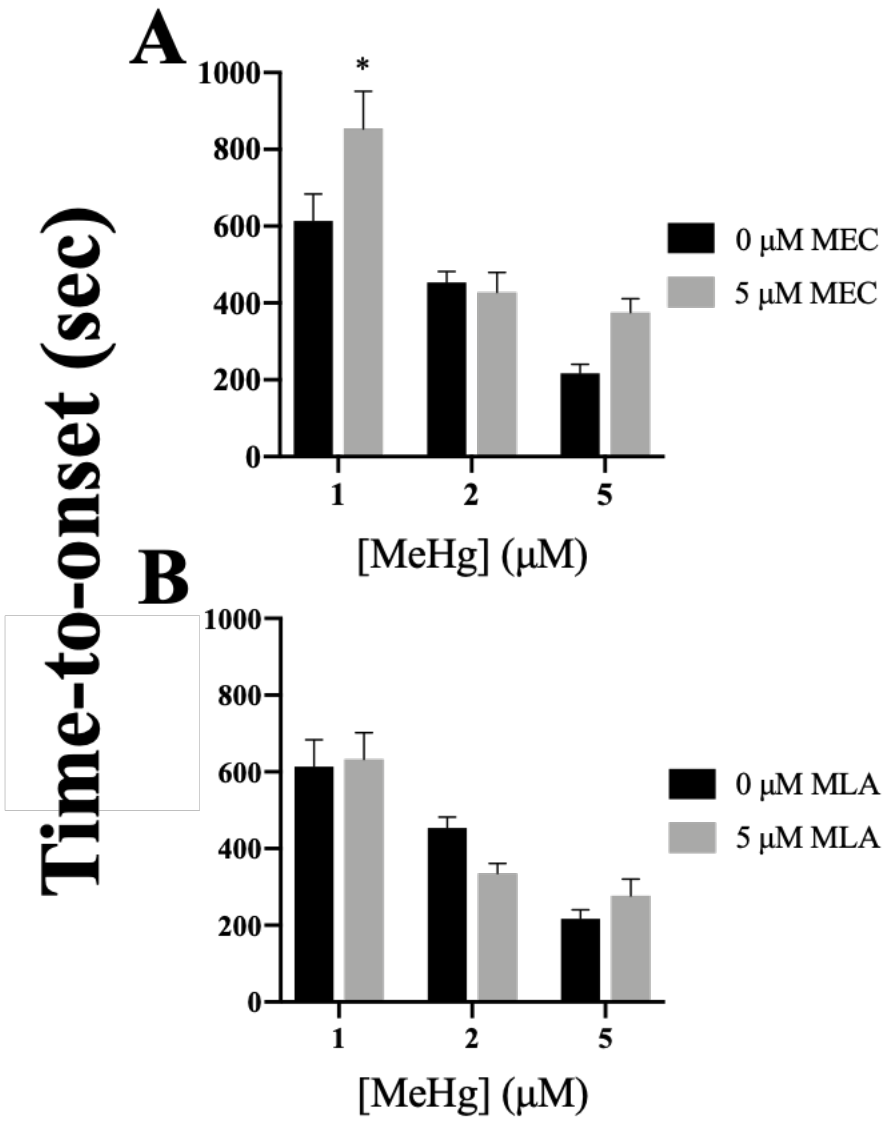

Figure 2.6. Comparative effects of Ca^{2+} on phase 1 time-to-onset of MeHg alone or the combination of MeHg + MEC or MLA during MeHg-mediated Ca^{2+}_i elevations. Differentiated PC12 cells were incubated in 5 μM MEC or 5 μM MLA, 5 min prior to perfusion with MeHg while simultaneously monitoring changes in fura-2 fluorescence. (A) Time-to-onset of phase 1 during 1 μM MeHg + MEC was significantly delayed from MeHg alone, denoted by the asterisk (*). (B) Presence of MLA during MeHg exposure did not affect MeHg-mediated fura-2 ratio for phase 1. Values are represented as mean ± SEM (n = 10) for 1, 2 and 5 μM MeHg.

Figure 2.6. (cont'd)

Values are represented as mean ± SEM (n = 10) for 1 μM MeHg + MEC and ± SEM (n = 8) for 2 and 5 μM MeHg + MEC. Values are represented as mean ± SEM (n = 5) for 1 μM MeHg + MLA, ± SEM (n = 7) for 2 μM MeHg + MLA and ± SEM (n = 9) for 5 μM MeHg + MLA. Each *n* represents the recording of fura-2 fluorescence value from the soma of 5-9 differentiated PC12 cells per cover dish. Each experiment was replicated three times. Two-way analysis of variance followed by Sidak's multiple comparison test was performed. Statistical significance is considered at $p < 0.05$.

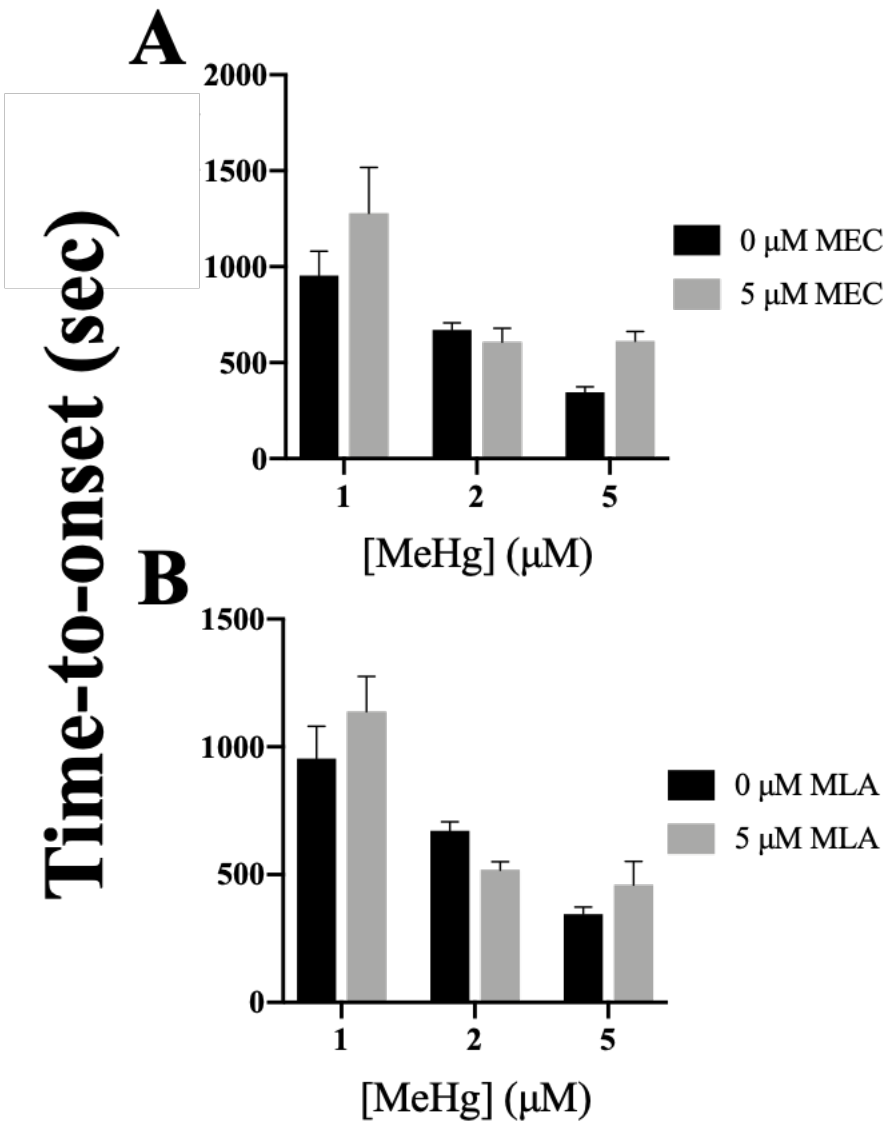

Figure 2.7. Comparative effects of Ca^{2+} on phase 2 time-to-onset of MeHg alone or the combination of MeHg + MLA during MeHg-mediated $Ca^{2+}{}_i$ elevations in differentiated PC12 cells. Differentiated PC12 cells were incubated in 5 μM MEC or 5 μM MLA, 5 min prior to perfusion with MeHg while simultaneously monitoring changes in fura-2 fluorescence. (A) Time-to-onset of phase 2 during MeHg + MEC or (B) phase 2 during MeHg + MLA did not affect MeHg-mediated fura-2 ratio fluorescence. Values are represented as mean ± SEM (n = 10) for 1, 2 and 5 μM MeHg. Values are represented as mean ± SEM (n = 10) for 1 μM MeHg + MEC and

Figure 2.7. (cont'd)

± SEM (n = 8) for 2 and 5 μM MeHg + MEC. Values are represented as mean ± SEM (n = 5) for 1 μM MeHg + MLA, ± SEM (n = 7) for 2 μM MeHg + MLA and ± SEM (n = 9) for 5 μM MeHg + MLA. Each *n* represents the recording of fura-2 fluorescence value from the soma of 5-9 differentiated PC12 cells per cover dish. Each experiment was replicated three times. Two-way analysis of variance followed by Sidak's multiple comparison test was performed. Statistical significance is considered at $p < 0.05$.

MEC-sensitive pathways protect against immediate MeHg-induced cell death in differentiated PC12 cells in the acute phase of degeneration

Studies have demonstrated that the blocking membrane receptors, such as VGCCs (Marty & Atchison, 1998) and mAChRs (Limke, Bearss, et al., 2004) besides reducing MeHg-mediated Ca^{2+} dysregulation, protects against cell death. We determined whether nAChRs participate in cell death by protecting against MeHg-induced cytotoxicity with MEC, MLA or MEC + MLA. MEC pre-incubation and co-exposure with 5 μM MeHg for 1 hr significantly improved cell viability 1 hr post-MeHg exposure (Fig 8A). MeHg + MLA treatment significantly reduced acute viability at 5 μM MeHg suggesting a potential toxic role from MLA in differentiated PC12 (Fig 2.8B). Combination of both antagonists did not change MeHg-induced cell death compared to control at 1 hr post-MeHg exposure (Fig 2.8C). None of the pharmacologic agents in combination with MeHg exposure did not successfully protect differentiated PC12 cells from MeHg-induced cell death at the 24 hr timepoint (Fig 2.9A, B, C). These data are consistent with the view that MEC-sensitive pathways protect viability in the acute phase of degeneration, but that protection does not persist over the long term. Therefore, heteromeric, but not homomeric, nAChRs contribute to MeHg-induce cell death 1 hr post-MeHg exposure in differentiated PC12 cells.

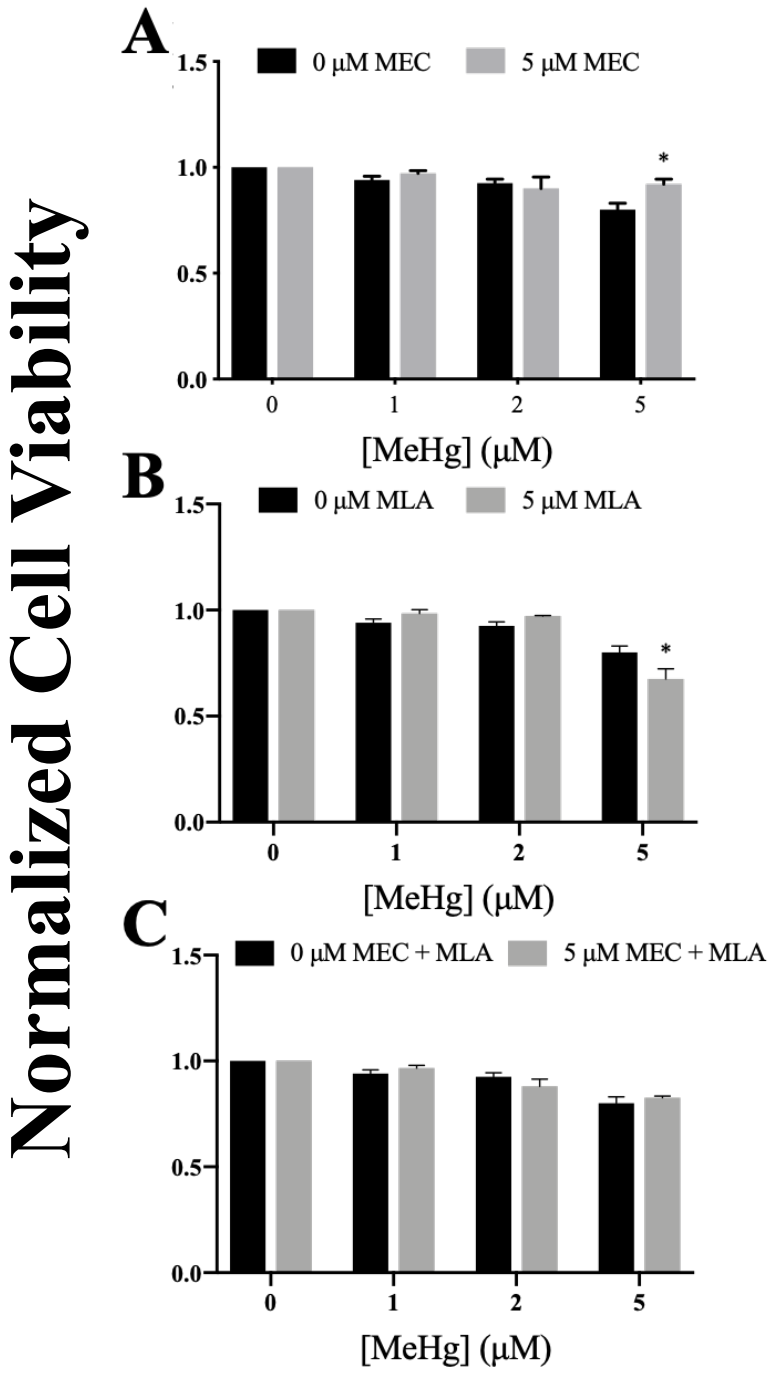

Figure 2.8. Viability of PC12 cells at immediate time point following acute *in vitro* MeHg exposure in the absence and presence of MEC, or MLA or MEC + MLA. (A) Following 1 hr of MeHg in combination with MEC, significantly increased the MeHg-induced cell death incidence at 5 µM MeHg exposure, denoted by asterisk (*). (B) MeHg in combination with MLA,

Figure 2.8. (cont'd)

significantly decreased the MeHg-induced cell death incidence at 5 μM MeHg exposure, denoted by asterisk (*). (C) Presence of MEC + MLA during MeHg exposure did not alter MeHg-induced cell death rate compared to controls. Values are represented as mean ± SEM (n = 7, 7, 7, 6) for 0, 1, 2 and 5 μM MeHg, respectively, for immediate viability. Values are represented as mean ± SEM (n = 7, 6, 6, 5) for 0, 1, 2 and 5 μM MeHg + MEC, mean ± SEM (n = 3, 3, 3, 3) for 0, 1, 2 and 5 μM MeHg + MLA, and mean ± SEM (n = 3, 3, 3, 3) for 0, 1, 2 and 5 μM MeHg + MEC + MLA. Each experiment was replicated three times. Two-way analysis of variance followed by Sidak's multiple comparison test was performed. Statistical significance is considered at $p < 0.05$.

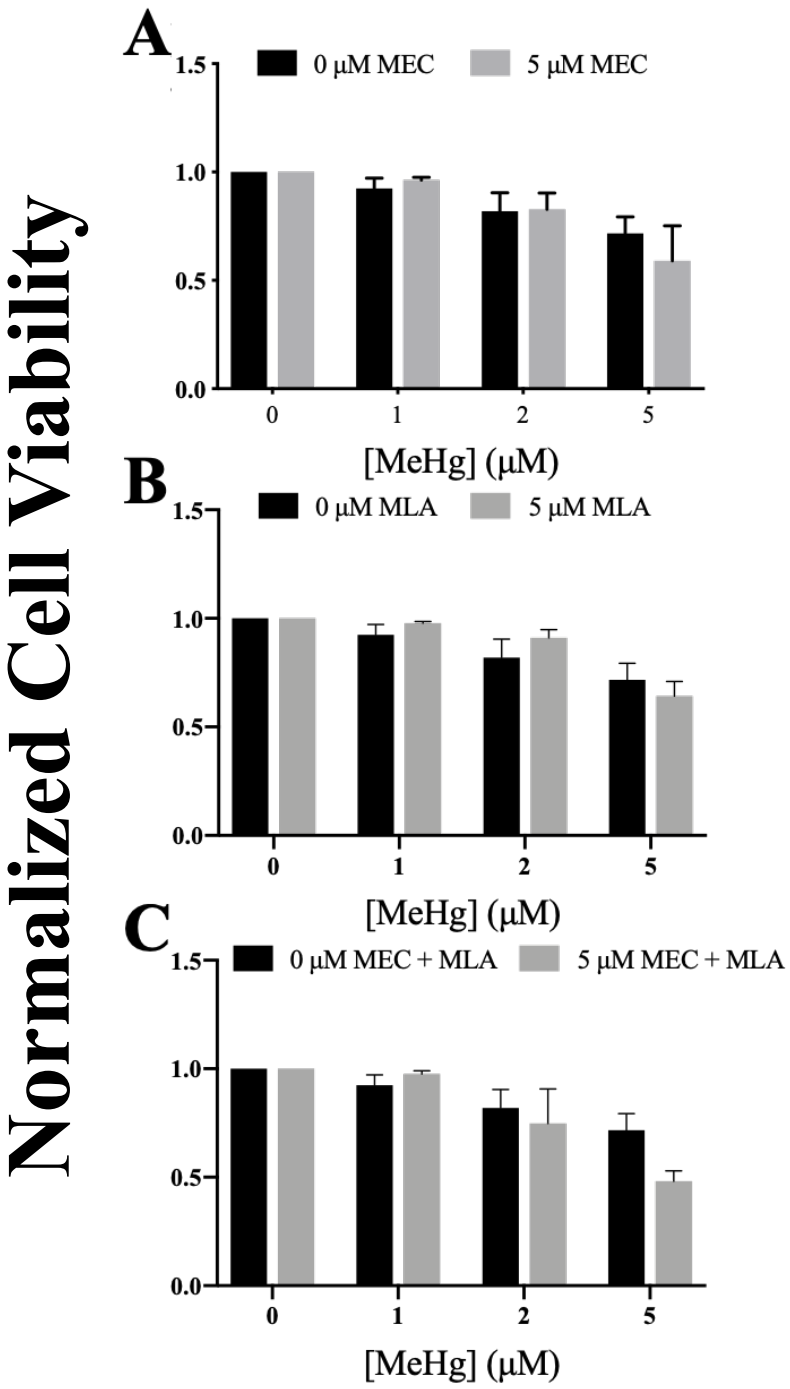

Figure 2.9. Viability of PC12 cells at delayed time point following acute *in vitro* MeHg exposure in the absence and presence of MEC, or MLA or MEC + MLA. (A) Following 1 hr of MeHg in combination with MEC, (B) MeHg in combination with MLA, or (C) Presence of MEC + MLA during MeHg exposure, all did not alter MeHg-induced cell death rate compared to

Figure 2.9. (cont'd)

controls. Values are represented as mean ± SEM (n = 7, 7, 6, 5) for 0, 1, 2 and 5 μM MeHg, respectively, for delayed viability. Values are represented as mean ± SEM (n = 7, 6, 6, 5) for 0, 1, 2 and 5 μM MeHg + MEC, mean ± SEM (n = 3, 3, 3, 3) for 0, 1, 2 and 5 μM MeHg + MLA, and mean ± SEM (n = 3, 3, 3, 3) for 0, 1, 2 and 5 μM MeHg + MEC + MLA. Two-way analysis of variance followed by Sidak's multiple comparison test was performed. Statistical significance is considered at $p < 0.05$.

Discussion

Experiments were designed to determine whether MeHg- mediated $[Ca^{2+}]_i$ dysregulation and if MeHg-induced $[Ca^{2+}]_i$ dysregulation correlates to cell death in differentiated PC12 cells. Furthermore, we aim to identify potential cholinergic mechanisms by which acute MeHg exposure causes alterations in $Ca^{2+}{}_i$ homeostasis and subsequent cytotoxicity. Uncontrolled and sustained dysregulation of $[Ca^{2+}]_i$ is a critical component of MeHg-induced cell death (Limke, Bearss, et al., 2004; Marty & Atchison, 1998). Our principal findings demonstrate for the first time that differentiated PC12 cells are sensitive to acute MeHg toxicity and that MeHg-mediated $[Ca^{2+}]_i$ dysregulation occurs in a biphasic manner. The biphasic response mediate by MeHg consists of phase 1: Ca^{2+} release from internal stores, followed by phase 2: $Ca^{2+}{}_e$ entry (Hare & Atchison, 1995; Hare et al., 1993; Levesque & Atchison, 1991; Limke & Atchison, 2002; Limke, Bearss, et al., 2004). Additionally, MeHg-mediated biphasic disruption of $[Ca^{2+}]_i$ and MeHg-induced cell death is dependent, but not exclusive, to heteromeric nAChRs in a MEC-sensitive manner. This is supported by previous *in vitro* and *in vivo* MeHg exposure studies from our laboratory. MeHg toxicity leads to a concentration-dependent increase in $[Ca^{2+}]_i$ in primary neurons and in immortalized cells. Studies suggest that inhibition of VGCCs, α-amino- 3-hydroxy-5-methyl-4-isoxazolepropionate (Campanari et al.), and NMDA receptors delay MeHg-mediated alterations in $Ca^{2+}{}_i$ homeostasis (Johnson et al., 2011; Marty & Atchison, 1997; Ramanathan & Atchison, 2011). Furthermore, inhibition of VGCCs protects against MeHg-induced cell death (Marty & Atchison, 1998; Sakamoto et al., 1996).

MeHg is able to cross the lipid bilayer through passive diffusion due to its high lipophilicity conferred by the methyl group (Atchison, 1987; Mirzoian & Luetje, 2002). MeHg triggers Ca^{2+}

release from internal Ca^{2+} stores (Hare & Atchison, 1995; Marty & Atchison, 1997). MeHg interacts with cysteine groups (Hisatome et al., 2000) and with cholinergic neurotransmission. Specifically, MeHg binds to nAChRs with high affinity and displaces ACh from the muscle-type nAChRs binding site on the electric ray (Eldefrawi et al., 1977; Shamoo et al., 1976). MeHg suppresses the depolarization of cholinergic neurotransmission suggesting that MeHg blocks the nicotinic response in N1E-115 neuroblastoma cells (Quandt et al., 1982). MeHg reduces nerve-evoked ACh release and promotes spontaneous release of ACh, in a Ca^{2+}-dependent manner (Atchison & Narahashi, 1982; Juang, 1976a). Lastly, MeHg has preferential affinity to α subunits on LGICs. For example, MeHg has differential sensitivity depending on the expression of the α subunit on the gamma-aminobutyric acid type A ($GABA_A$) receptor (Herden et al., 2008).

MeHg concentrations show an inversely related response to fura-2 time-to-onset ratio, suggesting a concentration-dependent behavior. The latter is qualitatively and quantitatively similar to that reported in cultures of mouse spinal cord MNs following MeHg exposure (Ramanathan & Atchison, 2011). Thus, differentiated PC12 cells and spinal MNs, both exhibit the characteristic MeHg-mediated biphasic $Ca^{2+}{}_i$ dysregulation. In differentiated PC12 cells, a significant change in fura-2 onset occurs at 2 and 5 μM MeHg exposure compared to 1 μM MeHg. Similarly, undifferentiated PC12 cells display a hastening in MeHg-mediated alterations in $Ca^{2+}{}_i$ homeostasis during 5 μM MeHg but not at lower MeHg concentrations at phase 2 (Edwards 2004 dissertation). This suggests that differentiated PC12 cells are susceptible to MeHg-mediated $Ca^{2+}{}_i$ dysregulation. Furthermore, differentiated PC12 cells are more susceptible to alterations in Ca^{2+} homeostasis than undifferentiated PC12 cells.

Previous studies in undifferentiated PC12 cells (Edwards 2004 dissertation), human derived MN-induced pluripotent stem cells (Colón-Rodriguez 2018 dissertation), spinal MN culture, CGCS and NG108-15 cells, exposure of EGTA treatment abolished MeHg-mediated phase 2 (Hare & Atchison, 1992; Marty & Atchison, 1997; Ramanathan & Atchison, 2011). However, the MeHg-mediated biphasic rise in Ca^{2+}_i persisted despite removal of Ca^{2+}_e with EGTA in differentiated PC12 cells. Specifically, phase 2 was significantly delayed but still observed during 0 mM Ca^{2+}_e conditions. This result, although surprising, is similar to acute MeHg exposure in HEK 293 cells which also displayed phase 2 during 1, 2, and 5 μM MeHg + EGTA, Ca^{2+}_e-free conditions (Hannon 2016 dissertation). Thus, data indicate that Ca^{2+}_e is responsible for time-to-onset of phase 1 and phase 2 during MeHg toxicity. However, the onset of phase 2 is attributed to Ca^{2+}_e influx. Therefore, the persistence of this phase under MeHg + EGTA conditions suggest that other cation-entry pathways independent of Ca^{2+}_e are involved. Ca^{2+}_e is not the only factor responsible for fura-2 biphasic fluorescence in differentiated PC12 cells. Other divalent cations could be contributing to this effect. Fura-2 fluorescence can be increased by non-Ca^{2+} divalent cations, like zinc (Zn^{2+}) (Arslan, Di Virgilio, Beltrame, Tsien, & Pozzan, 1985; Grynkiewicz et al., 1985). Similarly to Ca^{2+}, Zn^{2+} binds to fura-2 at 340 and 380 nm (Marty & Atchison, 1997). MeHg increases intracellular Zn^{2+} levels in rat brain synaptosomes (Denny & Atchison, 1994), Purkinje cells (Edwards 2004 dissertation), and NG108-15 cells (Denny & Atchison, 1994; Hare et al., 1993). Also, MeHg triggers Zn^{2+} release (Denny & Atchison, 1994, 1996) from vesicle terminals in differentiated PC12 cells (Salazar, Craige, Love, Kalman, & Faundez, 2005) and from cytoplasmic proteins like β-tubulin (Denny & Atchison, 1994). Administration of the heavy metal chelator N,N,N',N'-tetrakis(2- pyridylmethyl)ethylenediamine (TPEN) protects against MeHg-mediated divalent cation homeostasis in several cell types, including undifferentiated PC12 cells (Edwards

2004 dissertation). Furthermore, treatment with TPEN decreases fura-2 fluorescence during phase 1 (Denny & Atchison, 1994; Hare et al., 1993) (Edwards 2004 dissertation). Disruption of Zn^{2+}correlates with cytotoxicity of cerebellar neurons (Manev, Kharlamov, Uz, Mason, & Cagnoli, 1997). Thus, MeHg-mediated Zn^{2+} release could be the culprit associated with the MeHg-mediated biphasic rise in fura-2 fluorescence despite removal of Ca^{2+}_e. This is important because Zn^{2+} is released in a Ca^{2+}-dependent manner (Assaf & Chung, 1984; Howell, Welch, & Frederickson, 1984) and low Zn^{2+} concentrations can potentiate nAChRs (Hsiao, Dweck, & Luetje, 2001). In theory, Zn^{2+} can affect surface nAChRs and intracellular-Ca^{2+} stores. As a result, an increase in fura-2 fluorescence intensity can occur in differentiated PC12 cells.

Uncontrolled increase in $[Ca^{2+}]_i$ correlates to cytotoxicity (Kroemer et al., 1995; Kruman & Mattson, 1999). A consensus exists that MeHg-induced elevations in $[Ca^{2+}]_i$ result in reduced cell viability (Edwards et al., 2005; Limke, Bearss, et al., 2004; Marty & Atchison, 1998). Cholinergic pathways are involved in MeHg-induced neurotoxicity (Castoldi, Candura, Costa, Manzo, & Costa, 1996; Limke, Bearss, et al., 2004). The mAChRs blocker, bethanechol, effectively protected against MeHg-induced cytotoxicity in CGCs (Limke, Bearss, et al., 2004). In differentiated PC12 cells, MeHg increase the incidence of cell death in a concentration-dependent fashion at both 1- and 24-hr post-MeHg exposure. Specifically, incidence of cell death was significantly decreased 1 hr following exposure to 2 and 5 μM MeHg. This finding is similar to a previous study from our laboratory in that 2 and 5 μM MeHg, but not lower concentrations, caused reduced viability in undifferentiated PC12 cells (Edwards 2004 dissertation). Similarly, at 1 μM MeHg cell death rate did not change in differentiated PC12 cells. Perhaps, this suggests presence of a latency period due to the MeHg concentration being too low and thus needing a longer period for MeHg to reach its

target site. This is supported by a study from our laboratory. In detail, following 2 hr MeHg exposure, undifferentiated PC12 cells show a significant decrease in cell viability at 2.5 and 5 μM MeHg, but not 1 μM MeHg, at 24 hr post-MeHg exposure (Edwards 2004 dissertation). MeHg toxicity can trigger both cell death signals: apoptotic and necrotic (Castoldi et al., 2000; Fujimura et al., 2009; Nagashima et al., 1996). This suggests that different cell death pathways and involved in MeHg-induced cell death and future experiments need to address this.

Influx of Ca^{2+}_e during MeHg-mediated dysregulation of Ca^{2+}_i may be one of several mechanisms that contributes to MeHg-induced cytotoxicity. As observed, 5 μM MeHg caused a significant reduction in the biphasic fura-2 fluorescence intensity. However, this displays the ability of differentiated PC12 cells to retain and emit fura-2 fluorescence during high MeHg exposure. Conditions of 0 mM Ca^{2+}_e caused a significant delay of fura-2 fluorescence during 5 μM MeHg exposure. This suggests that membrane integrity is not compromised as a result of MeHg exposure because otherwise the cells would have not been able to emit large fura-2 fluorescence during MeHg + EGTA experiments. This indicates that Ca^{2+}_e is responsible for MeHg-induced degeneration of the plasma membrane and cell death. In agreement, conditions of 0 mM Ca^{2+}_e significantly protected against MeHg cytotoxicity and increased cell viability at 2 and 5 μM MeHg in differentiated PC12 cells. Similarly, EGTA treatment prevents 1, 2, 5 μM MeHg-induced cytotoxicity in cerebellar astrocyte cells (Jaiman-Cruz 2017 dissertation). Thus, Ca^{2+}-dependent pathways are involved during MeHg toxicity in differentiated PC12 cells.

Experiments were performed to determine the route(s) of Ca^{2+} entry in differentiated PC12 cells. The nonspecific heteromeric nAChRs blocker, MEC, afforded protection against MeHg-induced

alterations in $[Ca^{2+}]_i$. Specifically, MEC incubation prior to and during MeHg exposure, demonstrated that blockage of MEC-sensitive pathways significantly delayed fura-2 fluorescence only during phase 1 at 1 μM MeHg. At higher concentrations of MeHg perhaps the nAChRs are blocked or other means of Ca^{2+} entry are more significant or contribute more such that we are unable to see the effect of the channel expression. The delay of fura-2 fluorescence during MEC-sensitive pathways suggest that Ca^{2+}_e influx during phase 2 is not due to involvement of nAChRs pathways. The hypothetical reasoning for MEC delaying MeHg-mediated phase 1 is *three-fold*. *First*, MeHg activates several Ca^{2+} pathways that contribute to increases in $[Ca^{2+}]_i$. Thus, a concoction of multiple antagonists is required to block MeHg-induced Ca^{2+} increase. *Second*, the exact mechanism by which membrane receptor antagonists delay MeHg-induced changes in fura-2 fluorescence during phase 1 is not known. However, MeHg displaces w-conotoxin-GVIA from its binding site on N-type VGCCs in PC12 cells (Shafer, Contreras, & Atchison, 1990). Furthermore, radioligand experiments report that nAChRs have high affinity to metals in rats (Jett, Beckles, Navoa, & McLemore, 2002). These data demonstrate that MeHg competes with membrane antagonists for the same binding site. *Third*, nAChRs are serving as a route of entry for MeHg into the cell. Our laboratory has demonstrated that VGCCs facilitate MeHg movement across the plasma membrane (Atchison, 1986, 1987; Atchison & Narahashi, 1982). Also, MeHg could cross the plasma membrane on its own due to its high lipophilic properties (Mirzoian & Luetje, 2002). Once in the cytoplasm, MeHg could trigger Ca^{2+} influx from internal Ca^{2+} pools causing an increase $[Ca^{2+}]_i$. As a consequence, the cell membrane is depolarized, and perhaps it initiates Ca^{2+}-induce Ca^{2+}-release mechanisms, as revealed by fura-2 fluorescence increase in phase 1 (Hare & Atchison, 1992; Hare et al., 1993). Furthermore, the mAChR antagonist, atropine (10 μM) reduced the amplitude of MeHg-induced increase in $[Ca^{2+}]_i$ only during phase 1 without

affecting phase 2 in CGCs (Limke, Bearss, et al., 2004). Hence, cholinergic receptors contribute to MeHg-mediated increase in the time-to-onset of fura-2 fluorescence during phase 1. MEC treatment delayed time-to-onset of phase 1 by blocking the trajectory of MeHg to reach its target site or delaying entry of MeHg into the cell.

Phase 1 being delayed by membrane receptor inhibitors is in accordance with previous studies. Our laboratory has demonstrated that receptor antagonists significantly delay phase 1 time-to-onset. These blockers include: MK-801, AP-5, CNQX and *w*-conotoxin-MVIIA to block NMDA channels, NMDA receptor-operated ion channels, non-NMDA receptors and VGCCs, respectively, on spinal MNs in culture and CGCs. (Marty & Atchison, 1997; Ramanathan & Atchison, 2011). Xetospongin-C treatment to block the IP3-dependent Ca^{2+} increase, demonstrates that the SER contributes to elevations in $[Ca^{2+}]_i$ mediated through nAChRs-dependent pathways in differentiated PC12 cells (Gueorguiev et al., 2000). Thus, these results support the idea that MEC-sensitive, heteromeric nAChRs could provide a potential mechanism of entry for MeHg into differentiated PC12 cells.

Time-to-onset of phase 2 was unaffected with treatment of MEC or MLA antagonist during MeHg exposure. This could be because once phase 1 initiates, it activates $Ca^{2+}{}_e$ pathways that do not depend on MEC- or MLA-sensitive pathways. One $Ca^{2+}{}_e$ pathway could be Ca^{2+}-induced Ca^{2+} entry (CICE) mechanisms in order to replenish the mitochondria and the SER following activation of phase 1 (Mendelowitz, Bacal, & Kunze, 1992). Another $Ca^{2+}{}_e$ mechanisms could be activation of 2nd messenger-operated Ca^{2+} channels. The latter can be activated by IP3 mechanisms or Ca^{2+}

itself (Felder, Singer-Lahat, & Mathes, 1994). Nonetheless, MeHg can increase $[Ca^{2+}]_i$ by mechanisms independent of entry of MeHg into the cells (Limke, Bearss, et al., 2004).

Presence of MEC prior to and during 5 μM MeHg exposure significantly protected against MeHg-induced cytotoxicity at 1 hr post-MeHg. Since MeHg-mediated increase in $[Ca^{2+}]_i$ behaves in a concentration-dependent manner, 5 μM MeHg concentration disrupts $[Ca^{2+}]_i$ more than lower concentrations of MeHg (Marty & Atchison, 1997). As a result, the Ca^{2+} buffering mechanisms are overwhelmed at high MeHg concentrations. This was demonstrated by the significant hastening in the time-to-onset of phase 2 in differentiated PC12 cells. MeHg-mediated elevations in $[Ca^{2+}]_i$ trigger cell death (Marty & Atchison, 1998). Hence, the MEC afforded protection against cell death at 5 μM MeHg could be due to a direct relationship of enough accumulation of $[Ca^{2+}]_i$. Also, MEC-afforded protection could be due to the antagonist ability to prevent MeHg entry into the cell to reach its target site rather than an effect of $[Ca^{2+}]_i$ increase. MEC treatment failed to protect against MeHg toxicity at lower MeHg concentrations. Maybe because accumulation of $Ca^{2+}{}_i$ is less at 1 and 2 μM MeHg compared to 5 μM MeHg. If this is true, then concentrations less than 5 μM MeHg cause too slow of a Ca^{2+} dysregulation response that do not result in cell death at 1 hr post-MeHg.

MLA-sensitive, homomeric nAChRs failed to protect against MeHg-mediated $[Ca^{2+}]_i$ increase at 1 hr post-MeHg exposure. Perhaps, it was due to the well-known rapid desensitization of α7-subunit expressing nAChRs in differentiated PC12 cells (Blumenthal et al., 1997). Another possibility is that, MeHg has higher affinity to homomeric nAChRs than MLA or a lack of contribution from homomeric nAChRs. Neither MEC or MLA protect against 24 hr post-MeHg-

induced cytotoxicity. MeHg (1, 2, 5 μM) exposure compromises the neurofilaments in the cell membrane during development in carcinoma-derived neurons (Graff et al., 1997). Also, MeHg (5-7 μM) but not lower concentrations, caused undifferentiated PC12 cells, CGCs and Purkinje cells to detach from their substrate (Edwards 2004 dissertation). Together, degeneration of filaments may be a reason for the decrease measurements in cell viability at 24 hr post-MeHg exposure. Combination of MEC+MLA with MeHg did not protect against MeHg-induced cell death at any timepoint. The protection afforded by MEC and cancelled by MLA, is perhaps because nAChRs have higher affinity to MeHg than the antagonists. However, this needs to be studied further.

Overall, these results suggest that nAChRs are not the only receptor contributing to the MeHg-induced $[Ca^{2+}]_i$ increase and cell death. We cannot ignore the possibility of other Ca^{2+} entry sources, besides cholinergic pathways, are contributing to MeHg-induced Ca^{2+} dysregulation and subsequent cytotoxicity. Differentiated PC12 cells express VGCCs (Shafer & Atchison, 1991a) which have been demonstrated to be an important entry pathway for Ca^{2+}. In conclusion, MEC treatment delayed the MeHg-mediated $[Ca^{2+}]_i$ increase only at 1 μM MeHg exposure. Pharmacologic agents failed to completely abolish Ca^{2+} dysregulation. Blocking heteromeric nAChRs completely prevents cell death at 1 hr post-MeHg exposure. Thus, MeHg-induced $Ca^{2+}{}_i$ dysregulation and subsequent cell death are facilitated by heteromeric, but not homomeric, nAChRs in differentiated PC12 cells.

CHAPTER THREE:

ROLE OF SPINAL INHIBITORY AND EXCITATORY MECHANISMS DURING METHYLMERCURY NEUROTOXICITY IN THE RENSHAW AREA

Mónica Ríos-Cabanillas[1,2,3] and William D. Atchison[1,2,3]

[1]Comparative Medicine and Integrative Biology Program
[2]Department of Pharmacology and Toxicology
[3]Institute for Integrative Toxicology

Michigan State University
East Lansing, MI, 48824

Abstract

Methylmercury (MeHg) is an organic environmental neurotoxicant that accumulates in lumbar spinal cord alpha motor neurons (αMNs). MeHg exposure causes a multiphasic elevation in intracellular calcium ($[Ca^{2+}]_i$) and induces cytotoxicity ligand gated ion channels (LGICs)-dependent mechanisms. Lumbar spinal excitatory αMNs and local inhibitory Renshaw cells (RCs) interact in a negative feedback mechanism called 'recurrent inhibition'. Interruption of recurrent inhibition results in over excitation of αMNs or loss of inhibition from RCs. Either outcome results in hyperexcitability and subsequent cell death in the Renshaw area. Here, we study the effects of MeHg neurotoxicity in the Renshaw area. Additionally, we studied whether LGICs are responsible for recurrent inhibition mediate MeHg-induced $[Ca^{2+}]_i$ increase and subsequent cell death during acute exposure to MeHg *in situ*. To determine changes in $[Ca^{2+}]_i$ and viability we used fluo-4-AM microfluorimetry and calcein-AM, respectively. Recordings were made immediately at the conclusion of exposure (15 min) or 1 or 3 hr after MeHg application ceased. Mecamylamine (MEC), dihydro-β-erythroidine (DHβE), bicuculline (BCC) and strychnine, were selected to block α2, α4 nicotinic acetylcholine, γ-aminobutyric acid A ($GABA_A$) and glycine receptors, respectively. MeHg increased fluo-4 fluorescence from baseline at 15 min (51%) and 1 hr post-MeHg (57%). Presence of all the antagonist, except strychnine, during MeHg exposure significantly decreased calcium changes. Cell viability was significantly reduced at 3 hr post-MeHg (-48%) exposure compared to control, which was ablated in the presence of BCC. Thus, cholinergic and GABAergic pathways are involved during MeHg-mediated alterations in $Ca^{2+}{}_i$ homeostasis in the Renshaw area.

Key Words: Fluo-4-AM, Calcein-AM, Neurotoxicity, Intracellular Ca^{2+}, Motor Neurons, Renshaw Cells.

Introduction

Methylmercury (MeHg) is a persistent organic neurotoxicant produced from either natural or anthropogenic sources. Exposure to low-level MeHg from artisanal and small-scale gold mining is the current major pollution concern (Nakazawa et al., 2016; Veiga et al., 2004). Individuals poisoned by MeHg present degeneration of motor neuron (Wootz et al.), motor dysfunction and ataxia (Bakir et al., 1973; Eto, 1997). MeHg targets ubiquitous cysteine residues (Hughes, 1957; Roberts et al., 1980; Tsetlin et al., 2011). Thus, ligand-gate ion channels (LGICs), such as nicotinic acetylcholine (ACh) receptor (nAChRs), γ-aminobutyric acid (GABA) type A receptors ($GABA_ARs$) and glycine receptors (GlyRs) could be targets of MeHg neurotoxicity.

The Renshaw area is located in lamina VII of the ventral horn region of the lumbar spinal cord which is the location of lower MNs responsible for muscle contraction. These αMNs have an axon collateral that synapses on and excites Renshaw interneurons, which in turn inhibit the same αMNs, ultimately modulating their signaling. This negative-feedback mechanism is known as recurrent inhibition (Alvarez & Fyffe, 2007; Bhumbra et al., 2014; Eccles et al., 1954; Renshaw, 1946). It is important to control MN discharge and regulate motor output. ACh, GABA and glycine are the principal neurotransmitters that modulate recurrent inhibition (Dourado & Sargent, 2002; Geiman et al., 2002; Jonas et al., 1998; Schneider & Fyffe, 1992). Thus, MeHg-mediated MN excitation, resulting from either a decrease in inhibitory neurotransmission or activation of excitatory pathways, can lead to dysfunction of recurrent inhibition in the Renshaw area.

Studies *in vivo* have shown that oral administration of 10 mg/kg/day MeHg to adult rats accumulates in spinal cord αMNs and causes their degeneration (Moller-Madsen, 1990, 1991; M.

Su et al., 1998). MeHg-induced increases in intracellular calcium concentration ($[Ca^{2+}]_i$) have been reported in a variety of cell types, including spinal MNs (Ramanathan & Atchison, 2011), and contributes to cytotoxicity (Edwards et al., 2005; Limke, Bearss, et al., 2004; Marty & Atchison, 1998). Mechanisms underlying MeHg-induced neurotoxicity of MNs are not well characterized. This is the first report of MeHg neurotoxicity in the Renshaw area.

MeHg affects excitatory and inhibitory neurotransmission. The latter is affected earlier than the former. In detail, MeHg decreases GABA-induced Cl^- current, suggesting a direct interaction between MeHg and the GABAergic receptor (Arakawa et al., 1991; Huang & Narahashi, 1996). MeHg speedily suppress $GABA_AR$s-dependent current, suggesting that $GABA_AR$s are very sensitive to MeHg toxicity (Tsai et al., 2017; Yuan & Atchison, 2003). MeHg disrupts recurrent inhibition through inhibitory mechanisms and triggers hyperexcitability in hippocampal neurons (Yuan & Atchison, 1995, 1997). Also, MeHg induces a biphasic stimulation of synaptic transmission that consists of an initial asynchronous release of glutamate or GABA followed by a decrease in both amplitude and frequency to a complete current block (Atchison & Narahashi, 1982; Juang & Yonemura, 1975; Yuan & Atchison, 2003, 2005, 2007). Thus, MeHg suppression of GABA-induced Cl^- current could trigger hyperexcitability and subsequent excitotoxicity in the Renshaw area.

The purpose of this study is to determine for the first time the sensitivity of the Renshaw area to acute MeHg neurotoxicity and whether MeHg-induced Ca^{2+} dysregulation and subsequent cell death is prevented or ameliorated with antagonists of LGIC. We hypothesize that MeHg *in situ* exposure causes disruption of Ca^{2+} homeostasis in a time- and concentration-dependent manner

that will contribute to increased incidence of cell death. Furthermore, presence of the specific antagonists bicuculline (BCC) to block α (3, 5)-subunit containing $GABA_ARs$ (Alvarez & Fyffe, 2007; Geiman et al., 2002), strychnine to block α (Joint FAO/WHO Expert Committee on Food Additives. Meeting (33rd : 1989 : Geneva Switzerland) & International Program on Chemical Safety.)-subunit containing GlyRs (Geiman et al., 2002; Gonzalez-Forero & Alvarez, 2005), and mecamylamine (MEC) and dihydro-β-erythroidine (DHβE) to block α (2, 4)-subunit containing nAChRs (Dourado & Sargent, 2002; Lamotte d'Incamps & Ascher, 2013; Wada et al., 1989) will reduce neurotoxicity by MeHg. Our novel findings indicate that cholinergic and GABAergic, but not glycinergic, pathways contribute to MeHg-induced increase in $Ca^{2+}{}_i$ and subsequent cell death in the Renshaw area.

Materials and methods

Materials and experimental solutions

Tissue dissections were carried out in a slicing solution containing (in mM): 62.5, NaCl; 2.5, KCl; 5, $MgCl_2$; 1.25, KH_2PO_4; 26, $NaHCO_3$; 0.5, $CaCl_2$; 20, D-glucose; and 107, sucrose (pH 7.4 when saturated with 95% O_2 /5% CO_2 at 25°C). This solution contains low concentrations of Na^+ and Ca^{2+}, but high concentrations of Mg^{2+}, in order to reduce cellular damage during tissue slicing. N-methyl-D-glucamine (NMDG) solution contained (in mM): 125, NMDG; 2.5, KCl; 1.25 KH_2PO_4; 26, $NaHCO_3$; 5, $MgCl_2$; 0.5, $CaCl_2$; and 20, D-glucose (pH 7.4 when saturated with 95% O_2 /5% CO_2 at 25°C). Thus, it preserves the viability, morphology and the synaptic functions of spinal cord by causing the membrane potential to hyperpolarize (Tanaka, Tanaka, Furuta, Yanagawa, & Kaneko, 2008). Artificial cerebrospinal fluid (ACSF), in which all experiments were conducted, consisted of (in mM): 125, NaCl; 2.5, KCl; 1, $MgCl_2$; 1.25, KH_2PO_4; 26, $NaHCO_3$; 2, $CaCl_2$ and

20, D-glucose (pH 7.4 when saturated with 95% O_2 /5% CO_2 at 25°C). The 40 mM K^+ solution contained the same components as ACSF but with 40 mM K^+ and 115.4 mM NaCl. The K^+ solution depolarizes the cellular membrane of viable cells. MeHg chloride was purchased from ICN Biochemical Inc (Aurora, OH). A 10 mM MeHg stock solution was prepared in double-distilled water and stored at 4°C. Experimental solutions were prepared on the day of the experiment by diluting the MeHg stock solution at the desired working concentration in ACSF solution, in the absence or presence of pharmacologic drugs. A concentration of 20 μM MeHg was chosen for all experiments. It represents the concentration of Hg found in the blood of individuals contaminated with MeHg dicyandiamide through grain consumption during the outbreak in Iraq (Bakir et al., 1973). Additionally, 20 μM MeHg has been used in our laboratory for MeHg *in situ* exposure in rat cerebellar slices (Bradford, Mancini, & Atchison, 2016; Yuan & Atchison, 2003, 2005, 2007, 2016), rat hippocampal slices (Yuan & Atchison, 1993), and mouse striatal slices (Fox 2013 dissertation). A high MeHg (100 μM) concentration was used to shorten the time course of effects and examine effects on the concentration-respose curve that may have occurred at higher MeHg concentrations (Yuan & Atchison, 2003, 2005, 2016). The heteromeric α2 or α4 specific subunit nAChRs blockers, MEC (20 μM) (C. K. Su, Ho, Kuo, Wen, & Chai, 2009) and DHβE (20 μM) (Chavez-Noriega et al., 1997; Dourado & Sargent, 2002), respectively, were purchased from Sigma-Aldrich (St. Louis, MO). The $GABA_A$Rs competitive antagonist, BCC (20 μM) (Tsai et al., 2017; Yuan & Atchison, 1997) and the GlyRs antagonist, strychnine (20 μM) (Yuan & Atchison, 2005) were purchased from Sigma-Aldrich (St. Louis, MO). Antagonist stocks were prepared in double distilled H_2O or following manufacturers recommendations. Fluo-4 was purchased from Thermo Fisher Scientific (Waltham, MA) and the Live/Dead™ viability/cytotoxicity kit for mammalian cells was purchased from Molecular Probes (Invitrogen, Eugene, OR). Disposable or

MeHg-contaminated materials used during the preparation and experiment were discarded following the Michigan State University (MSU) Office of Radiation, Chemical, and Biological Safety (ORCBS) guidelines.

Lumbar C57BL6J slice

All animal procedures adhered to National Institute of Health (Aberg et al.) guidelines and were approved by the MSU Institutional Animal Care and Use Committee (IACUC). Adult C57BL6J mice (40-60 days postnatal, either gender) were obtained from Jackson Laboratories (Bar Harbor, ME). Mice were housed in pairs, fed standard diet (Harland, Teklab 18% Protein Global Rodent Diet), and exposed to normal light-dark cycle. Following anesthesia with CO_2 in a dedicated chamber, mice were quickly decapitated, the spinal cord was speedily removed, followed by lumbar region dissection. Tissue was rapidly submerged in ice-cold slicing solution, which is a low [Na^+], low [Ca^{2+}] and high [Mg^{2+}] solution, that helps to reduce cellular damage during tissue slicing. Working with very cold solutions protects against cellular swelling and death (Liang, Bhatta, Gerzanich, & Simard, 2007; Won, Kim, & Gwag, 2002). Experiments utilized tissue preparation and incubation methods previously described (Yuan & Atchison, 1999, 2007, 2016) with modifications specifically designed for spinal cord and described below. The lumbar tissue was sliced into thin (180 μm) transverse sections using a Leica VT100S Vibratome (Leica Microsystems Inc., Bannockburn, IL). Individual slices were transferred to a 15 min incubation chamber containing NMDG solution. The slices were then transferred and maintained to a 1:1 mix of oxygenated slicing solution and ACSF for approximately 30 min at room temperature. Then, slices were transferred to 100% ACSF in order to allow quick and controlled treatment of tissues with MeHg, without damaging much of the tissue morphology. Slices were incubated in ACSF

with fluo-4 acetoxymethyl ester (AM), which labels divalent cations, or in a viability assay that utilizes calcein AM, a green fluorescent dye that stains viable cells.

Confocal Ca^{2+} microscopy

Fluo-4 AM no wash (NW) (4 μM) in the presence of probenecid (2.5 μM) were obtained from Invitrogen Molecular Probes (Eugene, OR). Fluo-4 AM NW is a fluorophore that has been extensively used to monitor changes in $Ca^{2+}{}_i$. Thus, it is used to indicate relative MeHg-mediated increase in $[Ca^{2+}]_i$ (Bradford et al., 2016; Johnson et al., 2011; Yuan & Atchison, 2007, 2016). Probenecid inhibits organic-anion transporters, which can extrude dye loading. Slices where loaded for 40 min at room temperature in fluo-4 AM NW with probenecid in the presence of 0.02% (w/v^{-1}) pluronic F-127. The latter facilitates dye solubilization (Yuan & Atchison, 2016). Slices are then washed thoroughly with ACSF before Ca^{2+} recordings. Confocal images of fluo-4 $[Ca^{2+}]_i$ fluorescence were obtained using a Leica TCS SL laser scanning confocal microscope system equipped with Nomarski optics (10x water immersion objective) (Leica Microsystem, Heidelberg GmbH., Germany). Fluo-4 is excited at 485 nm from an argon laser and emits fluorescence at 520 nm. Images (512 x 512 pixels, xyz scan mode) were collected during perfusion with ACSF, 40 mM KCl, and during perfusion with ACSF-containing MeHg alone or MeHg with antagonists. MeHg-induced Ca^{2+} dysregulation was assessed immediately at the conclusion of exposure (15 min) or 1 or 3 hr after MeHg application ceased, in the absence or presence of antagonists. All experiments were oxygenated with 95% O_2 /5% CO_2 and performed at 25°C. An increase in fluo-4 fluorescence intensity corresponds to an increase in $Ca^{2+}{}_i$. Fluo-4 fluorescence was utilized to monitor spatial changes in $Ca^{2+}{}_i$ in the lumbar ventral region of the spinal cord in response to MeHg treatment. Recordings were made under visual guidance from fluo-4 fluorescent large cells,

presumably MNs (20 μm soma in diameter (McHanwell & Biscoe, 1981; Mitra & Brownstone, 2012)) located in the lumbar spinal lamina VII, known as the Renshaw area.

Measurement of tissue viability

MeHg-mediated loss of cell viability was measured using a commercial fluorimetric cell viability assay as previously described (Bradford et al., 2016; Limke, Bearss, et al., 2004; Marty & Atchison, 1998). Briefly, viability was indicated by calcein AM, a fluorescent dye that stains the cytoplasm of live, healthy cells in green (Papadopoulos et al., 1994). Calcein is excited at 495 nm and emits fluorescence at 515 nm. Lumbar spinal cord slices were monitored during perfusion with ACSF loaded with calcein for 40 min in oxygenated solution with 95% O_2/5% CO_2 and performed at 25°C. Viability was assessed immediately at the conclusion of exposure (15 min) or 1 or 3 hr after MeHg application ceased, in the absence or presence of antagonists. Visualization of the cytotoxicity assay was determined with a 10x water immersion objective and images were obtained using a Leica TCS SL laser scanning confocal microscope system equipped with Nomarski optics.

Statistics

Analysis of fluo-4 and calcein changes in fluorescence intensity were performed using the Leica software. In fluo-4 or calcein experiments, before MeHg exposure began, three scattered regions of interest (ROI) were selected within the Renshaw area. The same ROI were monitored from the beginning to the end of the experiment. The ROI in fluo-4 experiments consisted of the average from three different fluorescent cells easily observed with a 10x objective (Fig. 3.1A). Viability in the Renshaw area as indicated by calcein fluorescence was measured by three randomly selected ROI within the Renshaw area (Fig. 3.1B). Fluorescence intensity data in the same layer were

averaged and the background fluorescence was subtracted from all ROI before calculating fluo-4 and calcein mean fluorescence intensity. Untreated (MeHg control) slices with fluo-4 or calcein, were used to monitor photobleaching with the same duration as MeHg treated experimental slices. For each experiment the average from three ROI was taken and was expressed as ± standard error of the mean (SEM). To avoid variability between slices MeHg experiments in presence of pharmacologic drugs were conducted on the same experimental day. To analyze one or among different groups a one-way or two-way analysis of variance (ANOVA), respectively, was used with GraphPad Prism® software (GraphPad Software Inc., San Diego, CA). A *post hoc* comparison with Tukey's or Dunnett's was used when significant differences between means were found (Steel & Torrie, 1960). Values are considered statistically significant at $p < 0.05$.

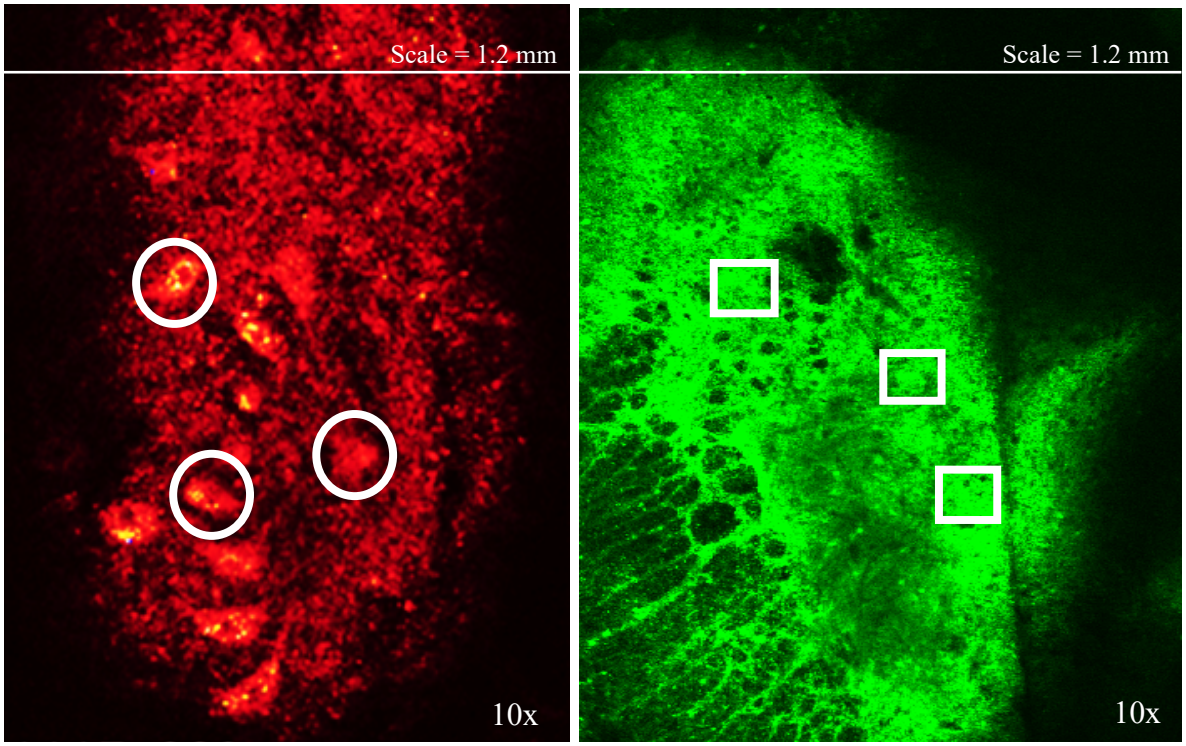

Figure 3.1. Representative pseudocolor epimicrograph of the Renshaw area isolated from a C57BL6J mouse. The Renshaw area is located in lamina VII of the ventral horn region of the lumbar spinal cord A) Fluo-4 (red) fluorescence indicates intracellular Ca^{2+} concentration. Depicted are three different MNs (defined as ROI) selected at random. B) Calcein (green) fluorescence indicates viable ROI in the tissue. Three scattered ROI were selected at random. Images were obtained using a Leica TCS SL laser scanning confocal microscope system equipped with Nomarski optics (10x water immersion objective). Scale bar represents 1.2 mm.

Results

Changes in fluo-4 fluorescence as a result of MeHg-mediated dysregulation of $[Ca^{2+}]_i$ in lower MNs in the Renshaw area

To examine early and delayed effects of MeHg on Ca^{2+} dysregulation we compared different MeHg concentrations (10, 20 and 100 μM) in lower MNs of the Renshaw area. The rationale for these concentrations has been previously described (Yuan & Atchison, 1993, 2003). Briefly, 10 and 20 μM MeHg are environmentally significant concentrations because they represent MeHg levels found within the blood of poisoned humans that caused symptoms of toxicity following an acute exposure to MeHg (Bakir et al., 1973). Additionally, these concentrations are consistent with the pattern and exposure reported in previous global outbreaks. The rationale for 100 μM MeHg is to determine if exposure to MeHg causes a concentration-dependent neurotoxicity and to shorten the time course of MeHg-induced effects (Yuan & Atchison, 1993, 2003). These concentrations are higher than those used in isolated cells in culture because MeHg presents higher capacities of nonspecific binding *in situ* (Bradford et al., 2016). The tissue diffusion barrier for MeHg and support cells can protect against MeHg toxicity more than in monolayer cultures (Yuan & Atchison, 2005). Presence of 10 μM MeHg caused the Ca^{2+}-selective indicator, fluo-4 fluorescence to significantly increase at 1 hr post-MeHg from baseline in lower MNs (Fig 3.2A). Treatment with MeHg (20 μM) caused an increase in $[Ca^{2+}]_i$ at both 15 min and 1 hr post-MeHg, but not at 3 hr post-MeHg exposure (Fig 3.2B). Presence of 100 μM MeHg at 1 hr post-MeHg caused fluo-4 fluorescence to significantly increase from baseline (Fig 3.2C). Conversely, at 3 hr post-MeHg exposure, there is a significant fluo-4 fluorescence reduction compared to 1 hr post-MeHg treatment for both 10 and 100 μM MeHg (Fig 3.2A, 3.2C). Taken together, results suggest that acute exposure to MeHg causes a direct effect upon cessation of treatment (15 min) which is

sustained at delay timepoints (1 hr post-MeHg), but subsided by 3 hr post-MeHg exposure. These suggest that reduction of Ca^{2+} signal after 3 hr exposure to MeHg is due to cytotoxicity.

Not shown, aplication of 40 mM KCl for 3 min before MeHg exposure caused a relative increase which ranges around 130% of the normalized control value. The purpose of using KCl is to confirm proper fluo-4 loading, cell viability and adequate Ca^{2+} buffering capacities of the lower MNs in the Renshaw area. After KCl was washed away and fluo-4 fluorescence returned to basal levels, MeHg exposure began. In slices not exposed to MeHg, there was no significant change in fluo-4 fluorescence over the 3 hr time course (result not shown). This indicates that fluo-4 treatment itself did not affect Ca^{2+} responses nor were the fluo-4 florescence changes due to fluo-4 photobleaching during confocal imaging. Increases in $[Ca^{2+}]_i$ are readily detected following exposure to 10, 20 or 100 μM MeHg in the Renshaw area. Henceforth, we use the epidemiologic dose of 20 μM MeHg in our remaining experiments since it is within the range of detectable changes in fluo-4 fluorescence.

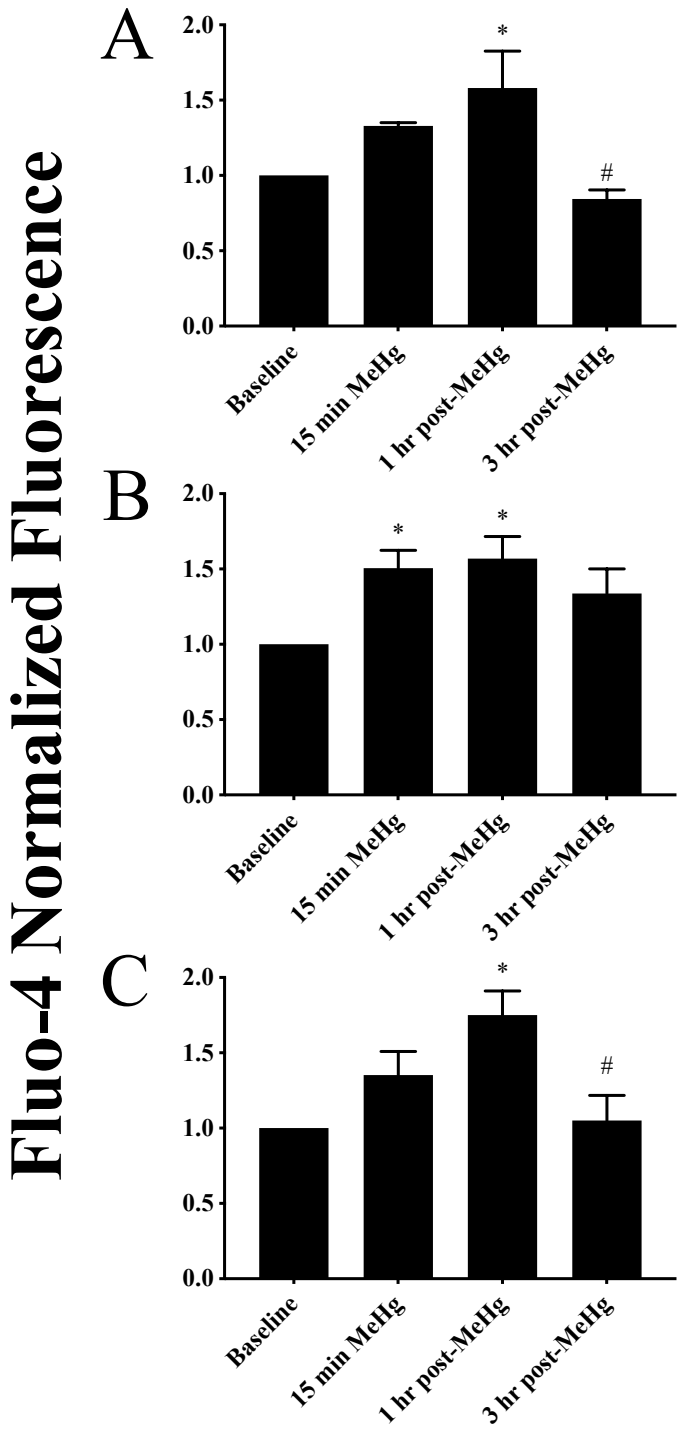

Figure 3.2. Immediate and delayed changes in $[Ca^{2+}]_i$ following acute exposure to 10, 20 or 100 µM MeHg *in situ* in the Renshaw area. A) Exposure to 10 µM MeHg, demonstrated no effect directly upon cessation of treatment (15 min) but a delayed increased ocured (1 hr post-

Figure 3.2. (cont'd)

MeHg) compared to baseline, denoted by the asterisk (*). The fluo-4 fluorescence increase was subsided by 3 hr post-MeHg from 1 hr post-MeHg, denoted by the pound (#). Data are presented as mean ± S.E.M. (n = 3). B) Exposure to 20 μM MeHg for 15 min significantly increases fluo-4 relative fluorescence at both 15 min MeHg and 1 hr post-MeHg compared to baseline, denoted by the asterisk (*). Data are presented as mean ± S.E.M. (n = 11). C) Exposure to 100 μM MeHg, demonstrated no effect directly upon cessation of treatment (15 min) but a delayed increased ocured (1 hr post-MeHg) compared to baseline, denoted by the asterisk (*). The fluo-4 fluorescence increase was subsided by 3 hr post-MeHg from 1 hr post-MeHg, denoted by the pound (#). Data are presented as mean ± S.E.M. (n = 4). All *n* values are averages of 3 replicates from the same slice. Statistics are performed using a one-way analysis of variance followed by Tukey's multiple comparison test. Statistical significance is considered at $p < 0.05$.

MeHg-induced cell death in the Renshaw area occurs at delayed time points

Dysregulation in $[Ca^{2+}]_i$ and following hyperexcitability mechanism is associated with loss of membrane integrity (Zipfel, Babcock, Lee, & Choi, 2000). Next, we aim to determine whether conditions shown to produce MeHg-mediated increase in $[Ca^{2+}]_i$ in the Renshaw area are related to MeHg-induced cell death. We used the same exposure paradigm used in Ca^{2+} microfluorimetry experiments, but Fluo-4 AM was replaced with calcein AM to stain viable cells. As illustrated in Fig. 3.3, MeHg (20 μM) exposure for 15 min, significantly decreases calcein fluorescence. Specifically, at 3 hr post-MeHg timepoint there is a significant fluorescence decline from all other timepoints (Fig 3.3). The immediate, 15 min MeHg exposure, did not affect calcein fluorescence. Over time, there was no significant decrease in calcein fluorescence in the absence of MeHg (result not shown). This suggests that calcein exposure alone does not affect viability. Therefore, any decrease in viability is the result of MeHg exposure. The cell viability in the Renshaw area is reduced following acute exposure to MeHg *in situ* at 3 hr post-MeHg but not at earlier timepoints. Thus, the Renshaw area is susceptible to the acute effects of MeHg neurotoxicity.

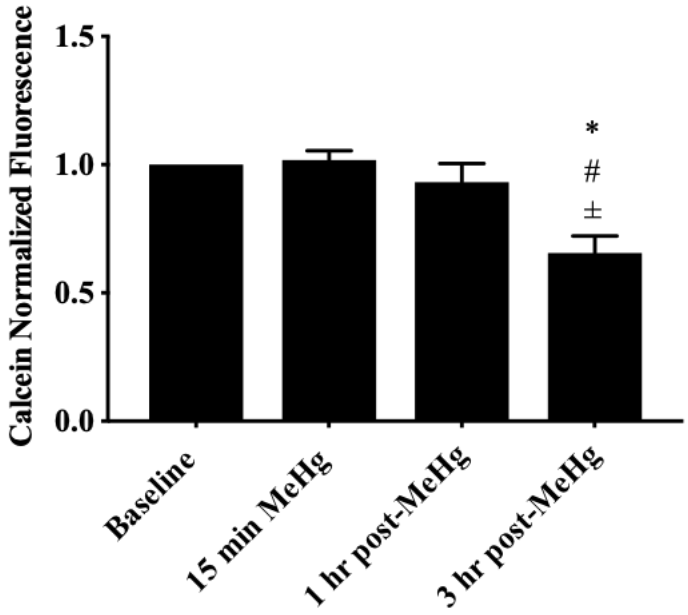

Figure 3.3. Calcein mean fluorescence in the Renshaw area is reduced at 3 hr post-MeHg but not 1 hr post-MeHg or 15 min MeHg. Exposure to 20 μM MeHg during 15 min significantly decreased calcein fluorescence at 3 hr post-MeHg exposure when compared to baseline, 15 min MeHg, and 1 hr post-MeHg denoted by the asterisk (*), pound (#), plus/minus (±), respectively. Data are presented as mean ± S.E.M. (n = 8) for all groups. All *n* values are averages of 3 replicates from the same slice. Statistics are performed using a one-way analysis of variance followed by Tukey's multiple comparison test. Statistical significance is considered at $p < 0.05$.

Membrane receptor antagonists suppress MeHg-mediated decrease in fluo-4 fluorescence intensity

To examine whether cholinergic, GABAergic or glycinergic pathways mediate MeHg-induced $[Ca^{2+}]_i$ increase due to external Ca^{2+} influx we used individual pharmacologic tools. Lumbar slices were exposed to a continuous perfusion with MeHg (20 μM) in the presence of individual antagonists. To block α2- and α4-subunit containing nAChRs, $GABA_A$Rs or GlyRs, the specific antagonists MEC, DHßE, BCC or strychnine, respectively, were administered prior to, as well as, during MeHg exposure. Pretreatment with antagonist alone did not cause any decrease in fluo-4 fluorescence (Fig 3.4A). Presence of MEC, DHßE and BCC, but not strychnine, attenuated the MeHg-induced increase in fluo-4 fluorescence intensity (Fig 3.4B). These data support the hypothesis that Ca^{2+} dysregulation through cholinergic and GABAergic pathways contributes to MeHg-induced $[Ca^{2+}]_i$ elevations. Strychnine treatment did not prevent the MeHg-induce increase in fluo-4 fluorescence intensity. Thus, the nAChRs and $GABA_A$Rs, but not GlyRs, participate of MeHg-mediated increase in $[Ca^{2+}]_i$ as determined by the intensity in fluo-4 fluorescence.

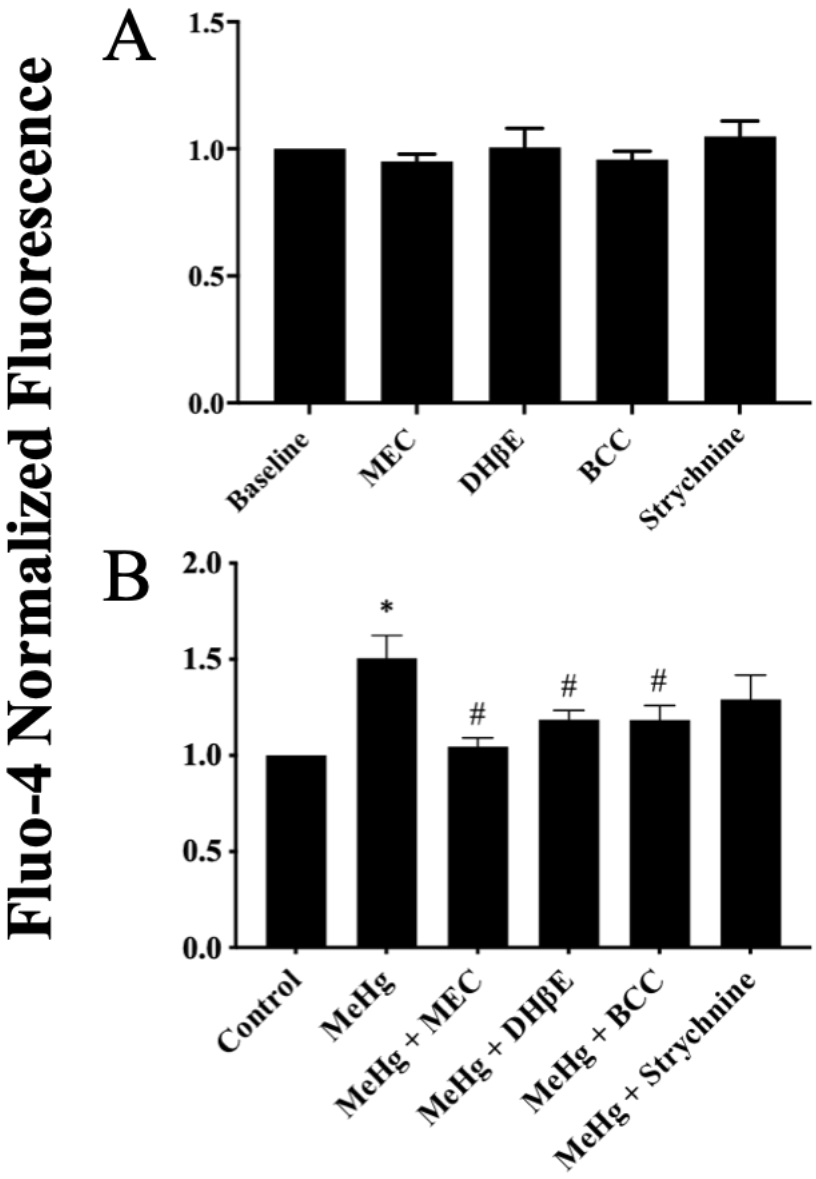

Figure 3.4. MeHg (20 µM) increase fluo-4 fluorescence intensity of the Renshaw area is reduced by antagonists of cholinergic and GABAergic, but not glycinergic receptors. A) Exposure to each antagonist for 5 min does not decrease or increase fluo-4 fluorescence intensity compared to baseline. Data are presented as mean ± S.E.M. (n = 3). All *n* values are averages of 3 replicates from the same slice. Statistics are performed using a one-way analysis of variance followed by Tukey's multiple comparison test. B) Following a 15 min real-time perfusion with

Figure 3.4. (cont'd)

MeHg treatment in the absence of inhibitors caused a significantly increased in fluo-4 fluorescence from control, denoted by the asterisk (*). The concentration for MEC, DHβE, BCC and strychnine was 20 μM. MeHg + MEC, MeHg + DHβE or MeHg + BCC, significantly decreased fluo-4 fluorescence from MeHg-induced fluo-4 increase compared to MeHg, denoted by pound (#). Data are presented as mean ± S.E.M. (n = 11) for all groups. All *n* values are averages of 3 replicates from the same slice. Statistics are performed using a one-way analysis of variance followed by Dunnett's multiple comparison test. Statistical significance is considered at $p < 0.05$.

BCC protects against MeHg-induced cytotoxicity in the Renshaw area

To verify whether cell death is related to MeHg interactions with nAChRs, $GABA_A$Rs or GlyRs a pharmacologic approach was used. Calcein fluorescence was determined at 15 min MeHg, 1 hr post-MeHg and 3 hr post-MeHg. No significant effect was observed with any drug treatment at 15 min MeHg and 1 hr post-MeHg (results not shown). Figure 3.5 shows the composite results for all the MeHg + drug treatments at 3 hr post-MeHg. Combination of MeHg with the GABAergic receptor blocker, BCC, significantly increase the intensity of calcein fluorescence compared to MeHg treatment at 3 hr post-MeHg exposure (Fig. 3.5). Presence of strychnine, MEC, and DHβE treatments were ineffective at preventing or reducing cell death following MeHg exposure (Fig 3.5). Perhaps, these drugs had an early effect in terms of a reduction in $[Ca^{2+}]_i$ but this was not sufficiently long lasting. Also, desensitization of nAChRs has been reported in CGCs (Fohrman, de Erausquin, Costa, & Wojcik, 1993; Giniatullin, Nistri, & Yakel, 2005). Thus, if nAChR desensitized in the Renshaw Area, then they would not be able to provide protection against MeHg-induced cell death. Furthermore, the stoichiometry in the nAChRs could underly the lack of protection afforded by MEC and DHβE. The Renshaw area express α2- and α4-containing nAChRs (Dourado & Sargent, 2002; Lamotte d'Incamps & Ascher, 2013; Wada et al., 1989). Whole-cell electrophysiology studies indicate that the GABA current is blocked faster in the α6-containig $GABA_A$Rs expressed in CGCs than in α1-containing $GABA_A$Rs in Purkinje cells (Herden et al., 2008). The lack of protection offered by strychnine against MeHg-induced cell death is consistent with our earlier findings in fluo-4 fluorescence. Thus, the only receptor involved in recurrent inhibition that delays MeHg-induced cytotoxicity in the Renshaw area is the $GABA_A$R.

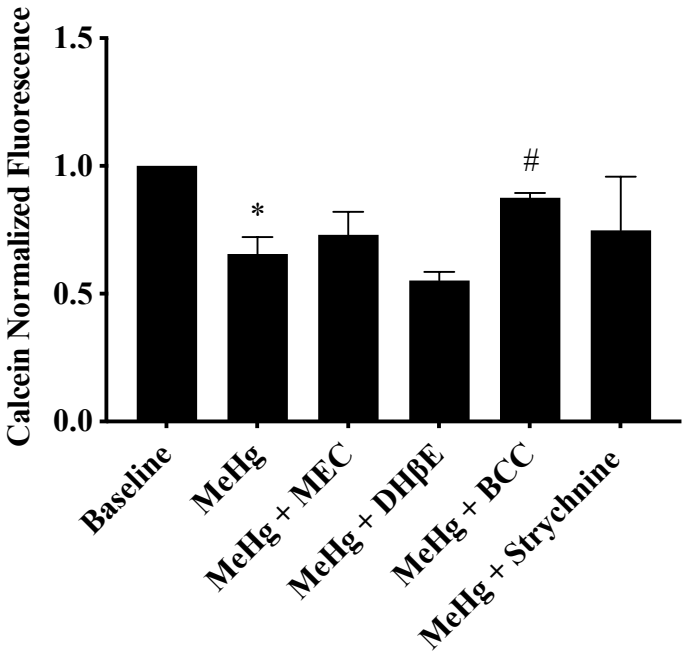

Figure 3.5. Comparison of effects of LGICs channels inhibitors on MeHg (20 µM) induced reduction in calcein fluorescence in the Renshaw area after 3 hr post-MeHg exposure. Exposure to 20 µM MeHg during 15 min significantly decreased calcein AM fluorescence at 3 hr post-MeHg exposure, denoted by asterisk (*). MEC or DHβE did not increase calcein fluorescence compared to MeHg treatment. MeHg + BCC significantly increased calcein fluorescence at 3 hr post-MeHg exposure compared to MeHg treatment, denoted by the number (#). D) MeHg + strychnine did not cause any significant increase in calcein fluorescence compared to MeHg treatment. Data are presented as mean ± S.E.M. (n = 8, 8, 5, 4, 5, 4) for MeHg, MeHg + MEC and BCC, MeHg + DHβE and strychnine, respectively. All *n* values are averages of 3 replicates from the same slice. Statistics are performed using a two-way analysis of variance followed by Sidak's multiple comparison test. Statistical significance is considered at $p < 0.05$.

Discussion

The present study was designed to determine the mechanism of MeHg susceptibility in the Renshaw area. Additionally, we aim to identify the membrane receptors that contribute to MeHg-induced $[Ca^{2+}]_i$ increase and subsequent cell death in the Renshaw area using fluo-4 and calcein fluorescence, respectively. Results show that acute exposure to MeHg *in situ* increases $[Ca^{2+}]_i$ and decreases cell viability in the Renshaw area. Specifically, 15 min perfusion with 20 μM MeHg caused a significant increase in fluo-4 fluorescence, an effect that is sustained at 1 hr post-MeHg exposure but not at 3 hr post-MeHg exposure. Presence of MEC, DHβE and BCC, but not strychnine, significantly decreased but did not abolish the MeHg-mediated increase in fluo-4 fluorescence. Thus, dysregulation of Ca^{2+}_i homeostasis is partially regulated by nAChRs and $GABA_A$Rs, but not GlyRs. MeHg-induced Ca^{2+}_i dysregulation is associated with cell death following 3 hr post-MeHg exposure (Marty & Atchison, 1998). Reduced cell viability was only prevented with BCC, the $GABA_A$R antagonist. This demonstrates that GABAergic pathways participate of MeHg neurotoxicity in the Renshaw area. Since the antagonists did not completely abolish MeHg-induced $[Ca^{2+}]_i$ increase and subsequent cell death, it is likely that other mechanisms participate. These mechanisms could involve activation of glutamate receptors (GluRs) because they are also expressed in the Renshaw area (Lamotte d'Incamps & Ascher, 2013). Furthermore, the contribution of GluRs to MeHg-mediated dysregulation in $[Ca^{2+}]_i$ has been reported in CGCs and primary MNs *in vitro* (Limke, Bearss, et al., 2004; Marty & Atchison, 1997, 1998; Ramanathan & Atchison, 2011).

Our findings demonstrate that LGICs participate in the MeHg-induced increase of $[Ca^{2+}]_i$ in the Renshaw area. This is in agreement with previous studies from our laboratory in which MeHg

drives an uncontrolled and sustained $[Ca^{2+}]_i$ increase through LGICs in isolated CGCs and primary MNs (Limke, Bearss, et al., 2004; Ramanathan & Atchison, 2011). Specifically, muscarinic AChRs, N-methyl D-aspartic acid (NMDA) receptors and VGCCs (Limke, Bearss, et al., 2004; Ramanathan & Atchison, 2011). Ca^{2+} microfluorimetry studies have consistently demonstrated the MeHg-mediated disruption of Ca^{2+} homeostasis in both primary and transformed cell lines, such as rat brain synaptosomes (Denny et al., 1993; Kauppinen et al., 1989), NG108-15 (Hare et al., 1993), CGCs (Limke, Bearss, et al., 2004; Marty & Atchison, 1997; T. A. Sarafian, 1993), Purkinje cells (Edwards et al., 2005), MNs (Edwards et al., 2005; Ramanathan & Atchison, 2011) and mice treated with 3 ppm MeHg administered through drinking water (Johnson et al., 2011). The MeHg-induced increase in $[Ca^{2+}]_i$ behaves in a characteristic kinetically different, biphasic manner, and in a time- and concentration-dependent fashion (Marty & Atchison, 1997).

To identify if nAChRs have a role in the observed increase in $[Ca^{2+}]_i$ at the lower MNs located in the Renshaw area we used a pharmacological approach. MEC- and DHβE -sensitive pathways significantly delayed the MeHg-induced increase in $[Ca^{2+}]_i$. Thus, MeHg may directly interact with nAChRs to cause an increase in $[Ca^{2+}]_i$. Previous findings demonstrate that MeHg exposure inhibits binding of ACh to the muscle-type nAChRs binding site on the electric ray (Shamoo et al., 1976). Also, muscarinic AChRs are involved during MeHg-mediated $[Ca^{2+}]_i$ dysregulation in CGCs (Limke, Bearss, et al., 2004). Thus, these finding support that MeHg interacts with ionotropic nAChRs to significantly dysregulate $Ca^{2+}{}_i$ homeostasis in the Renshaw area.

GABA and glycine are the primary and most widely distributed inhibitory neurotransmitters in the central nervous system. They are responsible for fast inhibitory synaptic transmission (Pycock &

Kerwin, 1981; Seeburg et al., 1990). Renshaw interneurons co-release GABA and glycine neurotransmitters to strengthen inhibitory inputs (Cullheim & Kellerth, 1981; Geiman et al., 2002; Jonas et al., 1998; Schneider & Fyffe, 1992). Also, their co-release induces postsynaptic currents that are larger in amplitude and longer in duration compared with synapses that are either GABAergic or glycinergic only (Russier, Kopysova, Ankri, Ferrand, & Debanne, 2002). However, our findings are in agreement with recurrent inhibition in the Renshaw area being BBC-, but not strychnine-, sensitive (Ryall, Piercey, & Polosa, 1972). Additionally, partial modulation of $GABA_AR$s during MeHg-induced $[Ca^{2+}]_i$ increase is in agreement with previous findings in which interactions between MeHg and $GABA_AR$s have been reported. Specifically, MeHg modulates the benzodiazepine binding site in $GABA_AR$s (Fonfria et al., 2001; Komulainen, Keranen, & Saano, 1995) and MeHg suppress the GABA-induced chloride current (Arakawa et al., 1991). Also, MeHg blocks inhibitory postsynaptic current (IPSC) through $GABA_AR$s resulting in the disinhibition of excitatory synaptic transmission (Herden et al., 2008; Yuan & Atchison, 1997, 2003, 2007). Thus, inhibitory synaptic transmission is a potential target of MeHg. BCC treatment during MeHg exposure reduced onset of fluo-4 fluorescence, suggesting that $GABA_AR$s play a role during MeHg-induced $[Ca^{2+}]_i$ increase (Bradford et al., 2016) and BCC blocked the MeHg-mediated evoked inward GABA currents (Tsai et al., 2017). In cerebellar slices, time-to-block of spontaneous IPSC is faster in CGCs than in Purkinje interneurons (Yuan & Atchison, 1997). These suggest that $GABA_AR$s might be primarily responsible for the initial MeHg-induced increase in excitability. In agreement, our findings demonstrate that presence of BCC prior to and during 20 μM MeHg exposure significantly reduces MeHg-induced fluo-4 fluorescence compared to MeHg only. Thus, BCC is acting as a competitive antagonist against MeHg, impeding the heavy metal to target $GABA_AR$s. As a consequence, the MeHg-induced heightened level of excitability decreases.

MeHg-mediated dysregulation of Ca^{2+}_i through GABAergic pathways unmasks an excitatory effect through disruption of Ca^{2+} homeostasis.

Dysregulation in Ca^{2+} homeostasis initiates the activation of cell death pathways (Berridge, 1998). MeHg-induced cell death is not an immediate effect (Marty & Atchison, 1998). We demonstrate that MeHg exposure significantly increased fluo-4 fluorescence at 15 min and 1 hr post-MeHg exposure, time points at which viability in the Renshaw area was not yet compromised. However, at 3 hr post-MeHg exposure the fluo-4 fluorescence trend decreases from 1 hr post-MeHg exposure. Perhaps this suggest that cellular membranes are compromised. The 3 hr post-MeHg time correlates to the time that a significant reduction in calcein fluorescence is observed. In agreement, MeHg-dependent cytotoxicity was reported following 24 hr post-MeHg treatment in rat CGCs (Edwards et al., 2005). Also, exposure to 0.5 or 1 μM MeHg for 45 or 38 min, respectively, caused no cell death following 30 min post-MeHg exposure but a significant calcein fluorescence decrease was observed following 3.5 hr post-MeHg exposure (Marty & Atchison, 1998). The lack of an immediate cell death effect suggests that extracellular Ca^{2+} entry is associated to cell death more than Ca^{2+} efflux from internal Ca^{2+}stores (Edwards et al., 2005; Marty & Atchison, 1998). Delaying the time-to-onset of MeHg-induced $[Ca^{2+}]_i$ increase protects against cell death (Edwards et al., 2005; Limke, Bearss, et al., 2004; Marty & Atchison, 1998). We demonstrate that $GABA_A$Rs mediate MeHg-induced cytotoxicity for the first time in the Renshaw area. Similarly, BCC treatment during MeHg exposure similarly protects against excitatory-induced death of CGCs (Babot, Cristofol, & Sunol, 2005). MeHg-induced excitotoxicity can trigger apoptotic (Ceccatelli, Dare, & Moors, 2010; Nagashima et al., 1996) or necrotic (Castoldi et al., 2000) mechanisms depending on the concentration of MeHg.

Lack of protection by strychnine suggests that GlyRs do not have a role during MeHg-induced Ca^{2+} dysregulation or subsequent cell death in the Renshaw area. Likewise, a study in the cat spinal cord confirms the recurrent inhibition of MNs is to some extent insensitive to strychnine (Larson, 1969). Furthermore, strychnine treatment did not prevent MeHg-induced early increase in population spikes in recurrent inhibition of hippocampal CA1 neurons *in situ* (Yuan & Atchison, 2005). Thus, it is possible that MeHg and strychnine compete for the same binding site in the GlyR and the interaction with MeHg overcomes the binding ability of strychnine. Also, the lack of contribution from GlyRs cannot be ruled out.

In conclusion, cholinergic, GABAergic and glycinergic neurotransmission control the negative feedback mechanism in the Renshaw area. The high lipophilic properties of MeHg allows it to easily cross the blood brain barrier and accumulate in the spinal cord (Arvidson, 1992; M. Su et al., 1998). A dysfunction with upper MNs impairs communication with lower MNs and vice versa. Pathologies in the Renshaw area could decrease generation, firing, modulation of strength and pattern of limb muscles (Mazzocchio & Rossi, 2010). A damaged signal integration causes poor muscle coordination and movement. If sustained for a prolonged period of time it culminates in muscle degeneration. Inhibitory synaptic transmission have received distinctive attention as a mechanism that contributes to MN dysfunction during neurological diseases, such as amyotrophic lateral sclerosis (Guallar et al.) (Mazzocchio & Rossi, 2010; Wootz et al., 2013). ALS seems to be a cell-autonomous disease affecting αMNs. However, loss of inhibitory RCs and deficiencies in recurrent inhibition have been reported in presymptomatic ALS animals (Q. Chang & Martin, 2009, 2011; Wootz et al., 2013) and humans (Hayashi et al., 1981; Niebroj-Dobosz & Janik, 1999). This is important because it may suggest that MeHg neurotoxicity and ALS syndrome may share

a toxic pathway that when activated could trigger the expression of ALS phenotype in susceptible individuals with genetic polymorphisms (Trojsi, Monsurro, & Tedeschi, 2013). Furthermore, primary, as well as, human derived pluripotent stem cell MNs show a hightened susceptibility to MeHg neurotoxicity (Ramanathan & Atchison, 2011) (Colón-Rodríguez 2018 dissertation). Also, evidence of gene and environment interactions between MeHg and susceptible organisms has been demonstrated (Johnson et al., 2011).

CHAPTER FOUR:

ROLE OF INTERNAL CALCIUM STORES DURING ACUTE METHYLMERCURY-NEUROTOXICITY IN THE RENSHAW AREA

Mónica Ríos-Cabanillas[1,2,3] and William D. Atchison[1,2,3]

[1]Comparative Medicine and Integrative Biology Program
[2]Department of Pharmacology and Toxicology
[3]Institute for Integrative Toxicology

Michigan State University
East Lansing, MI, 48824

Abstract

Methylmercury (MeHg) crosses the blood brain barrier resulting in neurotoxicity, presenting a significant risk to public health. Previous studies demonstrate that MeHg causes a multiphasic increase in intracellular calcium concentration ($[Ca^{2+}]_i$), dependent on Ca^{2+} efflux from internal Ca^{2+} stores, producing subsequent cytotoxicity. We present for the first time evidence of the contribution of intracellular Ca^{2+} stores to MeHg neurotoxicity in MNs. Our purpose is to understand how dysregulation of $[Ca^{2+}]_i$ affects synaptic function in neuronal circuits responsible for the regulation of motor function. One such critical circuit is recurrent inhibition in the spinal cord. This synaptic circuit is comprised of alpha motor neurons (αMNs) and interneurons know as Renshaw cells. The latter are inhibitory interneurons which regulate motor function. Previous work has demonstrated that MeHg causes death of αMNs and disrupts inhibitory synaptic function. Accordingly, we used Fluo4-AM to measure Ca^{2+} changes in the Renshaw area and calcein-AM to assess viability in lumbar spinal cord slices. MeHg (20 μM) was applied by perfusion for 15 min. Subsequently, recordings were made immediately at the conclusion of exposure (15 min) or at 1 or 3 hr after MeHg application ceased. Antagonists for the smooth endoplasmic reticulum Ca^{2+}-ATPase (SERCA) (thapsigargin (THP), 2 μM) or the mitochondrial oxidative phosphorylation uncoupler (carbonyl cyanide m-chlorophenyl hydrazine (CCCP), 10 μM) were applied in conjunction with MeHg following a 5 min pre-exposure in MeHg-free solution. MeHg increased fluo-4 fluorescence intensity from baseline at 15 min (51%) and 1 hr post-MeHg (57%). MeHg decreased calcein fluorescence at 3 hr post-MeHg (-48%). MeHg in presence of CCCP+THP significantly decreased fluo-4 fluorescence at 1 hr post-MeHg (64%) but did not preserve cell viability. Taken together, our results indicate that depletion of intracellular stores with CCCP+THP reduces MeHg-mediated $[Ca^{2+}]_i$ increase but does not protect against MeHg-

induced cytotoxicity, suggesting the participation of other mechanisms in MeHg-induced cell death.

Key Words: Fluo-4, Calcein, Neurotoxicity, Intracellular Calcium, Calcium-Induced Cytotoxicity, Recurrent Inhibition.

Introduction

The Renshaw area is located in the ventral lumbar lamina VII of the spinal cord, specifically medial to the lateral motor neurons (MNs). MNs stimulate muscles, and simultaneously through an axon collateral, they synapse inhibitory Renshaw interneurons (Geiman et al., 2000; Geiman et al., 2002; Wootz et al., 2013). In turn, Renshaw cells (RCs) inhibit MNs and participate in the negative feedback circuit known as recurrent inhibition (Eccles et al., 1954; Renshaw, 1946). Methylmercury (MeHg) is a persistent neurotoxicant that consistently alters internal calcium (Ca^{2+}_i) homeostasis in many cell types, including spinal MNs (Ramanathan & Atchison, 2011). MeHg accumulates in MNs located in the ventral horn of the spinal cord. As a result, MeHg exposure causes hind leg weakness and discoordination in rats (Moller-Madsen, 1990; M. Su et al., 1998). MeHg neurotoxicity is associated with "myasthenia gravis-like" syndromes (Rustam et al., 1975), ataxia and motor degeneration (Bakir et al., 1973; Eto, 2006; M. Harada, 1995). Additionally, protective effects of nimodipine on Ca^{2+} pathways suggest that MeHg-mediated disruption of Ca^{2+}_i homeostasis is associated to MeHg-induced motor dysfunction (Bailey et al., 2013).

MeHg-mediated disruption of nerve-evoked neurotransmitter release occurs through presynaptic mechanisms (Atchison & Narahashi, 1982; Juang, 1976b). Presynaptic Ca^{2+}_i determines the rate of spontaneous neurotransmitter release (Atchison & Narahashi, 1982; Bardo, Robertson, & Stephens, 2002; Kavalali, 2015; Levesque & Atchison, 1987; Savic & Sciancalepore, 1998). Thus, time-to-onset of elevations in MeHg-mediated Ca^{2+}_i concentrations ($[Ca^{2+}]_i$) correlate to MeHg-induced increase in both frequency and amplitude of excitatory and inhibitory postsynaptic currents (Yuan & Atchison, 1993). MeHg exposure disrupts mitochondrial Ca^{2+} regulation (Hare

et al., 1993; Levesque & Atchison, 1991; Levesque, Hare, & Atchison, 1992; Limke & Atchison, 2002; Limke et al., 2003). In a separate study, inhibition of mitochondrial Ca^{2+} regulation reduced acetylcholine (ACh) release (Levesque & Atchison, 1987; Levesque et al., 1992). Reduction of free $Ca^{2+}{}_i$ with 1,2-Bis(2-aminophenoxy)ethane-N,N,N′,N′-tetra acetic acid tetrakis (BAPTA) suppressed the MeHg-induced initial stimulation of spontaneous inhibitory postsynaptic current frequency (Yuan & Atchison, 2007). These findings suggest that presynaptic MeHg-mediated $[Ca^{2+}]_i$ increase is an important contributor to neurotransmitter release and postsynaptic responses.

The mitochondrion is a low-affinity, high-capacity Ca^{2+} pool (Budd & Nicholls, 1996; Nicholls & Akerman, 1982) and the smooth endoplasmic reticulum (SER) is a high-affinity, low capacity Ca^{2+} pool (Fohrman et al., 1993; Masgrau et al., 2000). MeHg induces a characteristic elevation of $[Ca^{2+}]_i$ consisting of two kinetically and temporally distinct phases. “Phase 1” represents Ca^{2+} efflux from both mitochondria and, principally, inositol-1,4,5-triphosphate (IP3)-mediated SER. “Phase 2” represents extracellular Ca^{2+} influx (Denny et al., 1993; Edwards et al., 2005; Hare & Atchison, 1995; Hare et al., 1993; Limke, Bearss, et al., 2004; Marty & Atchison, 1997; Ramanathan & Atchison, 2011). In CGCs, MeHg depolarizes the mitochondria and causes a biphasic $[Ca^{2+}]_i$ elevation. This increase was ablated during phase 1 with cyclosporin-A (CsA), the specific antagonist for the mitochondrial permeability transition pore (mPTP) (Limke & Atchison, 2002). Thus, time-to-onset of phase 1 but not phase 2 was significantly delayed. This suggests that the mitochondrial Ca^{2+} stores contribute to phase 1. Also it is known that the SER also contributes to phase 1 in cerebellar granule cells (CGCs) because, SER-Ca^{2+} depletion with thapsigargin (THP) reduced the Ca^{2+} amplitude in phase 1 (Hare & Atchison, 1995; Limke, Bearss, et al., 2004). Hence, both the mitochondria and the SER contribute to Ca^{2+} dysregulation during MeHg toxicity.

In detail, the initial Ca^{2+} wave in phase 1 originates from the IP3-sensitive store. Next, Ca^{2+} is buffered by the mitochondria matrix through the Ca^{2+} uniporter, only for Ca^{2+} to be released again through the mPTP into the cytosol (Limke & Atchison, 2002; Limke et al., 2003). The contribution from these Ca^{2+} stores to $[Ca^{2+}]_i$ is cell-type dependent because in neuroblastoma cells the initial effect of MeHg is Ca^{2+} release from the SER (Hare & Atchison, 1995). However, in CGCs, MeHg-mediated phase 1 occurs primarily due to mechanisms that involve the mitochondria (Limke & Atchison, 2002; Limke et al., 2003). Furthermore, Ca^{2+} release from the mitochondria has been reported to contribute to MeHg-induced ACh release in rat brain synaptosomes (Levesque & Atchison, 1991; Levesque et al., 1992).

Studies demonstrate that MeHg accumulates in the mitochondria (Sone, Larsstuvold, & Kagawa, 1977; Yoshino, Mozai, & Nakao, 1966), disrupts the mitochondrial membrane potential (Kauppinen et al., 1989), inhibits the mitochondrial respiration (Tiernan 2013 dissertation) and production of adenosine triphosphate (ATP) (Levesque & Atchison, 1991; Sone et al., 1977), generates reactive oxygen species (ROS) (LeBel, Ali, McKee, & Bondy, 1990), and increases intramitochondrial Ca^{2+} levels (Dreiem & Seegal, 2007; Limke et al., 2003). Likewise, at the whole organism level, MeHg-mediated disruption of $Ca^{2+}{}_i$ homeostasis has been reported to cause mitochondrial dysregulation, reduce mitochondrial membrane potential through opening of the mPTP and increase cytosolic cytochrome-c levels in CGCs (Bellum et al., 2007; Ceccatelli et al., 2010). In the SER, THP treatment depletes SER-Ca^{2+} during MeHg exposure and significantly reduced the contribution from intracellular Ca^{2+} stores to the elevations in $[Ca^{2+}]_i$ caused by MeHg (Limke, Bearss, et al., 2004).

Evidence suggest a relationship between MeHg-induced disruption of Ca^{2+}_i regulation and incidence of cytotoxicity (Limke, Bearss, et al., 2004; Marty & Atchison, 1998). Application of specific membrane receptor inhibitors improves survival (Choi, 1988) of MeHg-treated cells (Limke, Bearss, et al., 2004; Marty & Atchison, 1998; Sakamoto et al., 1996). The mitochondria (Hare et al., 1993; Levesque et al., 1992; Limke & Atchison, 2002; Limke et al., 2003) and the SER (Hare & Atchison, 1995; Limke et al., 2003) contribute to MeHg-induced neurotoxicity. MeHg-mediated dysregulation of $[Ca^{2+}]_i$ causes cell death in a time- and concentration-dependent manner (Limke & Atchison, 2002; Limke, Bearss, et al., 2004; Marty & Atchison, 1997, 1998). Increase in Ca^{2+}_i due to dysregulation of the mPTP or reversal of the uniporter contributes to cell death (Bernardi et al., 1999). However, inhibition of the mPTP with bcl-2 reduces MeHg-mediated neuronal mortality (T. A. Sarafian et al., 1994). CsA treatment to inhibit mPTP and atropine to cause downregulation and desensitization of muscarinic and IP3 receptors, respectively, caused partial protection against MeHg-induced cytotoxicity in CGCs (Limke & Atchison, 2002; Limke, Bearss, et al., 2004). Also, activation of IP3 receptors opens the mPTP and correlates with cell death mediated by cytochrome-c mechanisms (Szalai, Krishnamurthy, & Hajnoczky, 1999).

The consequences of MeHg-mediated increase in $[Ca^{2+}]_i$ due to contributions from the mitochondria and SER which could lead to cytotoxicity in the Renshaw area have not yet been elucidated. This study is the first to determine whether intracellular Ca^{2+} stores contribute to MeHg-induced $[Ca^{2+}]_i$ dysregulation and subsequent cytotoxicity in the Renshaw area. We hypothesize that Ca^{2+} depletion from intracellular Ca^{2+} stores with the combination of carbonyl cyanide m-chlorophenyl hydrazone (CCCP) and THP, superimposed upon MeHg-mediated Ca^{2+} dysregulation, will decrease MeHg-induced $[Ca^{2+}]_i$ increase and diminish subsequent cytotoxicity

in situ. In detail, CCCP depolarizes the inner mitochondrial membrane by increasing the membrane permeability to H^+. It uncouples oxidative phosphorylation and depletes mitochondrial Ca^{2+} causing an $[Ca^{2+}]_i$ increase while inhibiting mitochondrial Ca^{2+} accumulation (Budd & Nicholls, 1996). THP blocks the SER Ca^{2+}-ATPase (SERCA) pump and prevents the uptake of cytosolic Ca^{2+} (Denmeade & Isaacs, 2005; Thastrup et al., 1990). To test MeHg-induced neurotoxicity on the Renshaw area, $[Ca^{2+}]_i$ dysregulation and cell death was measured in the absence or presence of the pharmacology during an acute exposure to MeHg. We provide direct evidence that intracellular Ca^{2+} stores contribute to MeHg-mediated increase in $[Ca^{2+}]_i$ but they do not contribute to MeHg-induced cytotoxicity.

Materials and methods

Materials and experimental solutions

Tissue dissections were carried out in a slicing solution containing (in mM): 62.5, NaCl; 2.5, KCl; 5, $MgCl_2$; 1.25, KH_2PO_4; 26, $NaHCO_3$; 0.5, $CaCl_2$; 20, D-glucose; and 107, sucrose (pH 7.4 when saturated with 95% O_2 /5% CO_2 at 25°C). The slicing solution contains low concentrations of Na^+ and Ca^{2+} but high concentrations of Mg^{2+} in order to reduce cellular damage during tissue slicing. N-methyl-D-glucamine (NMDG) solution contained (in mM): 125, NMDG; 2.5, KCl; 1.25 KH_2PO_4; 26, $NaHCO_3$; 5, $MgCl_2$; 0.5, $CaCl_2$; and 20, D-glucose (pH 7.4 when saturated with 95% O_2 /5% CO_2 at 25°C). This solution preserves the spinal cord morphology and its synaptic functions by causing the membrane potential to hyperpolarize. Artificial cerebrospinal fluid (ACSF), in which all experiments were conducted, consisted of (in mM): 125, NaCl; 2.5, KCl; 1, $MgCl_2$; 1.25, KH_2PO_4; 26, $NaHCO_3$; 2, $CaCl_2$ and 20, D-glucose (pH 7.4 when saturated with 95% O_2 /5% CO_2 at 25°C). The 40 mM K^+ solution contained the same components as ACSF but with

40 mM K^+ and 115.4 mM NaCl. The K^+ solution depolarizes the cellular membrane of viable cells. MeHg chloride was purchased from ICN Biochemical Inc. (Aurora, OH). A 10 mM MeHg stock solution was prepared in double-distilled H_2O stored at 4°C. Experimental solutions were prepared on the day of the experiment by diluting the MeHg stock solution at the desired working concentration in ACSF solution in the absence or presence of pharmacologic drugs. The MeHg concentration of 20 μM was chosen for all experiments because it represents the concentration of mercury found in the blood of persons that was contaminated with MeHg dicyandiamide through grain consumption during the Iraq MeHg outbreak (Bakir et al., 1973). Additionally, this MeHg concentration has been used in numerous studies from our laboratory using tissue slices (Yuan & Atchison, 2005, 2007, 2016). CCCP and THP, the mitochondria uncoupler and SERCA pump specific inhibitors, respectively, were purchased from Tocris-Bioscience (Minneapolis, MN). Antagonist stocks were prepared in double distilled H_2O or following manufacturers recommendations. Fluo-4 was purchased from Thermo Fisher Scientific (Waltham, MA) and the Live/Dead™ viability/cytotoxicity kit, for mammalian cells, was purchased from Molecular Probes (Invitrogen, Eugene, OR). Disposable or MeHg-contaminated materials used during the preparation and experiment were discarded following the Michigan State University (MSU) Office of Radiation, Chemical, and Biological Safety (ORCBS) guidelines.

Lumbar C57BL6J slice

All animal procedures adhered to National Institute of Health (Aberg et al.) guidelines and were approved by the MSU Institutional Animal Care and Use Committee (IACUC). Adult C57BL6J mice (40-60 days postnatal, either gender) were obtained from Jackson Laboratories (Bar Harbor, ME). Mice were housed in pairs, fed standard diet (Harland, Teklab 18% Protein Global Rodent

Diet), and exposed to normal light-dark cycle. Following anesthesia with CO_2 in a dedicated chamber, mice were quickly decapitated, the spinal cord was speedily removed, the lumbar region dissected and rapidly submerged in ice-cold slicing solution. This solution is a low [Na^+], low [Ca^{2+}] and high [Mg^{2+}] solution, that helps to reduce cellular damage during tissue slicing. Working with very cold solutions protects against cellular swelling and death (Liang et al., 2007; Won et al., 2002). Experiments utilized tissue preparation and incubation methods previously described (Yuan & Atchison, 1999, 2007, 2016) with modifications specifically designed for spinal cord and described below. The lumbar tissue was sliced into 180 μm transverse sections using a Leica VT100S Vibratome (Leica Microsystems Inc., Bannockburn, IL). Individual slices were transferred to an incubation chamber containing NMDG solution for 15 min to preserve the function of chemical synapses for experiment conditions. Slices were then transferred and maintained to a 1:1 mix of oxygenated slicing solution and ACSF for approximately 30 min at room temperature. Then, lumbar slices were transferred to 100% ACSF in order to allow quick and controlled treatment of tissues with MeHg, without damaging much of the tissue morphology. Finally, slices were incubated for 40 min in ACSF with fluo-4 acetoxymethyl ester (AM), which labels divalent cations, or in a viability assay that utilizes calcein AM, a fluorescent dye that stains viable cells green.

Confocal Ca^{2+} microscopy

Fluo-4 AM no wash (NW) (4 μM) in the presence of probenecid (2.5 μM) were obtained from Invitrogen Molecular Probes (Eugene, OR). Fluo-4 AM NW is a fluorophore that has been extensively used to monitor MeHg-induced $Ca^{2+}{}_i$ changes. Thus, it is used to indicate relative changes in $[Ca^{2+}]_i$ (Bradford et al., 2016; Johnson et al., 2011; Yuan & Atchison, 2007, 2016).

Probenecid inhibits organic-anion transporters, which can extrude dye loading. Slices were loaded for 40 min at room temperature in fluo-4 AM NW with probenecid in the presence of 0.02% (w/v^{-1}) pluronic F-127, to facilitate dye solubilization (Yuan & Atchison, 2016). Slices are then washed thoroughly with ACSF before Ca^{2+} imaging recordings. Confocal images of $[Ca^{2+}]_i$ represented by fluo-4 fluorescence were obtained using a Leica TCS SL laser scanning confocal microscope system equipped with Nomarski optics (10x water immersion objective) (Leica Microsystem, Heidelberg GmbH., Germany). Fluo-4 is excited at 485 nm from an argon laser and emits fluorescence at 520 nm. Images (512 x 512 pixels, xyz scan mode) were collected during perfusion with ACSF, 40 mM KCl, during ACSF-containing MeHg and post MeHg exposure in the absence or presence of CCCP (10 μM) + THP (2 μM). A mitochondrial study on neurons *in situ* from C57BL6J mice used 10 μM CCCP (Stanford & Taylor-Clark, 2018) because this concentration depolarizes the mitochondria without inducing toxicity (Li et al., 2014). Also, due to non-specific binding capacities and tissue density, the concentration of CCCP (10 μM) *in situ* should be higher than in *in vitro* experiments that used 5 μM CCCP in CGCs (Limke et al., 2003). THP concentrations ranging from 2-4 μM are effective in reducing neurotransmitter release by reduction of Ca^{2+}_i (Behnisch & Reymann, 1995; Cong, Takeuchi, Tokuno, & Kuba, 2004; Haddock & Hill, 2002) and in previous studies from our laboratory we have used 1 μM THP in rat cerebellar slices (Yuan & Atchison, 2016). Dysregulation of Ca^{2+}_i homeostasis mediated by MeHg exposure was assessed at 15 min MeHg exposure, 1 and 3 hr post-MeHg exposure. All experiments were oxygenated with 95% O_2 /5% CO_2 and performed at 25°C. An increase in fluo-4 fluorescence intensity corresponds to an increase in cytosolic Ca^{2+}. Fluo-4 fluorescence was utilized to monitor spatial changes in Ca^{2+}_i in the lumbar ventral region spinal cord of C57BL6J mice in response to acute exposure of MeHg treatment *in situ*.

Measurement of tissue viability

MeHg-mediated loss of cell viability was measured using a commercial fluorimetric cell viability assay as previously described (Bradford et al., 2016; Limke, Bearss, et al., 2004; Marty & Atchison, 1998). Briefly, viability was indicated by calcein-AM, a fluorescent dye that stains the cytoplasm of live, healthy cells in green (Papadopoulos et al., 1994). Calcein is excited at 495 nm and emits fluorescence at 515 nm. Lumbar spinal cord slices were monitored during perfusion with ACSF loaded with calcein for 40 min in oxygenated solution with 95% O_2/5% CO_2 and performed at 25°C. Viability was assessed immediately at the conclusion of exposure (15 min) or 1 or 3 hr after MeHg application ceased, in the absence or presence of antagonists. Cytotoxicity assay visualization was determined with a 10x water immersion objective and images were obtained using a Leica TCS SL laser scanning confocal microscope system equipped with Nomarski optics.

Statistics

Analysis of fluo-4 and calcein changes in fluorescence intensity were performed using the Leica software. In fluo-4 or calcein experiments, before MeHg exposure began, three scattered regions of interest (ROI) were selected within the Renshaw area. The same ROI were monitored from the beginning to the end of the experiment. The ROI in fluo-4 experiments consisted of the average from three different fluorescent cells easily observed with a 10x objective (Fig 4.1A). Viability in the Renshaw area as indicated by calcein fluorescence was measured by three randomly selected ROI (Fig 4.1B). Fluorescence intensity data in the same layer were averaged and the background fluorescence was subtracted from all ROI before calculating fluo-4 and calcein mean fluorescence intensity. Untreated (MeHg control) slices with fluo-4 or calcein, were used to monitor photobleaching with the same duration as MeHg treated experimental slices. For each experiment

the average from three ROI was taken and was expressed as ± standard error of the mean (SEM). To avoid variability between slices MeHg experiments in presence of pharmacologic drugs were conducted on the same experimental day. To analyze one or among different groups a one-way or two-way analysis of variance (ANOVA), respectively, was used with GraphPad Prism® software (GraphPad Software Inc., San Diego, CA). A *post hoc* comparison with Tukey's, Dunnette's or Sidak's was used when significant differences between means were found (Steel & Torrie, 1960). Values are considered statistically significant at $p < 0.05$.

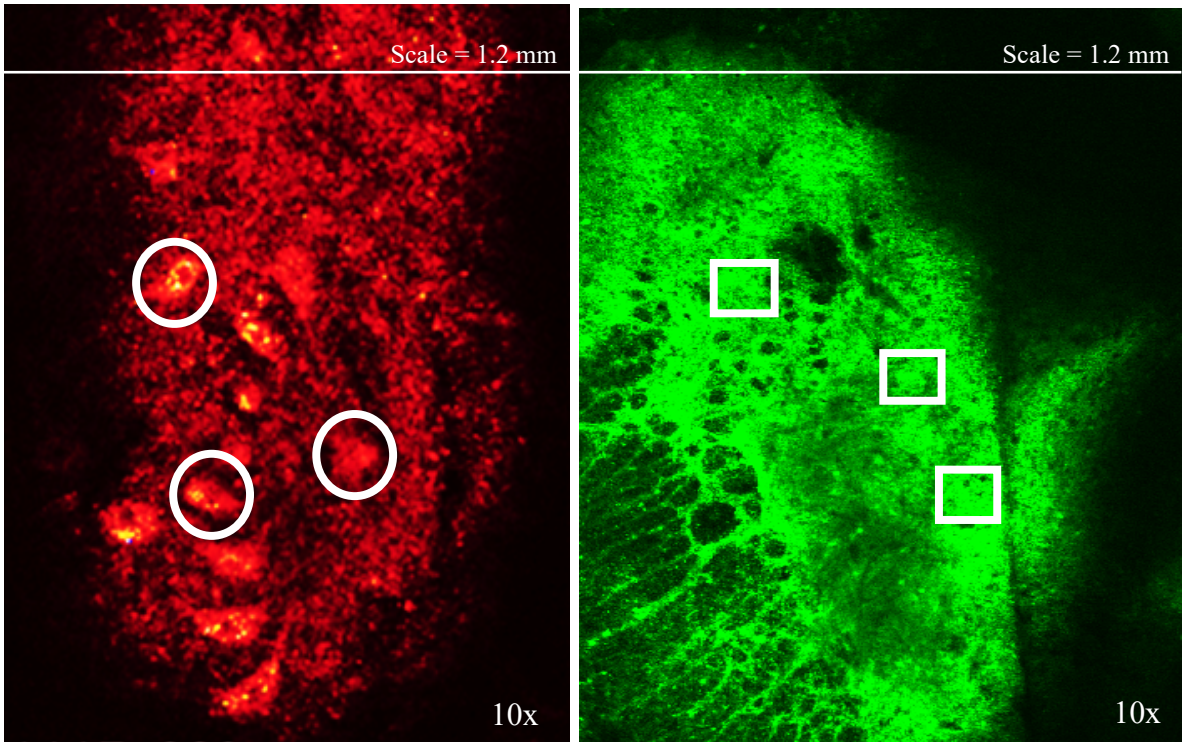

Figure 4.1. Representative pseudocolor epimicrograph of the Renshaw area from a C57BL6J mouse. The Renshaw area is located in the ventral lumbar lamina VII of the spinal cord. A) Fluo-4 (red) fluorescence indicates intracellular Ca^{2+} concentration. Depicted are three different MNs (defined as ROI) selected at random. B) Calcein (green) fluorescence indicates viable cells in the tissue. Three scattered ROI were selected at random. Images were obtained using a Leica TCS SL laser scanning confocal microscope system equipped with Nomarski optics (10x water immersion objective). Scale bar represents 1.2 mm.

Results

MeHg-mediated dysregulation of Ca^{2+} in the Renshaw area

MeHg-mediated increase in $[Ca^{2+}]_i$ previously has been demonstrated in isolated mouse spinal cord MNs *in vitro* (Ramanathan & Atchison, 2011). To determine if MeHg causes alterations in $Ca^{2+}{}_i$ homeostasis in the Renshaw area, recordings were performed *in situ*. Fura-4 fluorescence was measured after 15 min MeHg exposure, or 1 and 3 hr post 15 min MeHg exposure in order to account for both MeHg immediate and delayed effects. Treatment with 40 mM KCl for 3 min before MeHg exposure caused a slight increase in fluo-4 fluorescence associated with Renshaw area depolarization. This demonstrates that neurons *in situ* have healthy membranes before exposure to MeHg. MeHg exposure caused a significant increase in fluo-4 fluorescence intensity from baseline in a time-dependent manner at both 15 min and 1 hr post-MeHg by 51% and 57% mean increase, respectively (Fig 4.2). However, by 3 hr post-MeHg, fluo-4 fluorescence intensity had diminished back towards control levels (Fig 4.2). Perhaps, this suggests that the cell membrane is compromised due to the high $Ca^{2+}{}_i$ levels (Berridge, 1998). For this reason, the following fluo-4 fluorescence measurements will be limited to 15 min and 1 hr post-MeHg exposure. Over a period of 3 hr there was no significant change in fluo-4 fluorescence intensity in the absence of MeHg (result not shown). Thus, increases in fluo-4 florescence are not due to fluo-4 photobleaching during imaging. Together, results suggest that acute exposure to MeHg causes a direct effect directly upon cessation of treatment (15 min) which is sustained at delay timepoints (1 hr post-MeHg), but subsided by 3 hr post-MeHg exposure. Hence, the Renshaw area is susceptile to altreations in $Ca^{2+}{}_i$ homeostasis by MeHg.

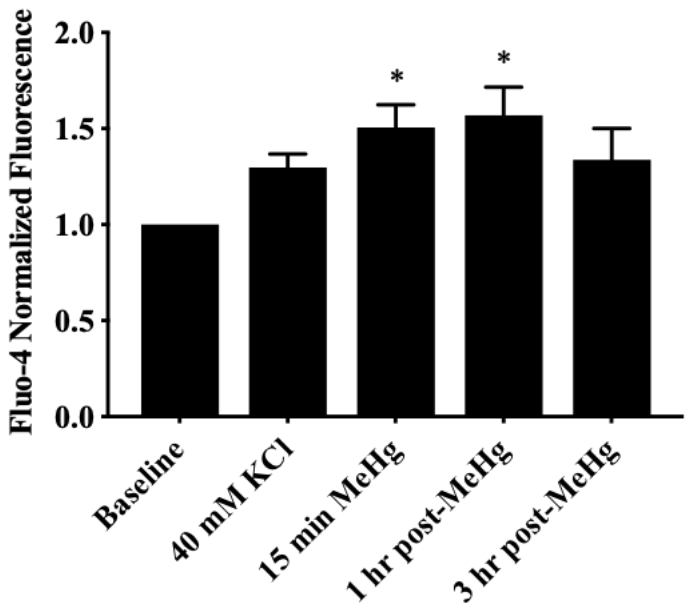

Figure 4.2. Immediate and delayed increase in $[Ca^{2+}]_i$ following acute exposure to 20 μM MeHg *in situ* in the Renshaw area. Perfusion with 40 mM KCl-induced depolarization of the plasma membrane slightly increases fluo-4 fluorescence intensity. Exposure to 20 μM MeHg for 15 min significantly increases fluo-4 fluorescence at both 15 min MeHg and 1 hr post-MeHg compared to baseline, denoted by asterisk (*). By 3 hr post-MeHg, fluo-4 fluorescence intensity had diminished back towards control levels. Data are presented as mean ± S.E.M. (n = 11). All *n* values are averages of 3 replicates. Statistics are performed using a one-way analysis of variance followed by Tukey's multiple comparison test. Statistical significance is considered $p < 0.05$.

MeHg-induced cell death in the Renshaw area

Next, we aim to determine whether MeHg-mediated $[Ca^{2+}]_i$ increase in the Renshaw area contributes to cytotoxicity. Exposure to MeHg for 15 min significantly decreased calcein fluorescence at 3 hr post-MeHg from baseline, 15 min MeHg and 1 hr post-MeHg by 48%, 46%, 31%, respectively (Fig 4.3). The immediate, 15 min, MeHg exposure did not affect calcein fluorescence. This suggests that MeHg does not cause a cytotoxicity effect directly upon cessation of MeHg treatment. Over time, there was no significant decrease in calcein fluorescence in the absence of MeHg (result not shown). Thus, MeHg exposure causes a delayed cytotoxicity in the Renshaw area.

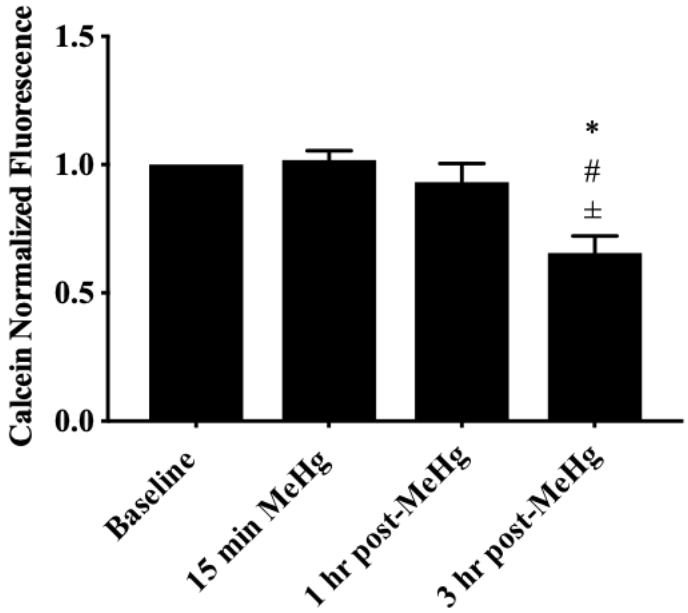

Figure 4.3. Calcein mean fluorescence in the Renshaw area is reduced at 3 hr post-MeHg but not 1 hr post-MeHg or 15 min MeHg. Exposure to 20 μM MeHg during 15 min significantly decreased calcein AM fluorescence at 3 hr post-MeHg exposure when compared to baseline, 15 min MeHg, and 1 hr post-MeHg denoted by the asterisk (*), pound (#), plus/minus (±), respectively. Data are presented as mean ± S.E.M. (n = 8) for all groups. All *n* values are averages of 3 replicates from the same slice. Statistics are performed using a one-way analysis of variance followed by Tukey's multiple comparison test. Statistical significance is considered at $p < 0.05$.

Internal Ca^{2+} stores contribute to MeHg-mediated Ca^{2+} dysregulation in the Renshaw area

To examine the contribution of internal Ca^{2+} stores to MeHg-induced $[Ca^{2+}]_i$ increase in the Renshaw area, CCCP + THP were used prior to, as well as during, MeHg (20 μM). CCCP depletes Ca^{2+} from the mitochondria and THP inhibits Ca^{2+} uptake mediated by the SERCA. In detail, THP with prolonged exposure will disrupt the normal Ca^{2+} cycling in the SER, involving tonic Ca^{2+} efflux and subsequently leading to depletion of Ca^{2+} (Berridge, 2016). CCCP + THP treatment in the absence of MeHg significantly increased fluo-4 fluorescence at 1 hr post-CCCP+THP compared to baseline (Fig 4.4). Thus, cytosolic Ca^{2+} stores released sufficient Ca^{2+} suggesting Ca^{2+} depletion. MeHg + CCCP + THP treatment did not increase fluo-4 fluorescence intensity at 15 min MeHg or 1 hr post-MeHg compared to baseline (Fig 4.5). Perhaps the mitochondria and the SER contribute to MeHg-mediated increase in $[Ca^{2+}]_i$ but because they have been depleted from Ca^{2+} there is no increase in fluo-4 fluorescence. Exposure to MeHg + CCCP + THP compared to MeHg alone significantly reduced fluo-4 fluorescence intensity at 1 hr post-MeHg exposure by 64% fluo-4 fluorescence (Fig 4.6). During MeHg alone or during CCCP + THP alone no reduction in fluo-4 fluorescence was observed at 1 hr post-MeHg. Thus, this reduction is due to an interaction between MeHg with the pharmacologic tools. These results suggest that internal Ca^{2+} stores contribute to disruption of $Ca^{2+}{}_i$ levels in MN during and following MeHg neurotoxicity.

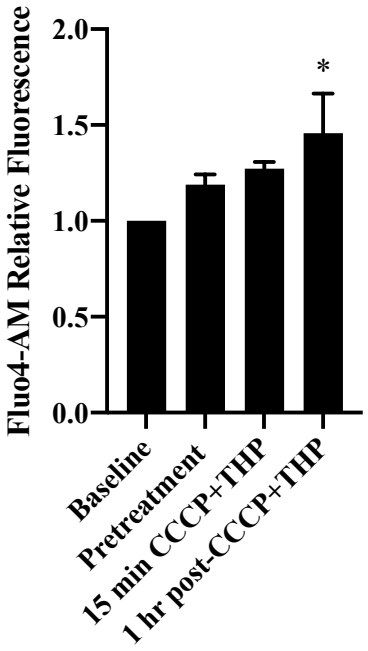

Figure 4.4. CCCP + THP treatment in the absence of MeHg deplete intracellular Ca^{2+} stores in the Renshaw area. Exposure to both antagonists for 20 min does not increase fluo-4 fluorescence intensity. However, at 1 hr after cessation of the antagonist treatment there is a significant increase in fluo-4 fluorescence, denoted by asterisk (*). Data are presented as mean ± S.E.M. (n = 3). All *n* values are averages of 3 replicates from the same slice. Statistics are performed using a one-way analysis of variance followed by Dunnett's multiple comparison test. Statistical significance is considered at $p < 0.05$.

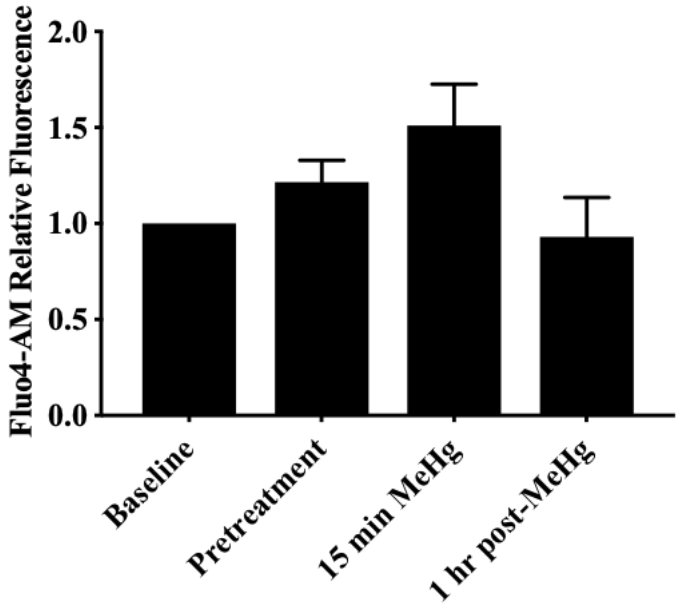

Figure 4.5. Immediate and delayed changes in $[Ca^{2+}]_i$ following acute exposure to MeHg + CCCP + THP *in situ* in the Renshaw area. Exposure to CCCP + THP prior to and during a continuous exposure of 20 μM MeHg for 15 min does not change fluo-4 fluorescence intensity at 15 min MeHg from baseline. CCCP + THP treatment prevents MeHg-induced fluo-4 fluorescence increase at 1 hr post-MeHg exposure. Data are presented as mean ± S.E.M. (n = 5) for baseline, pretreatment and 15 min MeHg, (n = 4) for 1 hr post-MeHg group. All *n* values are averages of 3 replicates. Statistics are performed using a one-way analysis of variance followed by Tukey's multiple comparison test. Statistical significance is considered $p < 0.05$.

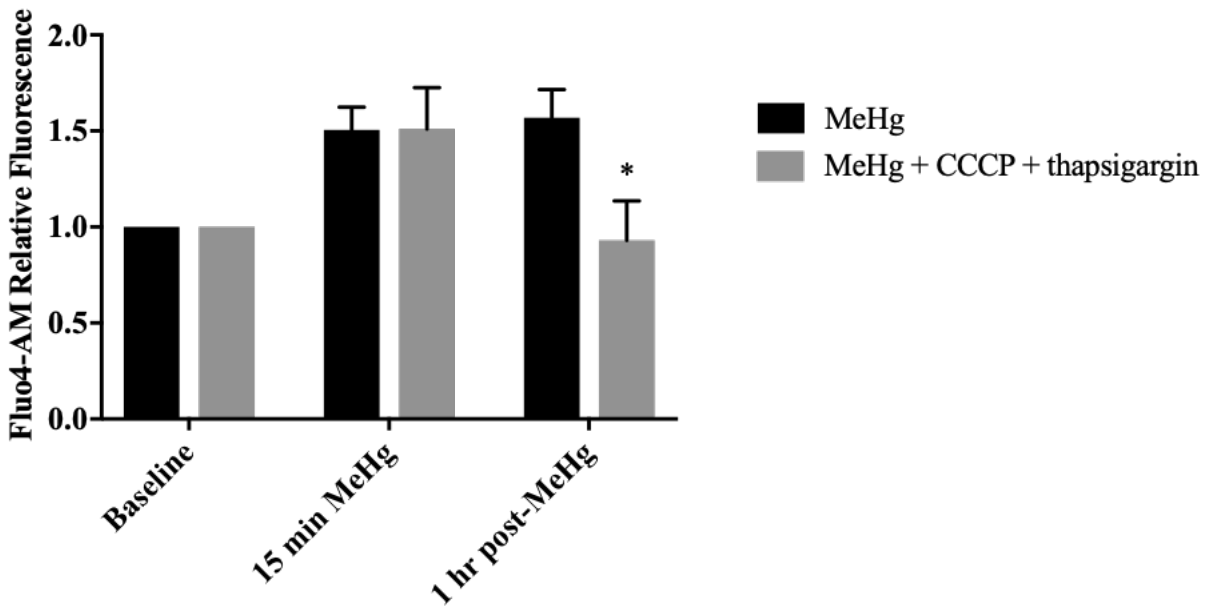

Figure 4.6. Fluo-4 fluorescence comparison between MeHg alone and MeHg + CCCP + THP in the Renshaw area. Mitochondria and SER depletion with CCCP and THP, respectively, did not affect MeHg-induced $[Ca^{2+}]_i$ at 15 min MeHg. However, at 1 hr post-MeHg, presence of CCCP + THP significantly reduced fluo-4 fluorescence intensity compared to 1 hr MeHg in the absence of CCCP + THP, denoted by asterisk (*). Data are presented as mean ± S.E.M. (n = 11) for all MeHg groups in the absence of CCCP + THP. MeHg in the presence of CCCP + THP, data are presented as mean ± S.E.M. (n = 5) for baseline, pretreatment and 15 min MeHg and (n = 4) for 1 hr post-MeHg group. Statistics are performed using a two-way analysis of variance followed by Sidak's multiple comparison test. Statistical significance is set at $p < 0.05$.

MeHg-induced cell death does not depend on internal Ca^{2+} stores in the Renshaw area

Next, we examined whether emptying Ca^{2+} from the mitochondria and the SER was protective against MeHg-induced reduction of viability at 15 min, 1 and 3 hr post-MeHg exposure. The Renshaw area was exposed to CCCP + THP for 5 min prior to, as well as, during MeHg treatment. MeHg exposure for 15 min significantly decreased calcein mean fluorescence intensity in a time-dependent fashion. MeHg + CCCP + THP treatment at 3 hr post-MeHg timepoint was significantly reduced from baseline, pretreatment, 15 min MeHg, and 1 hr post-MeHg by 48%, 51%, 46%, 31%, respectively (Fig 4.7). A similar pattern in calcein fluorescence is observed when comparing MeHg-induced cytotoxicity in the absence or presence of the pharmacologic drugs (Fig 4.8). Thus, depletion of internal Ca^{2+} stores with CCCP + THP treatment did not protect against MeHg-induced cell death in the Renshaw area.

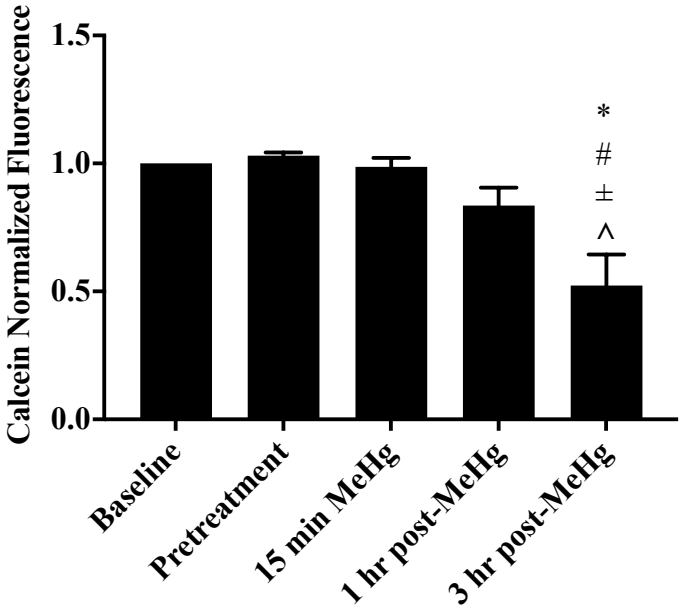

Figure 4.7. Incidence of cytotoxicity at immediate and delayed time points following MeHg perfusion with CCCP + THP in the Renshaw area. Acute 20 μM MeHg exposure in the presence of CCCP + THP did not cause a decrease in calcein fluorescence prior to 3 hr post-MeHg. A significant time-dependent decrease in calcein fluorescence is observed at 3 hr post-MeHg exposure when compared to all other groups, denoted by asterisk (*), pound (#), plus/minus (±), up (^), respectively. Data are presented as mean ± S.E.M. (n = 4). All *n* values are averages of 3 replicates. Statistics are performed using a one-way analysis of variance followed by Tukey's multiple comparison test. Statistical significance is considered $p < 0.05$.

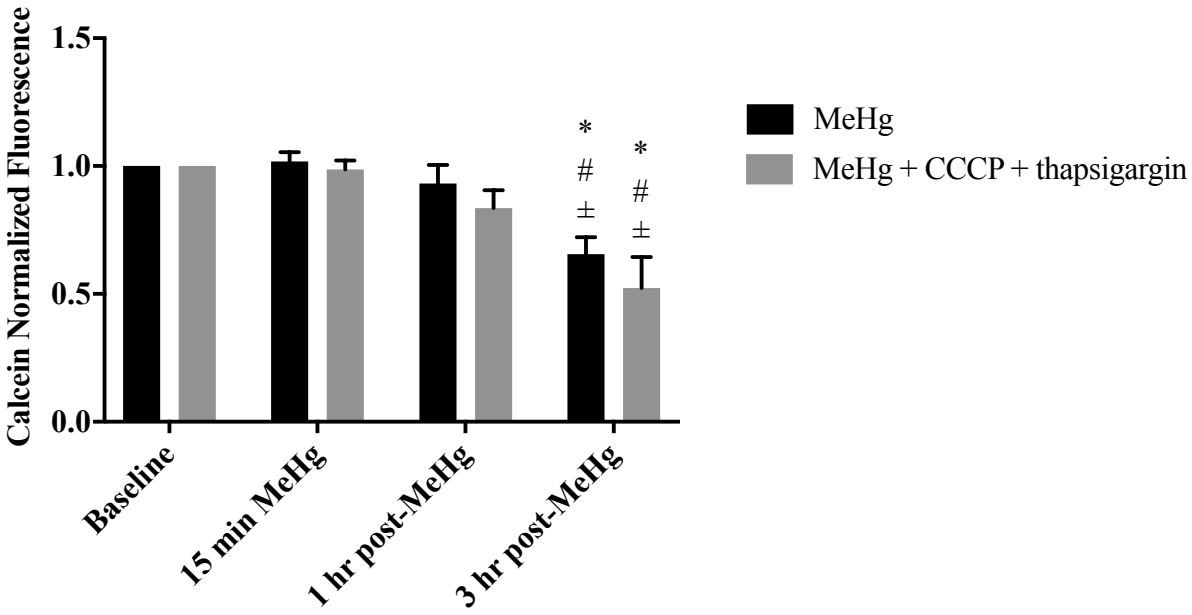

Figure 4.8. Comparison of calcein fluorescence intensity following continuous treatment with MeHg with or without CCCP + THP in the Renshaw area. Values were obtained at the conclusion of the 15 min MeHg incubation or 1 or 3 hr post incubation. Exposure to CCCP + THP prior to and during MeHg exposure did not increase calcein fluorescence intensity compared to MeHg alone treatment at any timepoint. A significant time-dependent decrease in calcein fluorescence is observed at 3 hr post-MeHg in the absence and presence of CCCP + THP. Significant is denoted by asterisk (*), pound (#), plus/minus (±) when compared to baseline, 15 min MeHg and 1 hr post-MeHg, respectively. Data are presented as mean ± S.E.M. (n = 8) for all MeHg groups in the absence of CCCP + THP. Data are presented as mean ± S.E.M. (n = 4) for all MeHg groups in the presence of CCCP + THP. Statistics are performed using a two-way analysis of variance followed by Sidak's multiple comparison test.

Discussion

This research highlights the contribution of internal Ca^{2+} stores during MeHg-induced increase in $[Ca^{2+}]_i$ of MN and subsequent cell death in the Renshaw area. Previous studies demonstrate supporting evidence for the contribution of intracellular Ca^{2+} stores to MeHg-induced increase in $[Ca^{2+}]_i$ (Denny et al., 1993; Dreiem & Seegal, 2007; Limke et al., 2003). In isolated rat forebrain mitochondria, MeHg stimulates mitochondrial $^{45}Ca^{2+}$ release and reduces both Ca^{2+} reuptake and buffering capacities through the Ca^{2+} uniporter (Levesque & Atchison, 1991). MeHg-induced elevations in $[Ca^{2+}]_i$ reduced when synaptosomes were pretreated with rotenone, a mitochondrial electron transport chain complex 1 inhibitor, or oligomycin A, the ATP synthase inhibitor (Komulainen and Bondy, 1987). Exposed to CCCP and oligomycin A, reduced but did not eradicate MeHg-induced increase in $[Ca^{2+}]_i$ in rat CGCs (Limke et al., 2003). These findings suggest that besides the mitochondrial Ca^{2+} efflux contributing to phase 1 another Ca^{2+} store participates of MeHg-induced elevations in $[Ca^{2+}]_i$. Specifically, treatment with bradykinin or caffeine to empty the SER (Hare & Atchison, 1995) and treatment with bethanechol to downregulate IP3 receptors caused a delay in the time-to-onset of phase 1. (Limke, Bearss, et al., 2004) Furthermore, MeHg exposure upregulates IP3 receptors in CGCs (T. A. Sarafian, 1993). Thus, MeHg interacts with the SER. Both intracellular Ca^{2+} stores influence the MeHg-induced biphasic disruption of $Ca^{2+}{}_i$ homeostasis.

MeHg-induced cell death mechanisms are not yet completely understood. However, Ca^{2+} dysregulation is reported to play a crucial role. Excessive high levels of $[Ca^{2+}]_i$ lead to mitochondria Ca^{2+} uptake causing mitochondrial membrane depolarization and it increases production of superoxide anion radicals that contribute to cell death (T. A. Sarafian et al., 1994).

Regardless of the presence of CCCP + THP treatment during exposure to MeHg a decrease in cell viability is absent during 15 min MeHg and 1 hr post-MeHg exposure. Viability in the Renshaw area was significantly decreased at 3 hr post-MeHg compared to all previous timepoints examined. Thus, the anterior lumbar tissue is susceptible to MeHg neurotoxic effects at delayed timepoints, but the mitochondria and the SER do not participate during MeHg-induced cytotoxicity. Results are in agreement with MeHg-induced cell death occurring at a long-term timepoints. In CGCs, which are very susceptible to MeHg-mediated cytotoxicity, MeHg did not produce immediate generalized cell damage or cell death regardless of whether the MeHg exposure occurred *in vitro* (T. A. Sarafian, 1993) or *in vivo* (M. Harada, 1995). Specifically, MeHg exposure elicits severe cytotoxicity after 3.5 hr but not at 30 min in CGCs (Marty & Atchison, 1998). This suggests that MeHg-induced elevations in $[Ca^{2+}]_i$ do not participate during the beginning stages of cell death because otherwise the elevations in fluo-4 fluorescence would correspond to a decrease in calcein fluorescence.

A possibility for the inability of $Ca^{2+}{}_i$ to increase during MeHg + CCCP + THP at 15 min or 1 hr post-MeHg may be that following treatment with the antagonists there was not enough $Ca^{2+}{}_i$ to be released by MeHg from the mitochondria and SER. Thus, CCCP + THP successfully depleted internal Ca^{2+} stores prior to and during MeHg exposure. Our results are in disagreement with CCCP treatment not causing a significant Ca^{2+} efflux from the mitochondrial and not delaying the time-to-onset of MeHg induced increase in $[Ca^{2+}]_i$ in CGCs (Budd & Nicholls, 1996; Limke et al., 2003). Perhaps these discrepancies could be due to different experimental parameters such as the MeHg concentration, duration of MeHg exposure, differences in protein concentrations and the experimental model.

CCCP treatment has been reported to deplete ATP levels (Budd & Nicholls, 1996). Similarly, MeHg reduces generation of ATP (Sone et al., 1977). Loss of ATP inhibits plasma membrane transporters and triggers onset of phase 2 in CGCs (Limke et al., 2003). Furthermore, multiple systems have demonstrated that besides Ca^{2+} release from intracellular Ca^{2+} stores, MeHg triggers extracellular Ca^{2+} entry that also contributes to increases in fluo-4 fluorescence (Atchison, 1986; Bradford et al., 2016; Hare & Atchison, 1995; Hare et al., 1993; Johnson & Atchison, 2009; Limke et al., 2003; Marty & Atchison, 1997; Ramanathan & Atchison, 2011). Therefore, the ability of MeHg + CCCP + THP to reduce fluo-4 fluorescence at 1 hr post-MeHg exposure may be due to high $[Ca^{2+}]_i$ levels that compromises the plasma membrane (Marty & Atchison, 1998). Although this possibility is not likely because incidence of viability in the Renshaw area did not decrease at 1 hr post-MeHg.

Another possibility for the absence of an increase in fluo-4 fluorescence during MeHg + CCCP + THP may involve the well-known expression of calbindin, the cytosolic Ca^{2+}-binding neuroprotective protein. RCs have a significant Ca^{2+} buffering machinery. They express calbindin and parvalbumin proteins (Alvarez et al., 2005; Geiman et al., 2000; Geiman et al., 2002). Levels of $[Ca^{2+}]_i$ regulate calbindin activity (Corradino, 1993). MeHg administration *in vivo* to rats caused an overexpression of calbindin proteins (de Oliveira Souza, de Marco, Laure, Rosa, & Barbosa, 2016). However, exposure to MeHg *in vivo* caused no change in the calbindin topographic distribution of cerebral motor cortex in rat offsprings (Kakita, Inenaga, Sakamoto, & Takahashi, 2002). Although these are conflicting results, perhaps depletion of Ca^{2+} by CCCP + THP treatments triggers Ca^{2+}-buffering proteins to quickly and efficiently buffer increases in $[Ca^{2+}]_i$

during and post-MeHg exposure in the Renshaw area. However, this possibility needs to be investigated furthered.

Failure of CCCP + THP to protect against MeHg-induced cell death suggests that other mechanisms are involved besides efflux of Ca^{2+} from the mitochondria and SER. Thus, MeHg-mediated $Ca^{2+}{}_i$-independent pathways may contribute to cell death in the Renshaw area. This likely reflects the substantial role of Ca^{2+} entry in inducing cell death. Furthermore, several studies have demonstrated the ability of MeHg to liberate and increase intracellular levels of zinc, which is itself cytotoxic (Denny & Atchison, 1994; Edwards et al., 2005; Hare et al., 1993; Johnson et al., 2011).

Lumbar slices were exposed to MeHg in a continuous perfusion to allow saturation of nonspecific binding sites. Monitoring temporal and spatial increases in $[Ca^{2+}]_i$ allows to understand the time course that follows MeHg-induced events that precede cell death. Acute exposure to MeHg *in situ* alters cytosolic Ca^{2+} homeostasis and cause cell death in the Renshaw area. Confocal Ca^{2+} imaging demonstrated that following a 15 min exposure to 20 μM MeHg caused a significant increase in fluo-4 fluorescence intensity. This effect was sustained at 1 hr post-MeHg but not at 3 hr post-MeHg exposure. Depletion of internal Ca^{2+} stores with CCCP + THP prevented the MeHg-induced elevation in fluo-4 fluorescence at 15 min MeHg and 1 hr post-MeHg exposure. When comparing between MeHg in the absence or presence of the antagonists there is a significant reduction in fluo-4 fluorescence intensity elicited by Ca^{2+} depletion from the mitochondria and SER at 1 hr post-MeHg. Calcein fluorescence indicates that viability of the Renshaw area decreased at 3 hr post-MeHg exposure irrespective of the presence of CCCP + THP treatment. Thus, MeHg-induced

$[Ca^{2+}]_i$ increase is dependent on Ca^{2+} release from intracellular Ca^{2+} stores whereas incidence of cell death is independent in the Renshaw area.

In summary, experiments were designed to determine whether there is a correlation between MeHg-mediated $[Ca^{2+}]_i$ increase and cell death in the Renshaw area. Depletion of the mitochondria and the SER prior to and during an acute exposure to MeHg (20 μM) *in situ* prevented MeHg-induced increase in $[Ca^{2+}]_i$ but did not protect against cell death. This study provides evidence for the first time the temporal events that take place during and after MeHg exposure regarding $Ca^{2+}{}_i$ dysregulation and its relationship to cytotoxicity in the Renshaw area. Due to the complexity of the biphasic $Ca^{2+}{}_i$ interactions we did not identify exactly how much each Ca^{2+} store contributes to the total $[Ca^{2+}]_i$ increase in the Renshaw area. Additionally, we did not determine whether MeHg-induced cell death in our model occurs through apoptotic or necrotic pathways (Castoldi et al., 2000; Fujimura et al., 2009; Nagashima et al., 1996).

CHAPTER FIVE:

SUMMARY AND CONCLUSIONS

Summary of experiments and conclusions

This dissertation was designed to understand whether known targets of MeHg neurotoxicity contribute to dysfunction in cells that degenerate in ALS disease. Prior work has demonstrated that exposure to MeHg causes an increase in $[Ca^{2+}]_i$ which behaves in a time- and concentration-dependent manner both primary and transformed cell lines (Edwards et al., 2005; Hare et al., 1993; Marty & Atchison, 1997; Ramanathan & Atchison, 2011). In detail, MeHg releases Ca^{2+} from the mitochondria and the SER into the cytosol, known as phase 1 (Hare & Atchison, 1995; Levesque & Atchison, 1991; Limke & Atchison, 2002). Then, MeHg causes extracellular Ca^{2+} to enter the cytoplasm via VGCCs and LGICs, known as phase 2 (Hare et al., 1993; Marty & Atchison, 1997; Ramanathan & Atchison, 2011). Additionally, MeHg induces cell death which is in part mediated by VGCCs (Edwards et al., 2005; Marty & Atchison, 1998). Furthermore, exposure to MeHg *in vivo* accumulates and degenerates αMNs in the spinal cord (Moller-Madsen, 1990, 1991; M. Su et al., 1998). Together, these findings highlight the participation of membrane receptors and Ca^{2+} stores during MeHg-mediated alterations in Ca^{2+} homeostasis and cell death.

My experimental design elucidates the involvement cholinergic receptors and extracellular Ca^{2+} in differentiated PC12 cells. Additionally, it reveals the participation of LGICs and intracellular Ca^{2+} stores during MeHg-mediated Ca^{2+} dysregulation and cell death in the Renshaw area. The central hypothesis guiding these studies was that LGICs and internal Ca^{2+} stores participate of MeHg-mediated increase in $[Ca^{2+}]_i$ leading to degeneration of the Renshaw area. I expand the neuroscience, as well as, the pharmacology and toxicology fields by presenting novel knowledge in the susceptibility of the Renshaw area to MeHg-induced neurotoxicity.

The original findings within this dissertation are the following:

1) MeHg neurotoxicity is modulated by, but not exclusive to, heteromeric nAChRs in differentiated PC12 cells.
2) Contribution of extracellular Ca^{2+} influx is crucial during MeHg-mediated increase in $[Ca^{2+}]_i$ and subsequent cytotoxicity in differentiated PC12 cells.
3) The neurotoxic effects of MeHg *in vitro* extend to an *in situ* model. The Renshaw area is susceptible to MeHg-mediated increase in $[Ca^{2+}]_i$ and subsequent cytotoxicity, via cholinergic and GABAergic, but not glycinergic, mechanisms.
4) Internal Ca^{2+} pools contribute to MeHg-mediated increase in $[Ca^{2+}]_i$ in the Renshaw area.

Experiments in Chapter 2 support the hypothesis that MeHg mediates increases in $[Ca^{2+}]_i$ through mechanisms that involve nAChRs in differentiated PC12 cells. Presence of the heteromeric nAChR antagonist, MEC, delayed MeHg-mediated $[Ca^{2+}]_i$ increase and subsequent cell death. Effects of MeHg in the cholinergic neurotransmission have been well established at the presynaptic and postsynaptic membranes. Presynaptic effects include the reduction of nerve-evoked ACh release and promotes spontaneous release of ACh, in a Ca^{2+}-dependent manner (Atchison & Narahashi, 1982; Juang, 1976a). The postsynaptic effects of MeHg include the inhibition of the fast depolarizing response in nAChRs (Quandt et al., 1982). MeHg inhibits binding of ACh to the mAChR and nAChR, suggesting that MeHg binds to the receptor itself (Eldefrawi et al., 1977; Shamoo et al., 1976). Furthermore, MeHg blocks the binding of carbachol, the mAChR agonist (Castoldi et al., 1996). Thus, the cholinergic system is a target of MeHg toxicity.

Differentiated PC12 cells express heteromeric and homomeric nAChRs (Blumenthal et al., 1997; Virginio et al., 2002). Furthermore, upon differentiation PC12 cells express the same nAChR stoichiometry as in the Renshaw area (Chavez-Noriega et al., 1997; Vincler & Eisenach, 2004; Virginio et al., 2002). The nAChR activates IP3 mechanisms to increase cytosolic Ca^{2+} through SER-dependent pathways (Dajas-Bailador & Wonnacott, 2004; Eberhard & Holz, 1987; Sharma & Vijayaraghavan, 2001). Binding of nicotine to the nAChR initiates a Ca^{2+}-induced Ca^{2+}-release cascade that triggers Ca^{2+} efflux via ryanodine and IP3 receptors in hippocampal cells (Brain, Trout, Jackson, Dass, & Cunnane, 2001; Sharma & Vijayaraghavan, 2001). Exposure to MeHg disrupts $Ca^{2+}{}_i$ homeostasis (Marty & Atchison, 1997) and this is one of the main mechanisms in which MeHg causes cell death. MeHg accumulates in the cerebellum and degenerates the granule cell layer in humans and animals (L. W. Chang, Reuhl, & Spyker, 1977; Hunter & Russell, 1954). Agents that block entry or buffer extracellular Ca^{2+} protect against MeHg-induced cell death (Limke, Bearss, et al., 2004; Marty & Atchison, 1998).

My findings agree with previous studies which demonstrate that MeHg increases $[Ca^{2+}]_i$ and cell death in primary and immortalized cell lines. (Edwards et al., 2005; Hare et al., 1993; Marty & Atchison, 1997, 1998). MeHg caused a biphasic increase in fura-2 fluorescence and induced cell death in differentiated PC12 cells. Treatment with MEC significantly delayed Ca^{2+} dysregulation produced by MeHg during phase 1 without affecting phase 2. Similarly, MeHg increases $[Ca^{2+}]_i$ during phase 1 by interacting with mAChRs in CGCs (Limke, Bearss, et al., 2004). MeHg exposure disrupts divalent cation regulation (Denny & Atchison, 1996; Limke, Heidemann, et al., 2004; Marty & Atchison, 1997). Failure of MEC and MLA treatment to delay the time-to-onset of phase 2 suggests that there is a non-Ca^{2+} divalent cation that is responsible for the phase 2 in

differentiated PC12 cells. Specifically, MeHg releases intracellular Zn^{2+} and this alters the estimation of $[Ca^{2+}]_i$ using fura-2 microfluorimetry (Denny & Atchison, 1994, 1996). Homomeric nAChRs do not contribute to the MeHg-mediated dysregulation of $[Ca^{2+}]_i$. This could be due to a low receptor expression or that MeHg has higher affinity to the receptor than MLA. Furthermore, the lack of contribution from homomeric nAChRs during MeHg neurotoxicity cannot be ruled out. MeHg effects on the homomeric α7-containing nAChRs have not been studied before.

Extracellular Ca^{2+} influx is critical during MeHg-mediated Ca^{2+} dysregulation and subsequent cell death. Chelation of external Ca^{2+} with EGTA delayed fura-2 fluorescence at phase 1 and phase 2. Our results are the second to indicate a contribution of Ca^{2+}_e in phase 1 Ca^{2+}_i dysregulation during EGTA conditions. Perhaps alterations in phase 1 are due to Ca^{2+}-induced Ca^{2+}-release mechanisms (Hannon 2016 dissertation). The delay in fura-2 fluorescence during phase 2 occurs via non-cholinergic pathways because treatment of MEC and MLA did not delay this phase. The mechanism(s) underlying this effect remain unclear, but data suggest that other divalent cations, such as Zn^{2+}, could be contributing to changes in fura-2 fluorescence intensity. Thus, external Ca^{2+} is involved in MeHg-mediated increase in $[Ca^{2+}]_i$ and this is linked to mechanisms of cell death in differentiated PC12 cells.

Experiments in Chapter 3 support the hypothesis that exposure to MeHg causes disruption of Ca^{2+} homeostasis and cell death in the Renshaw area. Furthermore, MeHg *in situ* neurotoxicity will be reduced with the presence of BCC to block $GABA_A$Rs, strychnine to bock GlyRs and both MEC and DHβE to block nAChRs. Recurrent inhibition in the Renshaw area is controlled by the negative feedback mechanism between excitatory and inhibitory neurotransmissions.

Communication between nAChRs, $GABA_A$Rs and GlyRs regulates synaptic input and the generation of the locomotor rhythm (Bhumbra et al., 2014). A disruption in this circuit by MeHg impedes the firing feedback between αMNs and RCs. Ultimately this leads to cell death via mechanisms of hyperexcitability (van Zundert, Izaurieta, Fritz, & Alvarez, 2012; Wootz et al., 2013).

Electrophysiology studies demonstrate that $GABA_A$Rs are susceptible to MeHg neurotoxicity. In detail, MeHg suppresses the GABA-induced Cl^- current (Arakawa et al., 1991). MeHg decreases the IPSP amplitude to a complete block (Yuan & Atchison, 1995), which occurs earlier than EPSPs (Yuan & Atchison, 1995, 1997). Hence, synaptic inhibitory neurotransmission is more sensitive to MeHg than excitatory neurotransmission. Furthermore, the sensitivity of $GABA_A$Rs to MeHg is greater in α6-containing CGCs than in α1-containing Purkinje cells because MeHg suppressed faster the IPSC in CGCs (Herden et al., 2008; Yuan & Atchison, 2003). Thus, the receptor stoichiometry influences the toxicity of MeHg. Also, MeHg potentiates binding of BZs in the $GABA_A$Rs (Fonfria et al., 2001). Together, these findings suggest that MeHg targets $GABA_A$Rs and disruption of inhibitory neurotransmission plays an important role in MeHg-induced MN excitotoxicity.

My findings demonstrate that $GABA_A$Rs participate of MeHg-mediated dysregulation of $[Ca^{2+}]_i$ and subsequent cell death in the Renshaw area. MeHg-mediated increase in $[Ca^{2+}]_i$ through $GABA_A$Rs precedes cell death mechanism(s). Treatment with BCC, MEC and DHβE reduced MeHg-mediated $Ca^{2+}{}_i$ dysregulation. Therefore, MeHg-mediated increase in $[Ca^{2+}]_i$ occurs through GABAergic and cholinergic pathways. MeHg does not affect α1-containing nAChRs at

the NMJ (Atchison & Narahashi, 1982). The Renshaw area expresses α3, α5-containing nAChRs (Alvarez et al., 2005; Geiman et al., 2002). MeHg does not affect nAChRs at the NMJ but it does affect nAChRs at the Renshaw area. This discrepancy could be due to the expression of the α subunit in the nAChRs. Besides these regions expressing different α subtypes, the nAChR structure could be slightly different perhaps making it easier for MeHg to reach sulfhydryl groups in the Renshaw area. Contrary to my hypothesis, glycine receptors do not participate in MeHg neurotoxicity. Blocking this receptor with strychnine did not protect against MeHg-mediated increase in $[Ca^{2+}]_i$ and subsequent cell death. A previous study demonstrated that strychnine treatment did not prevented the increase in population spikes caused by MeHg exposure in hippocampal CA1 neurons (Yuan & Atchison, 2005). Thus, MeHg and strychnine could compete for the same binding site in the GlyR, or MeHg has higher affinity to glycine receptors than strychnine. Moreover, strychnine could cross-react with $GABA_A$Rs because they both belong to the same family of LGICs, hence they share a similar receptor structure (Grenningloh et al., 1987; Langosch, Thomas, & Betz, 1988). Also, strychnine may not have an effect in the Renshaw area (Ryall et al., 1972). However, the lack of contribution from GlyRs during MeHg neurotoxicity cannot be ruled out.

MeHg cytotoxicity in the Renshaw area occurred at delayed, but not immediate, time points. My findings support that GABAergic mechanisms participate during MeHg-induced cell death. Similarly, MeHg exposure causes delayed cell death in CGCs (Edwards et al., 2005; Marty & Atchison, 1998). Blocking $GABA_A$Rs with BCC delayed MeHg-induced cytotoxicity in the Renshaw area. This area expresses α5-containing $GABA_A$Rs, which are involved in tonic-mediated inhibition (Castro, Aguilar, Andres, Felix, & Delgado-Lezama, 2011; Glykys, Mann, &

Mody, 2008; Lee & Maguire, 2014). If MeHg blocks this receptor and consequently decreases tonic inhibition it can lead to cell death via MN-mediated hyperexcitability. Furthermore, cerebellar ataxia and motor dysfunction occurs when GABA-mediated tonic inhibition is reduced in C57BL6J mice (Egawa et al., 2012). Furthermore, delayed cell death extends to reports of human poisoning. Specifically, Iraqi victims poisoned with MeHg presented symptoms weeks to months post-MeHg exposure (Bakir et al., 1973; B. Weiss et al., 2002). Similarly, Japanese victims did not show poisoning symptoms until years post-MeHg exposure (M. Harada, 1995; B. Weiss et al., 2002). Together, I conclude that the alterations in $Ca^{2+}{}_i$ homeostasis and cell death in the Renshaw area occur due to hyperexcitability via too much cholinergic excitation and not enough GABAergic inhibition. This chapter expands the current scientific knowledge by revealing the participation of nAChRs and $GABA_A$Rs in MeHg-mediated Ca^{2+} dysregulation and cell death in the Renshaw area.

Experiments in Chapter 4 support the hypothesis that depletion of Ca^{2+} from intracellular Ca^{2+} stores with the combination of CCCP and THP decreases MeHg-induced increase in $[Ca^{2+}]_i$ and subsequent cell death in the Renshaw area. The SER contains ryanodine and IP3-sensitive Ca^{2+} pools and the SERCA pump. These all regulate cytosolic Ca^{2+} homeostasis (Irving et al., 1992). Previous studies demonstrate that MeHg upregulates IP3 receptors (T. A. Sarafian, 1993), enhances the binding of IP3 to its receptor (Chetty et al., 1996) and releases Ca^{2+} through IP3 receptors (Hare & Atchison, 1995; Tan et al., 1993). Emptying of the IP3-sensitive pool in the SER delayed but not abolish phase 1 (Hare & Atchison, 1995), suggesting that the SER contributes to the overall cytosolic increase in $[Ca^{2+}]_i$. Additionally, MeHg-mediated increase in $[Ca^{2+}]_i$ during phase 1 contributes 30-40% of fura-2 fluorescence in CGCs (Limke, Bearss, et al., 2004) and 68%

in NG108-15 cells (Hare & Atchison, 1995). Perhaps the SER has a THP-insensitive Ca^{2+} pool in CGCs (Masgrau et al., 2000). Thus, the contribution of internal Ca^{2+} stores to disruption of $Ca^{2+}{}_i$ homeostasis by MeHg depends on the cell type. Data suggests that the SER is not the only target that contributes to increases of $Ca^{2+}{}_i$ during MeHg neurotoxicity. MeHg disrupts mitochondria function. In detail, MeHg depolarizes the mitochondrial membrane potential (Hare & Atchison, 1992; Kauppinen et al., 1989), opens the mPTP (Limke & Atchison, 2002), reduces production of ATP (Sone et al., 1977), and decreases Ca^{2+} reuptake by the Ca^{2+} uniporter (Levesque & Atchison, 1991). Thus, MeHg disrupts $Ca^{2+}{}_i$ homeostasis via a plethora of mechanisms. Furthermore, inhibition of ATP synthase with oligomycin-A, and inhibition of complex I of the mitochondrial electron transport chain with rotenone, reduce MeHg-mediated increase in $[Ca^{2+}]_i$ (Komulainen & Bondy, 1987). Thus, the mitochondria contribute to increases of $Ca^{2+}{}_i$ during MeHg neurotoxicity.

In agreement, my findings demonstrate that Ca^{2+} efflux from internal Ca^{2+} stores contribute to the cytosolic increase in $[Ca^{2+}]_i$ during MeHg neurotoxicity in the Renshaw area. However, contrary to my hypothesis, internal Ca^{2+} stores do not contribute to MeHg-induced cell death in the Renshaw area. In CGCs, MeHg caused cell death through activation of IP3-sensitive pathways via M3 mAChRs (Limke, Bearss, et al., 2004). Hence, the SER participates of MeHg-induced cell death in CGCs but not in the Renshaw area. This discrepancy could be due to different factors such as the MeHg concentration, exposure time, time of cell death measurement and the model system, *in vitro* vs *in situ*. Perhaps, in the Renshaw area, cell death is dependent on Ca^{2+} influx rather than Ca^{2+} efflux from internal Ca^{2+} stores.

Experiments in this dissertation considered MeHg concentrations relevant to human poisoning. The selected concentrations correlate to blood Hg (19.5 μM) levels of acutely poisoned individuals with motor impairment and ataxic phenotype (Bakir et al., 1973; Hunter & Russell, 1954). For the differentiated PC12 cells *in vitro* experiments 1, 2, and 5 μM MeHg are environmentally relevant concentrations because they are lower than whole-blood Hg concentrations in poisoned individuals. Experiments in the Renshaw area used 20 μM MeHg, which it is consistent with the MeHg concentration detected in poisoned individuals. Furthermore, symptoms of chronic MeHg poisoning in humans have been observed with blood and brain Hg levels of 4-80 μM (Skerfving, 1988). The concentrations of MeHg used *in vitro* and *in situ* did not produce outright cell death. Instead, the designated MeHg concentrations induce non-lethal effects. Otherwise, experiments lose relevance to actual human MeHg exposures. MeHg neurotoxicity was measured throughout a continuously monitored exposure that took into consideration MeHg toxicity during and post-MeHg exposure. Thus, experiments account for the MeHg effects during immediate and delayed toxicity.

In conclusion, experiments in this dissertation highlight new insights regarding the underlying mechanisms involved during MeHg neurotoxicity in the spinal cord. Simultaneously, this dissertation showcases that the Renshaw area is a target of MeHg neurotoxicity. Specifically, I demonstrate that nAChRs, $GABA_A$Rs, as well as, extracellular Ca^{2+} and internal Ca^{2+} stores participate of the characteristic Ca^{2+} dysregulation and subsequent cell death caused by MeHg exposure. These are all well-known targets of MeHg neurotoxicity. Furthermore, I demonstrate for the first time the susceptibility of these targets in the Renshaw area, which degenerates in ALS disease. GxE interactions have been speculated as a risk factor for the development of

neurodegenerative diseases. Due to the current concern of Hg emissions and environmental contamination the scientific field must continue the research. This dissertation inspires future work to have a better understanding of ALS disease.

I recognize that this dissertation has several limitations. First, internal Ca^{2+} pools contribute differently to MeHg-mediated disruption of $Ca^{2+}{}_i$ homeostasis in NG108-15 cells and CGCs (Hare et al., 1993; Limke, Heidemann, et al., 2004). Thus, the contribution of the internal Ca^{2+} stores following MeHg exposure depends on the cell type. The specific contribution the mitochondria and the SER during MeHg neurotoxicity has not been studied in αMNs. In Chapter 4, the participation of these pools was determined with a pharmacological approach. Simultaneously, the mitochondria were depleted and the SERCA pump blocked. Therefore, experiments cannot discriminate the individual contribution from each Ca^{2+} store in the Renshaw area. Consequently, I cannot confirm whether the protection afforded by the CCCP + THP treatment during MeHg exposure was because of an additive, synergistic effect or if a particular Ca^{2+} pool is responsible for MeHg neurotoxicity. Second, MeHg neurotoxicity *in situ* in the Renshaw area has not been previously studied. Thus, I must acknowledge and consider the presence of different cell populations within the lumbar tissue that are not necessarily equally susceptible to MeHg. Nonetheless they contribute to my results.

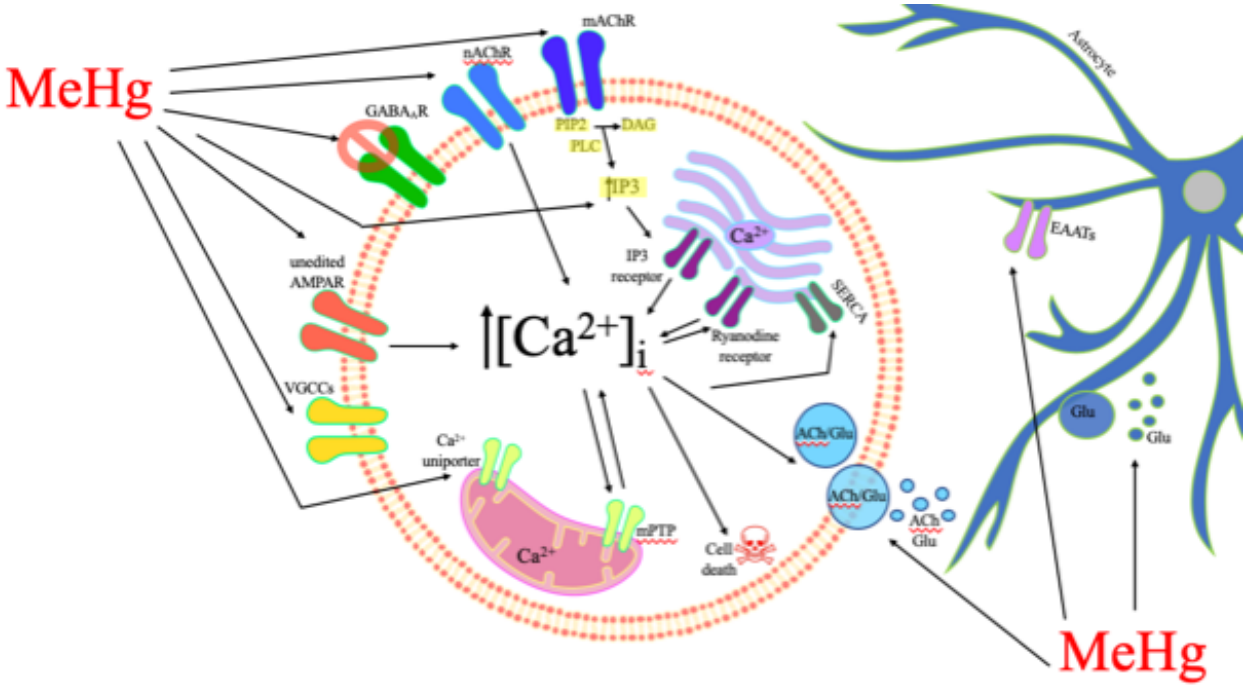

Figure 5.1. Schematic drawing of the targets of MeHg at the neuron and glia cell.

These mechanisms are present at the presynaptic membrane, axon terminal and throughout a neuron. Through various mechanisms MeHg increases $[Ca^{2+}]_i$. Uncontrolled and sustain increases in $[Ca^{2+}]_i$. lead to neurotransmitter release and hyperexcitability. It is hypothesized that MeHg utilizes the VGCCs, unedited AMPAR, nAChR and mAChR to reach the intracellular space. Also, MeHg can cross the phospholipid bilayer to reach the intracellular space. MeHg increases IP3 production, which triggers Ca^{2+} release from the SER into the cytoplasm from IP3 receptors. Furthermore, elevated cytosolic Ca^{2+} levels trigger Ca^{2+} release from the SER into the cytoplasm from ryanodine receptors, through a mechanism known as CICR. The excess of $Ca^{2+}{}_i$ is normally taken up by the SER through the SERCA pump. MeHg targets the SERCA pump. The mitochondria buffers Ca^{2+} released from the SER through the Ca^{2+} uniporter. The Ca^{2+} uniporter is a target of MeHg. MeHg impairs mitochondrial respiration and causes Ca^{2+} release from the mitochondria into the cytosol through the opening of the mPTP. At the glia cell, MeHg causes

Figure 5.1. (cont'd)

dysfunction of EAAT and triggers the release of glutamate from astrocytes, which contributes to hyperexcitability. Together, MeHg-mediated alterations in Ca^{2+}_i homeostasis lead to cell death through mechanisms that involve cytochrome-c, lipase and calpain enzymes.

APPENDIX

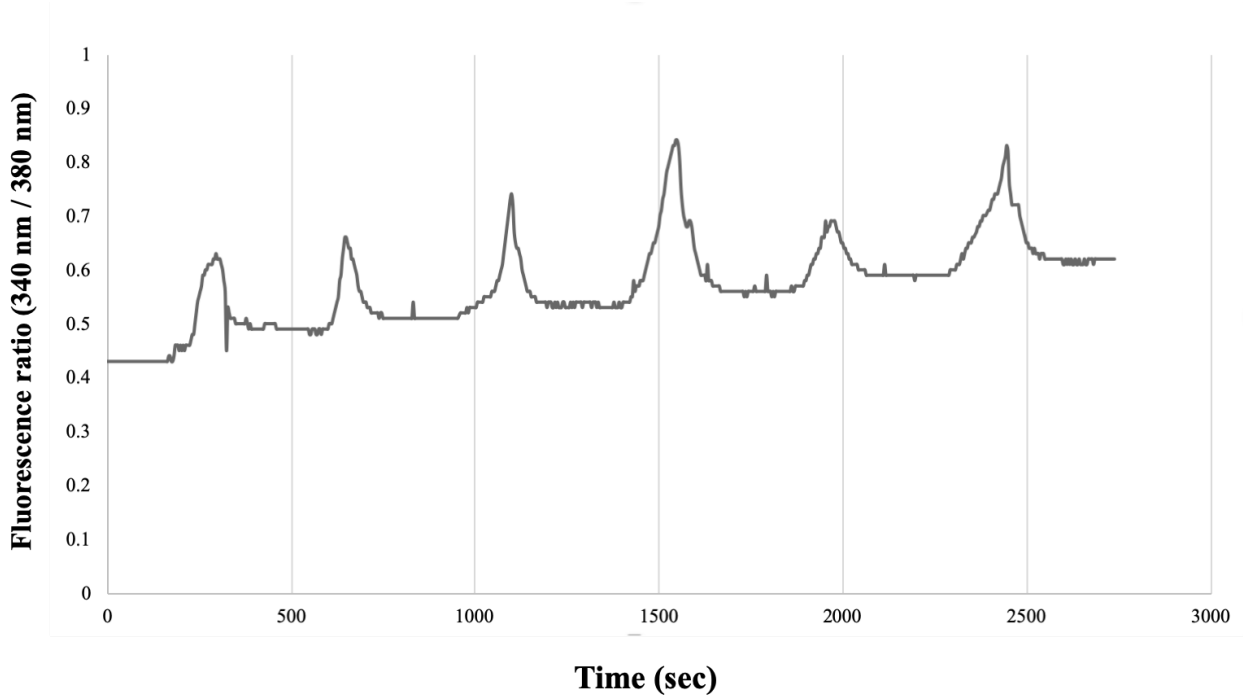

Figure A.1. Representative tracing of changes in fura-2 fluorescence intensity in a PC12 cell during exposure to low and high concentrations of nicotine. PC12 cells responded to a brief (2-4 min) 40 mM KCl-mediated transient depolarization followed by a return to baseline. This demonstrates the Ca^{2+}-buffering capacity upon K^+ cessation. The maximum fluorescence ratio induced by the different concentrations of nicotine (100-400 μM), intercalated with HBS, are the following:

Time Marks:

123.44 → 40 mM K^+

243.53 → HBS

409.98 → 100 μM Nicotine

610.82 → HBS

798.33 → 200 μM Nicotine

1064.3 → HBS

Figure A.1. (cont'd)

1310.47 → HBS

1523.56 → 250 μM Nicotine

1755.78 → HBS

1931.41 → 300 μM Nicotine

2160.33 → HBS

2418.71 → 400 μM Nicotine

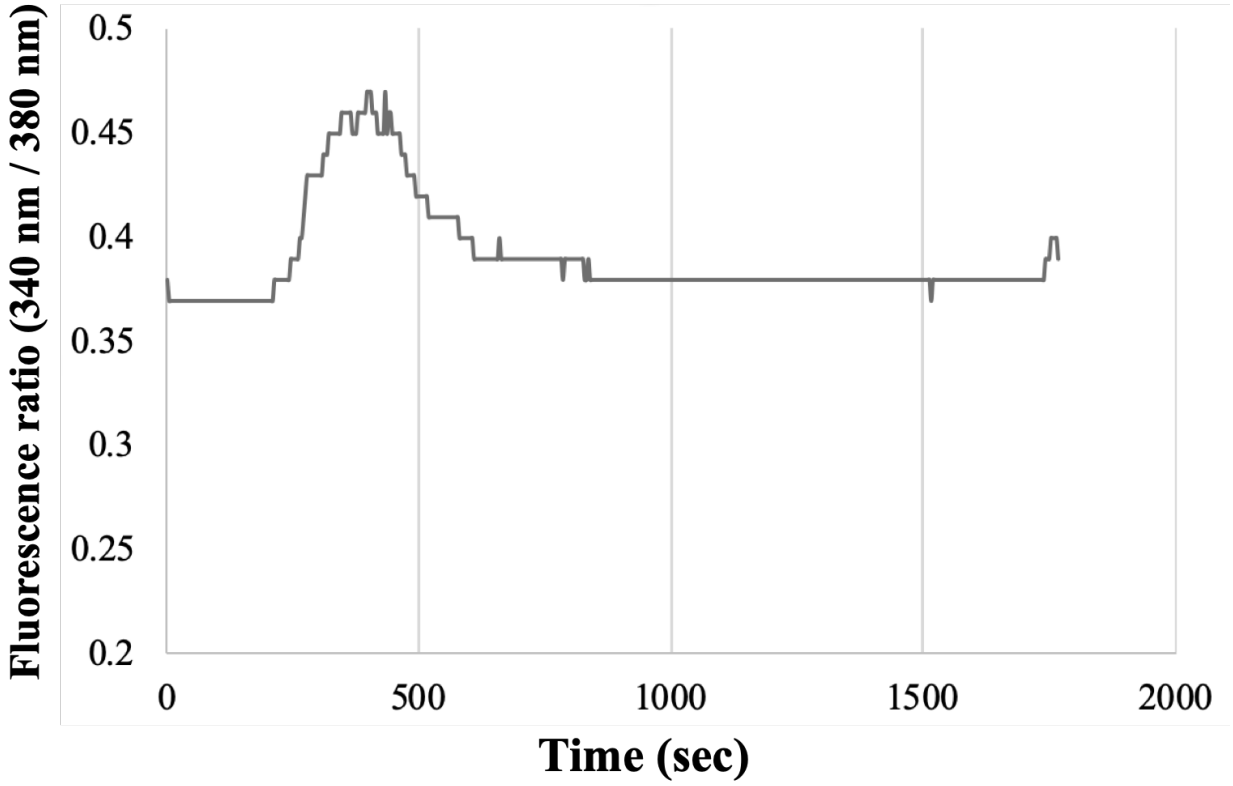

Figure A.2. Representative tracing of changes in fura-2 fluorescence intensity in a PC12 cell during exposure to MEC alone or in presence of nicotine (400 µM). PC12 cells responded to a brief (2-4 min) 40 mM KCl-mediated transient depolarization followed by a return to baseline, demonstrating Ca^{2+}-buffering capacity upon K^+ cessation. Pretreatment with MEC abolished the nicotine-induced increase in $[Ca^{2+}]_i$.

Time Marks:

119.53 sec → 40 mM K^+

347.95 sec → HBS

789.1 sec → 5 µM MEC

1181.49 sec → 400 µM Nicotine + 5 µM MEC

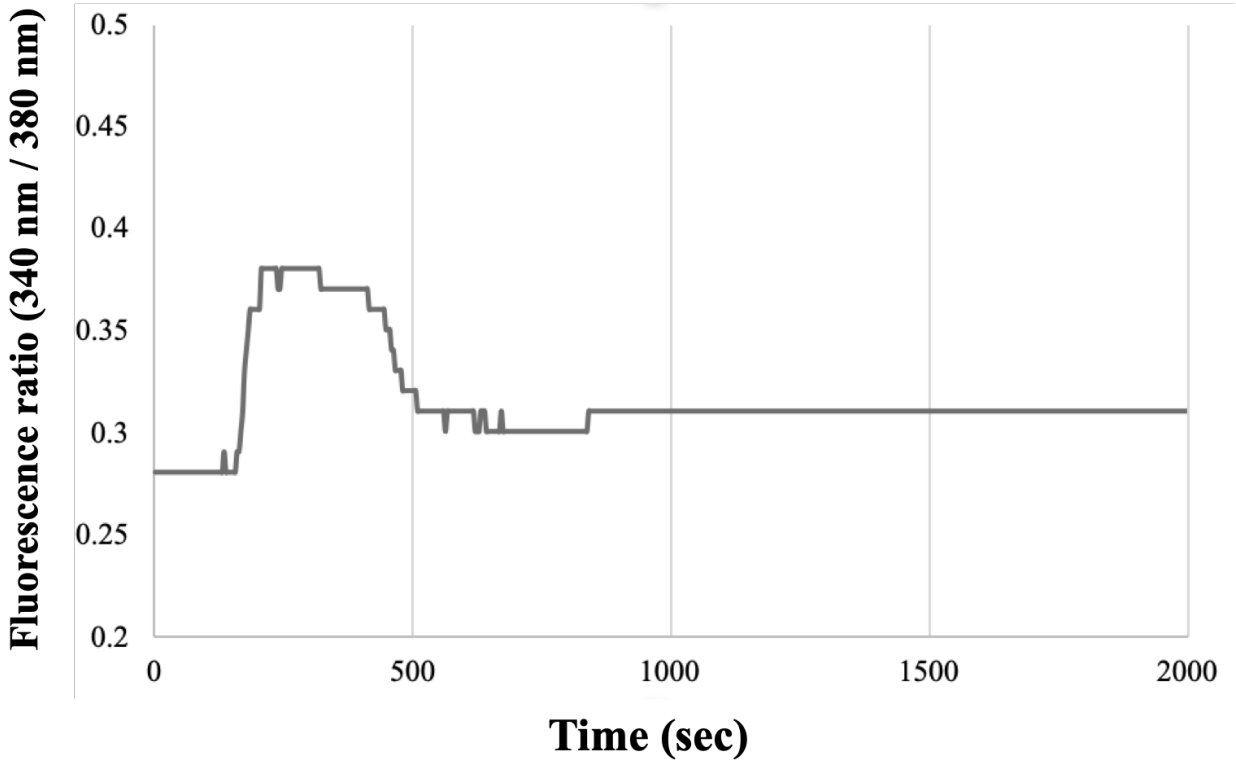

Figure A.3. Representative tracing of changes in fura-2 fluorescence intensity in a PC12 cell during exposure to MLA alone or in presence of nicotine (400 µM). PC12 cells responded to a brief (2-4 min) 40 mM KCl-mediated transient depolarization followed by a return to baseline, demonstrating Ca^{2+}-buffering capacity upon K^+ cessation. Pretreatment with MLA abolished the nicotine-induced increase in $[Ca^{2+}]_i$.

Time Marks:

126.11 sec → 40 mM K^+

298.71 sec → HBS

673.9 sec → 5 µM MEC

1066.58 sec → 400 µM Nicotine + 5 µM MEC

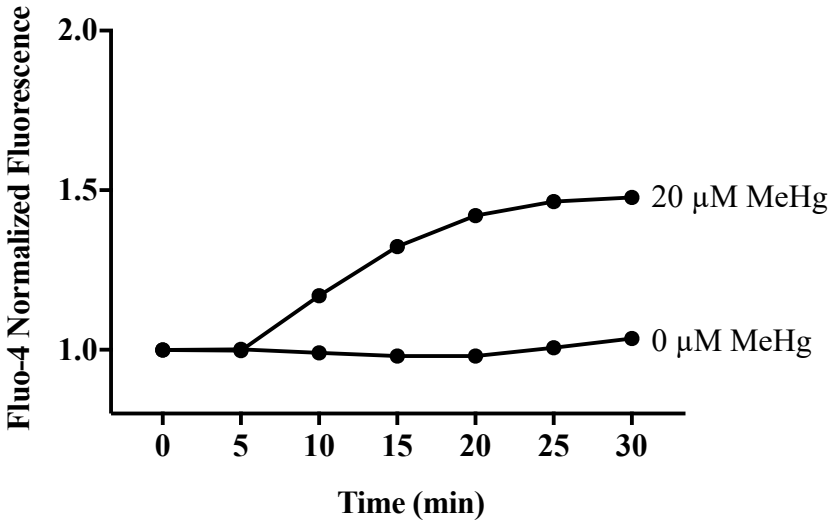

Figure A.4. Time series comparison of elevations in $[Ca^{2+}]_i$ between MeHg-treated and MeHg-untreated MNs in the Renshaw area. The trend indicates an increase in fluo-4 fluorescence during exposure to 20 μM MeHg compared to 0 μM MeHg. The graph suggests that following a 15 min exposure to 20 μM MeHg, dysregulation of $Ca^{2+}{}_i$ homeostasis is observed but not enough to reach fluo-4 plateau. For the MeHg group data are presented as (n = 3). For the 0 μM MeHg or ACSF group data are presented as (n = 1).

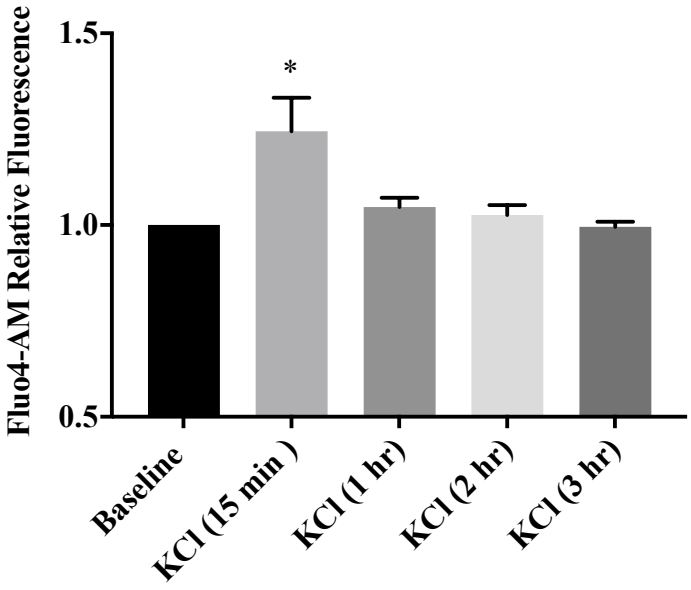

Figure A.5. The Renshaw area responds to KCl-mediated depolarizations only during early timepoints. KCl (40 mM) treatment was not continuous. It was only applied during the specific timepoints examined (15 min, 1 hr, 2 hr and 3 hr). Duration of the KCl treatment was 3 min at times. During the non-examined timepoints, the slice was exposed to ACSF. Thus, after the KCl exposure the tissue was perfused with oxygenated ACSF. Therefore, the KCl effects were washed away and the ability to buffer Ca^{2+} ion by MNs was determined. Data suggest that at 15 min post-baseline a significant increase in fluo-4 fluorescence is observed, denoted by asterisk (*). The other timepoints (1, 2 and 3 hr) examined did not respond to KCl depolarizations. Data are presented as mean ± S.E.M. (n = 3). All *n* values are averages of 3 replicates from the same slice. Statistics are performed using a one-way analysis of variance followed by Tukey's multiple comparison test. Statistical significance is considered at $p < 0.05$.

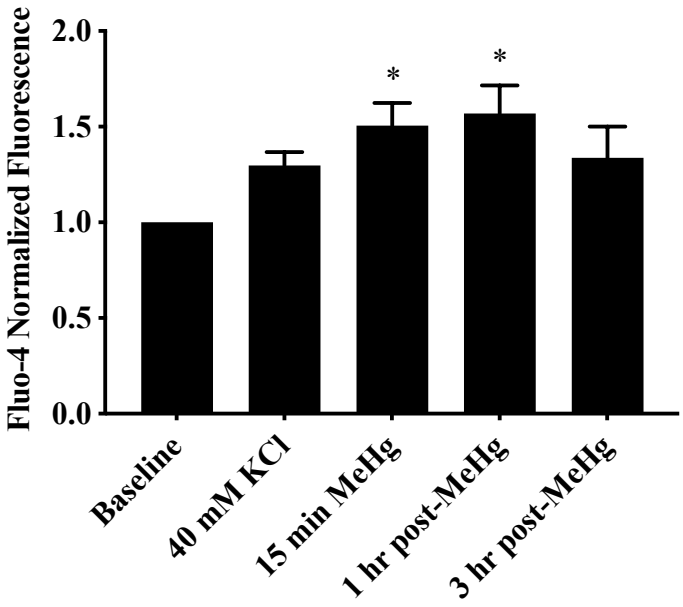

Figure A.6. Early and delayed onset changes in $[Ca^{2+}]_i$ following acute exposure to MeHg *in situ* in the Renshaw area. Exposure to 20 μM MeHg for 15 min significantly increases fluo-4 relative fluorescence at both 15 min MeHg and 1 hr post-MeHg compared to baseline, denoted by asterisk (*). Data are presented as mean ± S.E.M. (n = 11). All *n* values are averages of 3 replicates from the same slice. Statistics are performed using a one-way analysis of variance followed Tukey's multiple comparison test. Statistical significance is considered at $p < 0.05$.

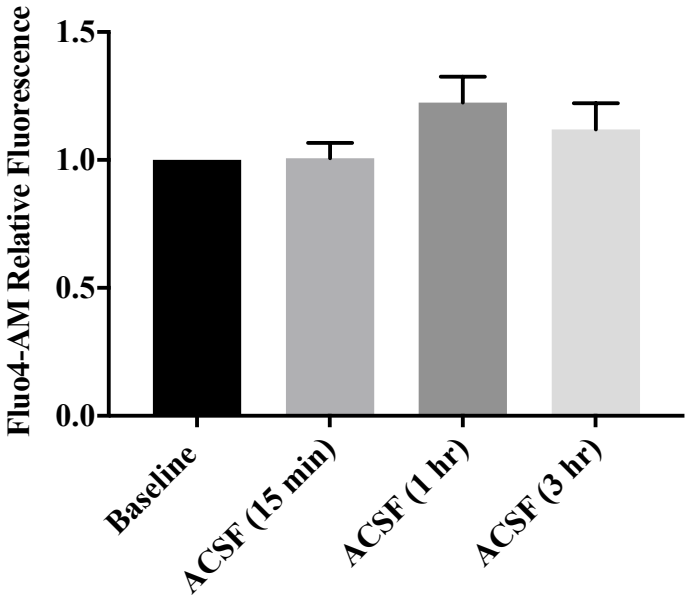

Figure A.7. Fluo-4 fluorescence intensity did not change as a function of time in the Renshaw area. Data are presented as ± S.E.M. (n = 3). A reduction of fluo-4 during a continuous perfusion with ACSF for 3 hr was not detected in the Renshaw area. Statistics are performed using a one-way analysis of variance followed by Tukey's multiple comparison test. Statistical significance is considered at $p < 0.05$.

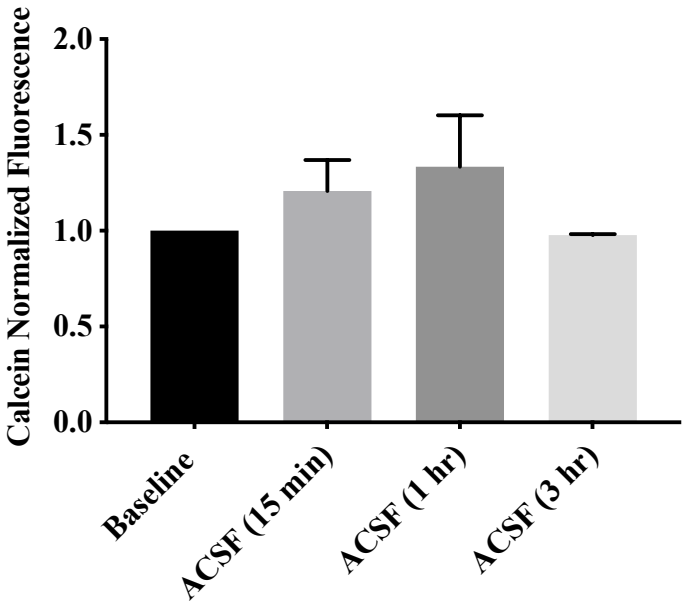

Figure A.8. Calcein fluorescence intensity did not change as a function of time in the Renshaw area. Data are presented as ± S.E.M. (n = 3). A reduction of calcein during a continuous perfusion with ACSF for 3 hr was not detected in the Renshaw area. Statistics are performed using a one-way analysis of variance followed by Tukey's multiple comparison test. Statistical significance is considered at $p < 0.05$.

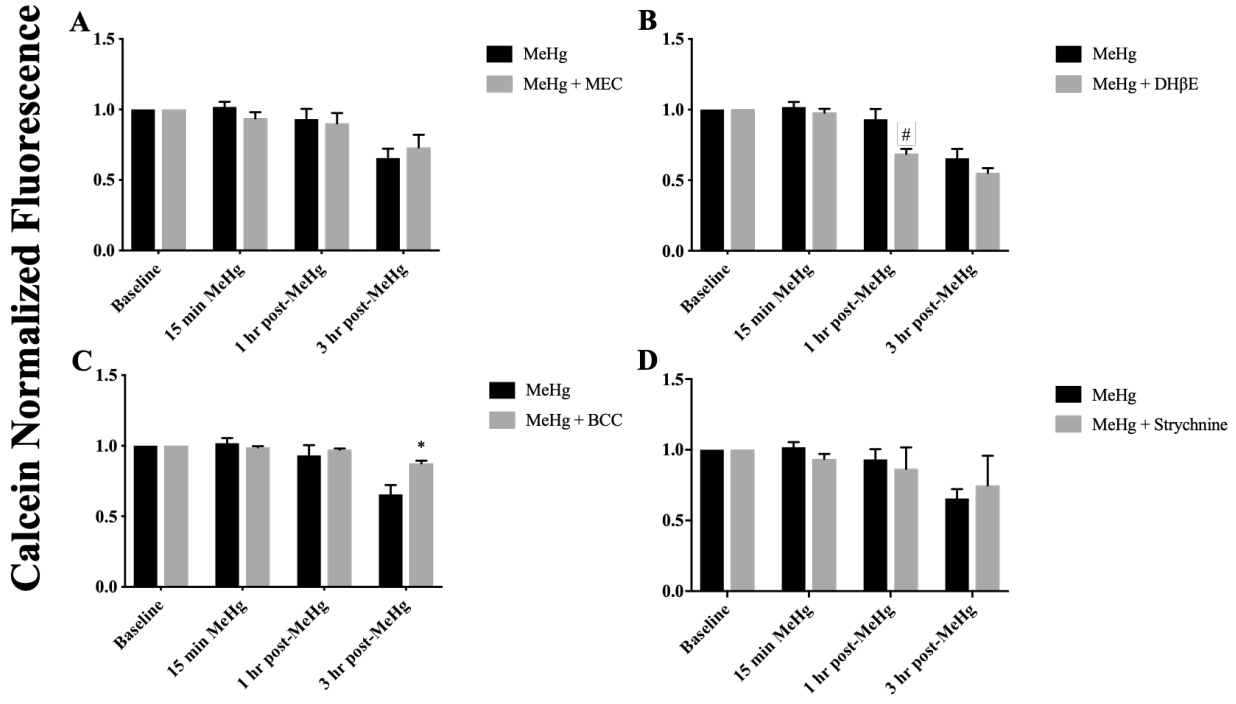

Figure A.9. Comparison of effects of ligand-gated ion channels inhibitors on MeHg (20 µM) induced reduction in calcein fluorescence in the Renshaw area after 3 hr post-MeHg exposure. A) MeHg + MEC did not cause a significant change in calcein fluorescence. B) MeHg + DHβE significantly reduced calcein fluorescence at 1 hr post-MeHg compared to MeHg treatment, denoted by asterisk (*). C) MeHg + BCC significantly increased calcein fluorescence at 3 hr post-MeHg exposure compared to MeHg treatment, denoted by asterisk (*). D) MeHg + strychnine did not change calcein fluorescence intensity. Data are presented as mean ± S.E.M. (n = 8, 5) for MeHg or MeHg + inhibitor, respectively. All *n* values are averages of 3 replicates. Statistics are performed using a two-way analysis of variance followed by a multiple comparison test. Statistical significance is considered at $p < 0.05$.

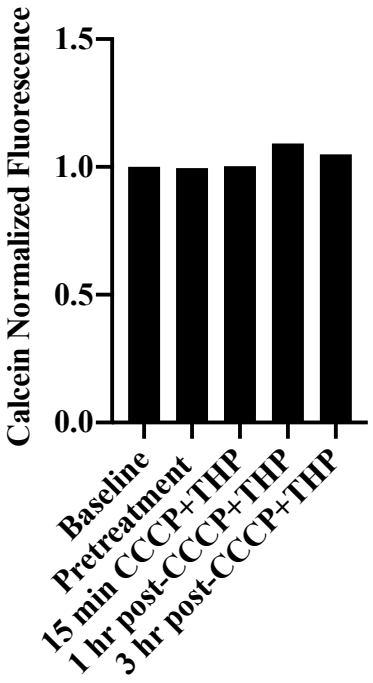

Figure A.10. CCCP with THP treatment did not change the intensity of calcein fluorescence in the Renshaw area. A reduction or increase in calcein fluorescence during a continuous perfusion with ACSF was not detected during any timepoint in the Renshaw area. Data are presented as ± S.E.M. (n = 1).

REFERENCES

REFERENCES

Abd-Elfattah, A. S., & Shamoo, A. E. (1981). Regeneration of a functionally active rat brain muscarinic receptor by D-penicillamine after inhibition with methylmercury and mercuric chloride. *Mol Pharmacol*, 20(3), 492-497.

Abe, T., Haga, T., & Kurokawa, M. (1975). Blockage of axoplasmic transport and depolymerisation of reassembled microtubules by methyl mercury. *Brain Res*, 86(3), 504-508.

Aberg, B., Ekman, L., Falk, R., Greitz, U., Persson, G., & Snihs, J. O. (1969). Metabolism of methyl mercury (203Hg) compounds in man. *Arch Environ Health*, 19(4), 478-484.

Abramson, J. J., Trimm, J. L., Weden, L., & Salama, G. (1983). Heavy metals induce rapid calcium release from sarcoplasmic reticulum vesicles isolated from skeletal muscle. *Proc Natl Acad Sci U S A*, 80(6), 1526-1530.

Adams, C. R., Ziegler, D. K., & Lin, J. T. (1983). Mercury intoxication simulating amyotrophic lateral sclerosis. *JAMA*, 250(5), 642-643.

Al-Mufti, A. W., Copplestone, J. F., Kazantzis, G., Mahmoud, R. M., & Majid, M. A. (1976). Epidemiology of organomercury poisoning in Iraq. I. Incidence in a defined area and relationship to the eating of contaminated bread. *Bull World Health Organ*, 53 Suppl, 23-36.

Albuquerque, E. X., Pereira, E. F., Alkondon, M., & Rogers, S. W. (2009). Mammalian nicotinic acetylcholine receptors: from structure to function. *Physiol Rev*, 89(1), 73-120.

Alvarez, F. J., & Fyffe, R. E. (2007). The continuing case for the Renshaw cell. *J Physiol*, 584(Pt 1), 31-45.

Alvarez, F. J., Jonas, P. C., Sapir, T., Hartley, R., Berrocal, M. C., Geiman, E. J., . . . Goulding, M. (2005). Postnatal phenotype and localization of spinal cord V1 derived interneurons. *J Comp Neurol*, 493(2), 177-192.

Andersen, P. M., Forsgren, L., Binzer, M., Nilsson, P., Ala-Hurula, V., Keranen, M. L., . . . Marklund, S. L. (1996). Autosomal recessive adult-onset amyotrophic lateral sclerosis associated with homozygosity for Asp90Ala CuZn-superoxide dismutase mutation. A clinical and genealogical study of 36 patients. *Brain*, 119 (Pt 4), 1153-1172.

Arakawa, O., Nakahiro, M., & Narahashi, T. (1991). Mercury modulation of GABA-activated chloride channels and non-specific cation channels in rat dorsal root ganglion neurons. *Brain Res*, 551(1-2), 58-63.

Armon, C. (2003). Western Pacific ALS/PDC and flying foxes: What's next? *Neurology*, 61(3), 291-292.

Arslan, P., Di Virgilio, F., Beltrame, M., Tsien, R. Y., & Pozzan, T. (1985). Cytosolic Ca2+ homeostasis in Ehrlich and Yoshida carcinomas. A new, membrane-permeant chelator of heavy metals reveals that these ascites tumor cell lines have normal cytosolic free Ca2+. *J Biol Chem*, 260(5), 2719-2727.

Arvidson, B. (1992). Inorganic mercury is transported from muscular nerve terminals to spinal and brainstem motoneurons. *Muscle Nerve*, 15(10), 1089-1094.

Arvidsson, U., Ulfhake, B., Cullheim, S., Ramirez, V., Shupliakov, O., & Hokfelt, T. (1992). Distribution of calbindin D28k-like immunoreactivity (LI) in the monkey ventral horn: do Renshaw cells contain calbindin D28k-LI? *J Neurosci*, 12(3), 718-728.

Aschner, M., Syversen, T., Souza, D. O., Rocha, J. B., & Farina, M. (2007). Involvement of glutamate and reactive oxygen species in methylmercury neurotoxicity. *Braz J Med Biol Res*, 40(3), 285-291.

Aschner, M., Yao, C. P., Allen, J. W., & Tan, K. H. (2000). Methylmercury alters glutamate transport in astrocytes. *Neurochem Int*, 37(2-3), 199-206.

Ashe, K. (2012). Elevated mercury concentrations in humans of Madre de Dios, Peru. *PLoS One*, 7(3), e33305.

Assaf, S. Y., & Chung, S. H. (1984). Release of endogenous Zn2+ from brain tissue during activity. *Nature*, 308(5961), 734-736.

Atchison, W. D. (1986). Extracellular calcium-dependent and -independent effects of methylmercury on spontaneous and potassium-evoked release of acetylcholine at the neuromuscular junction. *J Pharmacol Exp Ther*, 237(2), 672-680.

Atchison, W. D. (1987). Effects of activation of sodium and calcium entry on spontaneous release of acetylcholine induced by methylmercury. *J Pharmacol Exp Ther*, 241(1), 131-139.

Atchison, W. D., Joshi, U., & Thornburg, J. E. (1986). Irreversible suppression of calcium entry into nerve terminals by methylmercury. *J Pharmacol Exp Ther*, 238(2), 618-624.

Atchison, W. D., & Narahashi, T. (1982). Methylmercury-induced depression of neuromuscular transmission in the rat. *Neurotoxicology*, 3(3), 37-50.

Babot, Z., Cristofol, R., & Sunol, C. (2005). Excitotoxic death induced by released glutamate in depolarized primary cultures of mouse cerebellar granule cells is dependent on GABAA receptors and niflumic acid-sensitive chloride channels. *Eur J Neurosci*, 21(1), 103-112.

Bahr, G. F., & Moberger, G. (1954). Methyl-mercury-chloride as a specific reagent for protein-bound sulfhydryl groups; electron stains II. *Exp Cell Res*, 6(2), 506-518.

Bailey, J. M., Colon-Rodriguez, A., & Atchison, W. D. (2017). Evaluating a Gene-Environment Interaction in Amyotrophic Lateral Sclerosis: Methylmercury Exposure and Mutated SOD1. *Curr Environ Health Rep*, 4(2), 200-207.

Bailey, J. M., Hutsell, B. A., & Newland, M. C. (2013). Dietary nimodipine delays the onset of methylmercury neurotoxicity in mice. *Neurotoxicology*, 37, 108-117.

Bakir, F., Damluji, S. F., Amin-Zaki, L., Murtadha, M., Khalidi, A., al-Rawi, N. Y., . . . Doherty, R. A. (1973). Methylmercury poisoning in Iraq. *Science*, 181(4096), 230-241.

Ballatori, N., & Clarkson, T. W. (1985). Biliary secretion of glutathione and of glutathione-metal complexes. *Fundam Appl Toxicol*, 5(5), 816-831.

Ballatori, N., Gatmaitan, Z., & Truong, A. T. (1995). Impaired biliary excretion and whole body elimination of methylmercury in rats with congenital defect in biliary glutathione excretion. *Hepatology*, 22(5), 1469-1473.

Bannai, S. (1984). Transport of cystine and cysteine in mammalian cells. *Biochim Biophys Acta*, 779(3), 289-306.

Baraldi, M., Zanoli, P., Tascedda, F., Blom, J. M., & Brunello, N. (2002). Cognitive deficits and changes in gene expression of NMDA receptors after prenatal methylmercury exposure. *Environ Health Perspect*, 110 Suppl 5, 855-858.

Bardo, S., Robertson, B., & Stephens, G. J. (2002). Presynaptic internal Ca2+ stores contribute to inhibitory neurotransmitter release onto mouse cerebellar Purkinje cells. *Br J Pharmacol*, 137(4), 529-537.

Basu, N., Scheuhammer, A. M., Rouvinen-Watt, K., Evans, R. D., Trudeau, V. L., & Chan, L. H. (2010). In vitro and whole animal evidence that methylmercury disrupts GABAergic systems in discrete brain regions in captive mink. *Comp Biochem Physiol C Toxicol Pharmacol*, 151(3), 379-385.

Becker, C. M., Hoch, W., & Betz, H. (1988). Glycine receptor heterogeneity in rat spinal cord during postnatal development. *EMBO J*, 7(12), 3717-3726.

Behnisch, T., & Reymann, K. G. (1995). Thapsigargin blocks long-term potentiation induced by weak, but not strong tetanisation in rat hippocampal CA1 neurons. *Neurosci Lett*, 192(3), 185-188.

Bellingham, M. C. (2011). A review of the neural mechanisms of action and clinical efficiency of riluzole in treating amyotrophic lateral sclerosis: what have we learned in the last decade? *CNS Neurosci Ther*, 17(1), 4-31.

Bellum, S., Bawa, B., Thuett, K. A., Stoica, G., & Abbott, L. C. (2007). Changes in biochemical processes in cerebellar granule cells of mice exposed to methylmercury. *Int J Toxicol*, 26(3), 261-269.

Bennett, M. R., Farnell, L., & Gibson, W. G. (2000). The probability of quantal secretion within an array of calcium channels of an active zone. *Biophys J*, 78(5), 2222-2240.

Benoit, J. M., Mason, R. P., & Gilmour, C. C. (1999). Estimation of mercury-sulfide speciation in sediment pore waters using octanol-water partitioning and implications for availability to methylating bacteria. *Environ Toxicol Chem*, 18(10), 2138-2141.

Berlin, M., & Ullberg, S. (1963). Accumulation and retention of mercury in the mouse. I. An autoradiographic study after a single intravenous injection of mercuric chloride. *Arch Environ Health*, 6, 589-601.

Bernardi, P., & Petronilli, V. (1996). The permeability transition pore as a mitochondrial calcium release channel: a critical appraisal. *J Bioenerg Biomembr*, 28(2), 131-138.

Bernardi, P., Scorrano, L., Colonna, R., Petronilli, V., & Di Lisa, F. (1999). Mitochondria and cell death. Mechanistic aspects and methodological issues. *Eur J Biochem*, 264(3), 687-701.

Bernhoft, R. A. (2012). Mercury toxicity and treatment: a review of the literature. *J Environ Public Health*, 2012, 460508.

Berridge, M. J. (1998). Neuronal calcium signaling. *Neuron*, 21(1), 13-26.

Berridge, M. J. (2016). The Inositol Trisphosphate/Calcium Signaling Pathway in Health and Disease. *Physiol Rev*, 96(4), 1261-1296.

Bezprozvanny, I., Watras, J., & Ehrlich, B. E. (1991). Bell-shaped calcium-response curves of Ins(1,4,5)P3- and calcium-gated channels from endoplasmic reticulum of cerebellum. *Nature*, 351(6329), 751-754.

Bhumbra, G. S., Bannatyne, B. A., Watanabe, M., Todd, A. J., Maxwell, D. J., & Beato, M. (2014). The recurrent case for the Renshaw cell. *J Neurosci*, 34(38), 12919-12932.

Birke, G., Johnels, A. G., Plantin, L. O., Sjostrand, B., Skerfving, S., & Westermark, T. (1972). Studies on humans exposed to methyl mercury through fish consumption. *Arch Environ Health*, 25(2), 77-91.

Bjorklund, O., Kahlstrom, J., Salmi, P., Ogren, S. O., Vahter, M., Chen, J. F., . . . Dare, E. (2007). The effects of methylmercury on motor activity are sex- and age-dependent, and modulated by genetic deletion of adenosine receptors and caffeine administration. *Toxicology*, 241(3), 119-133.

Blumenthal, E. M., Conroy, W. G., Romano, S. J., Kassner, P. D., & Berg, D. K. (1997). Detection of functional nicotinic receptors blocked by alpha-bungarotoxin on PC12 cells and dependence of their expression on post-translational events. *J Neurosci*, 17(16), 6094-6104.

Booth, S., & Zeller, D. (2005). Mercury, food webs, and marine mammals: implications of diet and climate change for human health. *Environ Health Perspect*, 113(5), 521-526.

Braak, H., Brettschneider, J., Ludolph, A. C., Lee, V. M., Trojanowski, J. Q., & Del Tredici, K. (2013). Amyotrophic lateral sclerosis--a model of corticofugal axonal spread. *Nat Rev Neurol*, 9(12), 708-714.

Bradford, A. B., Mancini, J. D., & Atchison, W. D. (2016). Methylmercury-dependent increases in fluo4 fluorescence in neonatal rat cerebellar slices depend on granule cell migrational stage and GABAA receptor modulation. *J Pharmacol Exp Ther*, 356(1), 2-12.

Brain, K. L., Trout, S. J., Jackson, V. M., Dass, N., & Cunnane, T. C. (2001). Nicotine induces calcium spikes in single nerve terminal varicosities: a role for intracellular calcium stores. *Neuroscience*, 106(2), 395-403.

Bristow, D. R., Bowery, N. G., & Woodruff, G. N. (1986). Light microscopic autoradiographic localisation of [3H]glycine and [3H]strychnine binding sites in rat brain. *Eur J Pharmacol*, 126(3), 303-307.

Brown, I. A. (1954). Chronic mercurialism; a cause of the clinical syndrome of amyotrophic lateral sclerosis. *AMA Arch Neurol Psychiatry*, 72(6), 674-681.

Budd, S. L., & Nicholls, D. G. (1996). Mitochondria, calcium regulation, and acute glutamate excitotoxicity in cultured cerebellar granule cells. *J Neurochem*, 67(6), 2282-2291.

Burke, R. E., Levine, D. N., Tsairis, P., & Zajac, F. E., 3rd. (1973). Physiological types and histochemical profiles in motor units of the cat gastrocnemius. *J Physiol*, 234(3), 723-748.

Campanari, M. L., Garcia-Ayllon, M. S., Ciura, S., Saez-Valero, J., & Kabashi, E. (2016). Neuromuscular Junction Impairment in Amyotrophic Lateral Sclerosis: Reassessing the Role of Acetylcholinesterase. *Front Mol Neurosci*, 9, 160.

Cappello, V., & Francolini, M. (2017). Neuromuscular Junction Dismantling in Amyotrophic Lateral Sclerosis. *Int J Mol Sci*, 18(10).

Carr, P. A., Alvarez, F. J., Leman, E. A., & Fyffe, R. E. (1998). Calbindin D28k expression in immunohistochemically identified Renshaw cells. *Neuroreport*, 9(11), 2657-2661.

Carunchio, I., Mollinari, C., Pieri, M., Merlo, D., & Zona, C. (2008). GAB(A) receptors present higher affinity and modified subunit composition in spinal motor neurons from a genetic model of amyotrophic lateral sclerosis. *Eur J Neurosci*, 28(7), 1275-1285.

Castoldi, A. F., Barni, S., Turin, I., Gandini, C., & Manzo, L. (2000). Early acute necrosis, delayed apoptosis and cytoskeletal breakdown in cultured cerebellar granule neurons exposed to methylmercury. *J Neurosci Res*, 59(6), 775-787.

Castoldi, A. F., Candura, S. M., Costa, P., Manzo, L., & Costa, L. G. (1996). Interaction of mercury compounds with muscarinic receptor subtypes in the rat brain. *Neurotoxicology*, 17(3-4), 735-741.

Castoldi, A. F., Johansson, C., Onishchenko, N., Coccini, T., Roda, E., Vahter, M., . . . Manzo, L. (2008). Human developmental neurotoxicity of methylmercury: impact of variables and risk modifiers. *Regul Toxicol Pharmacol*, 51(2), 201-214.

Castro, A., Aguilar, J., Andres, C., Felix, R., & Delgado-Lezama, R. (2011). GABAA receptors mediate motoneuron tonic inhibition in the turtle spinal cord. *Neuroscience*, 192, 74-80.

Ceccatelli, S., Dare, E., & Moors, M. (2010). Methylmercury-induced neurotoxicity and apoptosis. *Chem Biol Interact*, 188(2), 301-308.

Celio, M. R. (1990). Calbindin D-28k and parvalbumin in the rat nervous system. *Neuroscience*, 35(2), 375-475.

Cernichiari, E., Myers, G. J., Ballatori, N., Zareba, G., Vyas, J., & Clarkson, T. (2007). The biological monitoring of prenatal exposure to methylmercury. *Neurotoxicology*, 28(5), 1015-1022.

Cernichiari, E., Toribara, T. Y., Liang, L., Marsh, D. O., Berlin, M. W., Myers, G. J., . . . et al. (1995). The biological monitoring of mercury in the Seychelles study. *Neurotoxicology*, 16(4), 613-628.

Chamley, J. H., Mark, G. E., Campbell, G. R., & Burnstock, G. (1972). Sympathetic ganglia in culture. I. Neurons. *Z Zellforsch Mikrosk Anat*, 135(3), 287-314.

Chang, L. W. (1977). Neurotoxic effects of mercury--a review. *Environ Res*, 14(3), 329-373.

Chang, L. W., Reuhl, K. R., & Spyker, J. M. (1977). Ultrastructural study of the latent effects of methyl mercury on the nervous system after prenatal exposure. *Environ Res*, 13(2), 171-185.

Chang, Q., & Martin, L. J. (2009). Glycinergic innervation of motoneurons is deficient in amyotrophic lateral sclerosis mice: a quantitative confocal analysis. *Am J Pathol*, 174(2), 574-585.

Chang, Q., & Martin, L. J. (2011). Glycine receptor channels in spinal motoneurons are abnormal in a transgenic mouse model of amyotrophic lateral sclerosis. *J Neurosci*, 31(8), 2815-2827.

Chavez-Noriega, L. E., Crona, J. H., Washburn, M. S., Urrutia, A., Elliott, K. J., & Johnson, E. C. (1997). Pharmacological characterization of recombinant human neuronal nicotinic acetylcholine receptors h alpha 2 beta 2, h alpha 2 beta 4, h alpha 3 beta 2, h alpha 3 beta 4, h alpha 4 beta 2, h alpha 4 beta 4 and h alpha 7 expressed in Xenopus oocytes. *J Pharmacol Exp Ther*, 280(1), 346-356.

Cherry, D., Lowry, L., Velez, L., Cotrell, C., & Keyes, D. C. (2002). Elemental mercury poisoning in a family of seven. *Fam Community Health*, 24(4), 1-8.

Chetty, C. S., Rajanna, S., Hall, E., Yallapragada, P. R., & Rajanna, B. (1996). In vitro and in vivo effects of lead, methyl mercury and mercury on inositol 1,4,5-trisphosphate and 1,3,4,5-tetrakisphosphate receptor bindings in rat brain. *Toxicol Lett*, 87(1), 11-17.

Chiu, V. C., Mouring, D., & Haynes, D. H. (1983). Action of mercurials on the active and passive transport properties of sarcoplasmic reticulum. *J Bioenerg Biomembr*, 15(1), 13-25.

Choi, D. W. (1988). Calcium-mediated neurotoxicity: relationship to specific channel types and role in ischemic damage. *Trends Neurosci*, 11(10), 465-469.

Clarkson, T. W. (1995). Environmental contaminants in the food chain. *Am J Clin Nutr*, 61(3 Suppl), 682S-686S.

Clarkson, T. W., & Magos, L. (2006). The toxicology of mercury and its chemical compounds. *Crit Rev Toxicol*, 36(8), 609-662.

Clarkson, T. W., Vyas, J. B., & Ballatori, N. (2007). Mechanisms of mercury disposition in the body. *Am J Ind Med*, 50(10), 757-764.

Cleveland, D. W., & Rothstein, J. D. (2001). From Charcot to Lou Gehrig: deciphering selective motor neuron death in ALS. *Nat Rev Neurosci*, 2(11), 806-819.

Coccini, T., Randine, G., Candura, S. M., Nappi, R. E., Prockop, L. D., & Manzo, L. (2000). Low-level exposure to methylmercury modifies muscarinic cholinergic receptor binding characteristics in rat brain and lymphocytes: physiologic implications and new opportunities in biologic monitoring. *Environ Health Perspect*, 108(1), 29-33.

Concas, A., Corda, M. G., Salis, M., Mulas, M. L., Milia, A., Corongiu, F. P., & Biggio, G. (1983). Biochemical changes in the rat cerebellar cortex elicited by chronic treatment with methyl mercury. *Toxicol Lett*, 18(1-2), 27-33.

Cong, Y. L., Takeuchi, S., Tokuno, H., & Kuba, K. (2004). Long-term potentiation of transmitter exocytosis expressed by Ca2+-induced Ca2+ release from thapsigargin-sensitive Ca2+ stores in preganglionic nerve terminals. *Eur J Neurosci*, 20(2), 419-426.

Corda, M. G., Concas, A., Rossetti, Z., Guarneri, P., Corongiu, F. P., & Biggio, G. (1981). Methyl mercury enhances [3H]diazepam binding in different areas of the rat brain. *Brain Res*, 229(1), 264-269.

Corradino, R. A. (1993). Calbindin D28K regulation in precociously matured chick egg shell gland in vitro. *Gen Comp Endocrinol*, 91(2), 158-166.

Cullheim, S., & Kellerth, J. O. (1981). Two kinds of recurrent inhibition of cat spinal alpha-motoneurones as differentiated pharmacologically. *J Physiol*, 312, 209-224.

Curtis, D. R., Hosli, L., & Johnston, G. A. (1967). Inhibition of spinal neurons by glycine. *Nature*, 215(5109), 1502-1503.

Dajas-Bailador, F., & Wonnacott, S. (2004). Nicotinic acetylcholine receptors and the regulation of neuronal signalling. *Trends Pharmacol Sci*, 25(6), 317-324.

Davidson, P. W., Cory-Slechta, D. A., Thurston, S. W., Huang, L. S., Shamlaye, C. F., Gunzler, D., . . . Myers, G. J. (2011). Fish consumption and prenatal methylmercury exposure: cognitive and behavioral outcomes in the main cohort at 17 years from the Seychelles child development study. *Neurotoxicology*, 32(6), 711-717.

de Oliveira Souza, V. C., de Marco, K. C., Laure, H. J., Rosa, J. C., & Barbosa, F., Jr. (2016). A brain proteome profile in rats exposed to methylmercury or thimerosal (ethylmercury). *J Toxicol Environ Health*, 79(12), 502-512.

Debes, F., Budtz-Jorgensen, E., Weihe, P., White, R. F., & Grandjean, P. (2006). Impact of prenatal methylmercury exposure on neurobehavioral function at age 14 years. *Neurotoxicol Teratol*, 28(5), 536-547.

Del Castillo, J., & Katz, B. (1954). Quantal components of the end-plate potential. *J Physiol*, 124(3), 560-573.

Denmeade, S. R., & Isaacs, J. T. (2005). The SERCA pump as a therapeutic target: making a "smart bomb" for prostate cancer. *Cancer Biol Ther*, 4(1), 14-22.

Denny, M. F., & Atchison, W. D. (1994). Methylmercury-induced elevations in intrasynaptosomal zinc concentrations: an 19F-NMR study. *J Neurochem*, 63(1), 383-386.

Denny, M. F., & Atchison, W. D. (1996). Mercurial-induced alterations in neuronal divalent cation homeostasis. *Neurotoxicology*, 17(1), 47-61.

Denny, M. F., Hare, M. F., & Atchison, W. D. (1993). Methylmercury alters intrasynaptosomal concentrations of endogenous polyvalent cations. *Toxicol Appl Pharmacol*, 122(2), 222-232.

Dineley, K. T., Pandya, A. A., & Yakel, J. L. (2015). Nicotinic ACh receptors as therapeutic targets in CNS disorders. *Trends Pharmacol Sci*, 36(2), 96-108.

Djiogue, S., Halabalaki, M., Njamen, D., Kretzschmar, G., Lambrinidis, G., Hoepping, J., . . . Vollmer, G. (2014). Erythroidine alkaloids: a novel class of phytoestrogens. *Planta Med*, 80(11), 861-869.

Dourado, M., & Sargent, P. B. (2002). Properties of nicotinic receptors underlying Renshaw cell excitation by alpha-motor neurons in neonatal rat spinal cord. *J Neurophysiol*, 87(6), 3117-3125.

Dreiem, A., & Seegal, R. F. (2007). Methylmercury-induced changes in mitochondrial function in striatal synaptosomes are calcium-dependent and ROS-independent. *Neurotoxicology*, 28(4), 720-726.

Dubinsky, J. M. (1993). Examination of the role of calcium in neuronal death. *Ann N Y Acad Sci*, 679, 34-42.

Dubinsky, J. M., & Rothman, S. M. (1991). Intracellular calcium concentrations during "chemical hypoxia" and excitotoxic neuronal injury. *J Neurosci*, 11(8), 2545-2551.

Dunn, J. D., & Clarkson, T. W. (1980). Does mercury exhalation signal demethylation of methylmercury? *Health Phys*, 38(3), 411-414.

Durisic, N., Godin, A. G., Wever, C. M., Heyes, C. D., Lakadamyali, M., & Dent, J. A. (2012). Stoichiometry of the human glycine receptor revealed by direct subunit counting. *J Neurosci*, 32(37), 12915-12920.

Dutczak, W. J., & Ballatori, N. (1992). gamma-Glutamyltransferase-dependent biliary-hepatic recycling of methyl mercury in the guinea pig. *J Pharmacol Exp Ther*, 262(2), 619-623.

Dutczak, W. J., & Ballatori, N. (1994). Transport of the glutathione-methylmercury complex across liver canalicular membranes on reduced glutathione carriers. *J Biol Chem*, 269(13), 9746-9751.

Dutertre, S., Becker, C. M., & Betz, H. (2012). Inhibitory glycine receptors: an update. *J Biol Chem*, 287(48), 40216-40223.

Eberhard, D. A., & Holz, R. W. (1987). Cholinergic stimulation of inositol phosphate formation in bovine adrenal chromaffin cells: distinct nicotinic and muscarinic mechanisms. *J Neurochem*, 49(5), 1634-1643.

Eccles, J. C., Fatt, P., & Koketsu, K. (1954). Cholinergic and inhibitory synapses in a pathway from motor-axon collaterals to motoneurones. *J Physiol*, 126(3), 524-562.

Edwards, J. R., Marty, M. S., & Atchison, W. D. (2005). Comparative sensitivity of rat cerebellar neurons to dysregulation of divalent cation homeostasis and cytotoxicity caused by methylmercury. *Toxicol Appl Pharmacol*, 208(3), 222-232.

Egawa, K., Kitagawa, K., Inoue, K., Takayama, M., Takayama, C., Saitoh, S., . . . Fukuda, A. (2012). Decreased tonic inhibition in cerebellar granule cells causes motor dysfunction in a mouse model of Angelman syndrome. *Sci Transl Med*, 4(163), 163ra157.

Ekstrom, E. B., Morel, F. M., & Benoit, J. M. (2003). Mercury methylation independent of the acetyl-coenzyme A pathway in sulfate-reducing bacteria. *Appl Environ Microbiol*, 69(9), 5414-5422.

Eldefrawi, M. E., Mansour, N. A., & Eldefrawi, A. T. (1977). Interactions of acetylcholine receptors with organic mercury compounds. *Adv Exp Med Biol*, 84, 449-463.

Elhassani, S. B. (1982). The many faces of methylmercury poisoning. *J Toxicol Clin Toxicol*, 19(8), 875-906.

Eto, K. (1997). Pathology of Minamata disease. *Toxicol Pathol*, 25(6), 614-623.

Eto, K. (2006). [Minamata disease: a neuropathological viewpoint]. *Seishin Shinkeigaku Zasshi*, 108(1), 10-23.

Eto, K., Tokunaga, H., Nagashima, K., & Takeuchi, T. (2002). An autopsy case of minamata disease (methylmercury poisoning)--pathological viewpoints of peripheral nerves. *Toxicol Pathol*, 30(6), 714-722.

Farrant, M., & Nusser, Z. (2005). Variations on an inhibitory theme: phasic and tonic activation of GABA(A) receptors. *Nat Rev Neurosci*, 6(3), 215-229.

Fasolato, C., Zottini, M., Clementi, E., Zacchetti, D., Meldolesi, J., & Pozzan, T. (1991). Intracellular Ca2+ pools in PC12 cells. Three intracellular pools are distinguished by their turnover and mechanisms of Ca2+ accumulation, storage, and release. *J Biol Chem*, 266(30), 20159-20167.

Felder, C. C., Singer-Lahat, D., & Mathes, C. (1994). Voltage-independent calcium channels. Regulation by receptors and intracellular calcium stores. *Biochem Pharmacol*, 48(11), 1997-2004.

Fischer, L. R., Culver, D. G., Tennant, P., Davis, A. A., Wang, M., Castellano-Sanchez, A., . . . Glass, J. D. (2004). Amyotrophic lateral sclerosis is a distal axonopathy: evidence in mice and man. *Exp Neurol*, 185(2), 232-240.

Fohrman, E. B., de Erausquin, G., Costa, E., & Wojcik, W. J. (1993). Muscarinic m3 receptors and dynamics of intracellular Ca2+ in cerebellar granule neurons. *Eur J Pharmacol*, 245(3), 263-271.

Fonfria, E., Rodriguez-Farre, E., & Sunol, C. (2001). Mercury interaction with the GABA(A) receptor modulates the benzodiazepine binding site in primary cultures of mouse cerebellar granule cells. *Neuropharmacology*, 41(7), 819-833.

Fraser, B. (2016). Peru's gold rush prompts public-health emergency. *Nature*, 534(7606), 162.

Frery, N., Maury-Brachet, R., Maillot, E., Deheeger, M., de Merona, B., & Boudou, A. (2001). Gold-mining activities and mercury contamination of native amerindian communities in French Guiana: key role of fish in dietary uptake. *Environ Health Perspect*, 109(5), 449-456.

Fujimura, M., Usuki, F., Sawada, M., Rostene, W., Godefroy, D., & Takashima, A. (2009). Methylmercury exposure downregulates the expression of Racl and leads to neuritic degeneration and ultimately apoptosis in cerebrocortical neurons. *Neurotoxicology*, 30(1), 16-22.

Fyffe, R. E. (1990). Evidence for separate morphological classes of Renshaw cells in the cat's spinal cord. *Brain Res*, 536(1-2), 301-304.

Garcia, F., Ortega, A., Domingo, J. L., & Corbella, J. (2001). Accumulation of metals in autopsy tissues of subjects living in Tarragona County, Spain. *J Environ Sci Health A Tox Hazard Subst Environ Eng*, 36(9), 1767-1786.

Gardner, E. (2012). Peru battles the golden curse of Madre de Dios. *Nature*, 486(7403), 306-307.

Gasso, S., Sunol, C., Sanfeliu, C., Rodriguez-Farre, E., & Cristofol, R. M. (2000). Pharmacological characterization of the effects of methylmercury and mercuric chloride on spontaneous noradrenaline release from rat hippocampal slices. *Life Sci*, 67(10), 1219-1231.

Geiman, E. J., Knox, M. C., & Alvarez, F. J. (2000). Postnatal maturation of gephyrin/glycine receptor clusters on developing Renshaw cells. *J Comp Neurol*, 426(1), 130-142.

Geiman, E. J., Zheng, W., Fritschy, J. M., & Alvarez, F. J. (2002). Glycine and GABA(A) receptor subunits on Renshaw cells: relationship with presynaptic neurotransmitters and postsynaptic gephyrin clusters. *J Comp Neurol*, 444(3), 275-289.

Gerstenberger, S. L., & Dellinger, J. A. (2002). PCBs, mercury, and organochlorine concentrations in lake trout, walleye, and whitefish from selected tribal fisheries in the Upper Great Lakes region. *Environ Toxicol*, 17(6), 513-519.

Ghasemi, M., & Brown, R. H., Jr. (2018). Genetics of Amyotrophic Lateral Sclerosis. *Cold Spring Harb Perspect Med*, 8(5).

Gilbertson, M., & Carpenter, D. O. (2004). An ecosystem approach to the health effects of mercury in the Great Lakes basin ecosystem. *Environ Res*, 95(3), 240-246.

Giniatullin, R., Nistri, A., & Yakel, J. L. (2005). Desensitization of nicotinic ACh receptors: shaping cholinergic signaling. *Trends Neurosci*, 28(7), 371-378.

Glykys, J., Mann, E. O., & Mody, I. (2008). Which GABA(A) receptor subunits are necessary for tonic inhibition in the hippocampus? *J Neurosci*, 28(6), 1421-1426.

Gonzalez-Forero, D., & Alvarez, F. J. (2005). Differential postnatal maturation of GABAA, glycine receptor, and mixed synaptic currents in Renshaw cells and ventral spinal interneurons. *J Neurosci*, 25(8), 2010-2023.

Goodman, L. S., Gilman, A., & Brunton, L. L. (2008). *Goodman & Gilman's manual of pharmacology and therapeutics*. New York: McGraw-Hill Medical.

Gotti, C., Zoli, M., & Clementi, F. (2006). Brain nicotinic acetylcholine receptors: native subtypes and their relevance. *Trends Pharmacol Sci*, 27(9), 482-491.

Graff, R. D., Falconer, M. M., Brown, D. L., & Reuhl, K. R. (1997). Altered sensitivity of posttranslationally modified microtubules to methylmercury in differentiating embryonal carcinoma-derived neurons. *Toxicol Appl Pharmacol*, 144(2), 215-224.

Grandjean, P., Weihe, P., White, R. F., Debes, F., Araki, S., Yokoyama, K., . . . Jorgensen, P. J. (1997). Cognitive deficit in 7-year-old children with prenatal exposure to methylmercury. *Neurotoxicol Teratol*, 19(6), 417-428.

Greene, L. A., & Rein, G. (1977). Synthesis, storage and release of acetylcholine by a noradrenergic pheochromocytoma cell line. *Nature*, 268(5618), 349-351.

Greene, L. A., & Tischler, A. S. (1976). Establishment of a noradrenergic clonal line of rat adrenal pheochromocytoma cells which respond to nerve growth factor. *Proc Natl Acad Sci U S A*, 73(7), 2424-2428.

Greenwood, M. R. (1985). Methylmercury poisoning in Iraq. An epidemiological study of the 1971-1972 outbreak. *J Appl Toxicol*, 5(3), 148-159.

Grenningloh, G., Gundelfinger, E., Schmitt, B., Betz, H., Darlison, M. G., Barnard, E. A., . . . Seeburg, P. H. (1987). Glycine vs GABA receptors. *Nature*, 330(6143), 25-26.

Grosskreutz, J., Van Den Bosch, L., & Keller, B. U. (2010). Calcium dysregulation in amyotrophic lateral sclerosis. *Cell Calcium*, 47(2), 165-174.

Grynkiewicz, G., Poenie, M., & Tsien, R. Y. (1985). A new generation of Ca2+ indicators with greatly improved fluorescence properties. *J Biol Chem*, 260(6), 3440-3450.

Guallar, E., Sanz-Gallardo, M. I., van't Veer, P., Bode, P., Aro, A., Gomez-Aracena, J., . . . Myocardial Infarction Study, G. (2002). Mercury, fish oils, and the risk of myocardial infarction. *N Engl J Med*, 347(22), 1747-1754.

Gueorguiev, V. D., Zeman, R. J., Meyer, E. M., & Sabban, E. L. (2000). Involvement of alpha7 nicotinic acetylcholine receptors in activation of tyrosine hydroxylase and dopamine beta-hydroxylase gene expression in PC12 cells. *J Neurochem*, 75(5), 1997-2005.

Gunson, A. J. (2004). *Mercury and artisanal and small-scale gold miners in China*. Vancouver: University of British Columbia.

Gunter, K. K., & Gunter, T. E. (1994). Transport of calcium by mitochondria. *J Bioenerg Biomembr*, 26(5), 471-485.

Gurney, M. E., Pu, H., Chiu, A. Y., Dal Canto, M. C., Polchow, C. Y., Alexander, D. D., . . . et al. (1994). Motor neuron degeneration in mice that express a human Cu,Zn superoxide dismutase mutation. *Science*, 264(5166), 1772-1775.

Haddock, R. E., & Hill, C. E. (2002). Differential activation of ion channels by inositol 1,4,5-trisphosphate (IP3)- and ryanodine-sensitive calcium stores in rat basilar artery vasomotion. *J Physiol*, 545(2), 615-627.

Haley, R. W. (2003). Excess incidence of ALS in young Gulf War veterans. *Neurology*, 61(6), 750-756.

Hammerschmidt, C. R., Fitzgerald, W. F., Lamborg, C. H., Balcom, P. H., & Tseng, C. M. (2006). Biogeochemical cycling of methylmercury in lakes and tundra watersheds of Arctic Alaska. *Environ Sci Technol*, 40(4), 1204-1211.

Harada, M. (1995). Minamata disease: methylmercury poisoning in Japan caused by environmental pollution. *Crit Rev Toxicol*, 25(1), 1-24.

Harada, Y., Miyamoto, Y., Nonaka, I., Ohta, S., & Ninomiya, T. (1968). Electroencephalographic studies of Minamata disease in children. *Dev Med Child Neurol*, 10(2), 257-258.

Hare, M. F., & Atchison, W. D. (1992). Comparative action of methylmercury and divalent inorganic mercury on nerve terminal and intraterminal mitochondrial membrane potentials. *J Pharmacol Exp Ther*, 261(1), 166-172.

Hare, M. F., & Atchison, W. D. (1995). Methylmercury mobilizes Ca++ from intracellular stores sensitive to inositol 1,4,5-trisphosphate in NG108-15 cells. *J Pharmacol Exp Ther*, 272(3), 1016-1023.

Hare, M. F., McGinnis, K. M., & Atchison, W. D. (1993). Methylmercury increases intracellular concentrations of Ca++ and heavy metals in NG108-15 cells. *J Pharmacol Exp Ther*, 266(3), 1626-1635.

Harris, H. H., Pickering, I. J., & George, G. N. (2003). The chemical form of mercury in fish. *Science*, 301(5637), 1203.

Harris, K. M., Kongsamut, S., & Miller, R. J. (1986). Protein kinase C mediated regulation of calcium channels in PC-12 pheochromocytoma cells. *Biochem Biophys Res Commun*, 134(3), 1298-1305.

Harris, R. C., Rudd, J. W., Amyot, M., Babiarz, C. L., Beaty, K. G., Blanchfield, P. J., . . . Tate, M. T. (2007). Whole-ecosystem study shows rapid fish-mercury response to changes in mercury deposition. *Proc Natl Acad Sci U S A*, 104(42), 16586-16591.

Harrison, M., O'Brien, A., Adams, L., Cowin, G., Ruitenberg, M. J., Sengul, G., & Watson, C. (2013). Vertebral landmarks for the identification of spinal cord segments in the mouse. *Neuroimage*, 68, 22-29.

Hayashi, H., Suga, M., Satake, M., & Tsubaki, T. (1981). Reduced glycine receptor in the spinal cord in amyotrophic lateral sclerosis. *Ann Neurol*, 9(3), 292-294.

Hebb, C. (1972). Biosynthesis of acetylcholine in nervous tissue. *Physiol Rev*, 52(4), 918-957.

Herden, C. J., Pardo, N. E., Hajela, R. K., Yuan, Y., & Atchison, W. D. (2008). Differential effects of methylmercury on gamma-aminobutyric acid type A receptor currents in rat cerebellar granule and cerebral cortical neurons in culture. *J Pharmacol Exp Ther*, 324(2), 517-528.

Hille, B. (1978). Ionic channels in excitable membranes. Current problems and biophysical approaches. *Biophys J*, 22(2), 283-294.

Hillered, L., Muchiri, P. M., Nordenbrand, K., & Ernster, L. (1983). Mn2+ prevents the Ca2+-induced inhibition of ATP synthesis in brain mitochondria. *FEBS Lett*, 154(2), 247-250.

Hinkle, P. M., & Osborne, M. E. (1994). Cadmium toxicity in rat pheochromocytoma cells: studies on the mechanism of uptake. *Toxicol Appl Pharmacol*, 124(1), 91-98.

Hirayama, K. (1985). Effects of combined administration of thiol compounds and methylmercury chloride on mercury distribution in rats. *Biochem Pharmacol*, 34(11), 2030-2032.

Hisatome, I., Kurata, Y., Sasaki, N., Morisaki, T., Morisaki, H., Tanaka, Y., . . . Shigemasa, C. (2000). Block of sodium channels by divalent mercury: role of specific cysteinyl residues in the P-loop region. *Biophys J*, 79(3), 1336-1345.

Horner, R. D., Kamins, K. G., Feussner, J. R., Grambow, S. C., Hoff-Lindquist, J., Harati, Y., . . . Kasarskis, E. J. (2003). Occurrence of amyotrophic lateral sclerosis among Gulf War veterans. *Neurology*, 61(6), 742-749.

Howell, G. A., Welch, M. G., & Frederickson, C. J. (1984). Stimulation-induced uptake and release of zinc in hippocampal slices. *Nature*, 308(5961), 736-738.

Hsiao, B., Dweck, D., & Luetje, C. W. (2001). Subunit-dependent modulation of neuronal nicotinic receptors by zinc. *J Neurosci*, 21(6), 1848-1856.

Huang, C. S., & Narahashi, T. (1996). Mercury chloride modulation of the GABAA receptor-channel complex in rat dorsal root ganglion neurons. *Toxicol Appl Pharmacol*, 140(2), 508-520.

Hughes, W. L. (1957). A physicochemical rationale for the biological activity of mercury and its compounds. *Ann N Y Acad Sci*, 65(5), 454-460.

Hunter, D., & Russell, D. S. (1954). Focal cerebellar and cerebellar atrophy in a human subject due to organic mercury compounds. *J Neurol Neurosurg Psychiatry*, 17(4), 235-241.

Ichas, F., & Mazat, J. P. (1998). From calcium signaling to cell death: two conformations for the mitochondrial permeability transition pore. Switching from low- to high-conductance state. *Biochim Biophys Acta*, 1366(1-2), 33-50.

Imura, N., Miura, K., Inokawa, M., & Nakada, S. (1980). Mechanism of methylmercury cytotoxicity: by biochemical and morphological experiments using cultured cells. *Toxicology*, 17(2), 241-254.

InSug, O., Datar, S., Koch, C. J., Shapiro, I. M., & Shenker, B. J. (1997). Mercuric compounds inhibit human monocyte function by inducing apoptosis: evidence for formation of reactive oxygen species, development of mitochondrial membrane permeability transition and loss of reductive reserve. *Toxicology*, 124(3), 211-224.

Ireland, L. M., Yan, C. H., Nelson, L. M., & Atchison, W. D. (1995). Differential effects of 2,4-dithiobiuret on the synthesis and release of acetylcholine and dopamine from rat pheochromocytoma (PC12) cells. *J Pharmacol Exp Ther*, 275(3), 1453-1462.

Irving, A. J., Collingridge, G. L., & Schofield, J. G. (1992). Interactions between Ca2+ mobilizing mechanisms in cultured rat cerebellar granule cells. *J Physiol*, 456, 667-680.

Ishii, K., Wong, J. K., & Sumikawa, K. (2005). Comparison of alpha2 nicotinic acetylcholine receptor subunit mRNA expression in the central nervous system of rats and mice. *J Comp Neurol*, 493(2), 241-260.

Jacob, T. C., Moss, S. J., & Jurd, R. (2008). GABA(A) receptor trafficking and its role in the dynamic modulation of neuronal inhibition. *Nat Rev Neurosci*, 9(5), 331-343.

Jensen, S., & Jernelov, A. (1969). Biological methylation of mercury in aquatic organisms. *Nature*, 223(5207), 753-754.

Jett, D. A., Beckles, R. A., Navoa, R. V., & McLemore, G. L. (2002). Increased high-affinity nicotinic receptor-binding in rats exposed to lead during development. *Neurotoxicol Teratol*, 24(6), 805-811.

Johnson, F. O., & Atchison, W. D. (2009). The role of environmental mercury, lead and pesticide exposure in development of amyotrophic lateral sclerosis. *Neurotoxicology*, 30(5), 761-765.

Johnson, F. O., Yuan, Y., Hajela, R. K., Chitrakar, A., Parsell, D. M., & Atchison, W. D. (2011). Exposure to an environmental neurotoxicant hastens the onset of amyotrophic lateral sclerosis-like phenotype in human Cu2+/Zn2+ superoxide dismutase 1 G93A mice: glutamate-mediated excitotoxicity. *J Pharmacol Exp Ther*, 338(2), 518-527.

Joint FAO/WHO Expert Committee on Food Additives. Meeting (33rd : 1989 : Geneva Switzerland), & International Program on Chemical Safety. (1989). *Toxicological evaluation of certain food additives and contaminants*. Cambridge ; New York: Cambridge University Press.

Jonas, P., Bischofberger, J., & Sandkuhler, J. (1998). Corelease of two fast neurotransmitters at a central synapse. *Science*, 281(5375), 419-424.

Jones, D. S., Walker, G. M., Johnson, N. W., Mitchell, C. P. J., Coleman Wasik, J. K., & Bailey, J. V. (2019). Molecular evidence for novel mercury methylating microorganisms in sulfate-impacted lakes. *ISME J*.

Juang, M. S. (1976a). Depression of frog muscle contraction by methylmercuric chloride and mercuric chloride. *Toxicol Appl Pharmacol*, 35(1), 183-185.

Juang, M. S. (1976b). An electrophysiological study of the action of methylmercuric chloride and mercuric chloride on the sciatic nerve-sartorius muscle preparation of the frog. *Toxicol Appl Pharmacol*, 37(2), 339-348.

Juang, M. S., & Yonemura, K. (1975). Increased spontaneous transmitter release from presynaptic nerve terminal by methylmercuric chloride. *Nature*, 256(5514), 211-213.

Kajiwara, Y., Yasutake, A., Adachi, T., & Hirayama, K. (1996). Methylmercury transport across the placenta via neutral amino acid carrier. *Arch Toxicol*, 70(5), 310-314.

Kakita, A., Inenaga, C., Sakamoto, M., & Takahashi, H. (2002). Neuronal migration disturbance and consequent cytoarchitecture in the cerebral cortex following transplacental administration of methylmercury. *Acta Neuropathol*, 104(4), 409-417.

Kanning, K. C., Kaplan, A., & Henderson, C. E. (2010). Motor neuron diversity in development and disease. *Annu Rev Neurosci*, 33, 409-440.

Kantarjian, A. D. (1961). A syndrome clinically resembling amyotrophic lateral sclerosis following chronic mercurialism. *Neurology*, 11, 639-644.

Karlin, A., Cox, R. N., Dipaola, M., Holtzman, E., Kao, P. N., Lobel, P., . . . Yodh, N. (1986). Functional domains of the nicotinic acetylcholine receptor. *Ann N Y Acad Sci*, 463, 53-69.

Kasischke, K., Buchner, M., Ludolph, A. C., & Riepe, M. W. (2001). Nuclear shrinkage in live mouse hippocampal slices. *Acta Neuropathol*, 101(5), 483-490.

Kass, G. E., & Orrenius, S. (1999). Calcium signaling and cytotoxicity. *Environ Health Perspect*, 107 Suppl 1, 25-35.

Katz, B., & Miledi, R. (1963). A Study of Spontaneous Miniature Potentials in Spinal Motoneurones. *J Physiol*, 168, 389-422.

Kauppinen, R. A., Komulainen, H., & Taipale, H. (1989). Cellular mechanisms underlying the increase in cytosolic free calcium concentration induced by methylmercury in cerebrocortical synaptosomes from guinea pig. *J Pharmacol Exp Ther*, 248(3), 1248-1254.

Kavalali, E. T. (2015). The mechanisms and functions of spontaneous neurotransmitter release. *Nat Rev Neurosci*, 16(1), 5-16.

Kazantzis, G., Al-Mufti, A. W., Al-Jawad, A., Al-Shahwani, Y., Majid, M. A., Mahmoud, R. M., . . . Dabagh, H. (1976). Epidemiology of organomercury poisoning in Iraq. II. Relationship of mercury levels in blood and hair to exposure and to clinical findings. *Bull World Health Organ*, 53 Suppl, 37-48.

Kazantzis, G., Al-Mufti, A. W., Copplestone, J. F., Majid, M. A., & Mahmoud, R. M. (1976). Epidemiology of organomercury poisoning in Iraq. III. Clinical features and their changes with time. *Bull World Health Organ*, 53 Suppl, 49-57.

Keating, M. H., United States. Environmental Protection Agency. Office of Air Quality Planning and Standards., & United States. Environmental Protection Agency. Office of Research and Development. (1997). *Mercury study report to Congress*. Washington, D.C.?: Office

of Air Quality Planning and Standards and Office of Research and Development, U.S. Environmental Protection Agency.

Kerper, L. E., Ballatori, N., & Clarkson, T. W. (1992). Methylmercury transport across the blood-brain barrier by an amino acid carrier. *Am J Physiol*, 262(5 Pt 2), R761-765.

Kershaw, T. G., Clarkson, T. W., & Dhahir, P. H. (1980). The relationship between blood levels and dose of methylmercury in man. *Arch Environ Health*, 35(1), 28-36.

King, J. K., Kostka, J. E., Frischer, M. E., & Saunders, F. M. (2000). Sulfate-reducing bacteria methylate mercury at variable rates in pure culture and in marine sediments. *Appl Environ Microbiol*, 66(6), 2430-2437.

Kirsch, J., & Betz, H. (1993). Widespread expression of gephyrin, a putative glycine receptor-tubulin linker protein, in rat brain. *Brain Res*, 621(2), 301-310.

Kirsch, J., Wolters, I., Triller, A., & Betz, H. (1993). Gephyrin antisense oligonucleotides prevent glycine receptor clustering in spinal neurons. *Nature*, 366(6457), 745-748.

Knight, M. M., Roberts, S. R., Lee, D. A., & Bader, D. L. (2003). Live cell imaging using confocal microscopy induces intracellular calcium transients and cell death. *Am J Physiol Cell Physiol*, 284(4), C1083-1089.

Knobeloch, L., Gliori, G., & Anderson, H. (2007). Assessment of methylmercury exposure in Wisconsin. *Environ Res*, 103(2), 205-210.

Komulainen, H., & Bondy, S. C. (1987). Increased free intrasynaptosomal Ca2+ by neurotoxic organometals: distinctive mechanisms. *Toxicol Appl Pharmacol*, 88(1), 77-86.

Komulainen, H., Keranen, A., & Saano, V. (1995). Methylmercury modulates GABAA receptor complex differentially in rat cortical and cerebellar membranes in vitro. *Neurochem Res*, 20(6), 659-662.

Kostyniak, P. J., & Clarkson, T. W. (1981). Role of chelating agents in metal toxicity. *Fundam Appl Toxicol*, 1(5), 376-380.

Kroemer, G., Petit, P., Zamzami, N., Vayssiere, J. L., & Mignotte, B. (1995). The biochemistry of programmed cell death. *FASEB J*, 9(13), 1277-1287.

Kruman, II, & Mattson, M. P. (1999). Pivotal role of mitochondrial calcium uptake in neural cell apoptosis and necrosis. *J Neurochem*, 72(2), 529-540.

Kunimoto, M. (1994). Methylmercury induces apoptosis of rat cerebellar neurons in primary culture. *Biochem Biophys Res Commun*, 204(1), 310-317.

Lamotte d'Incamps, B., & Ascher, P. (2013). Subunit composition and kinetics of the Renshaw cell heteromeric nicotinic receptors. *Biochem Pharmacol*, 86(8), 1114-1121.

Landis, M. S., Vette, A. F., & Keeler, G. J. (2002). Atmospheric mercury in the Lake Michigan basin: influence of the Chicago/Gary urban area. *Environ Sci Technol*, 36(21), 4508-4517.

Langosch, D., Thomas, L., & Betz, H. (1988). Conserved quaternary structure of ligand-gated ion channels: the postsynaptic glycine receptor is a pentamer. *Proc Natl Acad Sci U S A*, 85(19), 7394-7398.

Larson, M. D. (1969). An analysis of the action of strychnine on the recurrent IPSP and amino acid induced inhibitions in the cat spinal cord. *Brain Res*, 15(1), 185-200.

Laurie, D. J., Seeburg, P. H., & Wisden, W. (1992). The distribution of 13 GABAA receptor subunit mRNAs in the rat brain. II. Olfactory bulb and cerebellum. *J Neurosci*, 12(3), 1063-1076.

LeBel, C. P., Ali, S. F., McKee, M., & Bondy, S. C. (1990). Organometal-induced increases in oxygen reactive species: the potential of 2',7'-dichlorofluorescin diacetate as an index of neurotoxic damage. *Toxicol Appl Pharmacol*, 104(1), 17-24.

Lee, V., & Maguire, J. (2014). The impact of tonic GABAA receptor-mediated inhibition on neuronal excitability varies across brain region and cell type. *Front Neural Circuits*, 8, 3.

Lehninger, A. L., Nelson, D. L., & Cox, M. M. (2005). *Lehninger principles of biochemistry* (4th ed.). New York: W.H. Freeman.

Lemasters, J. J., Nieminen, A. L., Qian, T., Trost, L. C., Elmore, S. P., Nishimura, Y., . . . Herman, B. (1998). The mitochondrial permeability transition in cell death: a common mechanism in necrosis, apoptosis and autophagy. *Biochim Biophys Acta*, 1366(1-2), 177-196.

Levesque, P. C., & Atchison, W. D. (1987). Interactions of mitochondrial inhibitors with methylmercury on spontaneous quantal release of acetylcholine. *Toxicol Appl Pharmacol*, 87(2), 315-324.

Levesque, P. C., & Atchison, W. D. (1988). Effect of alteration of nerve terminal Ca2+ regulation on increased spontaneous quantal release of acetylcholine by methyl mercury. *Toxicol Appl Pharmacol*, 94(1), 55-65.

Levesque, P. C., & Atchison, W. D. (1991). Disruption of brain mitochondrial calcium sequestration by methylmercury. *J Pharmacol Exp Ther*, 256(1), 236-242.

Levesque, P. C., Hare, M. F., & Atchison, W. D. (1992). Inhibition of mitochondrial Ca2+ release diminishes the effectiveness of methyl mercury to release acetylcholine from synaptosomes. *Toxicol Appl Pharmacol*, 115(1), 11-20.

Leyshon-Sorland, K., Jasani, B., & Morgan, A. J. (1994). The localization of mercury and metallothionein in the cerebellum of rats experimentally exposed to methylmercury. *Histochem J*, 26(2), 161-169.

Li, N., Oquendo, E., Capaldi, R. A., Robinson, J. P., He, Y. D., Hamadeh, H. K., . . . Narayanan, P. K. (2014). A systematic assessment of mitochondrial function identified novel signatures for drug-induced mitochondrial disruption in cells. *Toxicol Sci*, 142(1), 261-273.

Liang, D., Bhatta, S., Gerzanich, V., & Simard, J. M. (2007). Cytotoxic edema: mechanisms of pathological cell swelling. *Neurosurg Focus*, 22(5), E2.

Limke, T. L., & Atchison, W. D. (2002). Acute exposure to methylmercury opens the mitochondrial permeability transition pore in rat cerebellar granule cells. *Toxicol Appl Pharmacol*, 178(1), 52-61.

Limke, T. L., & Atchison, W. D. (2009). Application of single-cell microfluorimetry to neurotoxicology assays. *Curr Protoc Toxicol*, Chapter 12, Unit 12 15.

Limke, T. L., Bearss, J. J., & Atchison, W. D. (2004). Acute exposure to methylmercury causes Ca2+ dysregulation and neuronal death in rat cerebellar granule cells through an M3 muscarinic receptor-linked pathway. *Toxicol Sci*, 80(1), 60-68.

Limke, T. L., Heidemann, S. R., & Atchison, W. D. (2004). Disruption of intraneuronal divalent cation regulation by methylmercury: are specific targets involved in altered neuronal development and cytotoxicity in methylmercury poisoning? *Neurotoxicology*, 25(5), 741-760.

Limke, T. L., Otero-Montañez, J. K., & Atchison, W. D. (2003). Evidence for interactions between intracellular calcium stores during methylmercury-induced intracellular calcium dysregulation in rat cerebellar granule neurons. *J Pharmacol Exp Ther*, 304(3), 949-958.

Liu, W., Wang, X., Zhang, R., & Zhou, Y. (2009). Effects of postnatal exposure to methylmercury on spatial learning and memory and brain NMDA receptor mRNA expression in rats. *Toxicol Lett*, 188(3), 230-235.

Long, P., Mercer, A., Begum, R., Stephens, G. J., Sihra, T. S., & Jovanovic, J. N. (2009). Nerve Terminal GABAA Receptors Activate Ca2+/Calmodulin-dependent Signaling to Inhibit Voltage-gated Ca2+ Influx and Glutamate Release. *J Biol Chem*, 284(13), 8726-8737.

Lukas, R. J., Changeux, J. P., Le Novere, N., Albuquerque, E. X., Balfour, D. J., Berg, D. K., . . . Wonnacott, S. (1999). International Union of Pharmacology. XX. Current status of the nomenclature for nicotinic acetylcholine receptors and their subunits. *Pharmacol Rev*, 51(2), 397-401.

Lynch, J. W. (2004). Molecular structure and function of the glycine receptor chloride channel. *Physiol Rev*, 84(4), 1051-1095.

Mahaffey, K. R., Clickner, R. P., & Jeffries, R. A. (2009). Adult women's blood mercury concentrations vary regionally in the United States: association with patterns of fish consumption (NHANES 1999-2004). *Environ Health Perspect*, 117(1), 47-53.

Mahaffey, K. R., Sunderland, E. M., Chan, H. M., Choi, A. L., Grandjean, P., Marien, K., . . . Yasutake, A. (2011). Balancing the benefits of n-3 polyunsaturated fatty acids and the risks of methylmercury exposure from fish consumption. *Nutr Rev*, 69(9), 493-508.

Mains, R. E., & Patterson, P. H. (1973). Primary cultures of dissociated sympathetic neurons. I. Establishment of long-term growth in culture and studies of differentiated properties. *J Cell Biol*, 59(2 Pt 1), 329-345.

Manev, H., Kharlamov, E., Uz, T., Mason, R. P., & Cagnoli, C. M. (1997). Characterization of zinc-induced neuronal death in primary cultures of rat cerebellar granule cells. *Exp Neurol*, 146(1), 171-178.

Marsh, D. O., Clarkson, T. W., Cox, C., Myers, G. J., Amin-Zaki, L., & Al-Tikriti, S. (1987). Fetal methylmercury poisoning. Relationship between concentration in single strands of maternal hair and child effects. *Arch Neurol*, 44(10), 1017-1022.

Marty, M. S., & Atchison, W. D. (1997). Pathways mediating Ca2+ entry in rat cerebellar granule cells following in vitro exposure to methyl mercury. *Toxicol Appl Pharmacol*, 147(2), 319-330.

Marty, M. S., & Atchison, W. D. (1998). Elevations of intracellular Ca2+ as a probable contributor to decreased viability in cerebellar granule cells following acute exposure to methylmercury. *Toxicol Appl Pharmacol*, 150(1), 98-105.

Masgrau, R., Servitja, J. M., Sarri, E., Young, K. W., Nahorski, S. R., & Picatoste, F. (2000). Intracellular Ca2+ stores regulate muscarinic receptor stimulation of phospholipase C in cerebellar granule cells. *J Neurochem*, 74(2), 818-826.

Mason, R. P., Heyes, D., & Sveinsdottir, A. (2006). Methylmercury concentrations in fish from tidal waters of the Chesapeake bay. *Arch Environ Contam Toxicol*, 51(3), 425-437.

Mattson, M. P. (2000). Apoptosis in neurodegenerative disorders. *Nat Rev Mol Cell Biol*, 1(2), 120-129.

Mattson, M. P., & Chan, S. L. (2003). Calcium orchestrates apoptosis. *Nat Cell Biol*, 5(12), 1041-1043.

Mattson, M. P., Rychlik, B., Chu, C., & Christakos, S. (1991). Evidence for calcium-reducing and excito-protective roles for the calcium-binding protein calbindin-D28k in cultured hippocampal neurons. *Neuron*, 6(1), 41-51.

Mazzocchio, R., & Rossi, A. (2010). Role of Renshaw cells in amyotrophic lateral sclerosis. *Muscle Nerve*, 41(4), 441-443.

Mc, A. D., & Araki, S. (1958). Minamata disease: an unusual neurological disorder caused by contaminated fish. *Lancet*, 2(7047), 629-631.

McGuire, V., Longstreth, W. T., Jr., Koepsell, T. D., & van Belle, G. (1996). Incidence of amyotrophic lateral sclerosis in three counties in western Washington state. *Neurology*, 47(2), 571-573.

McHanwell, S., & Biscoe, T. J. (1981). The sizes of motoneurons supplying hindlimb muscles in the mouse. *Proc R Soc Lond B Biol Sci*, 213(1191), 201-216.

McKeown-Eyssen, G. E., & Ruedy, J. (1983). Prevalence of neurological abnormality in Cree Indians exposed to methylmercury in northern Quebec. *Clin Invest Med*, 6(3), 161-169.

McMahon, A., Wong, B. S., Iacopino, A. M., Ng, M. C., Chi, S., & German, D. C. (1998). Calbindin-D28k buffers intracellular calcium and promotes resistance to degeneration in PC12 cells. *Brain Res Mol Brain Res*, 54(1), 56-63.

Mendelowitz, D., Bacal, K., & Kunze, D. L. (1992). Bradykinin-activated calcium influx pathway in bovine aortic endothelial cells. *Am J Physiol*, 262(4 Pt 2), H942-948.

Mergler, D., Anderson, H. A., Chan, L. H., Mahaffey, K. R., Murray, M., Sakamoto, M., . . . Toxicological Effects of, M. (2007). Methylmercury exposure and health effects in humans: a worldwide concern. *Ambio*, 36(1), 3-11.

Meyer, G., Kirsch, J., Betz, H., & Langosch, D. (1995). Identification of a gephyrin binding motif on the glycine receptor beta subunit. *Neuron*, 15(3), 563-572.

Mirzoian, A., & Luetje, C. W. (2002). Modulation of neuronal nicotinic acetylcholine receptors by mercury. *J Pharmacol Exp Ther*, 302(2), 560-567.

Mitchell, J. D. (2000). Amyotrophic lateral sclerosis: toxins and environment. *Amyotroph Lateral Scler Other Motor Neuron Disord*, 1(4), 235-250.

Mitra, P., & Brownstone, R. M. (2012). An in vitro spinal cord slice preparation for recording from lumbar motoneurons of the adult mouse. *J Neurophysiol*, 107(2), 728-741.

Miura, K., & Imura, N. (1987). Mechanism of methylmercury cytotoxicity. *Crit Rev Toxicol*, 18(3), 161-188.

Miyamoto, K., Nakanishi, H., Moriguchi, S., Fukuyama, N., Eto, K., Wakamiya, J., . . . Osame, M. (2001). Involvement of enhanced sensitivity of N-methyl-D-aspartate receptors in vulnerability of developing cortical neurons to methylmercury neurotoxicity. *Brain Res*, 901(1-2), 252-258.

Mogg, A. J., Whiteaker, P., McIntosh, J. M., Marks, M., Collins, A. C., & Wonnacott, S. (2002). Methyllycaconitine is a potent antagonist of alpha-conotoxin-MII-sensitive presynaptic nicotinic acetylcholine receptors in rat striatum. *J Pharmacol Exp Ther*, 302(1), 197-204.

Mohapatra, S. P., Nikolova, I., & Mitchell, A. (2007). Managing mercury in the great lakes: an analytical review of abatement policies. *J Environ Manage*, 83(1), 80-92.

Mohler, H., Fritschy, J. M., Luscher, B., Rudolph, U., Benson, J., & Benke, D. (1996). The GABAA receptors. From subunits to diverse functions. *Ion Channels*, 4, 89-113.

Moller-Madsen, B. (1990). Localization of mercury in CNS of the rat. II. Intraperitoneal injection of methylmercuric chloride (CH3HgCl) and mercuric chloride (HgCl2). *Toxicol Appl Pharmacol*, 103(2), 303-323.

Moller-Madsen, B. (1991). Localization of mercury in CNS of the rat. III. Oral administration of methylmercuric chloride (CH3HgCl). *Fundam Appl Toxicol*, 16(1), 172-187.

Moloney, E. B., de Winter, F., & Verhaagen, J. (2014). ALS as a distal axonopathy: molecular mechanisms affecting neuromuscular junction stability in the presymptomatic stages of the disease. *Front Neurosci*, 8, 252.

Mori, F., Tanji, K., & Wakabayashi, K. (2000). Widespread calcium deposits, as detected using the alizarin red S technique, in the nervous system of rats treated with dimethyl mercury. *Neuropathology*, 20(3), 210-215.

Myers, G. J., & Davidson, P. W. (1998). Prenatal methylmercury exposure and children: neurologic, developmental, and behavioral research. *Environ Health Perspect*, 106 Suppl 3, 841-847.

Myers, G. J., Davidson, P. W., Cox, C., Shamlaye, C. F., Palumbo, D., Cernichiari, E., . . . Clarkson, T. W. (2003). Prenatal methylmercury exposure from ocean fish consumption in the Seychelles child development study. *Lancet*, 361(9370), 1686-1692.

Nagase, M., Yamamoto, Y., Miyazaki, Y., & Yoshino, H. (2016). Increased oxidative stress in patients with amyotrophic lateral sclerosis and the effect of edaravone administration. *Redox Rep*, 21(3), 104-112.

Nagashima, K., Fujii, Y., Tsukamoto, T., Nukuzuma, S., Satoh, M., Fujita, M., . . . Akagi, H. (1996). Apoptotic process of cerebellar degeneration in experimental methylmercury intoxication of rats. *Acta Neuropathol*, 91(1), 72-77.

Nakai, K., & Satoh, H. (2002). Developmental neurotoxicity following prenatal exposures to methylmercury and PCBs in humans from epidemiological studies. *Tohoku J Exp Med*, 196(2), 89-98.

Nakazawa, K., Nagafuchi, O., Kawakami, T., Inoue, T., Yokota, K., Serikawa, Y., . . . Elvince, R. (2016). Human health risk assessment of mercury vapor around artisanal small-scale gold mining area, Palu city, Central Sulawesi, Indonesia. *Ecotoxicol Environ Saf*, 124, 155-162.

Neustadt, A., Frostholm, A., & Rotter, A. (1988). Topographical distribution of muscarinic cholinergic receptors in the cerebellar cortex of the mouse, rat, guinea pig, and rabbit: a species comparison. *J Comp Neurol*, 272(3), 317-330.

Ni, M., Li, X., Rocha, J. B., Farina, M., & Aschner, M. (2012). Glia and methylmercury neurotoxicity. *J Toxicol Environ Health A*, 75(16-17), 1091-1101.

Nicholls, D., & Akerman, K. (1982). Mitochondrial calcium transport. *Biochim Biophys Acta*, 683(1), 57-88.

Niebroj-Dobosz, I., & Janik, P. (1999). Amino acids acting as transmitters in amyotrophic lateral sclerosis (ALS). *Acta Neurol Scand*, 100(1), 6-11.

Nierenberg, D. W., Nordgren, R. E., Chang, M. B., Siegler, R. W., Blayney, M. B., Hochberg, F., . . . Clarkson, T. (1998). Delayed cerebellar disease and death after accidental exposure to dimethylmercury. *N Engl J Med*, 338(23), 1672-1676.

Nieto-Gonzalez, J. L., Moser, J., Lauritzen, M., Schmitt-John, T., & Jensen, K. (2011). Reduced GABAergic inhibition explains cortical hyperexcitability in the wobbler mouse model of ALS. *Cereb Cortex*, 21(3), 625-635.

O'Kusky, J. (1985). Synaptic degeneration in rat visual cortex after neonatal administration of methylmercury. *Exp Neurol*, 89(1), 32-47.

O'Kusky, J. R., & McGeer, E. G. (1985). Methylmercury poisoning of the developing nervous system in the rat: decreased activity of glutamic acid decarboxylase in cerebral cortex and neostriatum. *Brain Res*, 353(2), 299-306.

Obata, K., Ito, M., Ochi, R., & Sato, N. (1967). Pharmacological properties of the postsynaptic inhibition by Purkinje cell axons and the action of gamma-aminobutyric acid on deiters NEURONES. *Exp Brain Res*, 4(1), 43-57.

Odumo, B. O., Carbonell, G., Angeyo, H. K., Patel, J. P., Torrijos, M., & Rodriguez Martin, J. A. (2014). Impact of gold mining associated with mercury contamination in soil, biota sediments and tailings in Kenya. *Environ Sci Pollut Res Int*, 21(21), 12426-12435.

Olsen, R. W., DeLorey, T. M., Gordey, M., & Kang, M. H. (1999). GABA receptor function and epilepsy. *Adv Neurol*, 79, 499-510.

Pamphlett, R., & Coote, P. (1998). Entry of low doses of mercury vapor into the nervous system. *Neurotoxicology*, 19(1), 39-47.

Pamphlett, R., & Waley, P. (1996). Motor neuron uptake of low dose inorganic mercury. *J Neurol Sci*, 135(1), 63-67.

Papadopoulos, N. G., Dedoussis, G. V., Spanakos, G., Gritzapis, A. D., Baxevanis, C. N., & Papamichail, M. (1994). An improved fluorescence assay for the determination of lymphocyte-mediated cytotoxicity using flow cytometry. *J Immunol Methods*, 177(1-2), 101-111.

Pasinelli, P., & Brown, R. H. (2006). Molecular biology of amyotrophic lateral sclerosis: insights from genetics. *Nat Rev Neurosci*, 7(9), 710-723.

Perry, E., Norton, S. A., Kamman, N. C., Lorey, P. M., & Driscoll, C. T. (2005). Deconstruction of historic mercury accumulation in lake sediments, northeastern United States. *Ecotoxicology*, 14(1-2), 85-99.

Philip, N. S., Carpenter, L. L., Tyrka, A. R., & Price, L. H. (2012). The nicotinic acetylcholine receptor as a target for antidepressant drug development. *ScientificWorldJournal*, 2012, 104105.

Philips, T., & Rothstein, J. D. (2014). Glial cells in amyotrophic lateral sclerosis. *Exp Neurol*, 262 Pt B, 111-120.

Praline, J., Guennoc, A. M., Limousin, N., Hallak, H., de Toffol, B., & Corcia, P. (2007). ALS and mercury intoxication: a relationship? *Clin Neurol Neurosurg*, 109(10), 880-883.

Pycock, C. J., & Kerwin, R. W. (1981). The status of glycine as a supraspinal neurotransmitter. *Life Sci*, 28(24), 2679-2686.

Qian, K., Huang, H., Peterson, A., Hu, B., Maragakis, N. J., Ming, G. L., . . . Zhang, S. C. (2017). Sporadic ALS Astrocytes Induce Neuronal Degeneration In Vivo. *Stem Cell Reports*, 8(4), 843-855.

Qu, M., Nan, X., Gao, Z., Guo, B., Liu, B., & Chen, Z. (2013). Protective effects of lycopene against methylmercury-induced neurotoxicity in cultured rat cerebellar granule neurons. *Brain Res*, 1540, 92-102.

Quandt, F. N., Kato, E., & Narahashi, T. (1982). Effects of methylmercury on electrical responses of neuroblastoma cells. *Neurotoxicology*, 3(4), 205-220.

Rabe, C. S., Schneider, J., & McGee, R., Jr. (1982). Enhancement of depolarization-dependent neurosecretion from PC12 cells by forskolin-induced elevation of cyclic AMP. *J Cyclic Nucleotide Res*, 8(6), 371-384.

Rajaee, M., Long, R. N., Renne, E. P., & Basu, N. (2015). Mercury Exposure Assessment and Spatial Distribution in A Ghanaian Small-Scale Gold Mining Community. *Int J Environ Res Public Health*, 12(9), 10755-10782.

Ramanathan, G., & Atchison, W. D. (2011). Ca2+ entry pathways in mouse spinal motor neurons in culture following in vitro exposure to methylmercury. *Neurotoxicology*, 32(6), 742-750.

Raynor, E. M., & Shefner, J. M. (1994). Recurrent inhibition is decreased in patients with amyotrophic lateral sclerosis. *Neurology*, 44(11), 2148-2153.

Renshaw, B. (1946). Central effects of centripetal impulses in axons of spinal ventral roots. *J Neurophysiol*, 9, 191-204.

Rice, D. C. (1995). Neurotoxicity of lead, methylmercury, and PCBs in relation to the Great Lakes. *Environ Health Perspect*, 103 Suppl 9, 71-87.

Rice, D. C., & Gilbert, S. G. (1982). Early chronic low-level methylmercury poisoning in monkeys impairs spatial vision. *Science*, 216(4547), 759-761.

Rice, G., Swartout, J., Mahaffey, K., & Schoeny, R. (2000). Derivation of U.S. EPA's oral Reference Dose (RfD) for methylmercury. *Drug Chem Toxicol*, 23(1), 41-54.

Ridley, W. P., Dizikes, L. J., & Wood, J. M. (1977). Biomethylation of toxic elements in the environment. *Science*, 197(4301), 329-332.

Rigaud, M., Gemes, G., Barabas, M. E., Chernoff, D. I., Abram, S. E., Stucky, C. L., & Hogan, Q. H. (2008). Species and strain differences in rodent sciatic nerve anatomy: implications for studies of neuropathic pain. *Pain*, 136(1-2), 188-201.

Rizzuto, R. (2003). Calcium mobilization from mitochondria in synaptic transmitter release. *J Cell Biol*, 163(3), 441-443.

Rizzuto, R., Brini, M., Murgia, M., & Pozzan, T. (1993). Microdomains with high Ca2+ close to IP3-sensitive channels that are sensed by neighboring mitochondria. *Science*, 262(5134), 744-747.

Rizzuto, R., De Stefani, D., Raffaello, A., & Mammucari, C. (2012). Mitochondria as sensors and regulators of calcium signalling. *Nat Rev Mol Cell Biol*, 13(9), 566-578.

Roberts, L. R., Steinrauf, L. K., & Blickenstaff, R. T. (1980). New evaluation of potential methylmercury scavengers. *J Pharm Sci*, 69(8), 964-967.

Rooney, J. (2011). Further thoughts on mercury, epigenetics, genetics and amyotrophic lateral sclerosis. *Neurodegener Dis*, 8(6), 523-524.

Roos, P. M., Vesterberg, O., & Nordberg, M. (2006). Metals in motor neuron diseases. *Exp Biol Med (Maywood)*, 231(9), 1481-1487.

Roskoski, R., Jr., & Roskoski, L. M. (1989). Adenosine receptor activation and the regulation of tyrosine hydroxylase activity in PC12 and PC18 cells. *J Neurochem*, 53(6), 1934-1940.

Rowland, I. R., Davies, M. J., & Evans, J. G. (1980). The effect of the gastrointestinal flora on tissue content of mercury and organomercurial neurotoxicity in rats given methylmercuric chloride. *Dev Toxicol Environ Sci*, 8, 79-82.

Rowland, I. R., Robinson, R. D., & Doherty, R. A. (1984). Effects of diet on mercury metabolism and excretion in mice given methylmercury: role of gut flora. *Arch Environ Health*, 39(6), 401-408.

Rowland, L. P., & Shneider, N. A. (2001). Amyotrophic lateral sclerosis. *N Engl J Med*, 344(22), 1688-1700.

Russier, M., Kopysova, I. L., Ankri, N., Ferrand, N., & Debanne, D. (2002). GABA and glycine co-release optimizes functional inhibition in rat brainstem motoneurons in vitro. *J Physiol*, 541(Pt 1), 123-137.

Rustam, H., Von Burg, R., Amin-Zaki, L., & El Hassani, S. (1975). Evidence for a neuromuscular disorder in methylmercury poisoning. *Arch Environ Health*, 30(4), 190-195.

Ryall, R. W., Piercey, M. F., & Polosa, C. (1972). Strychnine-resistant mutual inhibition of Renshaw cells. *Brain Res*, 41(1), 119-129.

Sacco, K. A., Bannon, K. L., & George, T. P. (2004). Nicotinic receptor mechanisms and cognition in normal states and neuropsychiatric disorders. *J Psychopharmacol*, 18(4), 457-474.

Sager, P. R., Doherty, R. A., & Rodier, P. M. (1982). Effects of methylmercury on developing mouse cerebellar cortex. *Exp Neurol*, 77(1), 179-193.

Sakamoto, M., Ikegami, N., & Nakano, A. (1996). Protective effects of Ca2+ channel blockers against methyl mercury toxicity. *Pharmacol Toxicol*, 78(3), 193-199.

Sakamoto, M., Nakamura, M., & Murata, K. (2018). [Mercury as a Global Pollutant and Mercury Exposure Assessment and Health Effects]. *Nihon Eiseigaku Zasshi*, 73(3), 258-264.

Salazar, G., Craige, B., Love, R., Kalman, D., & Faundez, V. (2005). Vglut1 and ZnT3 co-targeting mechanisms regulate vesicular zinc stores in PC12 cells. *J Cell Sci*, 118(Pt 9), 1911-1921.

Sarafian, T., & Verity, M. A. (1991). Oxidative mechanisms underlying methyl mercury neurotoxicity. *Int J Dev Neurosci*, 9(2), 147-153.

Sarafian, T. A. (1993). Methyl mercury increases intracellular Ca2+ and inositol phosphate levels in cultured cerebellar granule neurons. *J Neurochem*, 61(2), 648-657.

Sarafian, T. A., Vartavarian, L., Kane, D. J., Bredesen, D. E., & Verity, M. A. (1994). bcl-2 expression decreases methyl mercury-induced free-radical generation and cell killing in a neural cell line. *Toxicol Lett*, 74(2), 149-155.

Sau, D., De Biasi, S., Vitellaro-Zuccarello, L., Riso, P., Guarnieri, S., Porrini, M., . . . Poletti, A. (2007). Mutation of SOD1 in ALS: a gain of a loss of function. *Hum Mol Genet*, 16(13), 1604-1618.

Savic, N., & Sciancalepore, M. (1998). Intracellular calcium stores modulate miniature GABA-mediated synaptic currents in neonatal rat hippocampal neurons. *Eur J Neurosci*, 10(11), 3379-3386.

Schinder, A. F., Olson, E. C., Spitzer, N. C., & Montal, M. (1996). Mitochondrial dysfunction is a primary event in glutamate neurotoxicity. *J Neurosci*, 16(19), 6125-6133.

Schmidt, S., Allen, K. D., Loiacono, V. T., Norman, B., Stanwyck, C. L., Nord, K. M., . . . Oddone, E. Z. (2008). Genes and Environmental Exposures in Veterans with Amyotrophic Lateral

Sclerosis: the GENEVA study. Rationale, study design and demographic characteristics. *Neuroepidemiology*, 30(3), 191-204.

Schneider, S. P., & Fyffe, R. E. (1992). Involvement of GABA and glycine in recurrent inhibition of spinal motoneurons. *J Neurophysiol*, 68(2), 397-406.

Schober, S. E., Sinks, T. H., Jones, R. L., Bolger, P. M., McDowell, M., Osterloh, J., . . . Mahaffey, K. R. (2003). Blood mercury levels in US children and women of childbearing age, 1999-2000. *JAMA*, 289(13), 1667-1674.

Schoen, D. (2004). Exceeding the methyl mercury reference dose: how dangerous is it? *Environ Health Perspect*, 112(6), A337; author reply A337-338.

Schwarz, S., Husstedt, I., Bertram, H. P., & Kuchelmeister, K. (1996). Amyotrophic lateral sclerosis after accidental injection of mercury. *J Neurol Neurosurg Psychiatry*, 60(6), 698.

Seeburg, P. H., Wisden, W., Verdoorn, T. A., Pritchett, D. B., Werner, P., Herb, A., . . . Sakmann, B. (1990). The GABAA receptor family: molecular and functional diversity. *Cold Spring Harb Symp Quant Biol*, 55, 29-40.

Seguela, P., Wadiche, J., Dineley-Miller, K., Dani, J. A., & Patrick, J. W. (1993). Molecular cloning, functional properties, and distribution of rat brain alpha 7: a nicotinic cation channel highly permeable to calcium. *J Neurosci*, 13(2), 596-604.

Shafer, T. J., & Atchison, W. D. (1991a). Methylmercury blocks N- and L-type Ca++ channels in nerve growth factor-differentiated pheochromocytoma (PC12) cells. *J Pharmacol Exp Ther*, 258(1), 149-157.

Shafer, T. J., & Atchison, W. D. (1991b). Transmitter, ion channel and receptor properties of pheochromocytoma (PC12) cells: a model for neurotoxicological studies. *Neurotoxicology*, 12(3), 473-492.

Shafer, T. J., Contreras, M. L., & Atchison, W. D. (1990). Characterization of interactions of methylmercury with Ca2+ channels in synaptosomes and pheochromocytoma cells: radiotracer flux and binding studies. *Mol Pharmacol*, 38(1), 102-113.

Shamoo, A. E., Maclennan, D. H., & Elderfrawi, M. E. (1976). Differential effects of mercurial compounds on excitable tissues. *Chem Biol Interact*, 12(1), 41-52.

Sharma, G., & Vijayaraghavan, S. (2001). Nicotinic cholinergic signaling in hippocampal astrocytes involves calcium-induced calcium release from intracellular stores. *Proc Natl Acad Sci U S A*, 98(7), 4148-4153.

Shaw, P. J., & Eggett, C. J. (2000). Molecular factors underlying selective vulnerability of motor neurons to neurodegeneration in amyotrophic lateral sclerosis. *J Neurol*, 247 Suppl 1, I17-27.

Shenker, B. J., Guo, T. L., & Shapiro, I. M. (2000). Mercury-induced apoptosis in human lymphoid cells: evidence that the apoptotic pathway is mercurial species dependent. *Environ Res*, 84(2), 89-99.

Sherlock, J., Hislop, J., Newton, D., Topping, G., & Whittle, K. (1984). Elevation of mercury in human blood from controlled chronic ingestion of methylmercury in fish. *Hum Toxicol*, 3(2), 117-131.

Sherlock, J. C., Lindsay, D. G., Hislop, J. E., Evans, W. H., & Collier, T. R. (1982). Duplication diet study on mercury intake by fish consumers in the United Kingdom. *Arch Environ Health*, 37(5), 271-278.

Siciliano, S. D., O'Driscoll, N. J., & Lean, D. R. (2002). Microbial reduction and oxidation of mercury in freshwater lakes. *Environ Sci Technol*, 36(14), 3064-3068.

Simmons-Willis, T. A., Koh, A. S., Clarkson, T. W., & Ballatori, N. (2002). Transport of a neurotoxicant by molecular mimicry: the methylmercury-L-cysteine complex is a substrate for human L-type large neutral amino acid transporter (LAT) 1 and LAT2. *Biochem J*, 367(Pt 1), 239-246.

Simpson, P. B., Nahorski, S. R., & Challiss, R. A. (1996). Agonist-evoked Ca2+ mobilization from stores expressing inositol 1,4,5-trisphosphate receptors and ryanodine receptors in cerebellar granule neurones. *J Neurochem*, 67(1), 364-373.

Simpson, P. B., & Russell, J. T. (1998). Role of mitochondrial Ca2+ regulation in neuronal and glial cell signalling. *Brain Res Brain Res Rev*, 26(1), 72-81.

Sine, S. M., & Engel, A. G. (2006). Recent advances in Cys-loop receptor structure and function. *Nature*, 440(7083), 448-455.

Sirois, J. E., & Atchison, W. D. (1996). Effects of mercurials on ligand- and voltage-gated ion channels: a review. *Neurotoxicology*, 17(1), 63-84.

Skerfving, S. (1988). Mercury in women exposed to methylmercury through fish consumption, and in their newborn babies and breast milk. *Bull Environ Contam Toxicol*, 41(4), 475-482.

Smith, T. A. (2001). Type A gamma-aminobutyric acid (GABAA) receptor subunits and benzodiazepine binding: significance to clinical syndromes and their treatment. *Br J Biomed Sci*, 58(2), 111-121.

Somlyo, A. P., Bond, M., & Somlyo, A. V. (1985). Calcium content of mitochondria and endoplasmic reticulum in liver frozen rapidly in vivo. *Nature*, 314(6012), 622-625.

Somogyi, P., Tamas, G., Lujan, R., & Buhl, E. H. (1998). Salient features of synaptic organisation in the cerebral cortex. *Brain Res Brain Res Rev*, 26(2-3), 113-135.

Sone, N., Larsstuvold, M. K., & Kagawa, Y. (1977). Effect of methyl mercury on phosphorylation, transport, and oxidation in mammalian mitochondria. *J Biochem*, 82(3), 859-868.

Stanford, K. R., & Taylor-Clark, T. E. (2018). Mitochondrial modulation-induced activation of vagal sensory neuronal subsets by antimycin A, but not CCCP or rotenone, correlates with mitochondrial superoxide production. *PLoS One*, 13(5), e0197106.

Steel, R. G. D., & Torrie, J. H. (1960). *Principles and Procedures of Statistics, With Special Reference to the Biological Sciences*. New York: McGraw-Hill.

Stone, C. A., Torchiana, M. L., Navarro, A., & Beyer, K. H. (1956). Ganglionic blocking properties of 3-methylaminoisocamphane hydrochloride (mecamylamine): a secondary amine. *J Pharmacol Exp Ther*, 117(2), 169-183.

Su, C. K., Ho, C. M., Kuo, H. H., Wen, Y. C., & Chai, C. Y. (2009). Sympathetic-correlated c-Fos expression in the neonatal rat spinal cord in vitro. *J Biomed Sci*, 16, 44.

Su, M., Wakabayashi, K., Kakita, A., Ikuta, F., & Takahashi, H. (1998). Selective involvement of large motor neurons in the spinal cord of rats treated with methylmercury. *J Neurol Sci*, 156(1), 12-17.

Sugita, S., Fleming, L. L., Wood, C., Vaughan, S. K., Gomes, M. P., Camargo, W., . . . Valdez, G. (2016). VAChT overexpression increases acetylcholine at the synaptic cleft and accelerates aging of neuromuscular junctions. *Skelet Muscle*, 6, 31.

Sutedja, N. A., Veldink, J. H., Fischer, K., Kromhout, H., Heederik, D., Huisman, M. H., . . . van den Berg, L. H. (2009). Exposure to chemicals and metals and risk of amyotrophic lateral sclerosis: a systematic review. *Amyotroph Lateral Scler*, 10(5-6), 302-309.

Swarup, V., & Julien, J. P. (2011). ALS pathogenesis: recent insights from genetics and mouse models. *Prog Neuropsychopharmacol Biol Psychiatry*, 35(2), 363-369.

Synofzik, M., Fernandez-Santiago, R., Maetzler, W., Schols, L., & Andersen, P. M. (2010). The human G93A SOD1 phenotype closely resembles sporadic amyotrophic lateral sclerosis. *J Neurol Neurosurg Psychiatry*, 81(7), 764-767.

Szalai, G., Krishnamurthy, R., & Hajnoczky, G. (1999). Apoptosis driven by IP(3)-linked mitochondrial calcium signals. *EMBO J*, 18(22), 6349-6361.

Takeuchi, T. (1982). Pathology of Minamata disease. With special reference to its pathogenesis. *Acta Pathol Jpn*, 32 Suppl 1, 73-99.

Takeuchi, T., Eto, K., & Tokunaga, H. (1989). Mercury level and histochemical distribution in a human brain with Minamata disease following a long-term clinical course of twenty-six years. *Neurotoxicology*, 10(4), 651-657.

Tan, X. X., Tang, C., Castoldi, A. F., Manzo, L., & Costa, L. G. (1993). Effects of inorganic and organic mercury on intracellular calcium levels in rat T lymphocytes. *J Toxicol Environ Health*, 38(2), 159-170.

Tanaka, Y., Tanaka, Y., Furuta, T., Yanagawa, Y., & Kaneko, T. (2008). The effects of cutting solutions on the viability of GABAergic interneurons in cerebral cortical slices of adult mice. *J Neurosci Methods*, 171(1), 118-125.

Tandan, R., & Bradley, W. G. (1985). Amyotrophic lateral sclerosis: Part 1. Clinical features, pathology, and ethical issues in management. *Ann Neurol*, 18(3), 271-280.

Tank, A. W., Ham, L., & Curella, P. (1986). Induction of tyrosine hydroxylase by cyclic AMP and glucocorticoids in a rat pheochromocytoma cell line: effect of the inducing agents alone or in combination on the enzyme levels and rate of synthesis of tyrosine hydroxylase. *Mol Pharmacol*, 30(5), 486-496.

Tarasov, A. I., Semplici, F., Li, D., Rizzuto, R., Ravier, M. A., Gilon, P., & Rutter, G. A. (2013). Frequency-dependent mitochondrial Ca(2+) accumulation regulates ATP synthesis in pancreatic beta cells. *Pflugers Arch*, 465(4), 543-554.

Thastrup, O., Cullen, P. J., Drobak, B. K., Hanley, M. R., & Dawson, A. P. (1990). Thapsigargin, a tumor promoter, discharges intracellular Ca2+ stores by specific inhibition of the endoplasmic reticulum Ca2(+)-ATPase. *Proc Natl Acad Sci U S A*, 87(7), 2466-2470.

Thomas, D. J., & Smith, J. C. (1979). Partial characterization of a low-molecular weight methylmercury complex in rat cerebrum. *Toxicol Appl Pharmacol*, 47(3), 547-556.

Traxinger, D. L., & Atchison, W. D. (1987). Comparative effects of divalent cations on the methylmercury-induced alterations of acetylcholine release. *J Pharmacol Exp Ther*, 240(2), 451-459.

Trojsi, F., Monsurro, M. R., & Tedeschi, G. (2013). Exposure to environmental toxicants and pathogenesis of amyotrophic lateral sclerosis: state of the art and research perspectives. *Int J Mol Sci*, 14(8), 15286-15311.

Tsai, T., Yuan, Y., Hajela, R. K., Philips, S. W., & Atchison, W. D. (2017). Methylmercury induces an initial increase in GABA-evoked currents in Xenopus oocytes expressing alpha1 and alpha6 subunit-containing GABAA receptors. *Neurotoxicology*, 60, 161-170.

Tsetlin, V., Kuzmin, D., & Kasheverov, I. (2011). Assembly of nicotinic and other Cys-loop receptors. *J Neurochem*, 116(5), 734-741.

Tsuda, T., Yorifuji, T., Takao, S., Miyai, M., & Babazono, A. (2009). Minamata disease: catastrophic poisoning due to a failed public health response. *J Public Health Policy*, 30(1), 54-67.

Tsuneki, H., Klink, R., Lena, C., Korn, H., & Changeux, J. P. (2000). Calcium mobilization elicited by two types of nicotinic acetylcholine receptors in mouse substantia nigra pars compacta. *Eur J Neurosci*, 12(7), 2475-2485.

Turek, J. W., Kang, C. H., Campbell, J. E., Arneric, S. P., & Sullivan, J. P. (1995). A sensitive technique for the detection of the alpha 7 neuronal nicotinic acetylcholine receptor

antagonist, methyllycaconitine, in rat plasma and brain. *J Neurosci Methods*, 61(1-2), 113-118.

United Nations Environment Programme., International Labour Organisation., World Health Organization., & International Program on Chemical Safety. (1990). *Methylmercury*. Geneva: World Health Organization.

van Zundert, B., Izaurieta, P., Fritz, E., & Alvarez, F. J. (2012). Early pathogenesis in the adult-onset neurodegenerative disease amyotrophic lateral sclerosis. *J Cell Biochem*, 113(11), 3301-3312.

Vanarsdale, A., Weiss, J., Keeler, G., Miller, E., Boulet, G., Brulotte, R., & Poissant, L. (2005). Patterns of mercury deposition and concentration in northeastern North America (1996-2002). *Ecotoxicology*, 14(1-2), 37-52.

Veiga, M. M., Baker, R. F., Fried, M. B., Withers, D., Global Mercury Project., & University of British Columbia. Department of Mining Engineering. (2004). *Protocols for environmental and health assessment of mercury released by artisanal and small-scale gold miners*. Vienna: Global Mercury Project, UNIDO.

Vernino, S., Amador, M., Luetje, C. W., Patrick, J., & Dani, J. A. (1992). Calcium modulation and high calcium permeability of neuronal nicotinic acetylcholine receptors. *Neuron*, 8(1), 127-134.

Vincler, M., & Eisenach, J. C. (2004). Plasticity of spinal nicotinic acetylcholine receptors following spinal nerve ligation. *Neurosci Res*, 48(2), 139-145.

Virginio, C., Giacometti, A., Aldegheri, L., Rimland, J. M., & Terstappen, G. C. (2002). Pharmacological properties of rat alpha 7 nicotinic receptors expressed in native and recombinant cell systems. *Eur J Pharmacol*, 445(3), 153-161.

Vogel, D. G., Margolis, R. L., & Mottet, N. K. (1985). The effects of methyl mercury binding to microtubules. *Toxicol Appl Pharmacol*, 80(3), 473-486.

Von Burg, R., Northington, F. K., & Shamoo, A. (1980). Methylmercury inhibition of rat brain muscarinic receptors. *Toxicol Appl Pharmacol*, 53(2), 285-292.

Wada, E., Wada, K., Boulter, J., Deneris, E., Heinemann, S., Patrick, J., & Swanson, L. W. (1989). Distribution of alpha 2, alpha 3, alpha 4, and beta 2 neuronal nicotinic receptor subunit mRNAs in the central nervous system: a hybridization histochemical study in the rat. *J Comp Neurol*, 284(2), 314-335.

Wade, L. (2013). Mercury pollution. Gold's dark side. *Science*, 341(6153), 1448-1449.

Wang, M. D., Little, J., Gomes, J., Cashman, N. R., & Krewski, D. (2017). Identification of risk factors associated with onset and progression of amyotrophic lateral sclerosis using systematic review and meta-analysis. *Neurotoxicology*, 61, 101-130.

Waxenbaum, J. A., & Futterman, B. (2019). Anatomy, Back, Lumbar Vertebrae. In *StatPearls*. Treasure Island (FL).

Wei, H., Wei, W., Bredesen, D. E., & Perry, D. C. (1998). Bcl-2 protects against apoptosis in neuronal cell line caused by thapsigargin-induced depletion of intracellular calcium stores. *J Neurochem*, 70(6), 2305-2314.

Weihe, P., Grandjean, P., Debes, F., & White, R. (1996). Health implications for Faroe islanders of heavy metals and PCBs from pilot whales. *Sci Total Environ*, 186(1-2), 141-148.

Weis, I. M. (2004). Mercury concentrations in fish from Canadian Great Lakes areas of concern: an analysis of data from the Canadian Department of Environment database. *Environ Res*, 95(3), 341-350.

Weiss, B., Clarkson, T. W., & Simon, W. (2002). Silent latency periods in methylmercury poisoning and in neurodegenerative disease. *Environ Health Perspect*, 110 Suppl 5, 851-854.

Weiss, B., Stern, S., Cox, C., & Balys, M. (2005). Perinatal and lifetime exposure to methylmercury in the mouse: behavioral effects. *Neurotoxicology*, 26(4), 675-690.

Weiss, J. H., & Sensi, S. L. (2000). Ca2+-Zn2+ permeable AMPA or kainate receptors: possible key factors in selective neurodegeneration. *Trends Neurosci*, 23(8), 365-371.

Weisskopf, M. G., Cudkowicz, M. E., & Johnson, N. (2015). Military Service and Amyotrophic Lateral Sclerosis in a Population-based Cohort. *Epidemiology*, 26(6), 831-838.

Welniarz, Q., Dusart, I., & Roze, E. (2017). The corticospinal tract: Evolution, development, and human disorders. *Dev Neurobiol*, 77(7), 810-829.

Werman, R., Davidoff, R. A., & Aprison, M. H. (1967). Inhibition of motoneurones by iontophoresis of glycine. *Nature*, 214(5089), 681-683.

White, R. J., & Reynolds, I. J. (1996). Mitochondrial depolarization in glutamate-stimulated neurons: an early signal specific to excitotoxin exposure. *J Neurosci*, 16(18), 5688-5697.

Whitehouse, P. J., Wamsley, J. K., Zarbin, M. A., Price, D. L., Tourtellotte, W. W., & Kuhar, M. J. (1983). Amyotrophic lateral sclerosis: alterations in neurotransmitter receptors. *Ann Neurol*, 14(1), 8-16.

Wisden, W., Gundlach, A. L., Barnard, E. A., Seeburg, P. H., & Hunt, S. P. (1991). Distribution of GABAA receptor subunit mRNAs in rat lumbar spinal cord. *Brain Res Mol Brain Res*, 10(2), 179-183.

Wojda, U., Salinska, E., & Kuznicki, J. (2008). Calcium ions in neuronal degeneration. *IUBMB Life*, 60(9), 575-590.

Won, S. J., Kim, D. Y., & Gwag, B. J. (2002). Cellular and molecular pathways of ischemic neuronal death. *J Biochem Mol Biol*, 35(1), 67-86.

Wood, J. M., Kennedy, F. S., & Rosen, C. G. (1968). Synthesis of methyl-mercury compounds by extracts of a methanogenic bacterium. *Nature*, 220(5163), 173-174.

Wootz, H., Fitzsimons-Kantamneni, E., Larhammar, M., Rotterman, T. M., Enjin, A., Patra, K., . . . Alvarez, F. J. (2013). Alterations in the motor neuron-renshaw cell circuit in the SOD1(G93A) mouse model. *J Comp Neurol*, 521(7), 1449-1469.

Yang, F., He, X. P., Russell, J., & Lu, B. (2003). Ca2+ influx-independent synaptic potentiation mediated by mitochondrial Na(+)-Ca2+ exchanger and protein kinase C. *J Cell Biol*, 163(3), 511-523.

Yin, Z., Jiang, H., Syversen, T., Rocha, J. B., Farina, M., & Aschner, M. (2008). The methylmercury-L-cysteine conjugate is a substrate for the L-type large neutral amino acid transporter. *J Neurochem*, 107(4), 1083-1090.

Yoshino, Y., Mozai, T., & Nakao, K. (1966). Biochemical changes in the brain in rats poisoned with an alkymercury compound, with special reference to the inhibition of protein synthesis in brain cortex slices. *J Neurochem*, 13(11), 1223-1230.

Yuan, Y., & Atchison, W. D. (1993). Disruption by methylmercury of membrane excitability and synaptic transmission of CA1 neurons in hippocampal slices of the rat. *Toxicol Appl Pharmacol*, 120(2), 203-215.

Yuan, Y., & Atchison, W. D. (1995). Methylmercury acts at multiple sites to block hippocampal synaptic transmission. *J Pharmacol Exp Ther*, 275(3), 1308-1316.

Yuan, Y., & Atchison, W. D. (1997). Action of methylmercury on GABA(A) receptor-mediated inhibitory synaptic transmission is primarily responsible for its early stimulatory effects on hippocampal CA1 excitatory synaptic transmission. *J Pharmacol Exp Ther*, 282(1), 64-73.

Yuan, Y., & Atchison, W. D. (1999). Comparative effects of methylmercury on parallel-fiber and climbing-fiber responses of rat cerebellar slices. *J Pharmacol Exp Ther*, 288(3), 1015-1025.

Yuan, Y., & Atchison, W. D. (2003). Methylmercury differentially affects GABA(A) receptor-mediated spontaneous IPSCs in Purkinje and granule cells of rat cerebellar slices. *J Physiol*, 550(Pt 1), 191-204.

Yuan, Y., & Atchison, W. D. (2005). Methylmercury induces a spontaneous, transient slow inward chloride current in Purkinje cells of rat cerebellar slices. *J Pharmacol Exp Ther*, 313(2), 751-764.

Yuan, Y., & Atchison, W. D. (2007). Methylmercury-induced increase of intracellular Ca2+ increases spontaneous synaptic current frequency in rat cerebellar slices. *Mol Pharmacol*, 71(4), 1109-1121.

Yuan, Y., & Atchison, W. D. (2016). Multiple sources of Ca2+ contribute to methylmercury-induced increased frequency of spontaneous inhibitory synaptic responses in cerebellar slices of rat. *Toxicol Sci*, 150(1), 117-130.

Zanette, G., Tamburin, S., Manganotti, P., Refatti, N., Forgione, A., & Rizzuto, N. (2002). Changes in motor cortex inhibition over time in patients with amyotrophic lateral sclerosis. *J Neurol*, 249(12), 1723-1728.

Zhang, Z. W., Vijayaraghavan, S., & Berg, D. K. (1994). Neuronal acetylcholine receptors that bind alpha-bungarotoxin with high affinity function as ligand-gated ion channels. *Neuron*, 12(1), 167-177.

Ziemann, U., Winter, M., Reimers, C. D., Reimers, K., Tergau, F., & Paulus, W. (1997). Impaired motor cortex inhibition in patients with amyotrophic lateral sclerosis. Evidence from paired transcranial magnetic stimulation. *Neurology*, 49(5), 1292-1298.

Zipfel, G. J., Babcock, D. J., Lee, J. M., & Choi, D. W. (2000). Neuronal apoptosis after CNS injury: the roles of glutamate and calcium. *J Neurotrauma*, 17(10), 857-869.

Zundorf, G., & Reiser, G. (2011). Calcium dysregulation and homeostasis of neural calcium in the molecular mechanisms of neurodegenerative diseases provide multiple targets for neuroprotection. *Antioxid Redox Signal*, 14(7), 1275-1288.